Catalytic Membrane Reactors for Synthesis Gas Production from Natural Gas via Partial Oxidation

Susanne Kelly Olsen

A thesis submitted in partial fulfilment of the
requirements of The Robert Gordon University for the degree of
Doctor of Philosophy

May 2004

ABSTRACT

Natural gas obtained during the extraction of liquid hydrocarbons is often undesired due to the lack of infrastructure to transport the natural gas to an onshore location. As a result the natural gas is often flared causing economic waste and environmental concern. It would therefore be desirable to either convert the natural gas into some other substance which can be transported easily, or transport the natural gas in a liquid state. In that way, new field development will be more financially viable through the use of the extensive infrastructure and technology already in place in the offshore industry for transporting liquid hydrocarbons.

It is considered that one feasible way of utilising offshore produced natural gas, is to convert it into synthetic gas (syngas) which can in turn be used to produce gases and fluids such as methanol, ammonia or a synthetic crude oil that can be readily pumped through the same pipelines as the produced oil.

For the production of synthetic gas, membrane technology presents an attractive advantage improving conversion efficiency by operating as catalyst support, which then also increases the catalyst dispersion, resulting in optimal catalyst load and complete consumption of oxygen and methane in the partial oxidation.

In the present investigation, an enhanced catalyst-dispersed ceramic membrane for low-cost synthesis gas production suitable for gas-to-liquids has been prepared, characterised and tested in a self-designed membrane reactor. The effect of temperature and feed flow rates has been studied and a kinetic model has been developed.

In the novel membrane reactor, an active porous layer is located on both sides facing the oxygen and methane containing gas, adjacent is a second active porous layer and is supported by layers with increasing pore radii. Here the active porous layer on the bore side enhances the reaction between permeated oxygen and fuel species.

In this study, it has also been demonstrated that the oxygen is activated prior to contacting the methane inside the membrane. This often results in 100% oxygen conversion, CO selectivity higher than 96% and syngas ratio (H_2 / CO) of 2.2 to 1.8.

Another advantage of the developed membrane system is that it can be used in high temperatures (> 1273.15K) and high pressure (80bars) processes with no variation on the flow rates, due to the mechanical strength of the ceramic support used.

DEDICATION

I would like to dedicate this work to the person that made me believe that this could be possible, supporting me and guiding me in every step and decision that needed to be made.

The person that can make dreams come true...

I dedicate this work to my brother, Johnar W. Olsen.

ACKNOWLEDGEMENTS

I would like to thank the following people who have made this project possible.

Firstly I would like to express sincere gratitude to my supervisor Dr. Gobina for believing in this work, giving me the chance, encouragement and guidance all the way. Thank you for the understanding and patience throughout this time. The lessons learned will remain for the rest of my life.

My complete appreciation and acknowledges to Ted Mason, my first contact at RGU, the person who opened the gates of the university giving me the chance of an interview and indicating me to potential projects and supervisors.

I would like to thank the best technical support team in the world, not only for the technical support, but for equally precious job of making me fell happy in my work. Milton Montgomery, Steven Pirie, Martin Johnstone, Stanley Buchan, Bill Walker, Allan Harkess. I would like to thank all the technicians just for being there, which made working days, "sunny" days. I can't forget to thank Gavin Murison for the motivation given from the next door.

All the secretarial staff of the school of engineering for helping me, and Professor Norman Deans on behalf of the school of engineering for the facility and financial support.

The overseas research award, for the financial support.

Scottish Enterprise, for accepting me as part time in the Proof of Concept, helping me with my financial situation.

I would like to thank my second supervisors - Bob Bradley for the acceptance to be my second supervisor and consent the use of his equipment and availability of his research team - and Helen Mill for the advices that made a good difference in my career.

Marcus Davidson, Marcella Browne, Sasha Poulsson and Stephen Mitchell from the Advanced Material group for the characterisation of my samples and friendship.

Iain Tough for the precious time and patience in explaining the bases of the SEM and analysis of the samples.

I would like to thank my colleagues from the centre for process integration and membrane technology Ramagopal Uppaluri, Khaled El-Zarouk, Bhavana Tripathi, Chee Chong Chen, and Sandhya Devala for the support, friendship and share of experiences.

Of course without my family's support I would not be able to even start this work, so I would like to thank my father Vilson Olsen and my mother Nerezi Olsen for the understanding of having me so far away, my brother Leonardo Olsen and his family for all the support. And my cousins and grandmother for not forgetting me while I was away.

I owe so much to my boyfriend Duncan Wiseman, to Zahra Izadi and my flat mate Sasha Poulsson, for being with me and listen to my complains giving me strength to carry on the work during the hard times and sharing the happiness of my conquests.

And all my friends that made me smile during the way.

This work would never be possible if it was not a gather of the effort of all the people mentioned. This is not just my thesis, but a result of **our** work.

Thank you.

NOMENCLATURE

A	Pre-exponential factor or frequency factor	[-]
C	Molar concentration	[mol/ml]
ΔH	Heat of reaction	[kJ/mol]
E	Activation energy	[kJ/mol K, kcal/mol K]
F	Molar flow rate	[mol/min]
id	Internal diameter	[mm]
k	Reaction rate constant	
od	External diameter	[mm]
P	Pressure	[bar]
r	Rate of reaction	[mol/ml min]
R	Gas constant	[83.12 bar ml/mol K]
S	Selectivity	
T	Temperature	[K]
ts	Internal thickness	[mm]
tw	External thickness	[mm]
V	Volume	[ml, cm^3]
v	Volumetric flow rate	[ml/min]
X	Conversion	[-]
Y	Yield	[-]
y	molar fraction	[-]
	Production rate	[ml/min cm^2]

SUBSCRIPTS

i	of specie i
n	place in the reactor
room	Room parameter
0	Initial condition

ABBREVIATIONS

AES	Auger Photoelectron Spectrum
ASAP	Surface Area and Porosimetry Analysis
ATR	Autothermal Catalytic Reforming
bcm	Billion Cubic Meter
BET	Stephen Brunauer; P.H. Emmet; Edward Teller
BJH	Elliot P. Barret; Leslie G. Joyner; Paul P. Halenda
BP	British Petroleum
CAR	Combined Autothermal Reforming
CMR	Catalytic Membrane Reactor
CNMR	Catalytic Non-permselective Membrane Reactor
CRM	Combined Reforming
CVD	Chemical Vapour Deposition
DRIFTS	Diffuse Reflectant Infrared Spectroscopy
EDXA	Energy Dispersive x-ray Analysis

FBCMR	Fluidized Bed Catalytic Membrane Reactor
FBMR	Fluidized Bed Membrane Reactor
F-T	Fischer-Tropsch
GC	Gas Chromatograph
GHR	Gas Heated Reforming
GHSV	Gas Hourly Space Velocity
GTL	Gas-to-Liquids
IFP	Intitut Francais du Petrole
LNG	Liquefied Natural Gas
MTG	Methanol-to-Gasoline
NC-POM	Non-catalytic Partial Oxidation
OCM	Oxidative Coupling of Methane
PBCMR	Packed Bed Catalytic Membrane Reactor
PBMR	Packed Bed Membrane Reactor
PDU	Pilot Demonstration Unit
PFA	Perfluoroalkoxy
POM	Catalytic Partial Oxidation
SCR	Selective Catalytic Reduction
SEM	Scanning Electron Microscopy
SMR	Steam Methane Reforming
STP	Standard Temperature and Pressure
Syngas	Synthesis Gas
TAP	Temporal Analysis of Products

WGS	Water-Gas-Shift
XPS	X-ray Photoelectron Spectroscopy

CONVERSIONS

Pressure

1 bar = 100 000 Pa = 0.9869 atmosphere

Energy

1 kcal = 4.1868kJ

Length

1 m = 100 cm = $1x10^6$ μm = $1x10^9$ nm = 3.2808 ft

Volume

1 bcm = $1x10^9$ m^3

1 m^3 = $1x10^6$ ml = $1x10^6$ cm^3 = 35.315 ft^3 = 6.2898 bbl

Area

1 m^2 = 10 000 cm^2 = 10.764 ft^2

Temperature

1°C = 273.15 K

CONTENTS

LIST OF FIGURES

LIST OF TABLES

1. INTRODUCTION

A new generation of ceramic catalyst impregnated membranes has been developed derived from commercially available ceramic support materials. These membranes have been incorporated into catalytic membrane reactors for achieving the conversion of natural gas to synthesis gas at commercially attractive rates with complete materials stability.

This porous catalyst impregnated membrane technology facilitates the control of atmospheric oxygen flowing to a desired reaction site in this case, natural gas partial oxidation to synthesis gas. Because this process is exothermic and eliminates the need for a separate oxygen plant, a significant reduction in synthesis gas production costs may be realized compared to currently available technology.

Current commercially available technology for synthesis gas production from natural gas is based on the endothermic steam reforming reaction which may be represented by:

$$CH_4 + H_2O \rightarrow 3\,H_2 + CO \qquad (1)$$

With CO also reacting with water via the water-gas-shift reaction:

$$CO + H_2O \rightarrow CO_2 + H_2 \qquad (2)$$

In contrast, the methane partial oxidation reaction:

$$CH_4 + \tfrac{1}{2}\,O_2 \rightarrow CO + 2\,H_2 \qquad (3)$$

is exothermic, with oxygen concentration being controlled for subsequent participation in the natural gas partial oxidation reaction at the membrane's porous matrix.

The two technical issues controlling development of membrane technology for achieving the partial oxidation of natural gas into synthesis gas have been:

1) the ability to control and activate a sufficiently high flux of oxygen across the membrane and

2) achieving this for materials which possess high thermal and mechanical stability.

Such membranes must be simultaneously stable to natural gas on the partial oxidation surface and air.

The majority of the work on membranes for syngas generation has focused on oxygen separating membranes of perovskite derived solid state lattice. In this material oxygen anion is controlled mainly through lattice oxygen vacancies. Such vacancies in the perovskite lattice are formed either through doping of the lattice or through oxygen loss when the material is exposed to atmospheres of low oxygen partial pressures. However, both of these vacancy formation mechanisms present problems. For example, doping of cations into the lattice can cause association between the dopants and the resulting oxygen vacancies. This leads to high activation energies for oxygen anion conduction. Loss of oxygen by reaction with the atmosphere leads to increases in lattice parameters and eventual phase decomposition, limiting the usefulness of such materials in commercial applications.

To overcome such problems we have developed an asymmetric catalytic ceramic membrane derived from a commercially available support consisting of α-alumina and a titania washcoat (Al_2O_3/TiO_2).

The rationale for selecting a specific porous architecture has evolved in part from recent studies performed at the Centre for Process Integration and Membrane Technology (CPIMT) which have identified clear correlations between catalyst dispersion and thermodynamic parameters relating to the activation of oxygen and its subsequent transport and reaction. These parameters include:

- the average metal-oxygen bond energy within the membrane matrix,
- pore size and surface area,
- partial pressure of oxygen and
- the feed methane to oxygen ratio

Of all potential applications for this type of membrane architecture the partial oxidation of methane to synthesis gas (syngas) is one of the most commercially important. Syngas can serve as precursor for a variety of products such as methanol, higher alcohols or Fisher-Tropsch products. This process is currently performed industrially but requires oxygen on a large scale, which is expensive (US$430-450/ton). By performing this

reaction with a membrane reactor, air can be used directly and oxygen need not be separated from air. This allows air to be used as the oxidant, greatly reducing syngas production costs.

In addition to the natural gas partial oxidation reaction, the study has considered partial oxidation / CO_2 reforming reactions. In these processes, CO_2 is added to the methane feed stream. This serves two purposes. First, since the natural gas partial oxidation reaction is highly exothermic and the CO_2 reforming reactions are highly endothermic, heat generated can be used to drive the reforming reactions. This allows for better thermal control of reactions within the membrane reactor. The second purpose for a mixed feedstream is that the syngas product composition can be varied. Specifically, the addition of CO_2 will decrease the H_2/CO ratio. The specific composition desired will depend upon the eventual use of the syngas product.

In order to promote the partial oxidation reaction utilising a catalytic membrane, the ceramic membrane material needs to be formed into an appropriate configuration. In the study a shell and tube configuration has been used in which one side of this reactor is exposed to oxygen or air. The membrane reactor then serves to control the amount of oxidant in the reaction zone where it goes on to react with methane present on the second side of the membrane yielding syngas.

As a means to develop commercially viable ceramic membrane reactors for the partial oxidation of natural gas, a novel catalytically active porous ceramic membrane has been prepared in tubular form. These tubes have been incorporated into membrane reactors for the partial oxidation of methane. These materials have shown complete chemical and mechanical stability under expected operating conditions, including long-term performance testing for over one year.

A dip coating technique was used to modify and incorporate catalytic material within the pores of the membrane. Membrane materials were characterised by SEM, EDXA, XPS and ASAP.

Sealing of reactors was achieved using moulded graphite seals. In reactor experiments, either pure oxygen or various oxygen/nitrogen mixtures were used as the oxidant. 100% methane was used primarily as the feedstock. However, experiments have been performed in which CO_2 or nitrogen was added by mixing gases prior to entry into the

reactor. Gas chromatography was used to analyse the syngas product stream as well as to detect any leakage of air across the membrane.

One of the most important properties necessary for industrial use of this technology is long term stability of the membrane materials under actual operating conditions. The catalytic membrane reactor technology has demonstrated stable continuous performance for more than one year. This reactor consisted of a shell and tube structure with separate feeding of methane and oxygen. The outside surface of the membrane tube contained a washcoat of titania while the inside surface was modified with γ-alumina. An adherent partial oxidation catalyst consisting of rhodium supported on the porous membrane matrix has been used. The experiments were performed at atmospheric pressure and up to 1073.15K. Following voluntary termination of the reaction after one year SEM and EDXA investigations showed no evidence of membrane material chemical instability.

At this time the performance of the novel reactor may be summarised as:

Syngas production rate: 1.68 ml/min cm^2

H_2/CO: 2.2 – 1.8

CO selectivity: >96%

O_2 conversion: 100% (also for air)

A unique class of porous ceramic membranes with dispersed catalytic material has been prepared. Incorporation of this membrane into a membrane reactor configuration has demonstrated stable, continuous performance for over one year at practical rates for the spontaneous conversion of natural gas into synthesis gas.

1.1. TARGETS OF THIS WORK

The majority of the research carried out to date on the production of syngas has been based on nickel catalysts. Some studies using rare earth – Ru mixed oxides, Ir or Pt were also carried out in fixed bed reactors. Group VIII metal catalysts were studied in a conventional fixed bed quartz microreactor over a silica support and the mechanism of the reaction using Rh/γ-alumina catalyst was studied in a TAP reactor.

Dense membrane reactors have been used to replace conventional air separation units using ion transport membranes.

The present investigation utilises a porous nonpermeselective membrane reactor, with the added advantage of the catalyst impregnation on the pores of the tubular alumina support, providing higher surface area and therefore less catalyst quantity requirement. Also, as the reactants are fed separately, their activation prior to contact is guaranteed, thus there is no flammability limit in feed concentration to be studied.

This nonpermeselective membrane reactor, modified by dipping technique and impregnated with noble metal catalyst can therefore be considered novel in the study of partial oxidation in a stainless steel reactor. Thus, the aims of the present investigation are:

- To select the appropriate support and modification process to impregnate the catalyst
- To prepare and characterise the appropriate catalytic membrane for carrying out the reaction.
- To design and characterise the reactor in order to determine whether mass and heat transfer limitations have any influence on the kinetic results.
- To design and carryout kinetic experiments to establish a reaction network and also to obtain the various kinetic parameters such as activation energies and pre-exponential factors.
- To determine the kinetic scheme by which this reaction takes place and thus postulate a possible reaction pathway.

- To develop a mathematical relationship between the reactor conversion and temperature using the kinetics data obtained in the study.

Based on the knowledge obtained from previous work on membrane technologies and chemical reactors, the partial oxidation process using a porous ceramic membrane catalyst reactor was defined as the best system to be studied experimentally.

Conceptually, from an engineering viewpoint, a tubular configuration for the membrane reactor could give better performance than the flat one due to the fluid-dynamic conditions [1]. Nickel and Rhodium based catalysts have presented the best results for partial oxidation of methane, demonstrating effective impregnation over a ceramic tubular membrane.

The partial oxidation focused on gas-to-liquids applications for stranded natural gas with a footprint able to be utilised offshore, presents the most attractive industrial application for a novel membrane technology.

To be commercially competitive, the reaction has to take place at lower temperatures than 1023.15K. The use of air instead of oxygen gives a product mixed with nitrogen, which doesn't affect the gas-to-liquids process to produce liquid fuel to be pipelined. The footprint will be increased due to a higher gas flow rate, consequence of the nitrogen containing gas stream, but the cost is still lower than existing processes and if 100% oxygen conversion is achieved this increase on the footprint is minor.

1.2. RELEVANT PUBLICATIONS OF THIS WORK

2004

OLSEN, S. K.; **GOBINA, E.** *Development of a High Performance Gas-To-Liquids (GTL) Synthesis Gas Generation Membrane for Monetizing Stranded Gas*. Membrane Technology Journal, June 2004.

2003

International (PCT) Patent Application No. PCT/GB 2004/001787 *A Membrane Apparatus and Method of Preparing a Membrane and a Method of Producing Hydorgen*. The Robert Gordon University 28 April 2004.

GOBINA, E.; **OLSEN, S. K.** *An Enhanced Catalyst-Dispersed Ceramic Membrane For Low-Cost Synthesis Gas Production Suitable For Gas-To-Liquids* The 21st Membrane Technology/Separation Conference, Newton, MA – USA, 1-2 December 2003.

GOBINA, E.; **OLSEN, S. K.** *Synthesis Gas Production Suitable For Gas-To-Liquids Processes Using Membrane Technology*, 4th Ibero-American Congress on Membrane Science and Technology, Brazil, July 2003.

GOBINA, E.; **OLSEN, S. K.** *Enhancement In Chemical Transformations Using Integrated Membrane Catalysts*, 4th Ibero-American Congress on Membrane Science and Technology, Brazil, July 2003.

GOBINA, E.; **OLSEN, S. K.;** TRIPATHI, B. *Preparation And Characterisation Of Hybrid Inorganic Membranes*, 4th Ibero-American Congress on Membrane Science and Technology, Brazil, July 2003.

OLSEN, S. K.; GOBINA, E. *The role of membrane technology/separations in the development of a hydrogen economy*, Fuel Cells and the hydrogen infrastructure. BCC, Stamford, March 2003.

2002

OLSEN, S. K.; GOBINA, E. *An Integrated Ceramic Membrane Process For Natural Gas Processing* 5th Monetizing Stranded Gas Reserves, Houston, Dec 4-6, 2002.

OLSEN, S. K.; TRIPATHI, B.; MILL, H.; GOBINA, E. Enhanced Productivity in the Hydrocarbon Processing Industry Using Hybrid Inorganic Membrane Technology Membrane and Separation Technology, September 2002

OLSEN, S. K.; TRIPATHI, B.; MILL, H.; GOBINA, E. *Hybrid Inorganic Membrane Technology Show Promise in Gas Processing.* Membrane Technology, July 2002.

OLSEN, S. K.; TRIPATHI, B.; GOBINA, E. *Novel Hybrid Inorganic Membrane Architectures in Natural Gas Processing.* The 2002 20th Membrane Technology/Separation Conference, Boston – USA, 19-20 November 2002.

OLSEN, S. K.; TRIPATHI, B.; GOBINA, E. *Multicomponent Gas Transport in Hybrid Inorganic Membranes.* North American Membrane Society - 13th Annual Meeting, Long Beach, California, May 11-15, 2002.

OLSEN, S.K.; TRIPATHI, B.; GOBINA, E. *Adsorption and Transport of CO_2 in Hybrid Inorganic Membrane.* - Carbon Adsorbents: Porosity, Surface Chemistry &Use.10-11 April 2002.

2001

OLSEN, S. K.; TRIPATHI, B.; FATOGUN, B.; GOBINA, E. *Predicting Gas Transport in Hybrid Inorganic Membranes.* The 19th 2001 Membrane Technology/Separation Conference, Boston – USA, 5-6 December 2001.

2. LITERATURE REVIEW

2.1. NATURAL GAS

When oil companies went looking for oil after the oil shocks of the 1970s they found natural gas in abundance. Proven world gas reserves are now estimated to be 140,000 billion cubic meters (bcm) and the figure is being constantly revised upwards. The annual consumption of natural gas is around 2,100 bcm, with most of the gas consumption occurring in the world's industrialised regions [2].

The chemical conversion of natural gas, one of the world's abundant resources, to produce basic chemicals is one of the desirable goals of the current chemical industry. The conversion of methane to useful chemicals has attracted attention in recent years and many technologies have been developed. Although the direct conversion of methane to valuable chemicals, such as ethylene or methanol and formaldehyde is a most fascinating route, no viable process or catalyst has yet been developed. For the time being, indirect transformation of methane via syngas is still the most competitive process [3].

According to a recent study almost 5,000 significant reservoirs of natural gas have been found worldwide [2], and estimates of stranded gas vary from 900 to 9,000 trillion cubic feet. This includes associated and flared/vented gas, and gas that is reinjected purely for regulatory compliance rather than for reservoir-pressure maintenance [4].

The conventional transport solution is gas compression/cryogenic cooling to produce liquefied natural gas. The liquefied gas accounts for 4% of world gas consumption and 23% of world gas exports [4]. The increasing acceptance of LNG as a method for developing stranded gas reserves has opened more competitive markets. However, to stay competitive project developers must continue to cut capital and operating costs [5].

One attractive option is to use gas-to-liquids (GTL) chemical conversion, which is where the development of improved syngas processes is so important. The liquid fuel produced is easily transported, can be used locally, can be used in existing fuel systems and is extremely clean.

One example of this process is shown in figure 1.

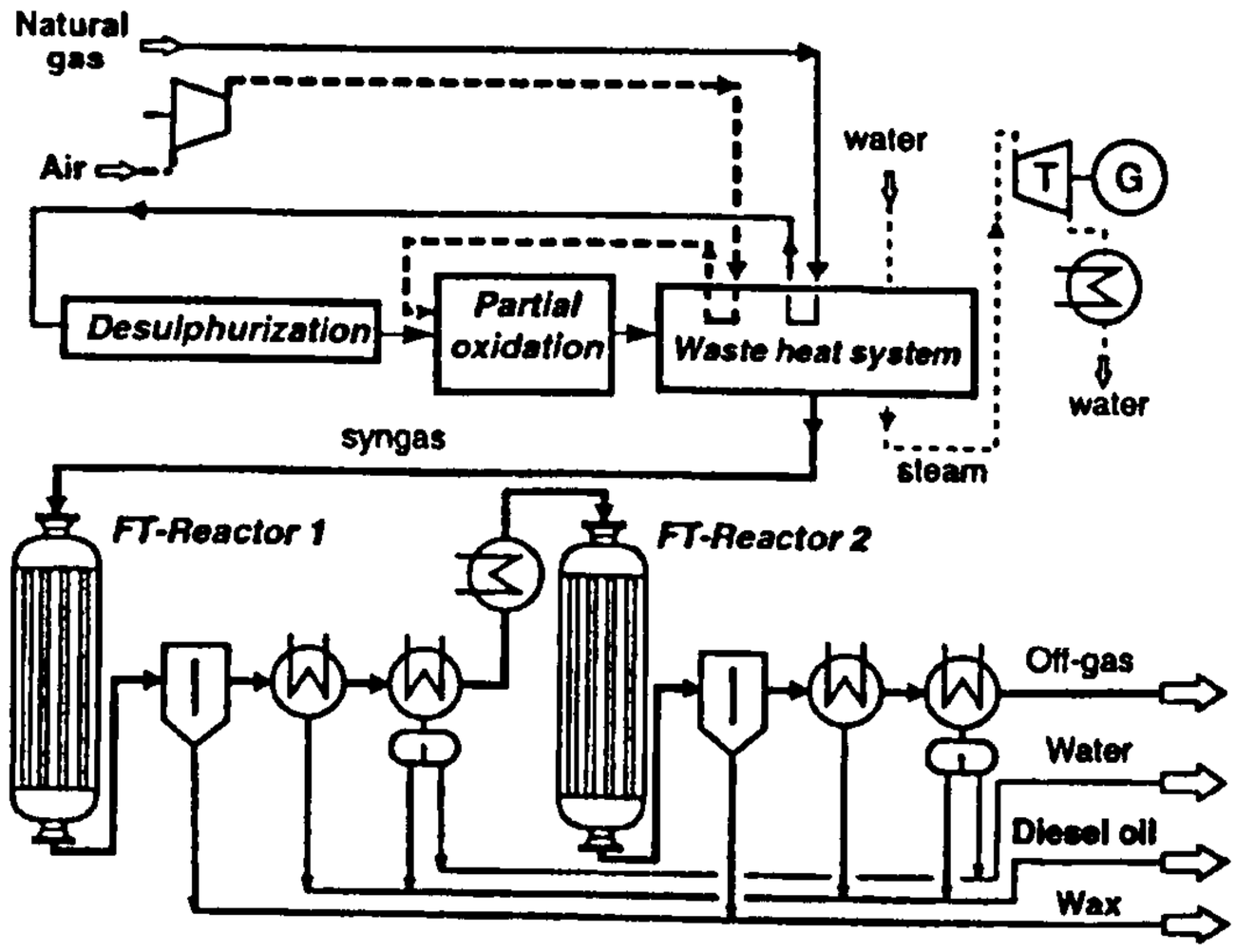

Flow sheet of the proposed low-cost process for the conversion of natural gas to diesel oil and wax based on nitrogen-rich syngas.

Figure 1: Example of GTL process using air [6].

In the first step of the process syngas is produced from the natural gas via partial oxidation. In the next step of the process, Fischer-Tropsch chemistry is used to produce hydrocarbon from the syngas. In some cases a further hydrocracking step is used to produce a liquid fuel. Fischer–Tropsch (F–T) chemistry understandably is often regarded as the key technological component of schemes for converting syngas to transportation fuels and other liquid products. However, syngas production itself accounts for more than half the capital investment and a disproportionate share of the operating costs for a GTL complex [7].

The development of new syngas technology is therefore absolutely critical for the commercialisation of GTL processes.

2.2. SYNTHESIS GAS (SYNGAS)

The production of syngas, a mixture of carbon monoxide and hydrogen has become something of a hot topic in the chemical and process industries over the past years. New technologies are changing the baseline economics of syngas production, making it an attractive feedstock for chemical synthesis and for the production of super-clean liquid fuels [5].

Almost any source of hydrocarbons, such as coal, oil shale, tar sands, bitumen or gasification of biomass can be used to produce syngas. Although coal reserves are large and coal remains available at lower prices than hydrocarbons, the investment in a coal-based syngas plant is ca. three times that required for natural gas-based plant [8]. Therefore it is in the production of syngas from natural gas where the most promise lies.

2.3. NATURAL GAS CONVERSION TO SYNGAS

Almost all options for the chemical conversion of methane (the main component of natural gas) involve its initial conversion to syngas ($CO + H_2$). Syngas can yield liquid hydrocarbons through the F-T reaction over Group VIII transition metal catalysts (Reaction (4)) or first to methanol over Cu/ZnO catalysts and then to gasoline by the methanol-to-gasoline (MTG) process over ZSM-5 zeolites (Reaction (5)):

$$CO + H_2 \rightarrow \text{Hydrocarbons} + H_2O \qquad (4)$$

$$CO + H_2 \rightarrow CH_3OH \rightarrow \text{gasoline} \qquad (5)$$

Ammonia synthesis is still the largest single consumer of syngas, but the growing interest during the last decade in C_1 chemistry and in large-scale conversion of natural gas into liquid fuels has created a need to explore the limits of the reforming technology.

It has been estimated that in the above industrial applications more than 60-70% of the cost of the overall process is associated with syngas production [9]. Therefore, reduction in syngas generation costs would have a large and direct impact on the overall economics of all these downstream industrial processes.

Because CH_4 is a very stable molecule, it has to be processed under very severe conditions. Although its conversion to syngas can be conducted at temperatures even below 700K, high yields to syngas need substantially higher temperatures, typically 1100K. The reaction products H_2, CO, CO_2 and H_2O are for all practical purposes stable at reaction conditions. There are two main reactions that are important in the conversion of natural gas to syngas: steam reforming and partial oxidation.

Steam reforming is a highly endothermic reaction of methane and steam whereas partial oxidation is slightly exothermic:

$CH_4 + H_2O \rightarrow CO + 3H_2$ ($\Delta H° = 206kJ/mol$) (1)

$CH_4 + ½O_2 \rightarrow CO + 2H_2$ ($\Delta H° = -36kJ/mol$) (3)

There are some unwanted reactions occurring simultaneously, namely carbon formation. Carbon deposited from the decomposition of CO into C and CO_2, from reduction of CO and from CH_4 decomposition on catalytic surfaces can be controlled by process conditions like steam concentration in the feed. Reactions (1) and (3) are involved in reforming processes of which there are five:

1) non-catalytic partial oxidation (NC-POM) (only reaction (3) is involved);

2) conventional steam reforming (SMR) (only reaction (1) participates);

3) autothermal catalytic reforming (ATR) (reaction (3) and reaction (1) take place simultaneously);

4) combined reforming (CMR) (reaction (1) is followed by reaction (3));

5) catalytic partial oxidation (POM) (mainly reaction (3) is involved).

While most syngas is produced by steam reforming, some of the other routes may be more attractive, depending on factors such as the required H_2/CO ratio, downstream use, product purity, the presence of CO_2, N_2, H_2O and CH_4, capacity, feedstock availability, purity and cost, including O_2 [10]. These five processes are described below.

2.3.1. NON-CATALYTIC METHANE PARTIAL OXIDATION (NC-POM)

In the non-catalytic process, a mixture of oxygen and natural gas is preheated, mixed and ignited in a burner. It has been stated above that only reaction (3) is involved in the process; however, this is a rough approximation of what is going on. In the absence of catalyst, the reactor temperature must be high enough to reach complete CH_4 conversion. Combustion products like CO_2 and H_2O are also formed to a certain extent. Subsequently, endothermic reactions like steam reforming are also involved, which determine the outlet temperature in the order of 1300-1400K. At this stage, the gas composition is near thermodynamic equilibrium. According to the stoichiometry of reaction (3) the consumption of O_2 should be, in the absence of combustion products, approximately $0.5O_2/CH_4$. However, actual use requires O_2/CH_4 ratios of about 0.7 [11].

One advantage of this process is that it can work at high pressures, thereby saving costly compressors. (Since CH_4 and O_2 are supplied under pressure)

Some carbon is formed by thermal cracking of methane and has to be removed by washing. The outer reactor walls are cold being insulated on the inside.

Using this technology, Texaco and Shell have commercialised this conversion process [12].

2.3.2. STEAM METHANE REFORMING (SMR)

Steam reforming is the established process for converting natural gas and other hydrocarbons into syngas [13]. SMR has been used for several decades since its first development in 1926 [14].

By the traditional process, natural gas is reacted with steam on a Ni-based catalyst in a primary reformer to produce syngas at residence time of several seconds, resulting in an H_2/CO ratio of 3 according to Reaction (1). Reformed gas is formed at ca. 1200K and pressures of 15-30 bar. Excess of steam is introduced to avoid carbon deposition and the feed H_2O/CH_4 mole ratios are typically 2-5, depending on the syngas end use.

Alkali (K) or alkali earths (Mg, Ca) are usually introduced in catalyst formulations so as to accelerate carbon removal from the catalyst surface. The CH_4 conversion at the exit is typically 90-92% and the mixture composition at the exit of the primary reformer approaches that predicted by thermodynamic equilibrium for a $CH_4:H_2O = 1:3$ feed.

A secondary autothermal reformer is placed just at the exit of the primary reformer in which the unconverted CH_4 is reacted with O_2 at the top of a refractory line tube. The mixture is then equilibrated on a Ni catalyst located below the oxidation zone.

Depending on the use, the water-gas shift (WGS) reactors adjust the H_2/CO ratio according to the reaction:

$$CO + H_2O \rightarrow CO_2 + H_2 \ (\Delta H^\circ = -41 \text{ kJ/mol}) \qquad (2)$$

In newer SMR configurations, reformed gas waste heat is recovered for steam generation, boiler feed water preheat and natural gas feed preheat. Over the years the SRM has been optimized with more precise designs of burners, highly creep resistant

materials for the tubes and new S-passivated catalysts which minimize carbon formation [15].

For methanol synthesis plants, the synthesis gas (after cooling and cleaning (water removal)) is compressed to synthesis pressure, typically 80-100 bar, which requires a considerable amount of electricity. For a 2500 Tm/day methanol plant for example the compressors require ca. 30-35 MW. In addition, the number of reforming tubes needed would be ca. 1000, which indicates clearly that the SMR is very costly. There is, however, an important advantage in SMR with respect to the other reforming processes: as it does not require oxygen, no oxygen plant is needed.

2.3.2.1. Carbon Formation

Carbon deposition takes place by the Boudouard reaction and by the direct decomposition of methane:

$$2CO \leftrightarrow C + CO_2 \ (\Delta H° = -172 kJ/mol) \quad (4)$$

$$CH_4 \leftrightarrow C+2H_2 \quad (\Delta H° = +75 kJ/mol) \quad (5)$$

Carbon formation, which is catalysed by Ni surfaces, usually takes place in the form of whiskers with a Ni particle at the top of a fibre [16]. Carbon formation may lead to breakdown of the catalyst, and carbon deposits and degraded catalyst may cause partial or total blockage of the reformer tubes. The uneven flow distribution will cause overheating of the hot tubes. Therefore, carbon deposition must be avoided in tubular reformers. For the SMR there are two limits to be considered:

1) Thermodynamic: carbon is formed if the equilibrated gas shows affinity for carbon. This is called the principle of equilibrated gas, and is justified by the fact that gas is at equilibrium in catalyst particles due to the low effectiveness factor [16].

2) Kinetic: it corresponds to conditions in the reformer where the CH_4 decomposes into carbon instead of reacting with steam, even if thermodynamics predicts no carbon formation after the equilibrium of SMR and WGS reactions has been reached. Carbon formation is then a question of kinetics, local process conditions and reformer design [12].

2.3.2.2. CO_2 reforming

Steam may be replaced by carbon dioxide in the reforming:

$$CH_4 + CO_2 \rightarrow 2CO + 2H_2 \ (\Delta H = +247kJ/mol) \qquad (6)$$

Also, this reaction offers opportunity to utilise CO_2 which is a greenhouse gas. This reaction is of interest because of the lower H_2/CO ratio in the product gas. $H_2/CO=1$ is used in the industrial manufacture of oxo-alcohols, where carbon monoxide is combined with hydrogen in a 1:1 ratio to form an aldehyde. This aldehyde is then reacted with pure hydrogen to form the desired oxo-alcohol product [17].

Reforming of natural gas with CO_2 is not only important in industry for CO production, but also attracts interest as a CO_2 consuming reaction [18]. The kinetics of reaction (6) were studied by Bodrov and Apel'baum [19] who found that the data could be represented by a kinetic expression obtained for steam reforming under similar conditions on a Ni film. A recent study [20] confirmed that replacing steam with CO_2 in the reforming reaction has no drastic influence on the mechanism. It was also observed that the activity trend for steam reforming on several supported metals is less marked for CO_2 reforming [16]. Thermodynamic calculations indicate that the carbon limits are approached when CO_2 is incorporated into the feed. When operating with CO_2 and CH_4 alone in the feed or with high CO_2 contents, thermodynamics predict the formation of carbon [13]. The rate of carbon formation is much lower on noble metals than on Ni, which is ascribed to a smaller dissolution of carbon into these metals. CO_2 reforming on noble metal catalysts was found to yield no carbon [18, 20, 21].

Nickel and noble metal-based catalysts have been reported to be active for CO_2 reforming [18]. Ir/Al_2O_3 catalyst is also active and no carbon deposits were observed [21]. This catalyst is active for the exothermic POM reaction and for the endothermic CO_2 reforming, thus both reactions can be performed simultaneously. This allows fine tuning of the thermodynamics using $CH_4 + CO_2 + O_2$ feeds. Ir or Ru supported on Eu_2O_3 have also been found to be active in syngas generation without significant coke formation [22]. Similarly, alumina-supported Rh catalysts have been shown to be effective in CO_2 reforming at low ratios of CH_4/CO_2 in the temperature range 870-1070K without coke formation [18]. The absence of carbon over noble metals has been attributed to high intrinsic reforming rates combined with low carbon formation rates on

the metals. Rhodium and ruthenium displayed the highest selectivity for the carbon-free operation [15], and this can be due to the high reforming activity combined with low carbon growth rates. Similar results were obtained with a Ni-passivated catalyst, although high operating temperatures were required to achieve reasonable reforming rates [23]. As discussed by Rostrup-Nielsen [24], carbon-free CO_2 reforming could be achieved on the Ni-passivated catalyst by ensemble control on a partly sulphur-poisoned surface. With this catalyst, the sites responsible for carbon formation are blocked, but sufficient sites remain available for the reforming reactions. This surface is generated by adding S-containing compounds to the reformer feed. The rate of carbon formation on a sulphur-passivated surface decreases more than does reforming indicating that the ensemble for the reforming reaction is smaller than that required for carbon deposition.

2.3.3. AUTOTHERMAL METHANE REFORMING (ATR)

Autothermal reforming (ATR) is a combination of non-catalytic partial oxidation and steam reforming developed by Haldor Topsoe in the late 1950s with the aim of carrying out reforming in a single reactor. The reformer basically consists of a ceramic lined tube, similar to the oxygen fired secondary reformer used in the SMR process, and a fixed catalyst bed for equilibration of the gas. The preheated feed streams ($CH_4 + H_2O$, and $H_2O + O_2$) are mixed in a burner placed at the top where the POM reactions take place. The final steam reforming and equilibration take place in the catalyst bed below the burner. Typically, the ATR operates at high temperatures ca. 2200K in the combustion zone and 1200-1400K in the catalytic zone. This results in a lower oxygen consumption (O_2/CH_4 = 0.55-0.60), however, with a certain amount of steam added to the feedstock to eliminate carbon formation. Carbon and soot formation in the combustion zone is an undesired reaction which leads to carbon deposition on downstream tubes causing equipment damage, pressure losses and heat transfer problems. Although the ATR was originally used to maximize H_2 production in ammonia plants, it can be applied in the production of CO-rich gases. In all cases, the H_2/CO ratio at the outlet of the reactor can be precisely adjusted by varying the H_2O/CH_4 and/or O_2/CH_4 molar ratios in the feed.

2.3.4. COMBINED METHANE REFORMING (CMR)

Steam reforming (Reaction (1)), carbon dioxide reforming (Reaction (6)) and partial oxidation of methane (Reaction (3)) supply synthesis gas with theoretical H_2-to-CO ratios of 3, 1 and 2, respectively. Combinations of the different processes can lead to the

desired synthesis gas composition. Syngas production by combined reforming (CMR) involves a primary steam reformer and a secondary oxygen reformer in series. This arrangement shifts a proportion of the reforming duty away from the primary reformer, reducing the required size of the primary reformer and the operation severity. This route produces stoichiometric syngas for methanol production but requires an oxygen plant. A new version of the CMR process, which is named the gas heated reforming (GHR), has been recently patented by ICI [25]. In this process, the heat required for the primary steam reformer is supplied directly by heat exchange with the reformed gas from the secondary oxygen reformer. This novel combination of the two reformers reduces the size of the syngas generation unit to approximately 25% of an equivalent conventional steam-reforming unit and should thus reduce also capital costs.

An all-in-one combined process, named combined autothermal reforming (CAR), wherein steam reforming is combined with partial oxidation of natural gas in a single fluidized bed reactor has been recently developed by Exxon [26]. In the pilot plant studies, natural gas and steam enter at the bottom of the fluidized bed reactor, while oxygen is separately sparged part way up the reactor into the fluidized catalyst bed of a reforming catalyst, e.g., Ni/α-Al_2O_3.

It has been suggested that reactor operation at steam to carbon ratios of as low as 0.5 is possible, with deposited carbon on the recirculating catalyst being burned off by oxygen [12]. In addition, the reverse methanation reaction over catalyst fines has been solved by rapid quenching of the syngas below the reaction threshold temperature.

In newer ammonia plants, the SMR reactors have been replaced by two reactors. The first reactor is the gas heated reformer (GHR) where ca. 75% of CH_4 is reformed to syngas at ca. 970K and 40 bar. The heat for the reforming is supplied by the effluent gases of the second reactor. This second reactor is an autothermal reformer (ATR), which transforms the unconverted CH_4 from the first reactor by partial catalytic air oxidation. This combination introduces the N_2 required in the NH_3 synthesis step and generates the heat that is required for the endothermic process in the first reactor, thus avoiding the need for the steam reformer furnaces. Heat transfer in the GHR is much better than in the old furnaces because both sides of the exchanger tubes are under pressure. In the newer ammonia plants, the combined autothermal reformer (CAR) replaces the two reactors.

The synthesis gas obtained by the conventional SMR is acceptable for methanol synthesis plants, even though the H_2 content is higher than required by the stoichiometry. The combined reforming concept is also applicable to methanol synthesis if pure O_2 is the oxidant in the second reformer. According to Supp [27], the process economics are more favourable for the CMR despite the need for an O_2 plant because of improved methane-to-methanol conversion efficiency. If inexpensive CO_2 is available at the plant site, a combination of SMR and CO_2 reforming results in more favourable synthesis gas composition and a higher methane-based conversion efficiency to methanol, because the CO_2 carbon also contributes to methanol according to reaction (7):

$$3CH_4 + 2H_2O + CO_2 \rightarrow 4CO + 2H_2 \qquad (7)$$

According to this equation, natural gas feeds with 10-25% carbon dioxide content might be particularly suited for methanol synthesis via SMR.

2.3.5. CATALYTIC PARTIAL OXIDATION OF METHANE (POM)

As steam reforming is a very energy intensive process, extensive work has been done over the years in order to develop other more attractive options.

In recent years syngas production has moved steadily from the SMR to direct dry catalytic oxidation of CH_4/O_2 mixtures. According to reaction (3), such a process, with a minimum of steam, yields the desired H_2/CO molar ratio of 2 required for methanol or Fischer-Tropsch synthesis [3]. From thermodynamic simulations [12] it is clear that the reaction is favoured at T>1100K with excess of CH_4, although both CO and H_2 selectivities are modified by the formation of H_2O and CO_2 in combustion reactions which are much more exothermic:

$$CH_4 + \tfrac{1}{2} O_2 \rightarrow CO + 2H_2O \ (\Delta H° = -519 kJ/mol) \qquad (8)$$

$$CH_4 + 2O_2 \rightarrow CO_2 + 2H_2O \ (\Delta H° = -802 kJ/mol) \qquad (9)$$

Since the POM reaction (3) is slightly exothermic, a process based on this reaction would be much more energy efficient than the energy intensive SMR process (Reaction (1)). In addition, the POM reaction is also much faster than the reforming reactions,

suggesting that a single-stage process for syngas production would be an attractive alternative to SMR and also results in smaller reactors and higher productivity.

The direct oxidation reaction has not been developed on an industrial scale, and it is difficult to study because it involves cofeeding CH_4/O_2 mixtures which might result in performing the reaction under flammable or even explosive conditions. Local hot spots are usually formed which can irreversibly damage the active ingredient. Moreover, the gas-phase reactions in a highly reducing atmosphere can lead to carbon and soot deposition over the catalyst surface. Nevertheless, different solutions have been applied as suggested in POM patents that have been issued regularly [28], including cofeeding of small quantities of water, reactor design or catalyst design. The use of catalysts, which overcome the problem of carbon deposition without any steam added into the feed, has renewed interest in the POM process [18, 21, 30, 31].

2.3.5.1. Catalysts

2.3.5.1.1. Early catalytic work on POM

The pioneering work on partial oxidation of CH_4 to synthesis gas was carried out by Prettre et al. [32] employing a 10% Ni catalyst and CH_4:O_2 = 2:1 mixtures at atmospheric pressure in the temperature range 1000-1170K.

Temperature profiles along the catalyst bed suggested that an initial exothermic reaction was followed by an endothermic step. The exothermic process just at the entry of the catalyst bed was attributed to complete combustion of the 25% CH_4 fed, which consumed 100% of the O_2 in the feed according to Reaction (9). The subsequent endothermic process was explained on the basis of the reforming of the remaining unreacted CH_4 with H_2O and/or CO_2 produced in the former step. The gas composition at the outlet of the reactor agreed with thermodynamic calculations based on the catalyst bed exit temperature, and almost complete CH_4 conversion was attained at temperatures above 1100K.

The influence of diffusional effects during POM reaction was then examined by Huszar et al. [33]. For the investigation, a 25% CH_4:air mixtures were reacted over a Ni/mullite catalyst in the temperature range 1030-1170K. They observed that the catalyst would deactivate in an oxidant environment but its activity could be partially recovered on H_2-treatment. This phenomenon was explained in terms of $NiAl_2O_4$ spinel like formation

which is inactive for the POM reaction. These authors concluded that the kinetics of the overall process is dominated by the rate of diffusion of O_2 through the gas film surrounding the catalyst grains and that syngas formation required the presence of metallic Ni obtained by using a CH_4-rich feed.

Working also on Ni catalysts, Gavalas et al. [34] studied the conversion of CH_4/O_2 mixtures at 820-1010 K on catalysts calcined and reduced at different temperatures. For CH_4/O_2 molar ratios 1.5-1.7, they observed a decrease in the initial activity for catalysts calcined at the highest temperatures and explained the observation as due to changes in the Ni^{3+} surface concentration. For a given calcination temperature, some activity decline with reaction time was also observed. CO_2 and H_2O were the only products observed under these conditions. However, prereduction in H_2 at 920-1030K led the initial activity to increase by one to three orders of magnitude, depending on the previous calcination temperature. According to this, these authors assumed that Ni obtained by prereduction is responsible for the reaction and converted to NiO under the reaction conditions, resulting in a decrease in activity with time on-stream. At a typical reaction temperature of 983K and CH_4/O_2 molar ratios of between 1.5-1.7 they found CO_2 as the only C-containing product, but when changing the CH_4/O_2 ratio at values as high as ca. 10, selectivities to CO and CO_2 were comparable.

2.3.5.1.2. Recent catalytic work on POM

In the last decade, many efforts have been devoted to producing synthetic and clean high molecular weight hydrocarbons from natural gas. Without doubt most of these efforts were focused on C-C bond formation by oxidative coupling of methane (OCM) on metal oxide catalysts with basic or redox properties [35]. Most of the researchers working on OCM observed that there seems to exist a limiting barrier in the production of C_{2+} hydrocarbons, which approaches to 22% C_{2+} yield. In addition, when working also on the CH_4 partial oxidation they found a dramatic change in product distribution when using metallic catalysts instead of basic oxide catalysts. Metals supported on refractory oxides yield H_2 and CO as the major products with small amounts of H_2O and CO_2.

Examples of the catalysts used in different reactors are given as follows.

2.3.5.2. Catalytic Reactors

A detailed analysis of the chemistry and reaction approaches in academic research using microcatalytic fixed-bed systems is analysed in the first instance [12]. Other approaches, including fluidized bed, honeycomb and membrane-type reactors are then reviewed subsequently. Figure 2 below depicts three of the reactor configurations normally adopted for syngas production via the POM process.

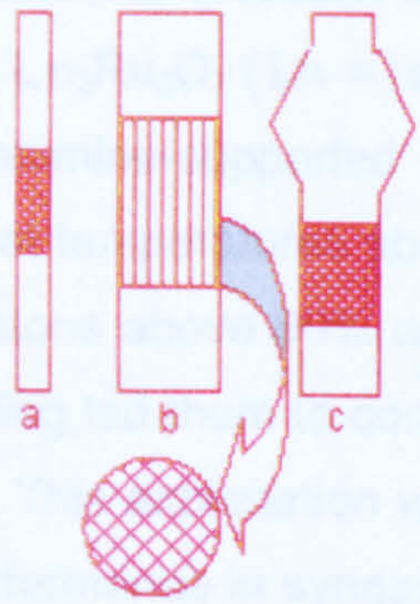

Figure 2: Reactor configurations used in POM processes: (a) fixed bed microreactor; (b) honeycomb reactor (the cross-section of the honeycomb is shown in the inset); (c) fluidized bed reactor.

The fixed bed microreactors are typically quartz tubes 2-6 mm in diameter with 20-80 mg of catalyst bed externally heated through the tube wall. The honeycomb reactor consists of a quartz tube 1-2 cm in diameter with the catalyst in the form of an extruded structure made of alumina or other refractory material. The fluidized bed reactors also consist of quartz tubes 4 - 6 cm in diameter and 20-30 cm tall, with an expansion on the top for catalyst disengagement, and 80-150 μm catalyst particles [12].

2.3.5.2.1. Fixed bed reactors.

Most of the studies on POM were focused on the reaction at atmospheric pressure using fixed bed quartz microcatalytic reactors.

The direct POM reaction at 1070-1270K and atmospheric pressure over a reforming-type Ni/Al_2O_3 catalysts was studied by Blanks et al. [36]. The reactor configuration used in this work allowed not only to operate adiabatically but also to reverse the flow direction periodically, thus reaching high temperatures.

At the entrance of the catalyst bed CH_4 combustion occurred, with a temperature close to 1220K, and downstream of this zone, steam reforming and CO_2 reforming reactions converted the CH_4 in excess to syngas. CH_4 conversions above 85% and H_2 and CO selectivities of 75-85% and 75-95% respectively, were obtained at residence times of 0.25s.

An important contribution to this field has been made by Ashcroft et al, [37, 38] and Vernon et al. [21], who studied methane oxidation to syngas on several rare earth-Ru mixed oxides, of general formula $Ln_2Ru_2O_7$ (Ln = lanthanide element) and pyrochlore structure, and also on several alumina-supported transition elements. Working with diluted feed (CH_4:O_2:N_2 = 2: 1: 4) at temperatures above 1020K and contact times close to 0.1s, they attained CH_4 conversions above 90% and H_2 selectivities in the range 95-99% for all the catalysts. This finding led them to conclude that the active component of the catalyst is the metallic phase. This explanation was then confirmed by Poirier et al. [39] in a study on the catalytic performance in syngas production and surface studies of a praseodymium-Ru pyrochlore. They concluded that once the $Pr_2Ru_2O_7$ is reduced and Ru metal is formed at catalyst surface, the catalyst becomes active in POM reaction to syngas. The effect of the overall pressure on the syngas production was also investigated on these type of catalysts. For a $Dy_2Ru_2O_7$ catalyst, CH_4 conversion and H_2 selectivity were 56 and 100%, respectively, at 1 bar, but fell to 30 and 88% at 20bar, which is in complete agreement with expectations from thermodynamic calculations. Similar high H_2 and CO yields were found on Ir/Al_2O_3 catalysts for the combined partial oxidation and CO_2 reforming [21]. This latter reaction is highly endothermic (Reaction (6)), but very attractive from the point of view of CO_2 removal from industrial emissions.

These authors suggested that the reaction mechanism may involve some CH_4 combustion to CO_2 and H_2O oxidation products, followed by steam reforming (Reaction (1)) and reverse water gas shift (Reaction (2)) reactions to yield equilibrium products. It is worth noting that in the above studies there is no comment upon the thermal gradients of the catalyst bed generated by the heat evolved at the catalyst surface during the POM reactions and their influence on product distributions.

The effect of temperature gradients in the catalyst bed was nicely illustrated by Vermeiren et al. [40] in the POM reaction over Ni-based catalysts. For a fixed temperature in the outer furnace, they found a peak temperature near the inlet zone of

the catalyst bed indicating the participation of exothermic reactions at the inlet and endothermic reactions in the latter part of the catalyst bed. Under the experimental conditions used in this work, the peak temperature was ca. 100K above the temperature of the catalyst bed in the absence of any reaction. In the analysis of the influence of residence time on CH_4 conversion and CO selectivity they observed different trends at high and low reaction temperatures.

While at 1070K both CH_4 conversion and CO selectivity were invariant irrespective of contact time, at 870K they decreased with increasing contact time.

This characteristic behaviour was explained by these authors by assuming a sequential reaction mechanism. Moreover, they also suggested that the POM process consists of a combination of the exothermic combustion and water-gas shift reactions and of the endothermic steam reforming process.

Similar conclusions were drawn by Dissanayake et al. [41] working with a 25% Ni/Al_2O_3 catalyst in the POM reaction. Under atmospheric pressure, oxygen deficient conditions (CH_4:O_2:He = 1.78:1:25) and temperatures in the range 720-1170K, contact times of ca. 0.1s were required to obtain equilibrium selectivities of H_2 and CO. Working at higher space velocities, they also found deviations from thermodynamic equilibrium with a decrease in both CH_4 conversion and H_2 and CO selectivities. Bulk study by X-ray diffraction and surface analysis by photoelectron spectroscopy revealed that under operating conditions the catalyst bed can be divided in three different regions. The first corresponding to the zone contacting the CH_2:O_2:He mixture was essentially $NiAl_2O_4$ which displayed moderate activity for complete combustion of CH_4. The second one consisted of NiO and Al_2O_3, on which complete oxidation of CH_4 to CO_2 and H_2O occurred, giving rise to an important temperature peak in this zone, typically 50K above that at the inlet. Finally, the third part consisted of reduced Ni on the alumina substrate, as expected due to complete O_2 consumption in the two former zones. Syngas production corresponding to thermodynamic equilibrium at the catalyst bed temperature occurred in this third zone through reforming reactions of the unreacted CH_4 and the CO_2 and H_2O products. For sufficiently short contact time, they observed breakthrough of unreacted O_2 causing reoxidation of metallic Ni to the inactive phase $NiAl_2O_4$.

In contrast, Choudhary et al. [42] found successful operation of a similar reactor at extremely low contact times (ca. 7ms) on Ni catalysts at temperatures below 950K. They

reported that the POM reaction is far from equilibrium and H_2 and CO selectivities higher than that predicted by the equilibrium are obtained. Although they attributed this to a change in reaction path, it was confirmed that the apparent deviations of CH_4/O_2 reaction mixture products from thermodynamic equilibrium at high space velocities may have resulted from a small hot zone in the reactor and consequently incorrect measurement of the true reaction temperature [43].

Prereduced nickel-containing substituted perovskite oxides of the type $Ca_{0.8}Sr_{0.2}TiO_{0.8}Ni_{0.2}O_3$ have also been used by Hayakawa et al. [44] in the POM reaction. These catalysts displayed high activity for syngas production. X-ray diffraction profiles of the used catalysts indicated that nickel oxide segregated from the perovskite structure and was reduced to nickel metal particles which were thought to be the active catalytic species. Similarly, Alqahtany et al. [45] have demonstrated syngas formation from methane over an Fe electrode in an yttria-stabilised zirconia reactor, they found that reduced iron was more active than oxidised iron for syngas formation. However, carbon deposition occurred on the iron electrode.

Silica-supported group VIII metal catalysts were used by Nakamura et al. [46] in the POM reaction using a conventional fixed bed quartz microreactor at atmospheric pressure and contact times of 0.15s. Above 900K, the conversion of CH_4 to CO and H_2 was near 90% over Rh, Ru and Ni catalysts respectively. They also share the model of combustion followed by reforming and shift reactions to explain the experimental results. As already observed by Huszar et al. [33] and Dissanayake et al. [41], they found that oxidized Ni surface becomes completely inactive for syngas production. These authors attributed this behaviour to a retardation of the CO_2 and H_2O reforming reactions in the absence of reduced metallic Ni. Platinum also showed activity for syngas formation at 900K, but Fe and Co exhibited activity in CH_4 combustion.

Concerning the mechanism, Lapszewicz et al. [47] pointed out that CO could be a primary product of CH_4 oxidation. Their objective was to identify the reaction pathway and to provide the information required for the development of catalysts suitable for industrial usage. In runs conducted at different space velocities they observed that on some catalysts the CO selectivity decreased with a decrease in contact time while on others it increased, providing evidence that either CO or CO_2 could be a primary product. This interpretation was then demonstrated by performing kinetic experiments with two

different feeds: one consisting of a CH_4:O_2 = 2:1 mixture and the other consisting of a CH_4:H_2O:CO_2 = 3:2:1 mixture, the latter corresponding to the mixture remaining after total O_2 consumption. They found important differences in the rates of CH_4 consumption and CO formation between the two feeds. While one catalyst was good for POM and reforming reactions, another was almost inactive for reforming but good for POM. Based on these observations, they suggested a free radical reaction mechanism on the catalyst surface. Following adsorption, CH_4 and O_2 undergo homolytic dissociation according to the sequence:

$$CH_4 \rightarrow [.CH_x]_{ads} + (4 - x)\,[.\,H]_{ads} \qquad (10)$$

$$O_2 \rightarrow 2\,[.O]_{ads} \qquad (11)$$

These authors then postulated that either CO or CO_2 could be primary products arising from the surface intermediates $[.CH_x]_{ads}$ and $[.O]_{ads}$. The secondary reactions included reforming of CH_4 with H_2O and CO_2, WGS and oxidation of H_2 and CO. The almost complete O_2 conversion suggested that the rate limiting step was the activation of CH_4. This was confirmed by the observed increase in CH_4 conversion and CO formation rates with increasing the metal loading in the catalyst.

Buyevska et al. [48] and Walter et al. [49] studied the mechanism over a Rh/γ-Al_2O_3 catalyst by a temporal analysis of products (TAP) reactor and diffuse reflectant infrared spectroscopy (DRIFTS). CH_4 activation is produced over reduced surface Rh, yielding carbon deposits, but it is oxided to CO_2 over Rh-O (oxided sites). CO is formed by reaction between these two primary products, C and CO_2 (reverse Boudouard reaction). Hydrogen is formed by CH_4 decomposition in the reduced sites. At steady-state condition, the product distribution is strongly affected by the degree of reduction of the surface. DRIFTS data showed also that groups on the support are involved in CH_4 conversion, and that formats are formed on the surface, like spectators of the reaction rapidly formed and reversibly bonded to the Al_2O_3 support. Finally, these spectroscopic data confirm that the initial oxygen coverage leads to different product distributions.

Mallens et al. [50] reported an investigation on the reaction mechanism for the partial oxidation of methane to syngas over Pt catalysts. The methodology involved admitting pulses of pure methane, pure oxygen and mixtures of methane and oxygen to a Pt sponge at temperatures ranging from 973 to 1073K and using the temporal analysis of

products (TAP) set-up. The reaction scheme is illustrated in Figure 3. Methane dissociates on reduced Pt to surface C and H atoms, but not on an oxidized Pt surface.

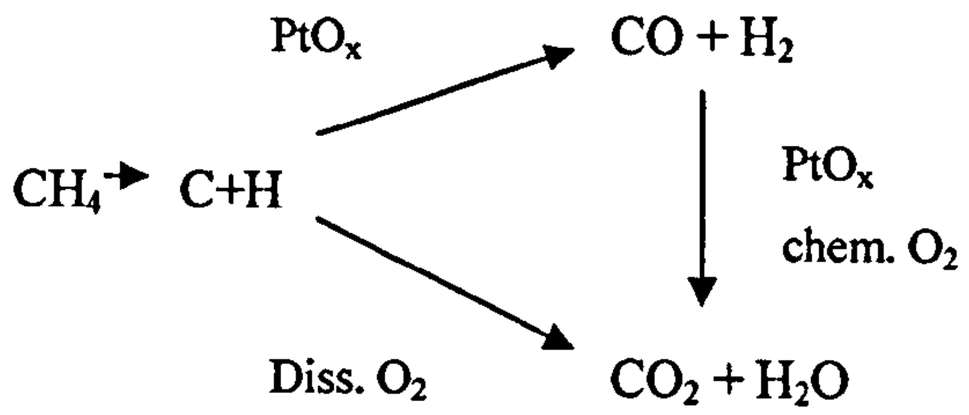

Figure 3: Reaction scheme for POM to syngas in the presence of oxygen over a Pt sponge at temperatures between 973K and 1073K.

Both Pt and PtO_x species seem to be present in platinum [51], even at temperatures as high as 1100K. It is also believed that the first layer of oxidized platinum consists of Pt atoms, although the Auger photoelectron spectrum (AES) of the oxide remained unchanged even after heating to 1300K [52]. The direct formation of CO from CH_4 occurs via oxygen present as PtO_x, which also favours recombination of H-atoms to yield H_2. In parallel to this reaction, CH_4 is directly converted to CO_2 and H_2O by participation of dissolved oxygen, which diffuses from the bulk Pt to its surface. The reaction is assumed to occur at the border between the subsurface oxygen region and the surrounding region were CO or H_2 is adsorbed. In this region the subsurface Pt phase is restructured and this process uncovers subsurface oxygen atoms, which in turn react with the chemisorbed CO or H_2. The consecutive oxidation of CO and H_2 occurs via oxygen present as Pt oxide and via chemisorbed oxygen species. In the presence of both methane and oxygen at a stoichiometric feed ratio the dominant reaction pathways are the direct formation of CO and H_2 followed by the consecutive oxidation to CO_2 and H_2O. The reaction proceeds via a redox cycle mechanism (Mars-van Krevelen) for selective oxidation reactions. The oxidation of methane is accompanied by the reduction of PtO_x, which is reoxidized by incorporation of O_2 into the catalyst.

2.3.5.2.2. Honeycomb reactors.

The most extensive use of honeycomb type catalysts is in pollution control applications such as stack gas cleanup and NO_x removal as in selective catalytic reduction (SCR) processes [53]. Honeycomb-based reactors have been proposed by Korchnak et al. [54]

for methane oxidation. In the patent by Korchnak et al. [54], the partial oxidation of methane is modulated by adding water to the feed. The reaction is performed at a temperature measured at the exit of the catalytic reaction zone which is equal to or greater than the minimum non-carbon-forming temperature.

This temperature is in the range from 1143K to 1313K, corresponding to a steam-to-carbon molar ratio (in the feed) from 0.4:1 to 0:1, and a space velocity in the range 20.000 to 500.000 h^{-1}. These reaction conditions produce essentially no free carbon deposits on the catalyst. The reactant gases are introduced to the catalyst bed at an inlet temperature not lower than 93K below the catalytic autoignition temperature of the feed mixture (typically 561-866K). Oxidant and methane are fed independently and only mixed immediately above the catalytic bed.

The catalyst comprises honeycomb structures with a surface area to volume ratio of 20 to 40 cm^2/cm^3. Noble metals supported by an alumina washcoat on cordierite extruded honeycombs of ca. 1m in diameter and 2m in length were used in catalytic combustion [12]. Based on this reactor configuration, Hochmuth [55] reported experimental results on the use of honeycombs for methane partial oxidation. The honeycombs containing 300 cells/in^2 were coated with a washcoat consisting of 1:1 weight ratio of Pd and Pt metals deposited on a CeO_2 . xAl_2O_3 powder. In general, the product distributions approached equilibrium values and the axial temperature profiles and product analysis revealed that combustion occurs just at the inlet of the honeycomb, with reforming and shift reactions occurring downstream to yield syngas.

Syngas production by the POM reaction on noble metals coated honeycomb catalysts was extensively investigated by Hickman and co-workers [30, 31].

Using air as an oxidant at atmospheric pressure and residence times between 0.1 and 10ms, they approached adiabatic operation. The Rh coated honeycomb catalyst was superior to its Pt counterpart. Hydrogen selectivities above 90% and CO selectivities in the order of 95% at CH_4 conversions somewhat above 90% were found on the Rh catalyst using O_2 as an oxidant. These authors used extruded honeycombs, noble metal coated ceramic foam and Pt-Rh alloy gauzes and studied the influence of reactor variables on syngas production. The results of this investigation revealed that the selectivity is enhanced by higher temperatures and by maintaining high rates of mass transfer through the boundary layer at the catalyst surface.

It was observed that the three types of catalysts (Pt, Rh and Pt-Rh alloy) give essentially the same CH_4 conversion and selectivities, however, these change to a significant extent when changing honeycomb geometry and thermal conductivity. It appears that the POM reaction on honeycomb-type reactors is governed by a combination of transport and kinetic effects. Thus, the diffusion of the reactants to the catalyst surface is a function of flow velocity and catalyst geometry, whereas the reaction kinetics depends on the honeycomb-wall temperature and on the nature of the catalytic function.

Perhaps the most striking observation in the above studies is the increase in both CH_4 conversion and CO and H_2 selectivities with decreasing contact time, which contrasts with earlier findings of Dissanayake et al. [41] and Ashcroft et al. [37]. In order to explain these data, Hickman et al. [31] suggested that the reaction mechanism involves direct formation of H_2 initiated by methane pyrolysis on the surface to form surface H and C species. Surface H species recombine to form H_2, while surface C reacts with oxygen to form CO. CO_2 would be formed at the surface by the CO + O reaction, while any OH forming reactions would give H_2O, as occurs on Pt honeycomb catalysts. In addition, they observed that the reaction occurs in the first few millimetres at the inlet of the honeycomb with complete O_2 conversion to give H_2 and CO, as opposed to the sequential mechanism of total oxidation followed by reforming.

Tomiainen et al. [56] also investigated the POM reaction on several group VIII metal coated honeycombs. Rh and Ni exhibited the best behaviour, although Ni was deactivated by aluminate formation. Pt and Ir were very stable, but somewhat less active and selective. Pd and Co deactivated rapidly and Ru and Fe were inactive. According to these results, it appears that Rh and Ni coated honeycombs are the most suitable systems for syngas production via POM reaction; however, coking on the Ni catalyst can be minimized by adding steam into the feed, although the process would not be conducted under adiabatic conditions. Gomez et al. [57] have reported studies disclosing the use of nickel honeycomb catalysts in the partial oxidation of methane (POM) to syngas at high pressure, at temperatures above 973K and with CH_4/O_2 molar ratios of 2 in the feed. It has been observed that both CH_4 conversion and CO and H_2 selectivities approach that predicted by thermodynamic equilibrium. Moreover, activity and stability during on-stream processing depend markedly on the method of nickel incorporation and on the nature of the phases present at catalyst surfaces, which in turn control the formation of metallic Ni, the active species in POM reaction. The CH_4 conversion

decreases slightly at times below 0.5h and is then stable. Upon increasing the temperature up to 1023K, the drop in activity is clearer and the catalyst becomes deactivated at 1073K. Selectivity to H_2 follows almost the same trend as conversion; however, CO selectivity was found to increase with time both at 973K or 1023K, although it decays drastically at higher temperatures (1073K). As important amounts of carbon were formed on the surface of deactivated catalyst, it appears that Ni sites became blocked by carbon deposits during on-stream operation.

2.3.5.2.3. Fluidized bed reactors.

Fluidized bed reactors for syngas production via direct oxidation of methane appear to be an interesting option which affords inherent advantages with respect to the conventional fixed bed catalyst configurations. As the partial oxidation reactions are highly exothermic, extreme safe precautions and careful control must be taken to avoid CH_4/O_2 compositions inside explosive limits. In fluidized bed reactors not only is the heat transfer good because of backmixing (ensuring uniform longitudinal and radial temperature profiles), but also the pressure drop is substantially lower than for a fixed bed of the same diameter and length for the same space velocity. These potential advantages have been investigated recently by British Petroleum (BP) researchers [58, 59], who developed a process for synthesis gas generation using spouted bed reactors, both non-catalytic and catalytic.

The patent for the non-catalytic process [58] describes the use of a bed of inert solids and refractory material through which a rich CH_4/O_2 mixture is passed with upward flow rate sufficient to cause a spouting action of the inert materials. This configuration also offers the option to inject steam into the bed along with the reactants and/or into the effluent gas as a quench agent. The quenching reduces the temperature of the product gases and hence minimizes further reaction to less useful gases and soot, particularly at pressures above 1bar. In order to maintain a stable flame on the spouted bed, a burner was also assembled at the outlet of the reactor. Quite different inert materials such as α-Al_2O_3, ZrO_2 and firebrick were used. Thus, in a typical experiment using α-Al_2O_3 beads to pack the reactor by feeding a CH_4/O_2 ratio of 1.78 and gas hourly space velocity (GHSV) of 26400 h^{-1}, CH_4 conversion of 68% was obtained with 56.7% selectivity to CO. Moderate proportions (26.5%) of C_{2+} hydrocarbons, mainly ethylene and acetylene, and

minor amounts (3%) of soot were also found. As these figures seem very high, they could make the process inapplicable.

The use of catalytic material is described in the second patent [59]. The catalyst employed for this purpose is very versatile as it can be used for both partial oxidation and steam reforming reactions. Basically, group VIII metals, optionally containing alkali promoters, on suitable carriers were employed. With a Pt catalyst a 87% CH_4 conversion with CO selectivity as high as 94.3% could be achieved. Similarly, working with a conventional steam reforming catalyst at 1050 K and a CH_4/O_2 ratio of 1.62, a CH_4 conversion of 91.2% with CO selectivity of 90.4% was observed. Using the same spouted bed reactor configuration, the performance of the catalysts under high pressure conditions was also investigated. In principle, no significant loss in CO selectivity was found under high pressure operation. Thus, at 25bar, CH_4 conversion in excess of 90% and CO selectivity greater than 88% could be reached with a steam reforming catalyst working at 1270K with CH_4/O_2 ratio of 1.7.

Within the framework of fluidized bed reactors, Sie [60] has developed a POM process in which catalyst particles are transferred by means of a gas stream to the burner device in such a way that the catalyst is already present during the intensive mixing of the reactants at the bottom of the reactor. The catalyst particles are moved up through the reactor and finally are separated from the product gas and recycled.

Recent work on the production of syngas by the catalytic partial oxidation of CH_4 in air or O_2 in fluidized beds working at nearly atmospheric pressure has been examined by Bharadwaj and Schmidt [61]. The catalysts used for this purpose consisted of 0.1mm α-Al_2O_3 beads coated with Pt, Rh and Ni metals.

With CH_4/air feeds, they found CH_4 conversions in excess of 90% and CO and H_2 selectivities as high as 95% on Rh and Ni catalysts. However, Pt catalysts exhibited significantly lower conversions and selectivities, probably because of more water forming reactions or the slow steam reforming behaviour of Pt.

Significant improvement of the optimal selectivities for the three catalysts was obtained by preheating the reaction mixture above the autothermal reaction temperature and also by using O_2 instead of air. Moreover, they investigated the influence of steam in the feed. With increasing steam in the feed, an increase in CH_4 conversion with the subsequent

decrease in CO selectivity was found indicating an approach to the water-gas shift equilibrium.

Similar reaction pathways to those in fixed beds can be envisaged for CH_4 oxidation in a fluidized bed, namely direct oxidation to CO and H_2 and total oxidation followed by steam reforming. In fluidized beds, longer contact times compared to honeycombs may yield more reforming while increasing backmixing may form more H_2O at the beginning.

2.3.5.2.4. Membrane reactors

Despite the impressive results achieved in partial oxidation, a major difficulty still exists. For autothermal behaviour to be attained a low methane/oxygen ratio mixture must be fed to the reactor. When such a mixture contacts a high temperature surface, the potential for an explosion exists.

Alibrando et al. [62] designed a fixed bed membrane reactor which allowed a low methane/oxygen ratio mixture to be fed at high flow rates while separating the methane and oxygen feeds. The reactor consisted of a porous permeable ceramic membrane tube placed concentrically inside a quartz reactor. The catalyst was prepared by the wet impregnation technique and placed on the bottom of the membrane tube were the permeation occurred. Methane was fed to the reactor on the shell side and oxygen was fed to the tube side. The permeate length was surrounded by catalyst on the outside of the tube allowing oxygen and methane to be mixed only over the catalyst surface. They concluded that the catalytic partial oxidation of methane on Rh/TiO_2 catalyst occurred at high conversions and selectivities under fast flow conditions when a membrane is used to separate the feeds. The Rh/TiO_2 catalyst exhibited a low ignition temperature and no deactivation during the experiments.

Wang et al. [63] developed a packed bed reactor using perovskite-type oxide as oxygen-permeable and $LiLaNiO/\gamma\text{-}Al_2O_3$ as catalyst with 10wt% nickel loading for ethane partial oxidation. They concluded that the tubular membrane reactor can operate steadily for 100h at 1150K obtaining 100% ethane conversion and CO selectivity higher than 91%.

Another tubular perovskite-type membrane reactor packed with Ni/Al_2O_3 catalyst was developed by Jin et al. [64] for the partial oxidation of methane to syngas. The $La_{0.6}Sr_{0.4}Co_{0.2}Fe_{0.8}O_{3-\delta}$ membrane reactor presented 97% CO selectivity and CH_4 conversion larger than 96% at low carbon space velocity.

Lafarga et al. [35] and Coronas et al. [65] developed a new reactor concept that provides low oxygen concentrations in the reactor in order to increase hydrocarbon selectivity. The porous ceramic membrane reactor was used for methane oxidative coupling. The commercial alumina microfiltration membranes were modified with silica to reduce the oxygen flow. The addiction of lithium and subsequent calcinations have an important influence on the pore structure and flow characteristics of the membrane, improving its use as oxygen distributors.

2.3.5.3. POM process considerations.

The most efficient process is one in which the operation conditions such as temperature, pressure, space velocity and CH_4/O_2 molar ratio in the feed are integrated with a catalyst exhibiting high activity, selectivity and on-stream lifetime [66]. A number of aspects with respect to process conditions are summarized below.

2.3.5.3.1. Temperature. If the process works close to thermodynamic equilibrium, depending on the pressure, temperatures in excess of 1020K at 1bar and 1270K at 30 bar can be used to achieve conversions ca. 90% for the POM reaction, with no steam added to the feed. The use of high temperatures, typically above 1270K, will invalidate the advantage of materials used by a lower temperature process, i.e., special refractory and alloy materials will have to be used, which will add to investment costs. Incorporation of steam to the feed improves methane conversion and decreases temperature for a required conversion level.

Thus, at 30bar the temperature required for 90% conversion can be lowered to ca. 1220K if a H_2O/CH_4 ratio of 3.0 is used [26, 67].

2.3.5.3.2. Pressure. As most downstream processes operate under pressure, it is essential that at least some compression be performed before reaction. For instance, for the methanol synthesis the power requirement for the total process can be almost halved by increasing the pressure of the partial oxidation from 10 to 80 bar [67]. Moreover, this also precludes the use of air as an oxidant due to the large increase in compression requirements caused by the presence of nitrogen.

2.3.5.3.3. Space velocity. High space velocities facilitate good mixing and minimize mass transfer effects [30, 31]. The majority of processes use high GHSV, with values of over 100,000 h^{-1}. This makes the use of fixed bed reactors difficult as large pressure

drops will be generated across the catalyst bed. To overcome this problem, honeycomb-supported catalysts [54, 55, 60] and fluidized or spouted-bed reactors [26, 59, 67] have been used. Fluidized bed reactors have the advantage of uniform mixing, but can suffer from problems involving catalyst entrainment. An example of this is the Exxon process, which uses a fluidized-bed reactor and utilizes a Ni catalyst [26]. In this case, the syngas products have to be cooled at the outlet of catalyst bed to stop the formation of methane by any entrained Ni catalyst. On the contrary, honeycomb catalysts can accommodate high flow rates, but may still give rise to hot spots.

Finally, Shell has patented a method of contacting catalyst and gas feed via an entrained bed reactor [60]. In this process, finely divided Pt/α-Al_2O_3 or Pt-Pd/α-Al_2O_3 catalyst particles are transported into the reaction zone with the methane, where they are mixed with the other reactants under intensive mixing conditions. The catalyst is subsequently entrained in the product gases, then it is separated via cyclones and recycled. However, Ni-containing catalysts, which catalyse the reverse methanation reaction, will be unsuitable for this process, unless a rapid quench, similar to that described for the Exxon fluidized-bed process [26], is used.

2.3.5.3.4. Feed composition. For stoichiometric syngas (H_2/CO = 2) a CH_4/O_2 ratio of 2 is needed. Increasing the oxygen content of the feed gas alters catalyst performance. There is an increase in conversion, e.g., at 1 bar and thermodynamic equilibrium, the temperature for 90% conversion is 1053K with CH_4/O_2 = 2, whereas it is 973K with CH_4/O_2 = 1.54. A concomitant drop in CO selectivity, as a result of CO_2 formation, is observed. Moreover, increasing the CH_4/O_2 ratio above 2 results in lower methane conversion and carbon deposition. Introducing a premixed feed with CH_4/O_2 ratio of 2 at high pressure, a very rapid transfer of the gas mixture to the catalytic zone is required if the flashback and the occurrence of gas-phase reactions are to be minimized [12]. To avoid this, there are several options:

i) introduction of steam into the feed;

ii) staging the introduction of oxygen;

iii) introducing oxygen and methane separately;

iv) novel reactor design.

Institut Francais du Petrole (IFP) has developed a process which uses a series of adiabatic reactor beds containing Ni/Al_2O_3 catalysts [68]. Oxygen is fed separately so that the gas mixture entering each bed is below the explosive limit.

However, the products formed in each bed will be exposed to oxygen, favouring combustion reactions. A variation of this consists of two fixed-bed reactors in series, where the methane feed is divided into two streams. One stream is fed with oxygen to the first reactor where essentially combustion takes place. The product stream from the first reactor, is then mixed with the second methane stream and fed to the second reactor where reforming to the final syngas product takes place.

The introduction of steam into the feed not only enhances methane conversion but also lowers the oxygen partial pressure and hence decreases explosion risks. When catalysts are prone to carbide formation, e.g. Ni, the steam cofeed limits the formation of carbon on the surface. Korchnak and Dunster [54] determined the CH_4/O_2 and CH_4/H_2O ratios for which carbon is formed. Thus, at 1223K with a feed CH_4/O_2 of 2 the minimum CH_4/H_2O ratio is also 2. As the steam added also contributes to the SMR reaction, the degree of SMR relative to POM will vary depending on the catalyst used and the amount of steam added. An excess of steam into the feed also facilitates the WGS reaction, which results in decreased CO selectivity and an H_2/CO ratio greater than 2.

Other methods involve separate introduction of oxygen into the reaction zone.

Exxon developed a fluidized-bed system in which the CH_4/H_2O is fed to the bottom of the reactor and oxygen is fed into the middle of the fluidized bed [26].

Accordingly, SMR occurs at the base of the fluidized-bed, with the POM occurring in its upper region. In this catalytic system, where high GHSV result in large heat release rate, and where the stoichiometric feed composition is near the explosion limit, particularly under pressure, it is unlikely that conventional fixed-bed reactor technology will be suitable. A logical extension would be the use of membrane reactors which could facilitate differential addition of oxygen to the methane feed, thus avoiding hot spots and explosion risk.

Thus, to summarize the process conditions:

i) methane conversions and CO and H_2 selectivities indicate that the reactors operate at thermodynamic equilibrium;

ii) most of the processes operate at temperatures and pressures above 1100K and 20 bar, respectively;

iii) the most common reactors used are fluidized bed and the use of fixed-bed reactors appears essentially limited to their use with honeycomb catalysts;

iv) in most cases steam is cofed with methane and the oxygen is then mixed with this stream just prior to, or in, the reaction bed;

v) catalysts consist mainly of Pt, Pd, Rh, Ni or combinations thereof supported on an alumina substrate;

vi) the oxidant is pure or enriched oxygen, but not air.

2.4. MEMBRANE TECHNOLOGY

In the common membrane processes, separation of chemical components is the main objective and is in a stage of rapid growth and innovation [69]. In catalytic membrane reactors (CMR), however, the membrane process is combined with a catalysed chemical conversion. The actual task of the membrane in a CMR depends on the process, and may, for example, be to separate the reaction products or feed streams, or to control the mixing of reactants, as well being a catalyst for the chemical reaction [70].

2.4.1. MEMBRANE TYPES

Membranes are often divided into different types and classes. Distinctions are usually made between polymeric and inorganic membranes, dense membranes and porous membranes, composite and homogeneous membranes, and symmetric and asymmetric membrane configurations. The resistance to mass transport is usually proportional to the thickness, and the membrane is therefore made as thin as possible. A common membrane configuration is therefore a thin membrane layer on a mechanically strong support. This membrane configuration is called composite. The membrane material may differ from the support material, and such a configuration is called an asymmetric composite membrane configuration. Conversely, both dense and porous membranes

can be made of inorganic and organic materials. Liquid membranes supported in porous structure are special types of dense membranes.

The membrane operating conditions, - high or low temperature, harsh or mild conditions, etc., - and the requirements of membrane performance, as selectivity, flux, mechanical strength, etc., determine the necessary chemical and physical proprieties of the membrane. In low temperature membrane applications both polymeric and inorganic membranes are possible candidates. For such applications membrane cost versus lifetime considerations are often decisive. For high temperature applications (above approximately 425-475K) inorganic membranes are the only choice available.

2.4.2. CLASSIFICATION OF CATALYTIC MEMBRANE REACTORS

In a membrane reactor two processes, membrane operation and catalytic conversion, are combined in the same unit. These processes can be combined in different ways depending on the application. If the membrane is permselective and the sole catalyst for the reaction, the configuration is called a catalytic membrane reactor (CMR). If, however, the membrane is not permselective, but acts as the sole catalyst for the reaction, it is called a catalytic nonpermeselective membrane reactor (CNMR). If the membrane is catalytic and permselective, and a packed or fluidised bed of catalyst also exist inside or outside the membrane, these configurations are called packed-bed (PBCMR) or fluidised-bed (FBCMR) catalytic membrane reactors. Alternatively, if the membrane is permselective, but not catalytic, the configurations are called packed-bed (PBMR) or fluidised-bed (FBMR) membrane reactors, respectively. If the membrane material is not catalytic, one may apply a catalyst in the pores or on the membrane surface. In this case the membrane is regarded as catalytic with respect to the configurations described above [70].

Inorganic membranes are the most frequently used in catalytic membrane reactors. The membrane configuration is usually asymmetric, i.e. a thin selective membrane layer is supported on a porous substrate of different material determining the mechanical strength. The membrane shape can be tubular, (tubes or monolithic multichanel units), or flat (disks and plates) [70].

Porous membranes are often divided into classes of macroporous (pore diameter, $d > 50$ nm), mesoporous (2 nm $< d < 50$ nm) and microporous ($d < 2$nm) [71]. Existing

commercial inorganic membranes mainly cover the macro and mesoporous types. These membranes are typically made from binary metal oxides such as TiO_2, ZrO_2, Al_2O_3, also from glass, C, SiC, and some metal types. Commercial microporous membranes of SiO_2 and zeolite membranes are available only for small-scale applications from a few companies [70].

In high temperature applications, the macroporous membranes have no ability to separate gases due to only laminar flow in pores in this size range. Possible uses of macroporous membranes in gas treatment are therefore limited to non-separative membrane operations. The mesoporous and microporous membranes with pores less than 5-20 nm may separate gases by various mechanisms. The possible utilisation of porous membranes in gas separation and CMRs is a strong driving force for the present large effort to develop membranes with smaller pores [70].

2.4.3. MEMBRANE PREPARATION

Several routes can be used to modify mesoporous and prepare microporous membranes. Some examples are: sol-gel deposition method, thin-film deposition, controlled pyrolysis of polymeric fibres or repeated impregnation are used to prepare microporous membranes [70].

2.4.3.1. Sol-gel deposition method

The sol-gel can be divided into two main routes: the colloidal suspension route and the polymeric gel route. In both cases, a precursor is hydrolysed while a condensation or polymerisation reaction occurs simultaneously. The precursor is either an inorganic salt or a metal organic compound.

In the colloidal route, a faster hydrolysis rate is obtained by using a water excess. A precipitate of gelatinous hydroxide (or oxohydroxide) particles is formed and then peptized to give a stable colloidal suspension. By different processes, this suspension is transformed in a gel structure consisting of a network of particles or agglomerate chains.

In the polymeric gel route, the hydrolysis is kept low by using a lack of water. The final stage of the process is a strongly interlinked gel network.

The final structure obtained in both ways is totally different [72].

2.4.3.2. Thin-film deposition

Various techniques are available to produce thin films on a substrate. Some of these techniques are also applicable to the preparation of inorganic membranes. Chemical vapour deposition, plasma deposition, sputtering, dip-coating technique, ion plating, and metal plating can be used to coat a porous support in ways to control the pore size. Deposition of various materials can be used to reduce the pore size of the support and to modify the surface characteristics of the support. As examples, one side of a porous polycarbonate membrane was coated with a thin layer of titania by sputtering; and $SiCl_4$ in the gas phase was introduced into a flame to form fine SiO_2 particles which were deposited on a target to give a porous glass membrane. Porous silicon nitride has been coated with alumina by chemical vapour deposition. Thin metal films of gold and palladium have been formed by plasma deposition.

2.4.3.3. Pyrolysis

Here, polymers are coated onto porous supports, and then degraded by controlled pyrolysis to produce a membrane. Silica membranes can be produced from silicone rubber, while carbon membranes can be produced from thermosetting polymers such as polyacrylonitrile.

This technique is also used to produce commercial porous composite membranes. The support is formed by the pyrolysis of an appropriate polymer tube in a controlled environment. One or two layers are added to the support. For medium size pores, an organic solution of phenolic resins is deposited on the support, followed by controlled pyrolysis. To produce smaller pores, a film is produced by in-situ polymerisation, followed by stepped pyrolysis. Surface properties, pore sizes, and morphology are controlled by additives and the degree and type of pyrolysis. Film thickness is 100 to 1000 nm with a porosity of 65 to 75%. Pore sizes of these membrane ranges from 4 to 1000 nm.

2.4.4. APPLICATION OF CATALYTIC MEMBRANE REACTORS

In general, membranes are used in three different modes of operation in catalytic membrane reactors:

1) The membrane is selective with respect to one of the components in the process, and this component is removed from the reaction zone through the membrane during the process.

2) A reactant is fed through the membrane in a controlled manner to the reaction zone in the reactor.

3) The membrane acts as a catalyst nonpermeselective medium where a controlled chemical reaction takes place within its pores.

2.4.4.1. Equilibrium-limited reactions

The first mode of operation has been exploited to increase conversion in equilibrium-limited reactions. In reversible reactions such as:

$$A \leftrightarrow B + C \qquad (12)$$

where the conversion is thermodynamically limited, a membrane permselective to B or C can increase the conversion of A by selective removal of products from the reaction zone. Typical examples are dehydrogenation reactions, where hydrogen selective membranes are used to remove hydrogen from the reaction zone. Another benefit normally obtained in such membrane reactors is a shift to lower operation temperatures, i.e. the same or even higher conversions can be obtained at lower working temperatures.

2.4.4.2. Controlled feeding of reactant through the membrane

In many chemical reactions, the desired product is an intermediate product in a sequence of possible reactions. For instance, in oxidative reactions of hydrocarbons further oxidation of valuable products to CO_2 and water must be hindered. Another example is hydrogenation reactions, where control of unsaturated bound is desirable [70].

Generally, the idea of using a membrane to feed a reactant is to better control the reaction so that selectivity is enhanced. This can be achieved by controlling the operation conditions so that the local concentration of the fed reactant, e.g. oxygen can be produced continuously from air through an oxygen selective membrane. Some other possible advantages of this membrane reactor concept are:

There is no need for subsequent separation of unreacted reactant (the reactant which is fed through the membrane) and it can therefore be recirculated in a continuous mode.

The reaction rate can be controlled by adjusting the permeation rate. This can, for instance, be important in strongly exothermic or endothermic reactions.

Impure reactants may be used if the membrane is selective. For instance, impure hydrogen from a refinery could be used to feed hydrogen through a Pd-based membrane instead of more expensive high purity hydrogen [70].

2.4.4.3. Nonpermeselective catalytic membrane for chemical conversion and reaction control

In so-called catalytic membrane contactors the membrane provides a restricted well-defined structure/body that facilitates contact between reactants and catalyst. The catalytic membrane usually generates an interface between two separate feed streams (reactants) which can be gas-gas, gas-liquid or liquid-liquid.

Gas-gas catalytic membrane contactors have been studied in the destruction of H_2S and NO_x [73]. The idea is that the reactants enter the nonpermeselective membrane from opposite sides, and diffuse into the membrane where they meet and react. If the reaction occurs instantaneously and irreversibly, a sharp reaction zone is formed in the membrane at the position of stoichiometric ratio of reactants. If a change in the feed concentration occurs, the diffusion profiles of the reactants into the membrane are also changed. The effect is to move the reaction zone inside the membrane to a position where the flow of reactants gives the stoichiometric ratio. A change in concentration of reactants is therefore compensated by a self-regulating displacement of the reaction zone inside the membrane. This concept may therefore be used to reduce problems of slip related to dangerous reactants in applications where variations in their concentrations may occur [70].

It should also be emphasised that these types of CMRs have the advantage of separated feed streams thereby restricting other possible unwanted side reactions in mixtures of the feed streams.

2.4.5. MEMBRANE TECHNOLOGY IN SYNGAS PRODUCTION

The primary advantage of utilising the membrane reactor configuration is that it provides a safer reaction environment, and this allows operations at conditions that could be hazardous in a traditional fixed bed reactor. In the membrane reactor, it is possible to lower the methane/oxygen feed ratios without the potential for an explosion. It is also possible to operate at both high and low contact times.

Preliminary cost estimates indicate that ceramic membrane reactors could decrease the capital cost for syngas by more than one third. This reduction would have a very significant impact on the costs of liquid transportation fuels derived from natural gas [74].

This fact definitely provides a substantial incentive for developing an alternative strategy for syngas production using membranes.

One of the emerging membrane technologies is the ion transport membrane. For either, partial oxidation or auto-thermal reforming, the cryogenic oxygen plant may be replaced by a high temperature membrane that can separate oxygen from air and supply it directly into the reactor for converting CH_4 to $CO+H_2$. The extremely low partial pressure of oxygen in the reaction zone of an autothermal reformer (mole fraction of the order of 10^{-16} – 10^{-18}) creates a large driving force for oxygen separation in oxygen ion conducting membranes. Using such membranes, only compression work need to overcome the friction losses in the system would be required [75].

Some limitations concerning the oxygen selective mixed conducting materials are worth mentioning. The thermodynamic stability of these materials is not yet fully documented. The very reduced conditions in the syngas reactor may be a problem, particularly since the material contains a significant amount of $Sr_4Fe_6O_{13}$ type phase [70]. A surface limited reaction on the syngas side could help the situation due to a reduction of the oxygen gradient in the material, however such a system will depend on sufficient oxygen supply. Any phase change, e.g. between the perovskite ($SrFe_{1-x}Co_xO_{3-y}$) and $Sr_4Fe_6O_{13}$ due to variations in temperature or oxygen pressure, or demixing or segregation of components during operation, could lead to internal stress and crack formation. Another problem occasionally observed in perovskites is internal stress generation due to variations in molar volume across the membrane during operation in an oxygen potential gradient.

However, at lower temperatures an equilibrium shift towards the product gases could be obtained with H_2 selective membranes which continuously remove the hydrogen formed in the reaction [76]. The reversible nature of these reactions imposes a limit, determined by thermodynamic equilibrium, on the conversion and yields of CO and H_2 that is well below commercially acceptable levels, unless the reaction temperature is very high (>1000K). However, if H_2 is selectively and continuously removed from the reaction zone the equilibrium limitations of a conventional reactor can be circumvented. Alternatively, this offers the possibility of obtaining a given level of conversion at a much lower operating temperature than that realised in a conventional reactor [77].

A heat balance can be obtained between available waste heat from the reformer process and heat required for process steam generation and feed preheating. In current steam reforming processes excess steam is produced, which has to be either exported or used for power generation. Although a lower reformer temperature seems to be economically more attractive, operating problems associated with carbon formation may well occur and have to be carefully investigated. Hydrogen suppresses carbon formation and the much lower hydrogen content in reformer retentate streams may increase the risk of carbon formation [75].

Lower temperatures would allow the use of considerably cheaper tubing materials. Furthermore, the reformer size can be substantially reduced due to the lower reformer duty and the lower reforming temperature enabling the use of more compact reformers of the heat exchanger type. A decrease in reformer duty, which can be as high as 30-35%, can result in lower fuel gas consumption [75].

Another attractive application of membrane technology in GTL processes is for a Fischer-Tropsch reaction that does not require air separation. It can be improved by using the membrane as catalyst support, which increases the catalyst dispersion, resulting in higher conversion of the separated feeds, which are activated prior to their contact inside the reactor. This results in many cases of 100% oxygen conversion.

3. EXPERIMENTAL WORK

3.1. APPARATUS:

The experimental rig consisted of three sections: feed delivery system, reaction system and analytical system.

The schematic diagram of the feed, reactor and analytical section of the apparatus is shown in figure 4. Mass-flow-controllers were used to meter and control the gases flow rates. The oxygen (and nitrogen for air tests) flow, were led to a stainless steel mixing chamber before entering into the reactor. The methane flow was led directly into the reactor, except for experimental reactions involving carbon dioxide in the feed in which case the pure methane feed was disconnected from the reactor and connected in a secondary rig. In the secondary rig, methane and carbon dioxide were led to a stainless steel mixing chamber and into the reactor.

The product streams from the reactor system were led through a water trap before being analysed by gas chromatography. A pictorial view of the entire experimental rig is shown in Figure 5.

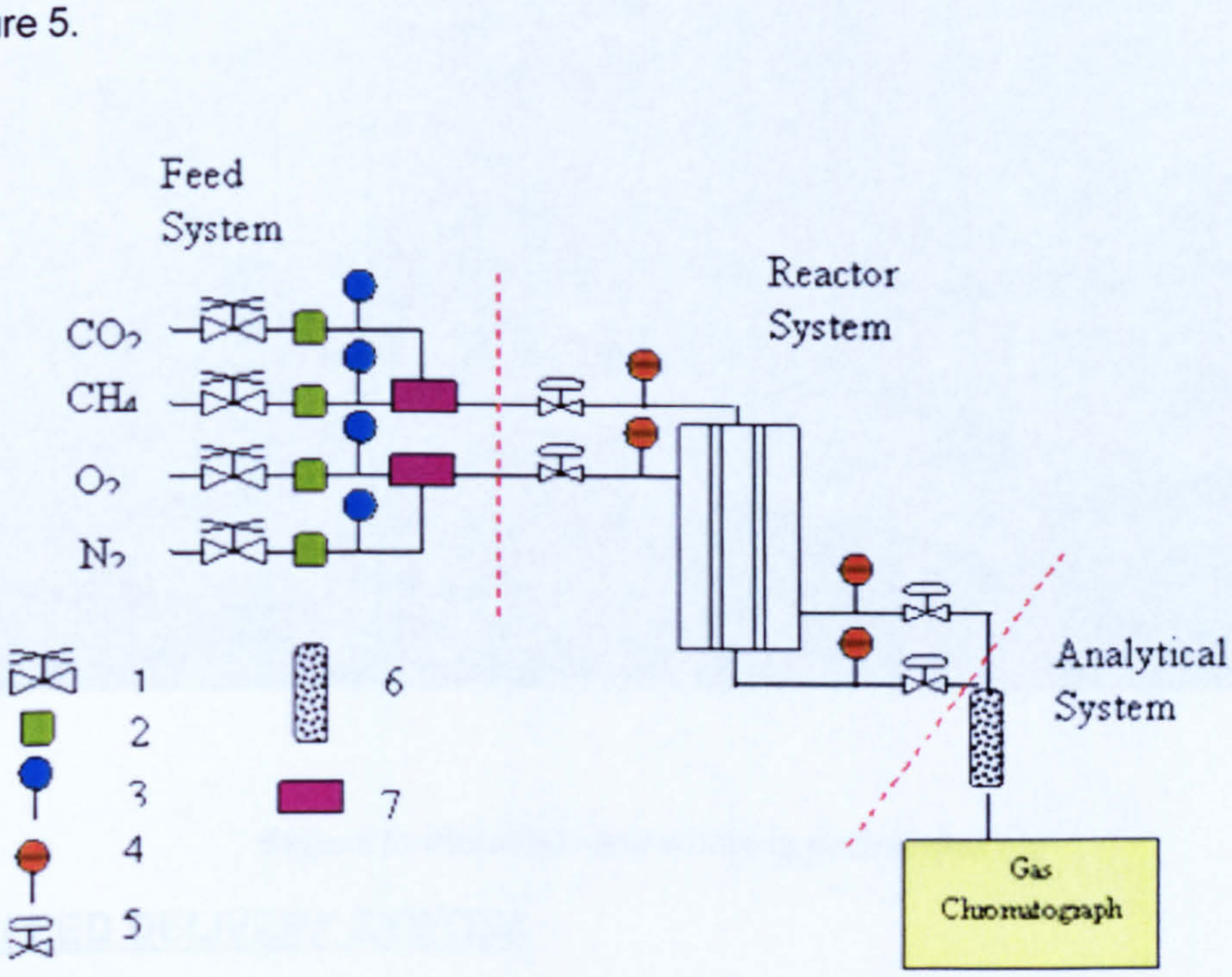

Figure 4: Schematic diagram of the feed, reactor and analytical sections

Where:

1 – On/off valve

2 – Non-return check valve

3 – Mass flow controller

4 – Pressure gauge

5 – Needle valve

6 – Water trap

7 – Mixing chamber

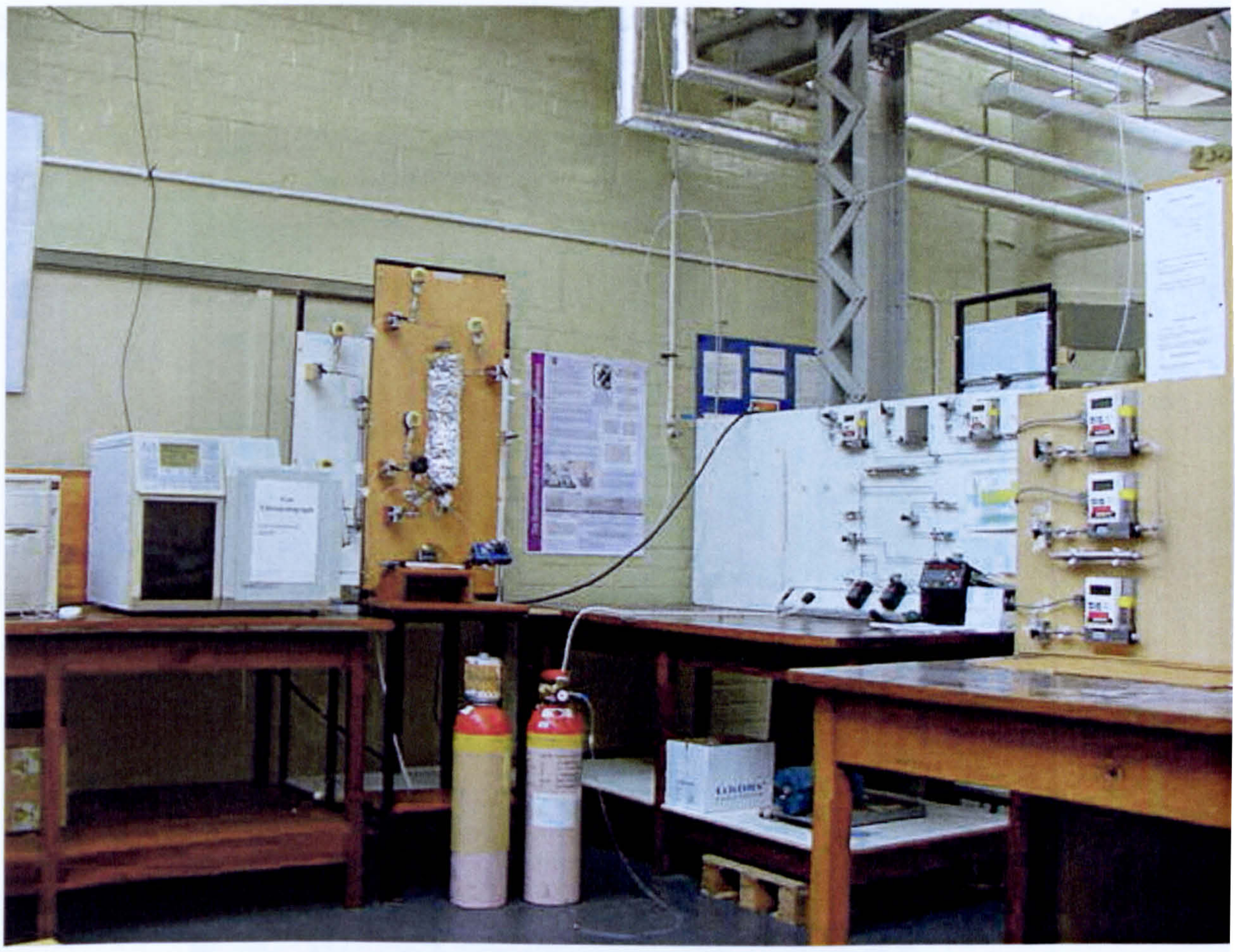

Figure 5: Pictorial view of the experimental rig

3.1.1. FEED DELIVERY SYSTEM

The feed system comprises of gas cylinders, containing pure oxygen, nitrogen, carbon dioxide and methane. Each cylinder was provided with a pressure regulator. The back-

up pressures were kept constant and monitored by the mentioned pressure regulators. Separate on/off valves ((1) – Figure 6 and 7) situated just before non-return check valves ((2) – Figure 6 and 7), controlled the gas flows to the mass flow controllers ((3) – Figures 6 and 7). The feed flow rates were set using the digital mass flow controllers 810 series Mass-Trak from Sierra instruments, Inc ((3) – Figure 6 and 7). Variation on the feed ratio were also controlled by the mass flow controllers. The feed system is shown in figures 6 and 7. Figure 6 shows the feed system for tests with methane/oxygen and methane/air as feed. The secondary rig (figure 7) was used for tests using carbon dioxide in the feed stream. The experimental procedure is explained in more detail at the end of this section.

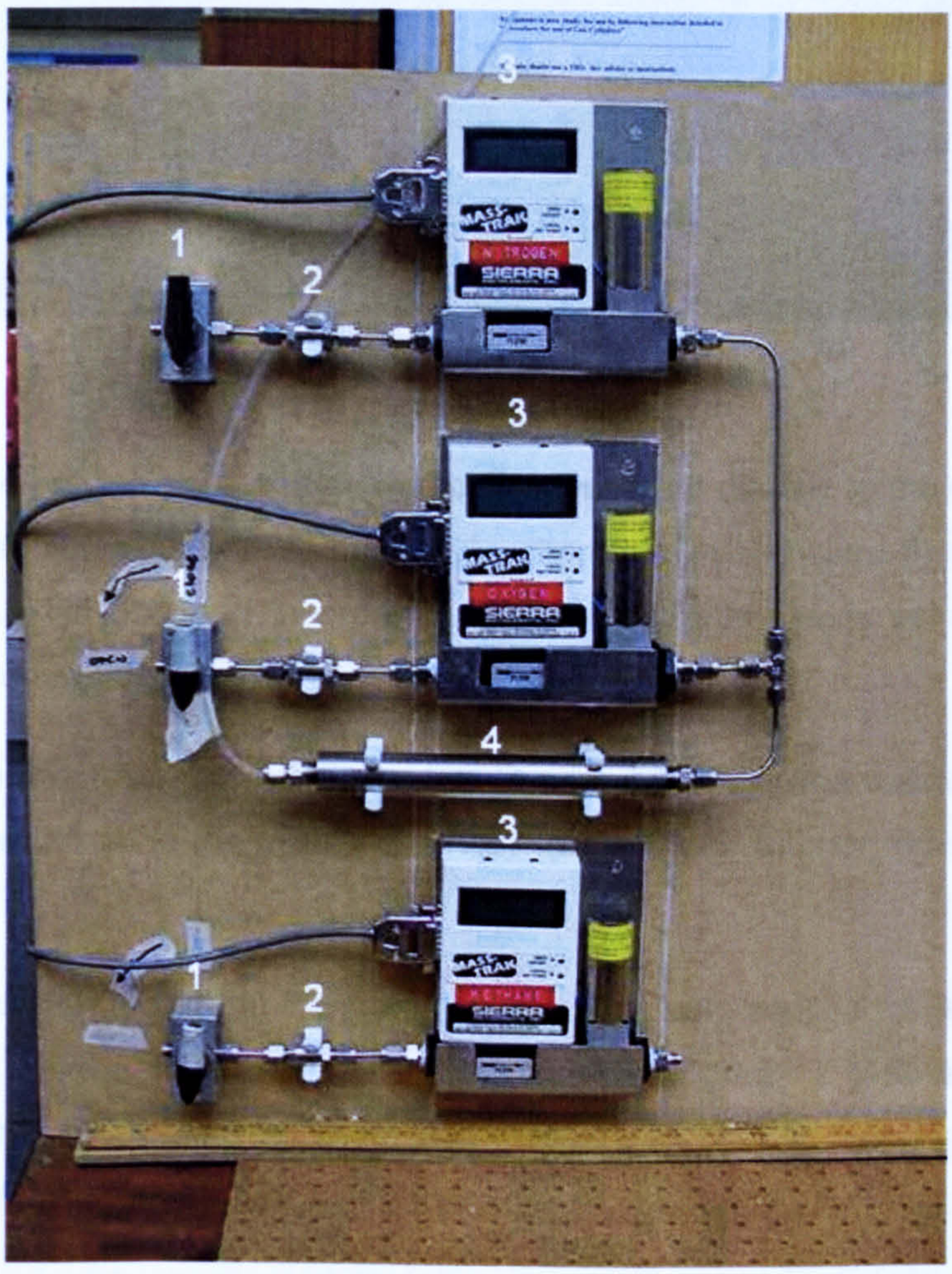

Figure 6: Feed mass flow control system

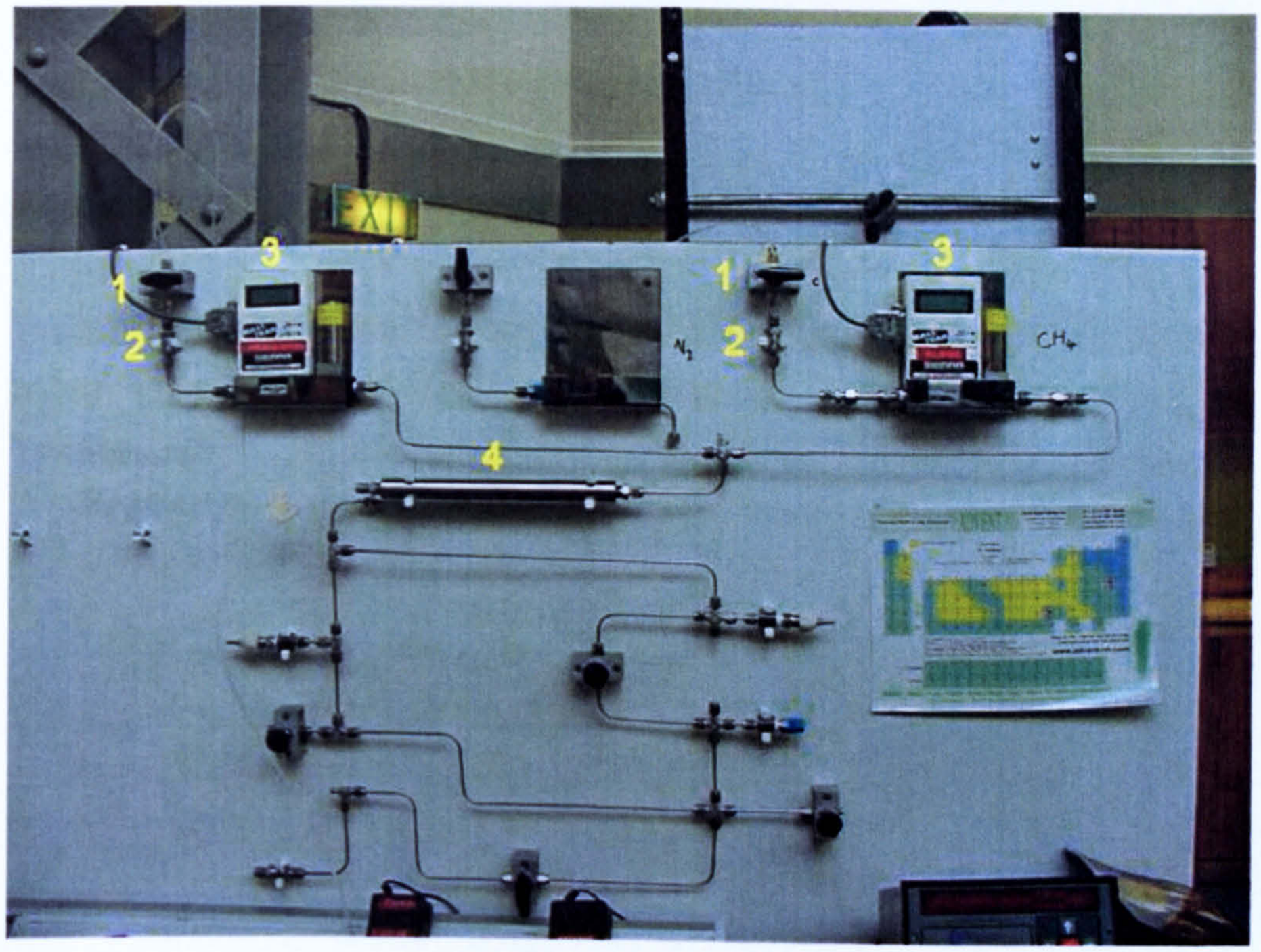

Figure 7: Secondary feed system

For the methane/oxygen tests, the methane flow was sent directly to the reactor system, while the oxygen flow was sent to the mixing chamber ((4) – Figure 6) and then to the reactor system. This occurred in order to proceed to further tests using a mixture of oxygen and nitrogen (air).

For the methane/air tests, methane was again sent directly to the reactor and nitrogen and oxygen were mixed in the mixing chamber ((4) – Figure 6) prior to being sent to the reactor system.

For tests with carbon dioxide in the feed, pure oxygen was sent to the shell side of the membrane in a similar rig but set for carbon dioxide (Figure 7). Methane and carbon dioxide were sent to a mixing chamber ((4) – Figure 7) prior to being sent to the tube side of the reactor in a similar fashion to the air experiments.

All connectors were made of stainless steel and so were the connecting lines for the mass-flow-controller. From the feed system to the reactor system, PFA (perfluoroalkoxy) tubing was used due to its heat resistance, as connecting lines as shown in the schematic diagram of the feed system (Figure 8).

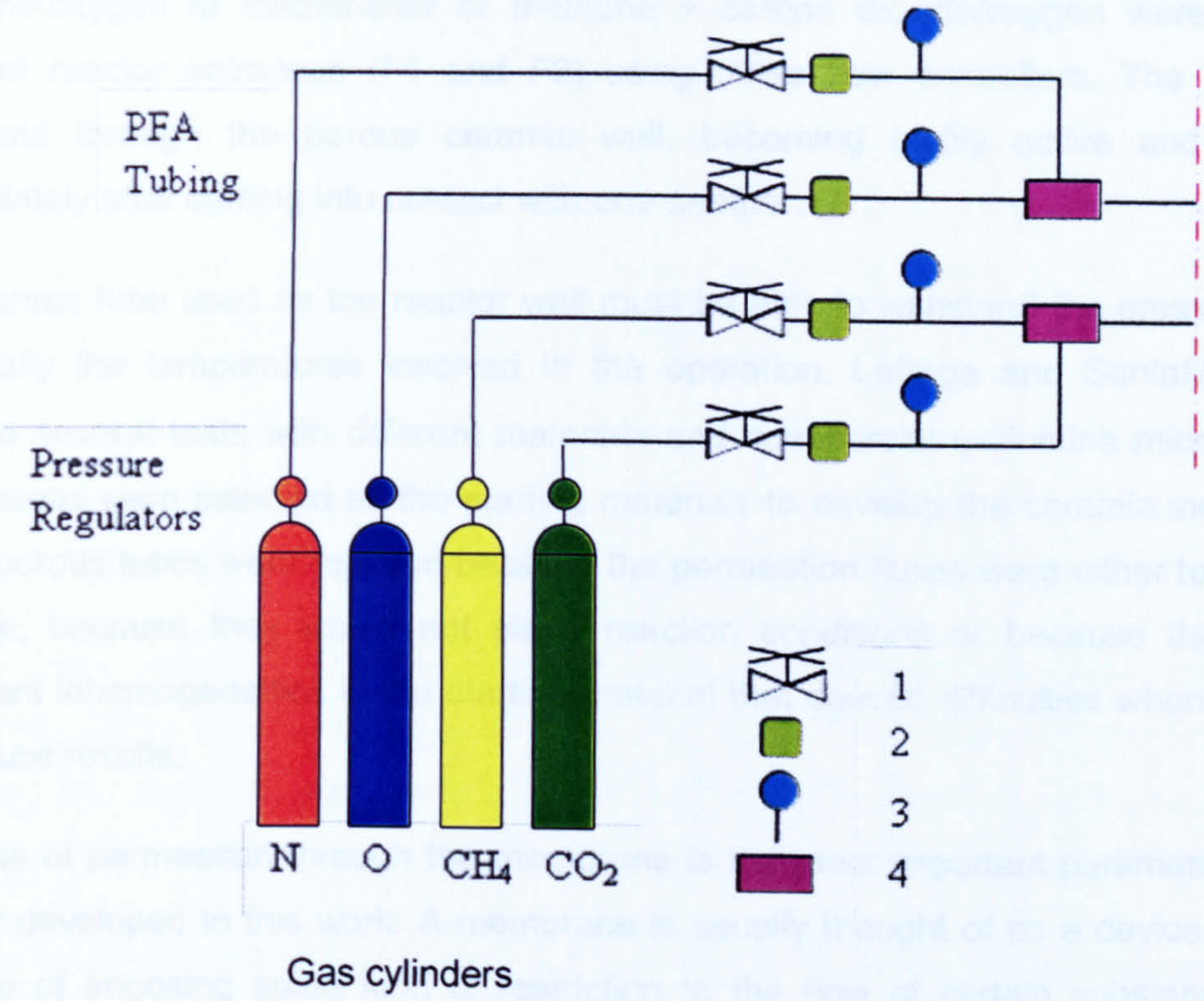

Figure 8: Schematic diagram of the feed gas delivery system

Where:

1 – On/off valve

2 – Non-return check valve

3 – Mass flow controller

4 – Mixing chamber

3.1.2. REACTOR SYSTEM

The reactor concept presented in this work is illustrated in Figure 11. It consists of a membrane catalyst reactor, impregnated with a suitable catalyst onto the porous ceramic tube, acting as oxygen distributor and activator. In any such system, the design of the reactor has a strong influence in determining the selectivity towards the desired product.

Methane/oxygen or methane/air or methane + carbon dioxide/oxygen were led into different reactor entrances (F1 and F2) using mass flow controllers. The reactants permeate through the porous ceramic wall, becoming highly active and reacting immediately after coming into contact with one another.

The porous tube used as the reactor wall must be able to withstand the pressures and especially the temperatures involved in the operation. Lafarga and SantaMaria [35] indicate several tests with different materials and commercial α-alumina microfiltration membranes were selected as the starting materials to develop the ceramic membrane. Other porous tubes were rejected because the permeation fluxes were either too high or too low, because they would not stand reaction conditions or because there were important inhomogeneities in the starting material that caused difficulties when trying to reproduce results.

The rate of permeation through the membrane is the most important parameter for the reactor developed in this work. A membrane is usually thought of as a device which is capable of imposing some kind of restriction to the flow of certain substances. The restriction may apply only to some components of a fluid (selective permeation), or may be of a more general type. In this work, the membrane effect consists of allowing flow of the species towards the other side of the tube, forcing its activation within the membrane, and preventing the contact of non active reactants. This is of great importance for methane partial oxidation, since there is no oxygen mixed with methane in the feed, and there is no oxygen left after the reaction, different feed ratios could be tested with no hazard of explosion and no total oxidation products.

The reactants may also migrate to the other side of the tube by leaking through the seals between the ceramic tube and the stainless steel enclosure. Several materials and different designs were tested by Lafarga and Santamaria [35] as candidates for gaskets, with the requirements of being able to maintain gas tightness at 1073K and 6 bar of pure oxygen for at least 30 hours of experiment. After the tests, graphite was selected and gaskets were made using several compressed 3 mm thick graphite rings.

Therefore the reaction experiments were performed at atmospheric pressure using a stainless steel reactor. The tubular membrane was placed and sealed in the interior of the reactor using 98% pure graphite seals 24mm outer diameter (od) x 10mm inner diameter (id) x 7mm thick (tw) from Geegraf moulded graphite. The reaction temperature

was controlled by 5 NiCr/NiAl – K type fibre glass thermocouples ((1) – Figure 12) 2m long, placed at different locations of the external surface of the reactor tube (Figure 11). The thermocouples were connected to a K – type 6-way switch box bench selector ((2) – Figure 12). Heating tapes 2.4 m long were used to provide heating along the reactor. The temperature was controlled by a 5A intermittent power controller ((3) – Figure 12) and finally read from the Digitron 3208 digital thermometer ((4) – Figure 12).

The reactor, thermocouples and heating tapes were covered with fibre glass and foil tapes to maintain the heating of the reactor system as shown in figure 10 (see also the schematic diagram of the reactor system in figure 11).

The reactants were fed separately ((F1 and F2) – Figure 9) and pressures in the reactor were metered by 4 pressure gauges ((P1, P2, P3, P4) – Figure 9); the flows were controlled by needle valves ((V1, V2, V3, V4) – Figure 9) placed in each channel ((F1, F2, F3, F4) – Figure 9) of the reactor. See picture of the reactor in figures 9 and 10.

The reactants and product mixtures ((F3 and F4) – Figure 9) were analysed by gas chromatography with a thermal conductivity detector, using both molecular sieve and porapak columns. The water formed in the reaction was removed from the effluent in a water trap at room temperature.

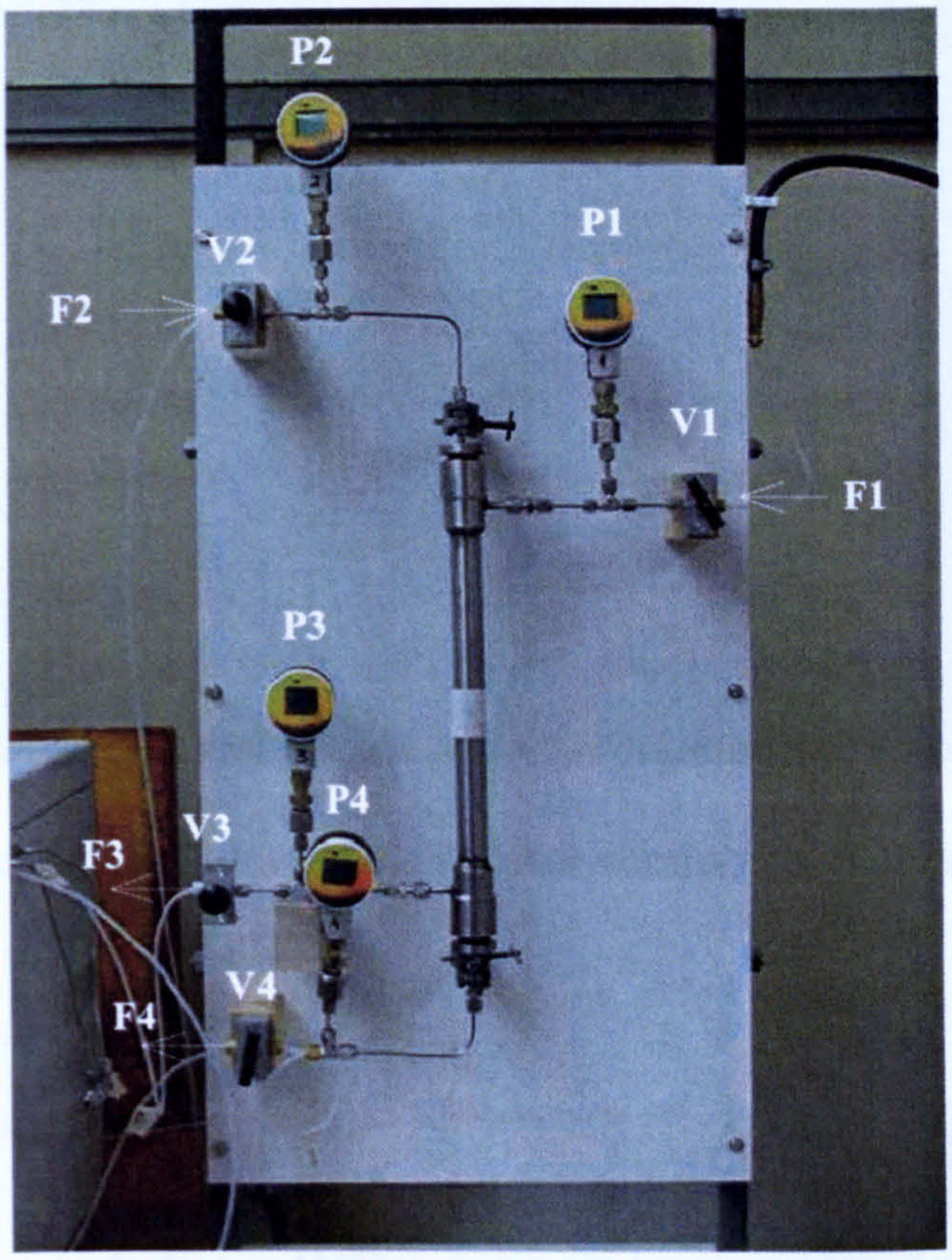

Figure 9: Pictorial view of the reactor section without heating system

Figure 10: Pictorial view of the reactor section and heating system

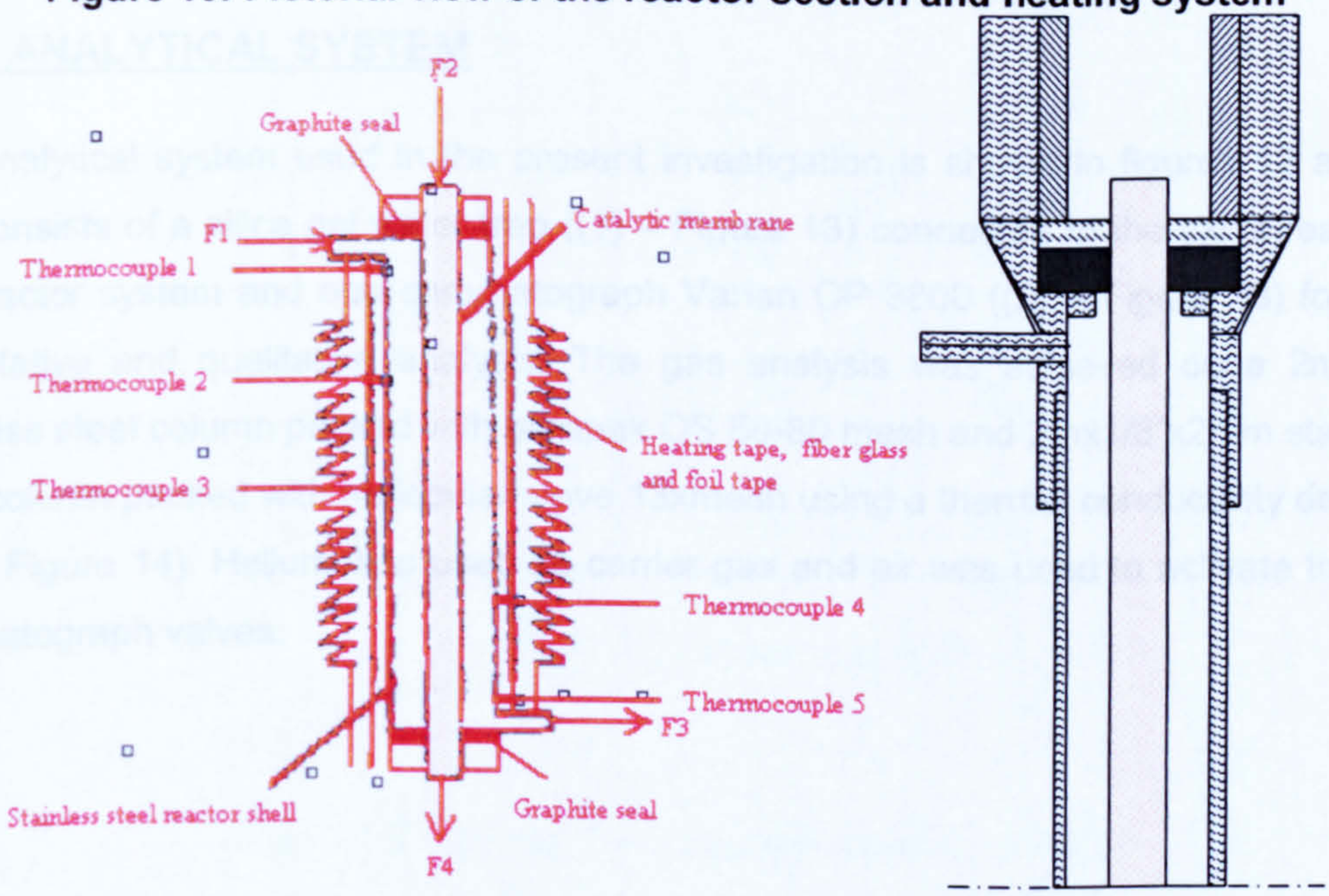

Figure 11: Schematic diagram of the reactor section – detailed design of the reactor

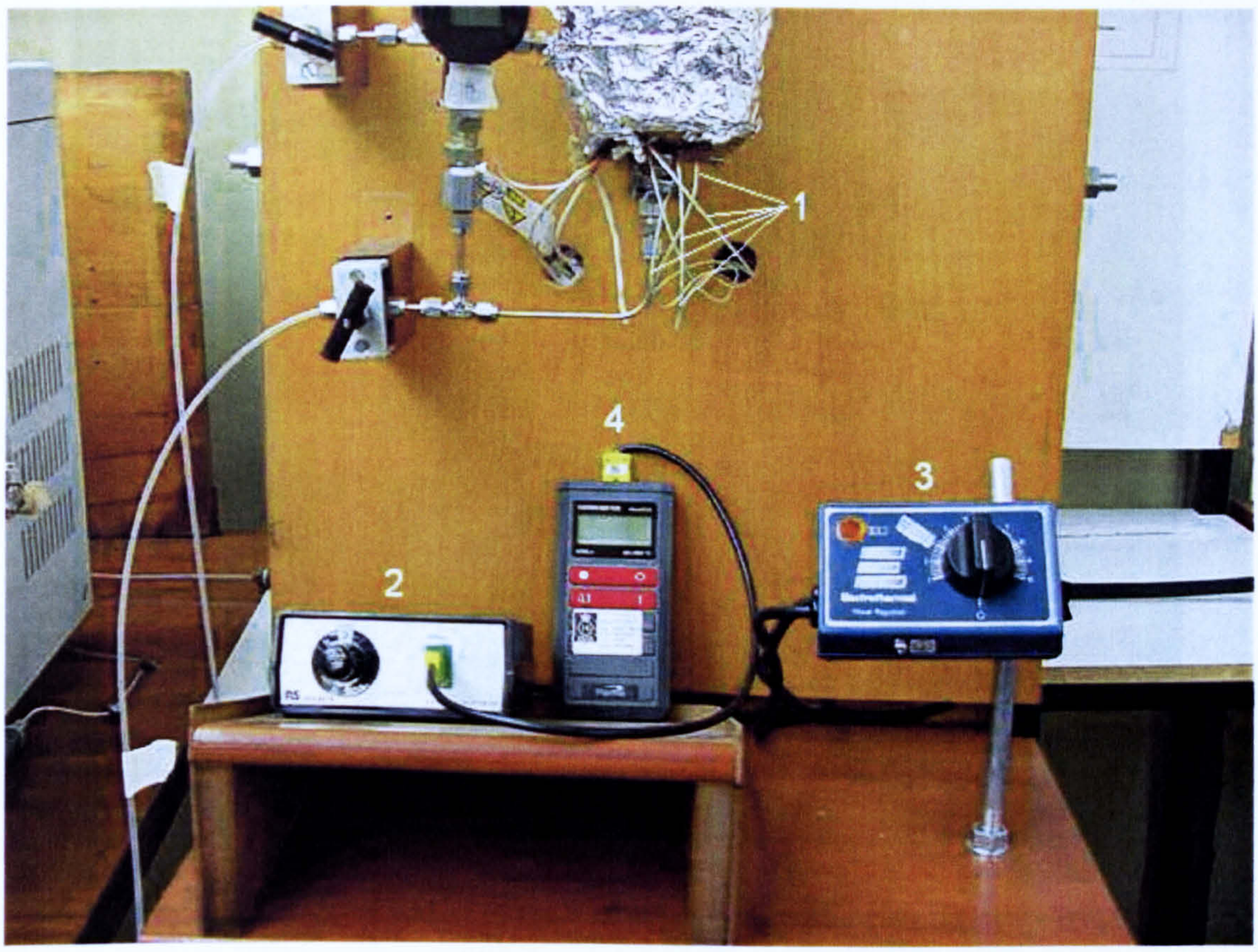

Figure 12: Reactor heating system and cotroller

3.1.3. ANALYTICAL SYSTEM

The analytical system used in the present investigation is shown in figures 13 and 14 and consists of a silica gel water trap ((1) – Figure 13) connected to the exit streams of the reactor system and one chromatograph Varian CP 3800 ((2) – Figure 13) for both quantitative and qualitative analysis. The gas analysis was achieved on a 2m long stainless steel column packed with porapak QS 50-80 mesh and 2mx1/8"x2mm stainless steel column packed with molecular sieve 13xmesh using a thermal conductivity detector ((A) – Figure 14). Helium was used as carrier gas and air was used to activate the gas chromatograph valves.

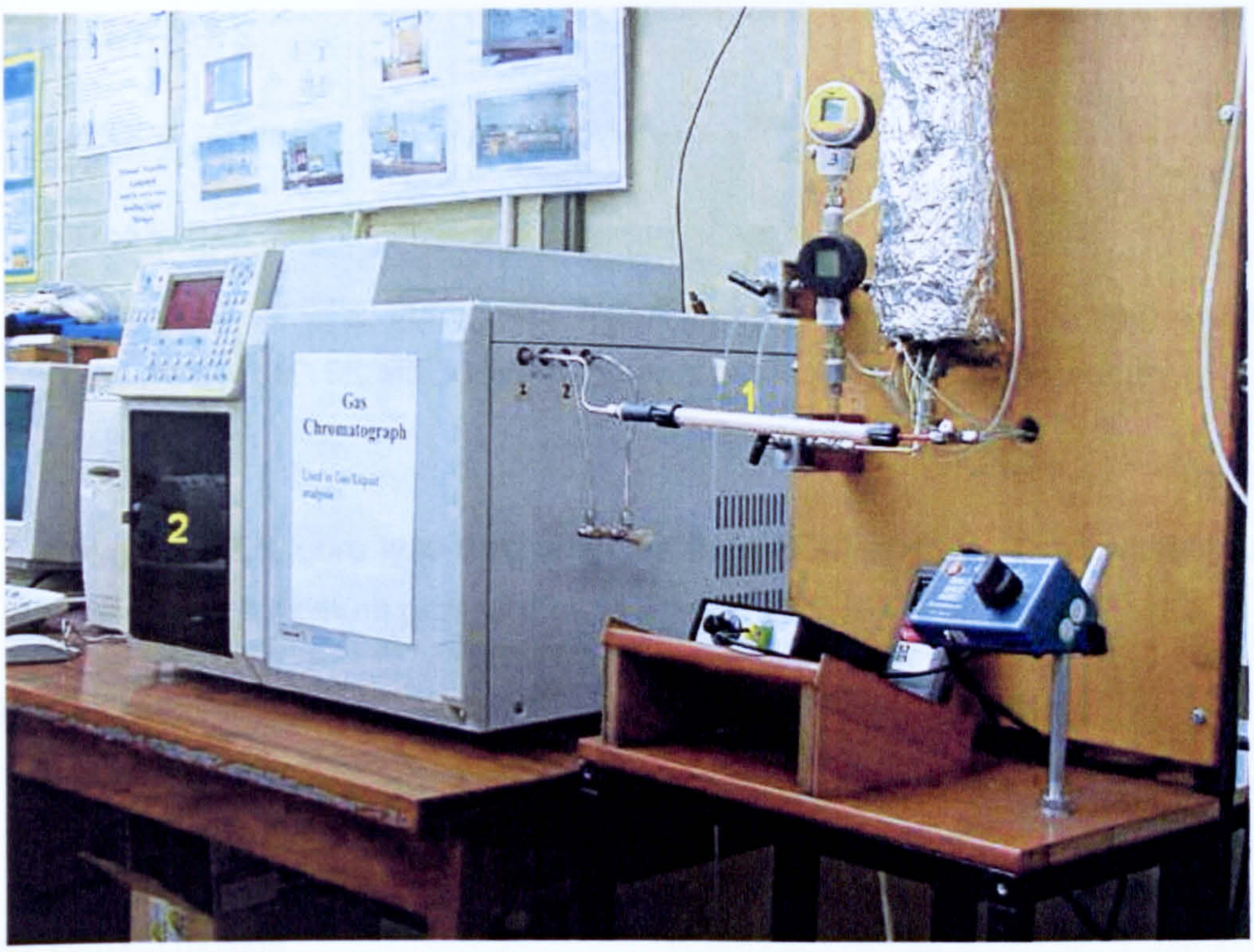

Figure 13: Pictorial view of the analytical system showing moisture trap

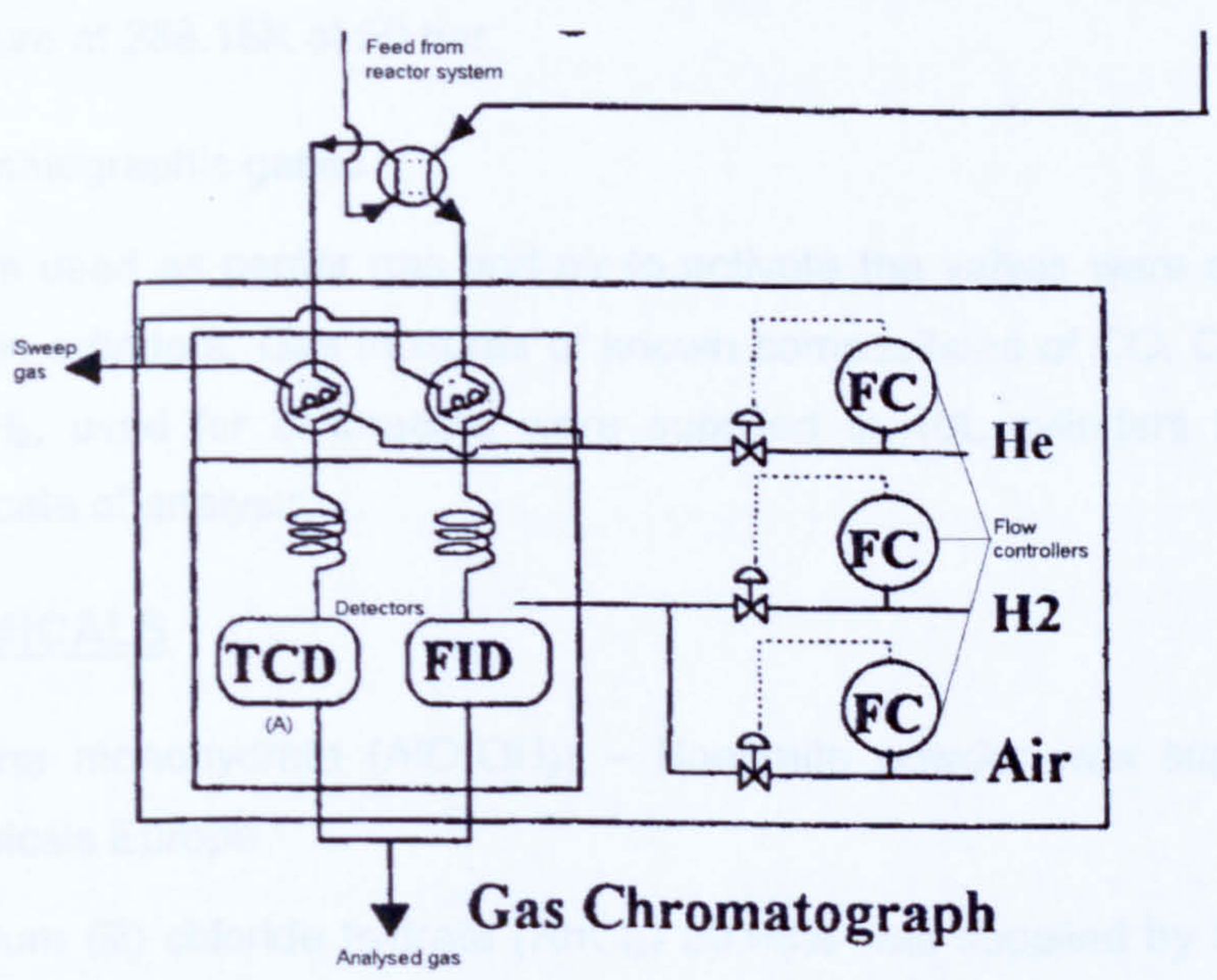

Figure 14: Schematic details of gas chromatograph

3.2. MATERIALS

3.2.1. GASES

i) Nitrogen

Nitrogen of 99.97% purity was supplied in cylinders by BOC with maximum pressure at 288.15K of 230bar. Additional purification was unnecessary.

ii) Oxygen

Oxygen 99.5% pure was also obtained from BOC and was used without further purification. Maximum pressure of delivery at 288.15K is 230 bar.

iii) Methane

Methane was supplied in cylinders 99.9% pure, with maximum pressure at 288.15K of 137 bar. Also from BOC.

iv) Carbon dioxide

Carbon dioxide 99.8% was also supplied by BOC in cylinders of maximum pressure at 288.15K of 50 bar.

v) Chromatographic gases

Helium used as carrier gas and air to activate the valves were also supplied by BOC in cylinders. Gas mixtures of known compositions of CO, CO_2, O_2, N_2, CH_4 and H_2, used for calibration, were supplied in 10L cylinders by BOC with a certificate of analysis.

3.2.2. CHEMICALS

i) Alumina monohydrate (AlO(OH)) – Boehmite powder was supplied by Alcan Chemicals Europe

ii) Rhodium (iii) chloride hydrate ($RhCl_3$) 99.98% was supplied by Sigma/Aldrich in 250mg ampoules.

iii) Nickel (II) nitrate hexahydrate $Ni(NO_3)_2$ 99.999% supplied by Sigma/Aldrich in 100g bottles.

3.2.3. CERAMIC SUPPORT

i) α- alumina tubes washcoated externally with titania supplied by Ceramiques Techniques et Industrielles (CTI SA) in France.

3.3. SAFETY

3.3.1. FLAME AND EXPLOSION

The flammables in this investigation include all the organic materials and are classed either highly or moderately flammable [78].

3.3.1.1. Safety Characteristics of Methane: At room temperature, methane is a gas less dense than air. It melts at 90.15K and boils at 109.15K. It is not very soluble in water. Methane is combustible, and mixtures of about 5 to 15 percent in air are explosive. Methane is not toxic when inhaled, but it can produce suffocation by reducing the concentration of oxygen inhaled. An undetected gas leak could result in an explosion or asphyxiation.

3.3.1.2. Safety Characteristics of Oxygen: Oxygen is heavier than air. It is a violent oxidiser and will explode when petrochemicals (oil & grease) are in contact with pressurised oxygen.

3.3.1.3. Safety Characteristics of Hydrogen: Specific Gravity - 0.0694 - Air 1.0. It is much lighter than air. Practically no toxicity except it may asphyxiate. Highly dangerous fire and severe explosion hazard when exposed to heat, flame or oxidizers. The small size of the molecule makes containing of hydrogen more difficult than larger gaseous molecules. It has a flammable range in air of 4% to 72%. It is also flammable or explosive when mixed with O_2 and chlorine.

3.3.1.4. Safety Characteristics of Carbon Monoxide: Carbon monoxide is an extremely dangerous poison. Because it is an odourless and tasteless gas, it gives no warning of its presence. It binds to the haemoglobin in blood to form a compound that is so stable that it cannot be broken down by body processes. When the haemoglobin is combined with carbon monoxide, it cannot combine with oxygen; this destroys the ability of haemoglobin to carry essential oxygen to all parts of the body. Suffocation can occur if

sufficient amounts of carbon monoxide are present to form complexes with the haemoglobin. Dangerous fire hazard when exposed to flame.

3.3.1.5. Safety Characteristics of Carbon Dioxide: Carbon dioxide is a colourless and essentially odourless gas that is 1.5 times as dense as air. It is not toxic, although a large concentration could result in suffocation simply by causing a lack of oxygen in the body. Carbon dioxide is also used as a fire extinguisher, because most substances do not burn in it, and it is readily available and inexpensive. Air containing as little as 2.5 percent CO_2 extinguishes a flame.

3.3.1.6. Safety Characteristics of Boehmite: Boehmite is a non-hazardous product.

3.3.1.7. Safety Characteristics of Rhodium Chloride: When heated to decomposition it emits toxic fumes of Cl^-. Rhodium can be a sensitizer. Flammable when exposed to heat or flame. Most rhodium compounds have only moderate toxicity by ingestion.

3.3.1.8. Safety Characteristics of Nickel Nitrate: Suspect carcinogen. Moderately toxic by ingestion. When heated to decomposition it emits fumes of NO_x.

3.4. MEMBRANE PREPARATION

3.4.1. SUPPORT MODIFICATION

The alumina tube used in this work as a starting material is commercially sold as membrane for microfiltration applications. It consists of an α-alumina structure washcoated externally with TiO_2 resulting ~ 77% α-alumina + ~23% TiO_2. The outer diameter (od) is ~10.2mm, inner diameter (id) ~ 7.6mm and ~ 1.3mm thickness (tw) with an average pore size of 3nm (see figure 15).

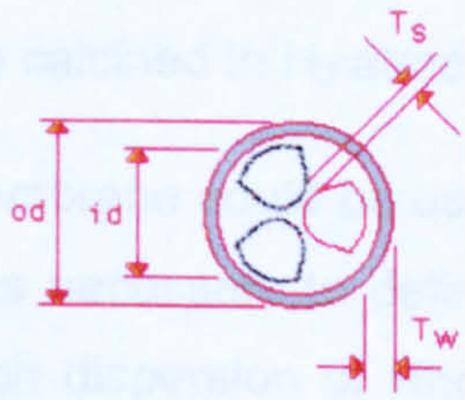

Figure 15: Support internal structure

In order to modify the surface of the substrate a 0.6mol/L boehmite sol was used as γ-alumina source.

The internal surface of the coarse alumina tube was exposed to the boehmite sol, coating the internal wall of the tube for a period of 2 minutes, maintaining the titanium on the external surface. After this the membrane was air-dried overnight and then heat-treated on the temperature profile showed bellow (Figure 16):

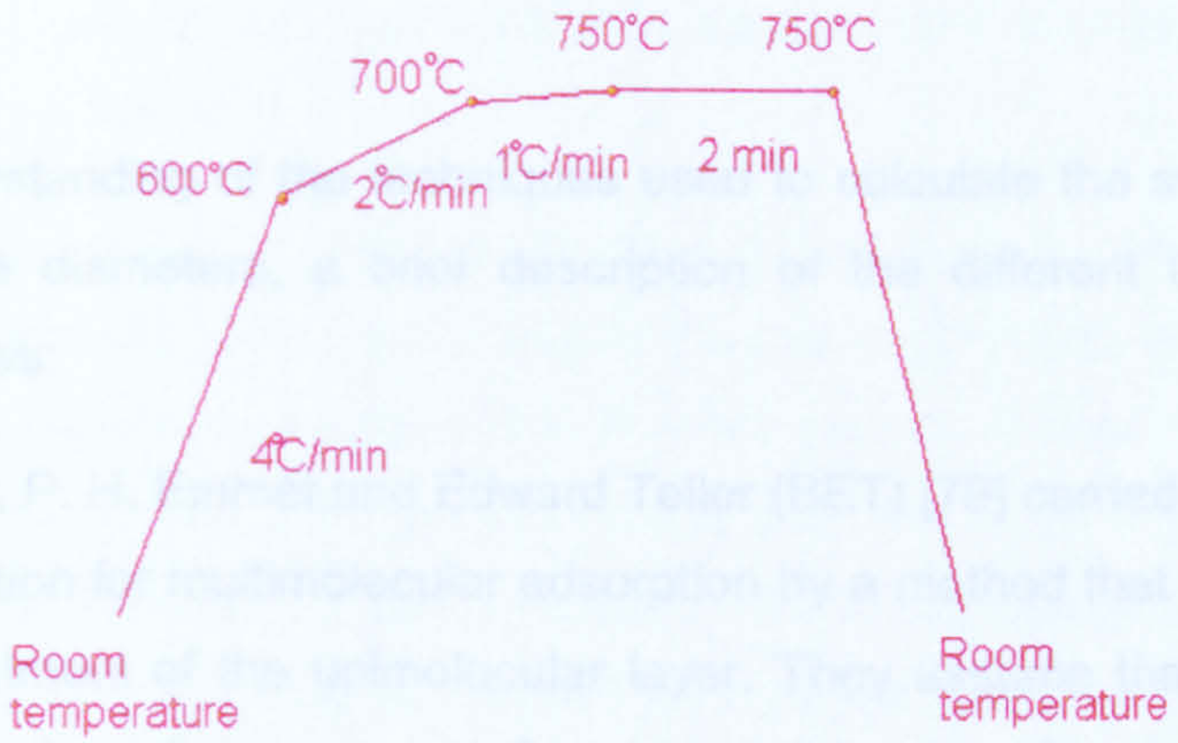

Figure 16: Heat-treatment profile

The control of the heating rate was optimised, with the experimental work, to maximise the transition of boehmite to γ-alumina. It was necessary to repeat this dipping-drying-firing procedure once more to achieve the required γ-alumina layer on the coarse support.

3.4.2. CATALYTIC MEMBRANE COATING

The membranes were prepared by a repeated dip-coating technique of the modified porous substrate in a saturated solution of $Rh_3Cl.2H_2O$ and deionised water. The support was immersed into the solution for about 30 minutes followed by draining and drying in air at 338.15K for 24hours. This procedure was repeated 4 times.

The resulting membrane was then calcined in H_2 atmosphere for 2 hours at 673.15K.

After the above processes the membrane could be used as a reactor. However, in order to define a reaction volume it was necessary to define the region in which permeation was taking placing. Assuming high dispersion of Rhodium over the surface, the entire permeate membrane volume was considered as reaction volume.

3.5. MEMBRANE CHARACTERISATION

3.5.1. SURFACE AREA AND POROSIMETRY ANALYSIS (ASAP)

To characterise the surface of the porous catalytic membrane, the surface area, pore volume and pore diameter were evaluated. Nitrogen adsorption of the samples was measured at –195.8°C (77.35K) with an ASAP 2010 Micrometrics apparatus. Prior to the measurements the samples were degassed at 673.15K overnight at a pressure less than 1.4Pa.

For a better understanding of the techniques used to calculate the surface areas, pore volumes and pore diameters, a brief description of the different theories has been presented as follows:

Stephen Brunauer, P. H. Emmet and Edward Teller (BET) [79] carried out a derivation of the isotherm equation for multimolecular adsorption by a method that is a generalisation of Langmuir's treatment of the unimolecular layer. They assume that the same forces that produce condensation are chiefly responsible for the binding energy of multimolecular adsorption. As nitrogen is a non-polar gas and assuming the samples analysed are not ionic, the DeBoer and Zwicker's method, which assume dipole formation for adsorption calculation is not used in this work, but the BET method has been used.

But, considering Shull's assumption that the BET thickness becomes much larger than experimental thicknesses for flat surfaces in the high pressure region, the BJH (Elliot P. Barret, Leslie G. Joyner and Paul P. Halenda) [80] technique for estimating volumes of porous materials was also used. This technique was developed to deal with relatively coarsely porous materials exhibiting a wide range of pore sizes, but the procedure appears to be applicable to porous solids of any nature.

BJH carried out a formal analysis of the relationship between nitrogen desorption isotherms at liquid nitrogen temperatures and the distribution of pore volume and area with respect to the pore radius. For this they assumed that the equilibrium between the gas phase and the adsorbed phase during desorption is determined by two mechanisms: (1) physical adsorption *on* the pore walls (which would occur to the same extent whether the area involved constituted wall of pores or a flat surface impenetrable to nitrogen), and (2) capillary condensation *in* the inner capillary volume [80].

The experimental values of the volume of nitrogen adsorbed in cm^3 STP/g of adsorbent are obtained as a function of the relative pressure (P/Po), and may be transformed to functions of thickness of the multimolecular layer of adsorbed nitrogen. By plotting the volume of adsorbed nitrogen for an unknown sample as a function of the experimental thickness, a straight line is obtained as long as the multilayer is formed unhindered. The straight line goes to the origin and its slope is a measure of surface area. The surface area will not be exactly equal to the BET surface area, as the BET equation depends on the sample and the plot indicated as t-plot (see appendix for examples) is independent of the nature of the sample [81].

As the adsorption behaviour of nitrogen depends on the surface characteristics and on the pore diameter, and both can change during the membrane preparation, the results of nitrogen adsorption have to be interpreted with much caution. It must also be considered that the values of the surface and the pore volume are referenced to the sample weight. Nevertheless, the BJH method is usually applied as the standard method for pore size determination and is well suited to analyse trends in similar samples [82]. An example of the values obtained for the pore structure of the original alumina tube is as follows:

Surface Area	**[m^2/g]**
Single Point	99.6606
BET	260.9962
BJH	181.4751
Pore Volume	**[cm^3/g]**
Single Point	0.213349
BJH	0.195347
Pore Size (diameter)	**[nm]**
Average BET	3.2698
BJH	4.3057

3.5.2. X-RAY PHOTOELECTRON SPECTROSCOPY (XPS)

X-ray photoelectron spectroscopy (XPS) also known by the synonym ESCA (electron spectroscopy for chemical analysis), is the method of choice to provide high-resolution compositional material surfaces [83]. XPS identifies all elements, except H and He present in the outer 10 nanometres of a surface at concentrations exceeding 0.1 atomic percent. It determines the approximate surface composition (10%) semi-quantitatively. It gives bonding information and molecular environments (oxidation states, bonding partners) in surface zone and so on [83].

XPS is based on photoemission of core levels electrons in an atom. Incident X-rays with energy, usually monochromatic on modern systems, liberate core-level electrons with sufficient kinetic energy to escape from the material and pass through the vacuum chamber to the energy spectrum analyser.

In this work, the XPS was used mainly for quantitative and qualitative compositional surface analyses. The equipment used was a Kratos Axis Hsi 5 channel imaging x-ray photoelectron spectrometer using monochromated AlK (alpha) radiation.

3.5.3. SCANNING ELECTRON MICROSCOPY (SEM)

The SEM generates a finely focused beam of electrons which is made to scan across the sample under inspection. The beam originates from the heating of tungsten wire filament (thermionic emission) housed in an electron gun at the top of the microscope column. The beam electrons are accelerated towards the specimen by means of an applied accelerating voltage between the filament assembly and an anode plate. The SEM column and sample chamber are maintained under a high vacuum to allow the electrons forming the beam unhindered path from the filament to the sample surface [84].

As the beam travels down the column, it undergoes electron optical demagnification as it passes through two electromagnetic lenses (condenser lenses). Just above the specimen the beam comes under the influence of a set of scan coils which deflect the beam in a faster pattern across the sample surface. This scanning section is synchronised with the display monitor where an image of the surface, with high magnification is obtained. Available magnification may exceed 300,000x with resolution of 3-4nm [84]. This compares with a resolution capability of a light microscope of

approximately 2550nm. The equipment used was a Leo model S430 Scanning Electron Microscopy (SEM).

As an example, the SEM of the support used in this study is shown in figure 17.

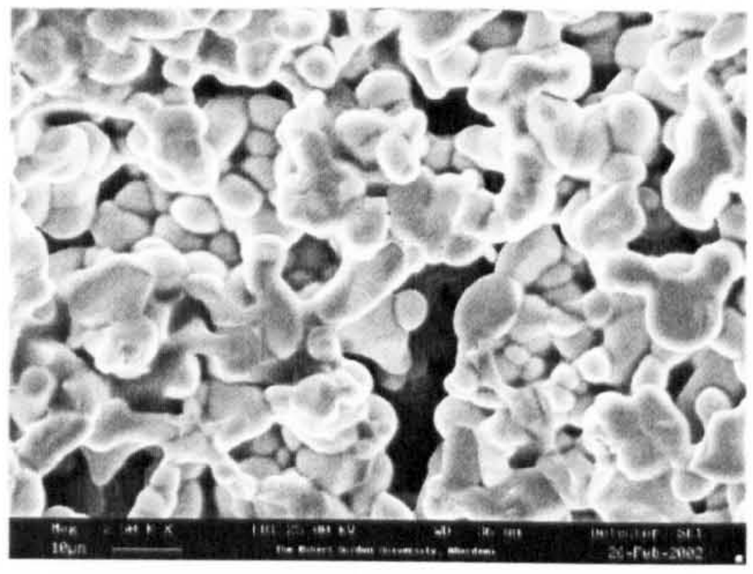

Figure 17: SEM Support – Surface

3.5.4. ENERGY DISPERSIVE X-RAY ANALYSIS (EDXA)

As the scanning electron microscope uses a high energy electron beam to illuminate a specimen, one of the by-products is the generation of x-rays as primary beam electrons interact with specimen electrons. The production of x-rays occurs in two basic ways. As an electron in the primary beam enters the volume of a specimen atom, it can be scattered inelastically in various ways [85].

Primary electrons may slow down by interaction with forces present within the volume of an atom resulting in the electron giving up energy. This energy loss can be accomplished by the emission of x-ray radiation. This type of radiation is known as braking radiation and is observed as a continuous spectrum. This continuous spectrum is regarded as background radiation for EDXA spectrometers [85].

Inelastic scattering also occurs due to collisions between primary electrons and electrons within specimen atoms. The consequent rearrangement of electrons within electron shells, as atoms strive to reach their lowest energy states, results in the release of energy in the form of x-ray photons. As the energy of these photons is related to the energy between electron shells, the x-ray photons are characteristic of the element present in the specimen. By collecting and analysing these x-rays, qualitative and quantitative information about the component elements of a specimen may be obtained [85]. The additional hardware required to detect and measure the energy of the

characteristic x-rays, used to characterise the membrane was a Link exL2 EDXA system (Oxford Microanalysis Group).

3.6. PRODUCTS IDENTIFICATION

Gas chromatography (GC) was used to identify the products of the reaction. Literature information acted as a guide to the spectrum of the products to be expected.

A gas chromatography apparatus consists of a pressurized tank of carrier gas, usually He, a pressure regulator to control the flow rate of the gas through the chromatograph, a sample inlet, the column, a detector with associated electronics, some kind of interface to the outside world such as a recorder (computer), and a flow meter to measure the flow rate of carrier gas. Chromatographs also provide heating for the column, the sample inlet, and the detector. The temperatures of these three components can usually be controlled independently.

On this work, the on-line GC (Varian) was equipped with two air actuated automatic valves including a sampling valve and a bypassing valve, and the GC Star Workstation for data collection and analysis. Two isothermal (323.15K) stainless steel columns, porapak QS and molecular sieve 13X was used. An external standard method was used for product analysis. Multiple point calibration curves were created, and recalibrated routinely with standard gas mixture (O_2, N_2, CH_4, CO and CO_2) for long-term studies. The quantity of H_2O was calculated based on hydrogen atomic balance.

The calibration involved injecting pure H_2, CO_2, CH_4 and O_2 for qualitative analysis, i.e. to obtain the retention times of each of the gases used in the specified GC configurations. For quantitative calibration a known gas composition (standard gas) containing H_2, CO, CO_2, CH_4 and O_2 was injected also in both columns, to obtain the area of the peaks. The analysis could then be carried out. The respective retention times were recorded and compared to the standard gas using the method described. The equipment was calibrated before every run.

For the identification of carbon dioxide the porapak column was used, and all the other products were analysed in the molecular sieve column. A thermal conductivity detector (TCD) was used to identify the gases exiting from both columns. One example of the peaks for the products is shown in figure 18.

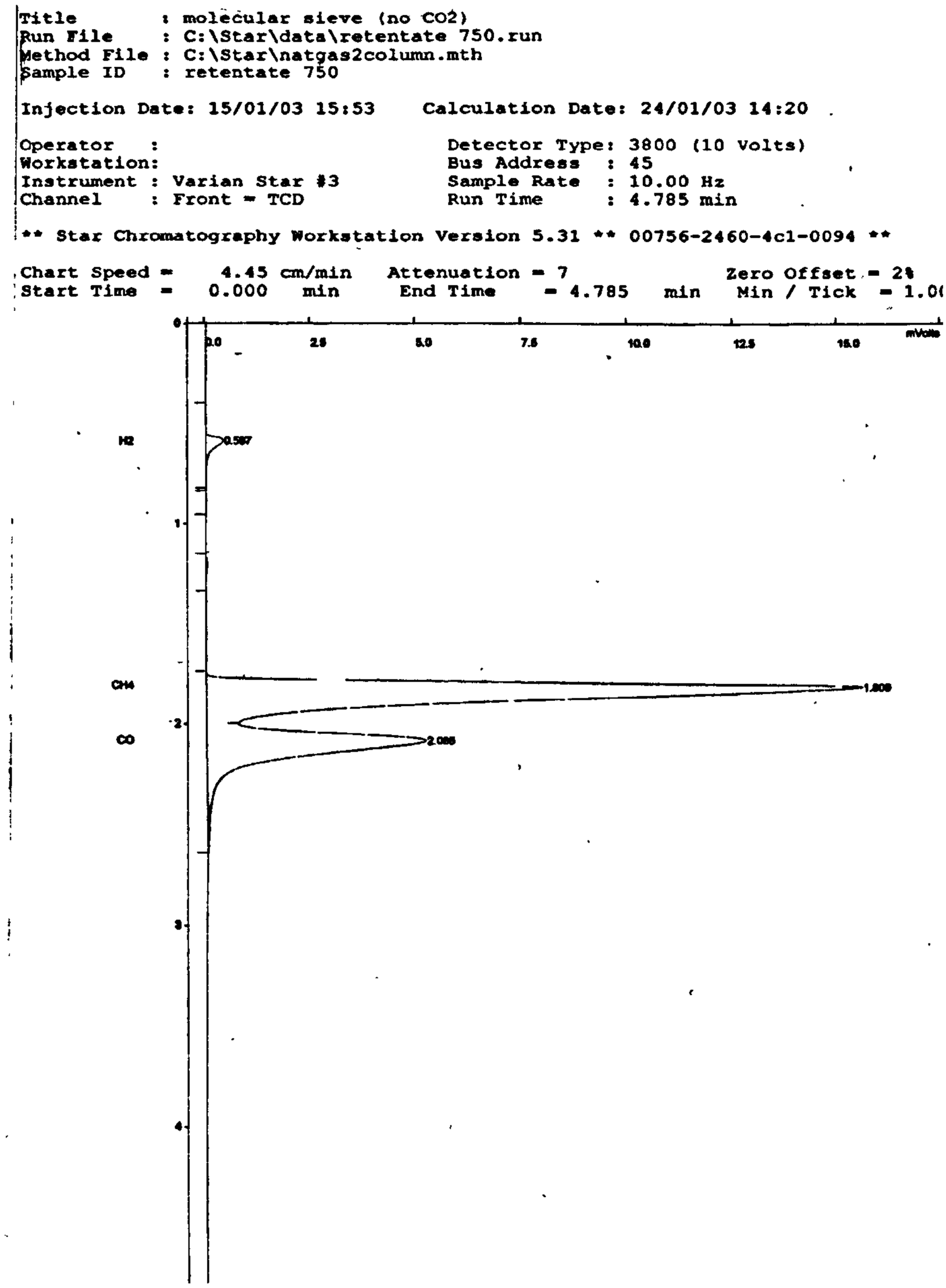

Figure 18: Products chromatograph

3.7. SCREENING TESTS

A series of trial membranes was prepared and reaction runs were carried out to identify the best catalytic membrane composition, define inlet parameters and also guide the precise identification of the reaction products using gas chromatography.

The literature review (chapter 2) shows a wide range of supports, support modifications, catalysts, reactor design and membrane specifications that could potentially be used to

enhance research and produce very good partial oxidation reactors. (See also Appendix for exploratory table from literature review.)

Some references such as the work done by Wang et.al. [3] have called special attention to the membrane stability. Various other research works ([86], [62]) together with novel ideas of membrane reactor utilisation provided the initial foundation in this work to define the parameters and specifications of the membrane reactor that was built and tested in order to reach an optimised partial oxidation reaction for syngas production. The trials carried out prior to the actual experimental work are described below.

3.7.1. SUPPORT MODIFICATION

Over the basic support described earlier in this chapter (support (A)) boehmite was dip-coated 2 and 4 times in both sides of the tube (support (B) and support (C) respectively), followed by heat treatment in each coating, in order to obtain the γ-alumina crystal structure. The heat treatment has already been described in detail in Section 3.4.

A third type of support modification was carried out using boehmite over the internal part of the row support, maintaining the titania on the external surface (support (D)). This support gave the best results.

3.7.2. CATALYTIC SOLUTION

3.7.2.1. Solution 1

A magnesium based solution was prepared aiming to achieve a concentration of 4mmols Mg/m^2 of support. $Mg(NO_3)_2$ was dissolved in distilled water at room temperature.

3.7.2.2. Solution 2

The nickel based solutions were prepared using 15%NiO and 20%NiO per grams of raw sample. The appropriate amount of $Ni(NO_3)_2$ was dissolved in 1 litre of distilled water at room temperature in order to obtain 15%NiO/g of γ-alumina. A second Nickel based solution was prepared in the same manner, but for 20%NiO/g of γ-alumina.

3.7.2.3. Solution 3

1 litre of a saturated rhodium solution was prepared by dissolving $RhCl_3$ in distilled water at room temperature.

3.7.3. PREPARATION OF CATALYSTS/MEMBRANE

3.7.3.1. CATALYST

The nickel based catalyst was prepared using 10g of the support (B), cut in small pieces (~3mm x 3mm x 1mm) and immersed in the solution for 10 minutes in each of the Nickel based solutions (15% and 20% - samples CSY01and CSY02 respectively). The coated pieces were then dried at 383.15K for 10 hours. The samples thus formed were calcined in air at 1025.15K for 4 hours to yield NiO/γ-alumina catalyst. The amounts of NiO are expressed as wt%.

The sample coated using the 15% NiO solution (CSY01) was filtered to remove the remaining solution before drying. This procedure not done for the solution using 20% NiO (CSY02).

This samples were prepared in order to test the effectiveness of a packed bed reactor, but with the success of the Rh based catalytic membrane, these tests were discontinued.

3.7.3.2. CATALYTIC MEMBRANE COATING

The catalytic membranes were prepared using wet impregnation dip-coating technique. The support tubes were dip-coated in two different catalytic solutions based on magnesium, nickel and rhodium respectively.

Six different membranes (SY00, SY01, SY02, SY03, SY04 and SY05) were prepared using the previously described supports and solutions. SY05 showed the best results, and consequently this was the membrane type used for the final tests.

3.7.3.2.1. SY00

The support B was dip-coated for 2 minutes in the magnesium based solution (solution 1). Dried at 298.15K 24 hours in air and heated up to 673.15 K for 30 min in order to obtain MgO from $Mg(NO_3)_2$.

3.7.3.2.2. SY01

The support B was dip-coated for 10 minutes in the 15% nickel based solution (solution 2). Dried at 383.15K 10 hours and calcined in air at 1023.15K for 4 hours in order to obtain NiO from $Ni(NO_3)_2$.

3.7.3.2.3. SY02

The same procedure as SY01 was used, but over support A.

3.7.3.2.4. SY03

The support A was dip-coated for 30 minutes in the rhodium based solution (solution 3) at room temperature. The tube was then dried at 338.15K 24 hours and calcined in air at 873.15K for 2 hours.

3.7.3.2.5. SY04

The same procedure as SY03 was used, but the calcination proceeded in hydrogen for 2 hours at 673.15K.

3.7.3.2.6. SY05

The internally modified support D was dip-coated 4 times in the rhodium based solution (solution 3) at room temperature. After drying the tube at 338.15K for 24 hours, it was calcined in hydrogen atmosphere for 2 hours at 673.15K.

In total, 6 tubular catalytic membranes and 2 catalysts for packed bed reactors were prepared to define the final catalytic membrane. The samples are summarised in table 1.

Table 1: Summary of the catalysts prepared

Sample	Support used	Solution
CSY01	B	2 15%
CSY02	B	2 20%
SY00	B	1
SY01	B	2 15%
SY02	A	2 15%
SY03	A	3
SY04	A	3
SY05*	C	3

*SY05 = final membrane

3.7.4. CHARACTERISATION OF CATALYSTS & MEMBRANES

3.7.4.1. ASAP

The boehmite powder used to prepare the solution for γ- alumina support modification was characterised in order to observe the heat-treatment effect on it.

The ceramic pieces prepared for packed bed reactors (samples CSY01 and CSY02) were also characterised for each step of its preparation. The surface area [m^2/g], pore volume [m^3/g] and pore diameter [nm] of the boehmite powder heat treatment steps and of the catalyst manufacturing step are shown in tables 2, 3 and 4.

Table 2: Catalyst surface area

Sample	Surface area m^2/g		
	Single Point	BET	BJH Desorption cumulative
alpha-alumina powder - row boehmite	118.3649	187.2944	206.04
1st Heating treatment of boehmite powder	126.0587	201.7164	201.2089
2nd Heating treatment of boehmite powder	115.8117	210.6230	196.6921
CSY first heat treatment	99.5301	261.3714	169.8327
CSY second heat treatment	99.5059	260.9744	169.7199
15% NiO on CSY twice heat treated – CSY01	99.6884	260.1799	169.8562
*20% NiO on CSY twice heat treated – CSY02	99.7585	248.3975	167.2601

Table 3: Catalyst pore volume

Sample	Pore Volume m^3/g	
	Single point	BJH Desorption cumulative
alpha-alumina powder - row boehmite	0.216504	0.215934
1st Heating treatment of boehmite powder	0.242083	0.230745
2nd Heating treatment of boehmite powder	0.234681	0.223766
CSY first heat treatment	0.213862	0.187411
CSY second heat treatment	0.213400	0.187499
15% NiO on CSY twice heat treated – CSY01	0.213607	0.187678
*20% NiO on CSY twice heat treated – CSY02	0.212975	0.189715

Table 4: Catalyst pore diameter

Sample	Pore Diameter [nm]	
	BET average	BJH Desorption average
alpha-alumina powder - row boehmite	4.62382	4.19208
1st Heating treatment of boehmite powder	4.80048	4.58718
2nd Heating treatment of boehmite powder	4.45690	4.55058
CSY first heat treatment	4.327292	4.41402
CSY second heat treatment	3.27082	4.41902
15% NiO on CSY twice heat treated – CSY01	3.28398	4.41968
*20% NiO on CSY twice heat treated – CSY02	3.42958	4.53700

*The solution was not removed from the sample prior to drying.

Surface area analysis of the catalytic membranes SY00, SY02, SY03, SY04 and SY05 are showed in table 5, 6 and 7. The catalytic membrane SY01 was not characterised due to the need of its whole length for further reaction tests in the reactor.

Table 5: Catalytic membrane surface area

Sample	Surface area [m^2/g]				
	Single Point	BET	Langmuir	BJH Adsorption cumulative	BJH Desorption cumulative
SY00	95.8036	249.2468	-	-	167.1009
SY02	98.2756	262.7124	22391.506	180.1987	168.6517
SY03	100.5232	261.339	6290.2831	182.0516	169.1859
SY04	98.9405	259.5253	7522.0405	180.2705	169.2345
SY05	99.4755	261.4715	8763.9821	181.1238	169.7357

Table 6: Catalytic membrane pore volume

Sample	Pore Volume [cm^3/g]		
	Single point	BJH Adsorption cumulative	BJH Desorption cumulative
SY00	0.209297	-	0.183771
SY02	0.212461	0.193246	0.186053
SY03	0.214371	0.196234	0.186102
SY04	0.212727	0.191621	0.186169
SY05	0.213523	0.195629	0.184523

Table 7: Catalytic membrane pore diameter

Sample	Pore Diameter [nm]		
	BET average	BJH Adsorption average	BJH Desorption average
SY00	3.3588	-	4.39904
SY02	3.23488	4.28962	4.4127
SY03	3.28112	4.31162	4.39994
SY04	3.27872	4.25184	4.40028
SY05	3.2665	4.3203	4.3485

3.7.4.2. SEM

Scanning electron micrographs were taken for the catalysts CSY01 and CSY02 (Figures 19 and 20) and from the catalytic membranes SY00, SY02, SY03, SY04 and SY05 (Figures 21, 22, 23, 24 and 25). It is possible to observe the excess of nickel on the CSY02 (Figure 20). This occurred due to lack of rinsing before drying.

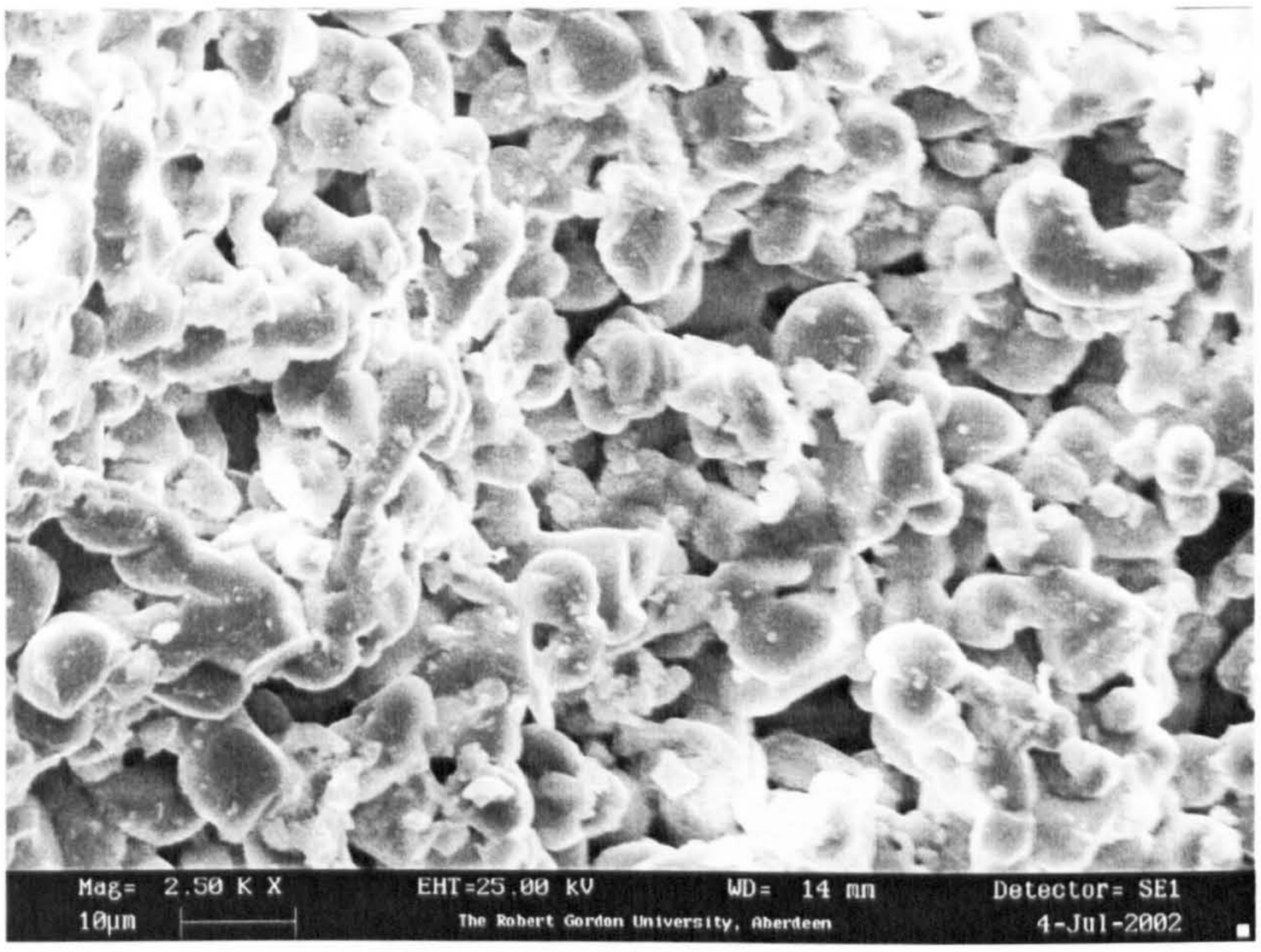

Figure 19: Nickel catalyst 15% - CSY01

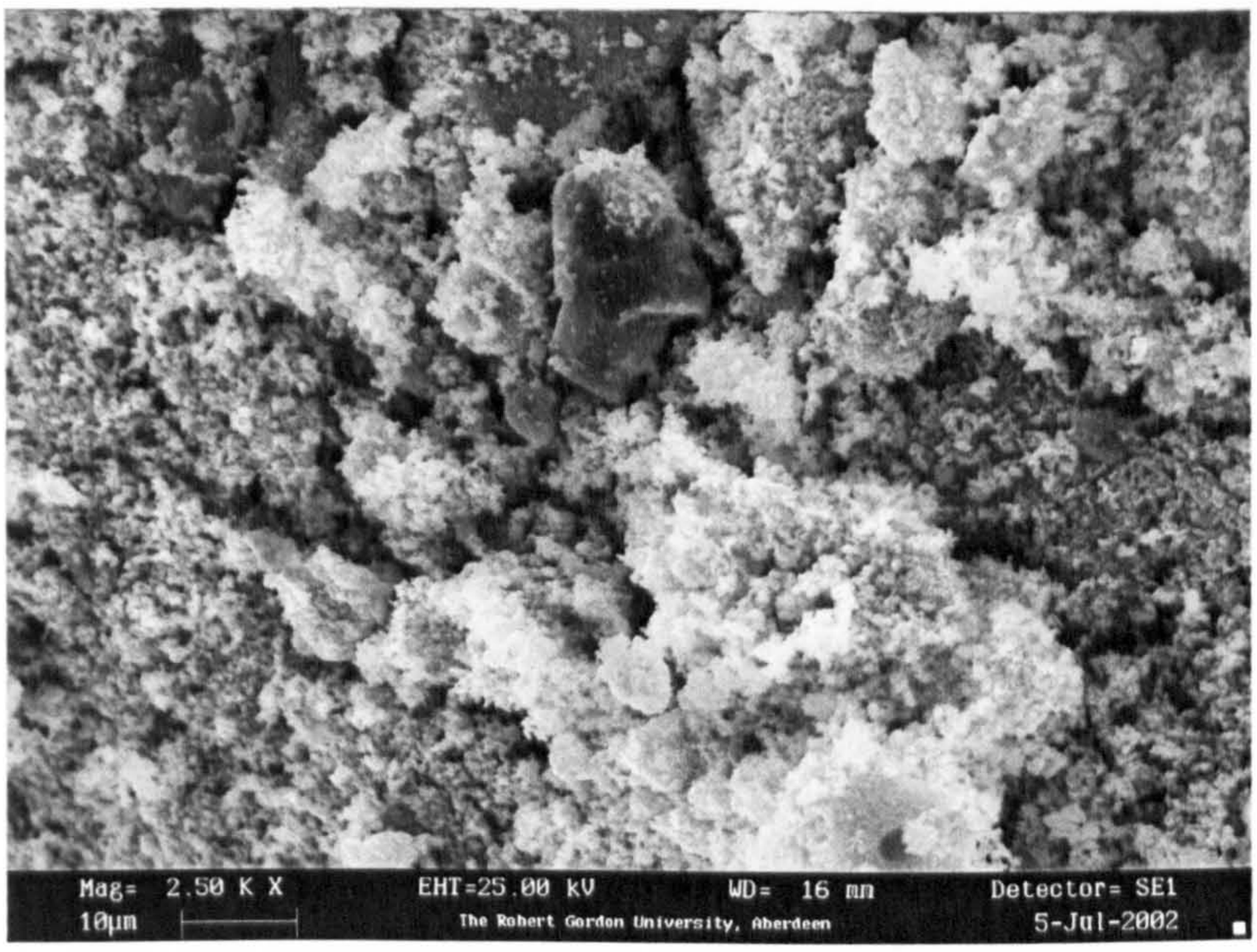

Figure 20: Nickel catalyst 20% - CSY02

For the catalytic membrane, it is possible to examine the magnesium, nickel and rhodium crystals over the support.

Figure 21 shows the magnesium covering the outer surface of the membrane.

In figure 22, it is possible to observe the small concentration of nickel over the ceramic support.

Comparing figures 23 and 24 is possible to examine the effect of the calcination procedure. In sample SY03 (Figure 23) the rhodium chloride is not reduced as when the sample is calcined in a hydrogen atmosphere which is the case of sample SY04 (Figure 24). Figure 25 shows the rhodium membrane previously modified with γ-alumina.

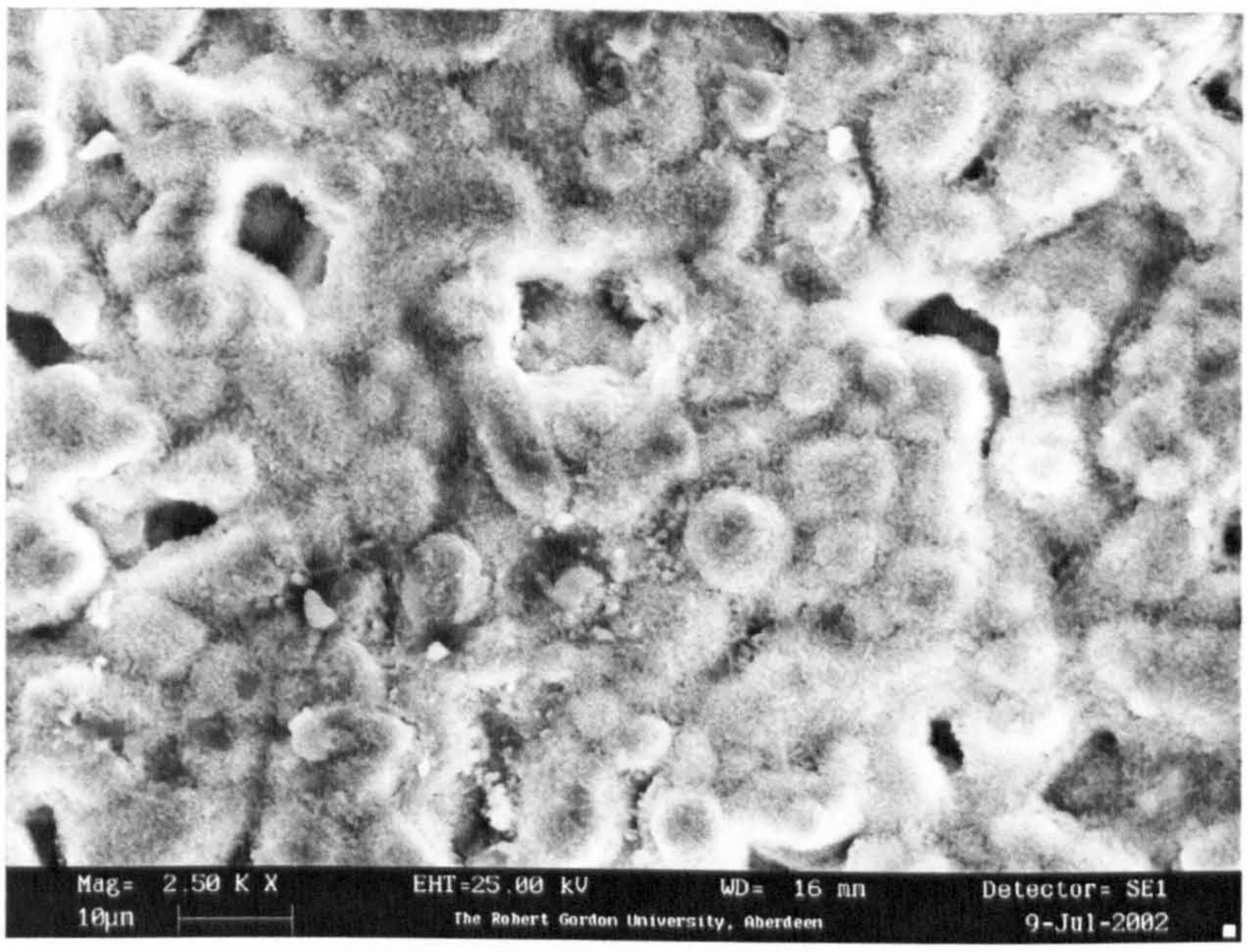

Figure 21: Magnesium catalytic membrane – SY00

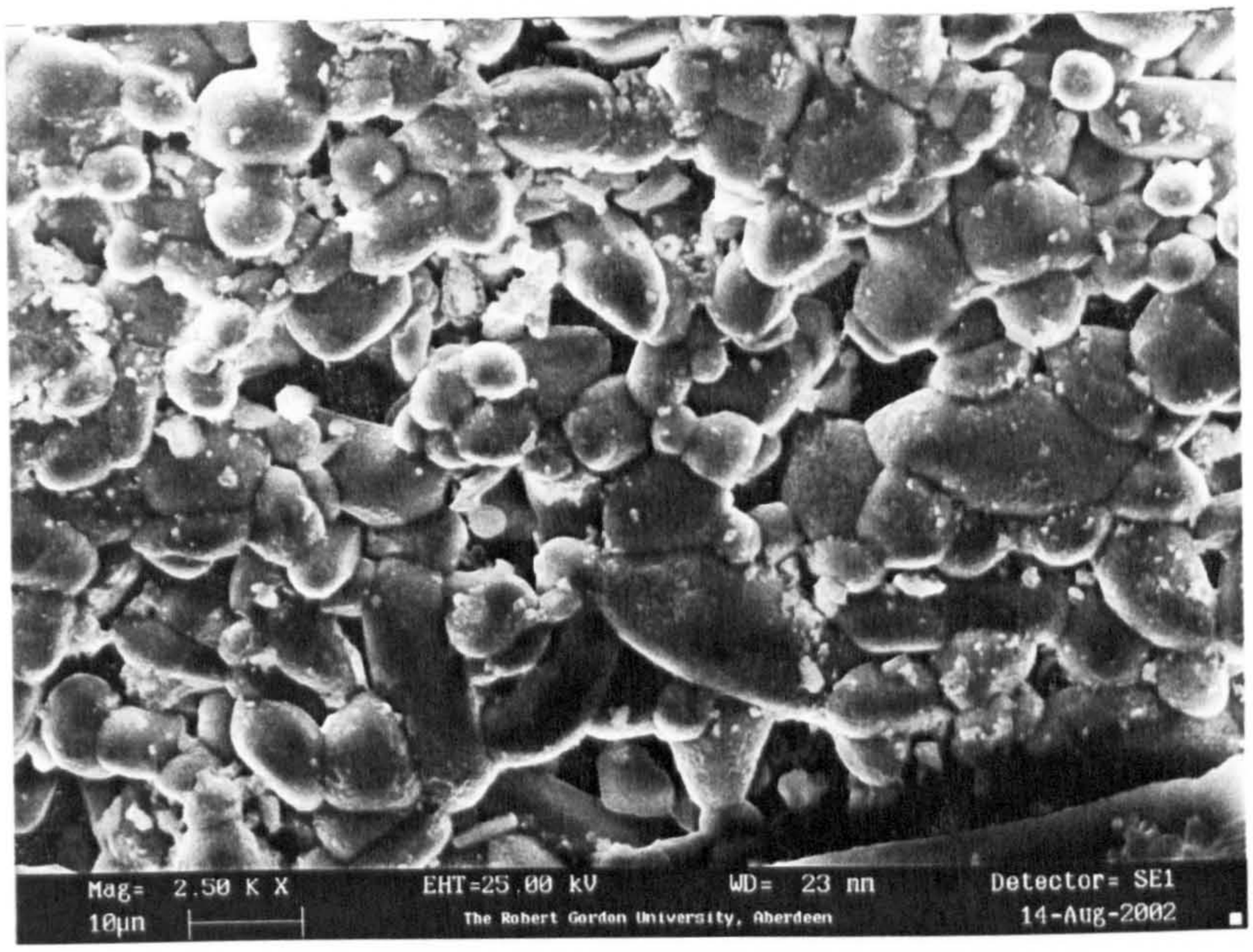

Figure 22: Nickel catalytic membrane - SY02

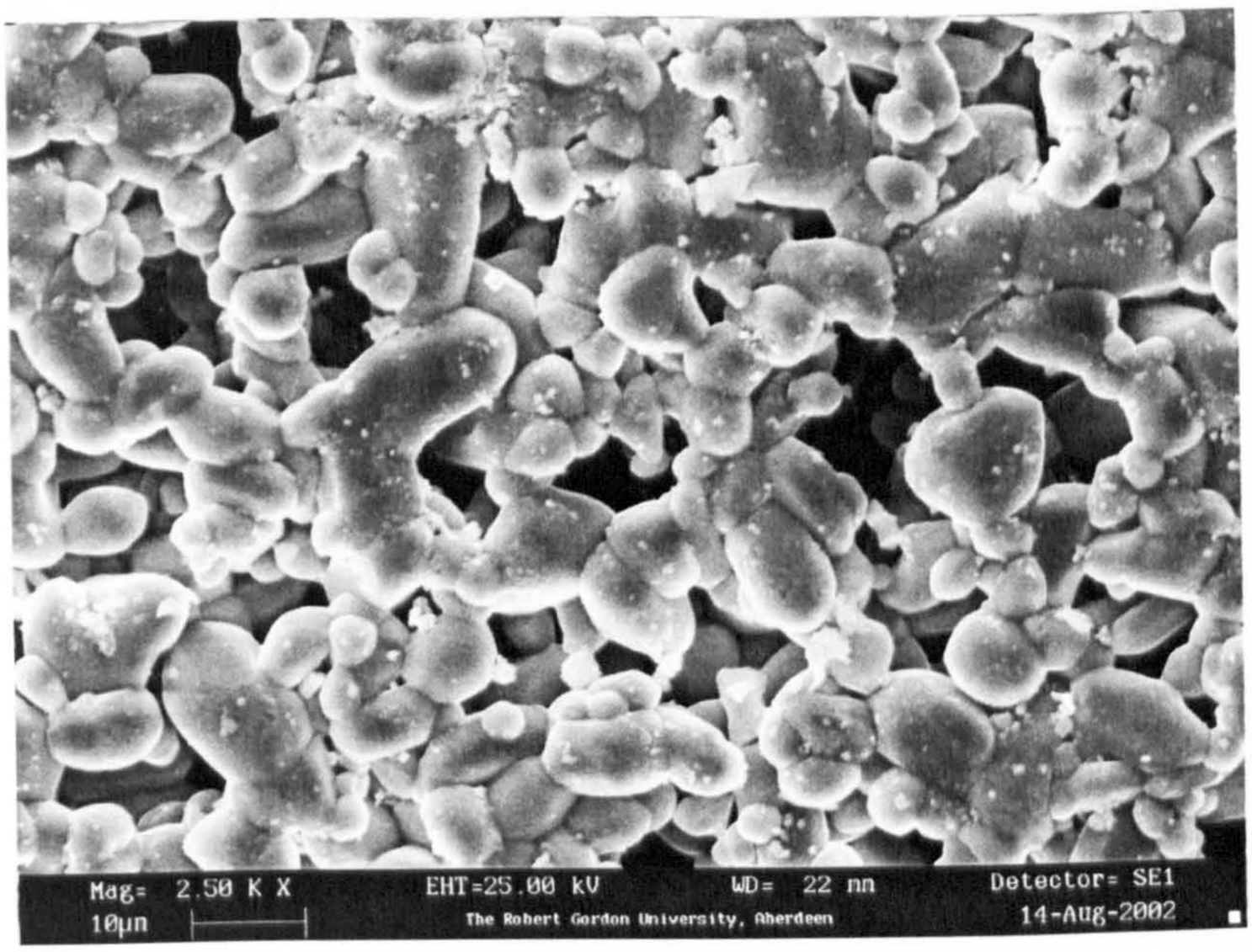

Figure 23: Rhodium catalytic membrane - SY03

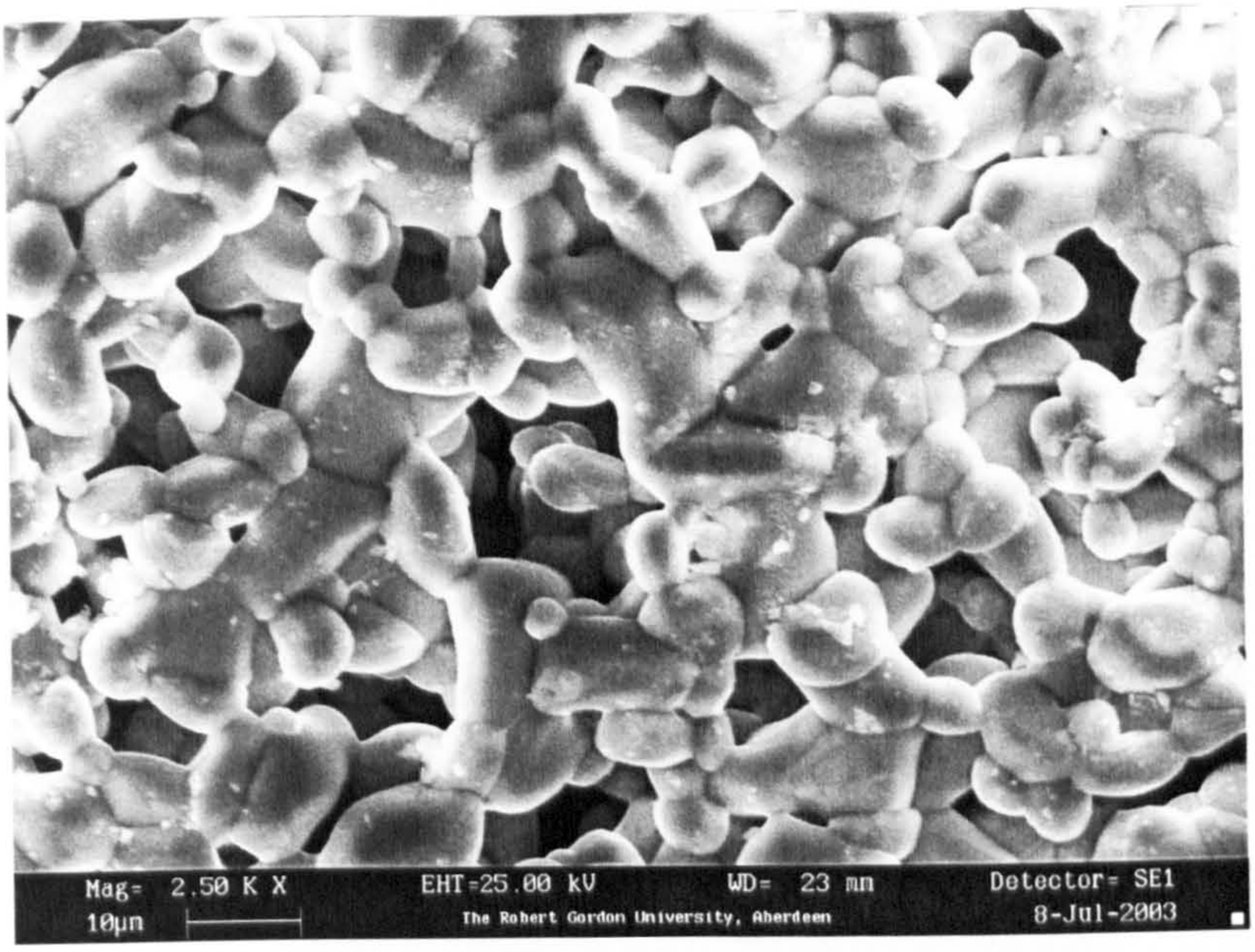

Figure 24: Rhodium catalytic membrane – SY04

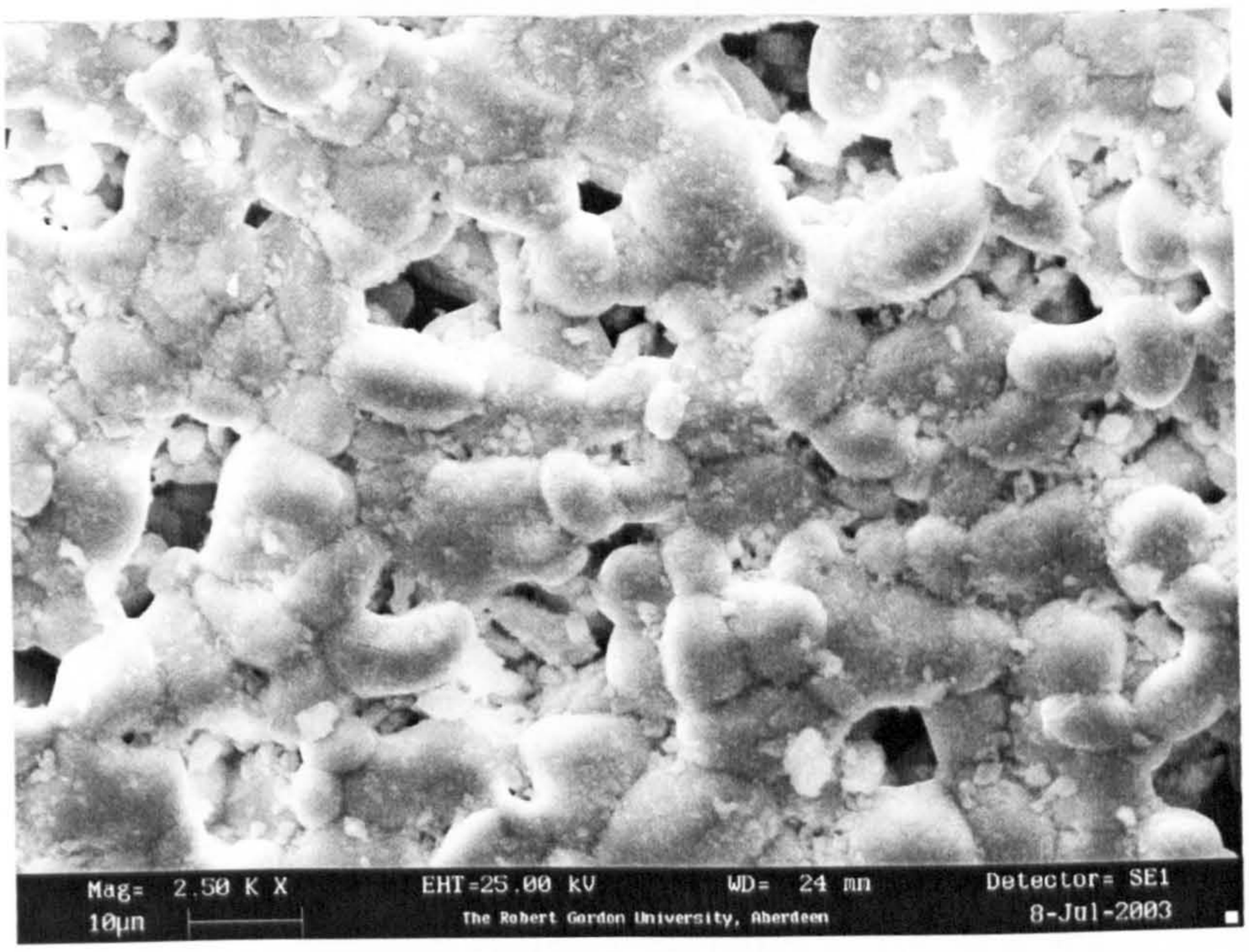

Figure 25: Rhodium catalytic membrane – SY05

3.7.4.3. EDXA

The quantitative analyses of the samples were also evaluated.

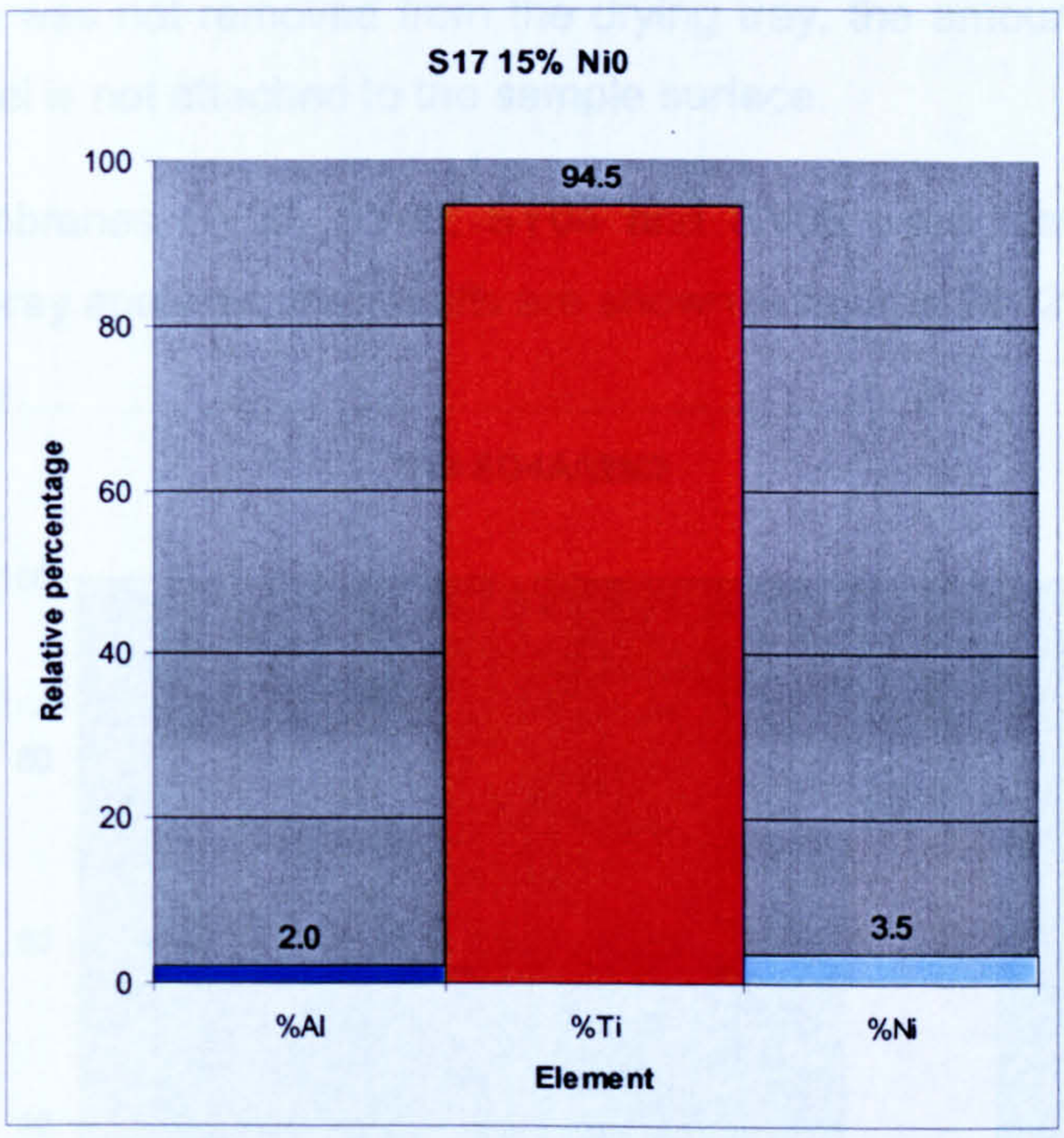

Figure 26: EDXA – CSY01

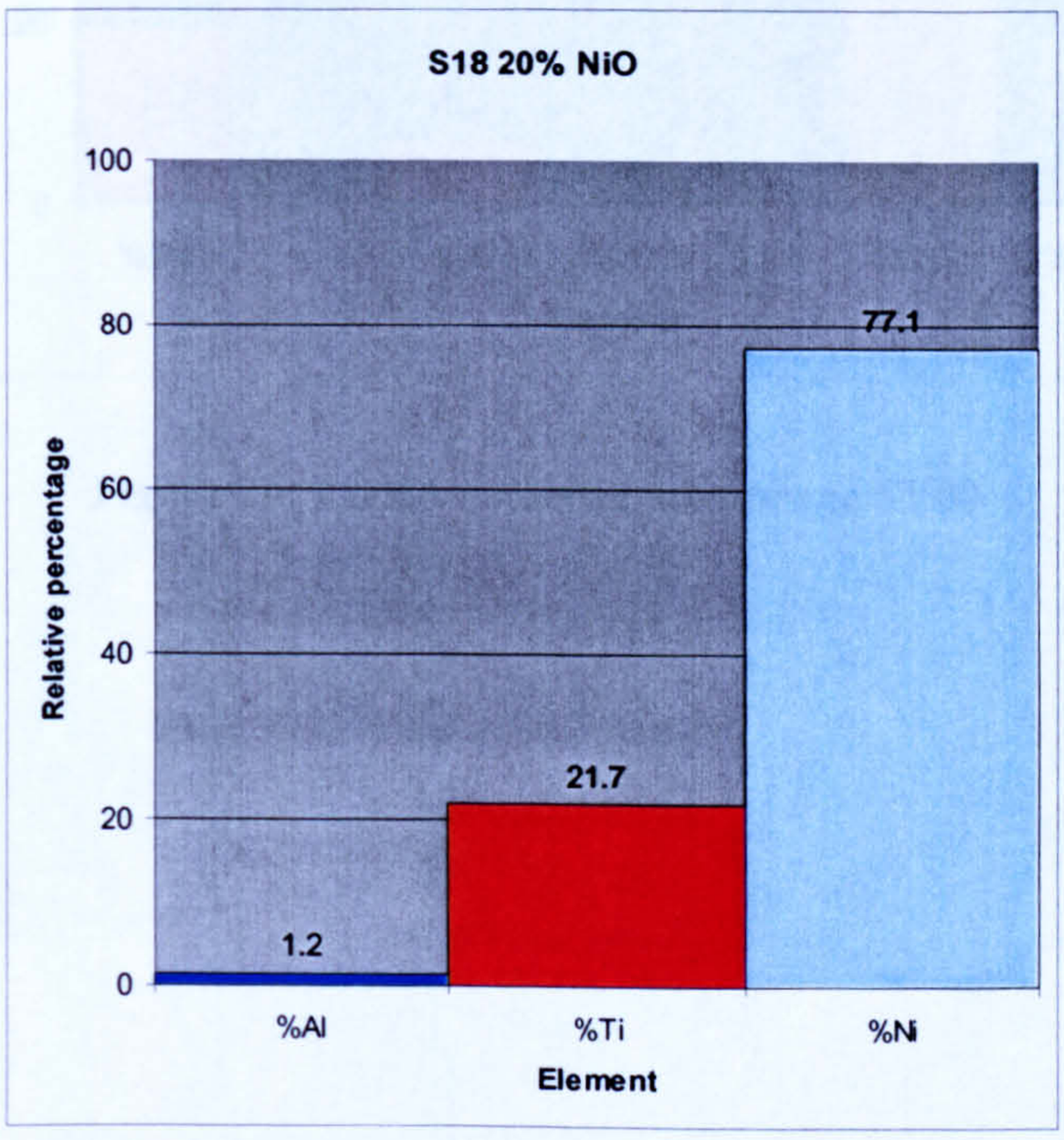

Figure 27: EDXA – CSY02

From these samples (Figures 26 and 27) is possible to observe the non-attachment of the nickel onto the ceramic material. For the samples where the solution was removed from the drying tray, the amount of nickel is minimal. On the other hand, on the sample where the solution was not removed from the drying tray, the amount of nickel is much higher but the nickel is not attached to the sample surface.

The catalytic membranes SY00, SY02, SY04 and SY05 were also analysed on the energy disperse X-ray analyser; the results are shown in figures 28, 29, 30 and 31.

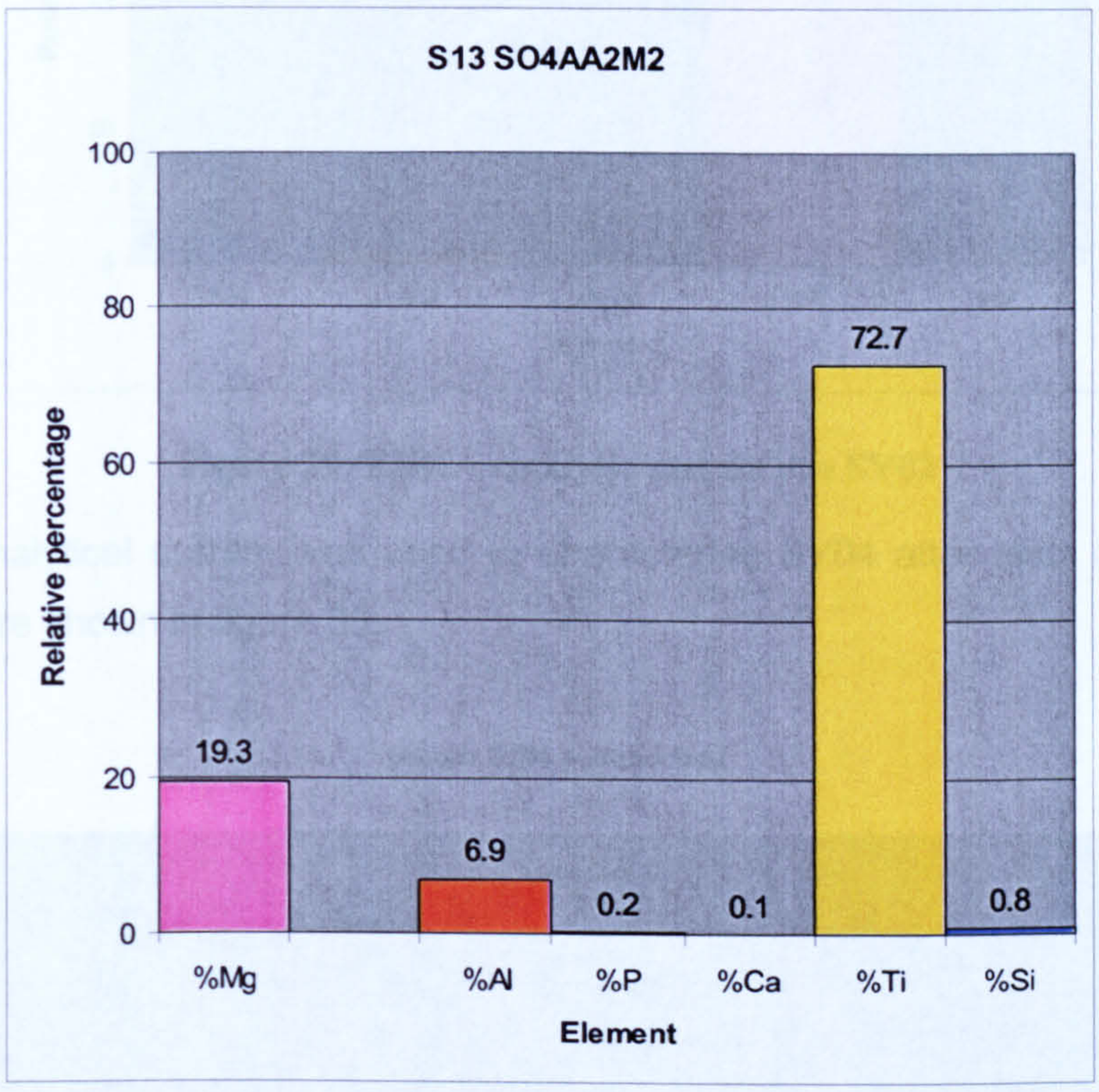

Figure 28: EDXA catalytic membrane SY00

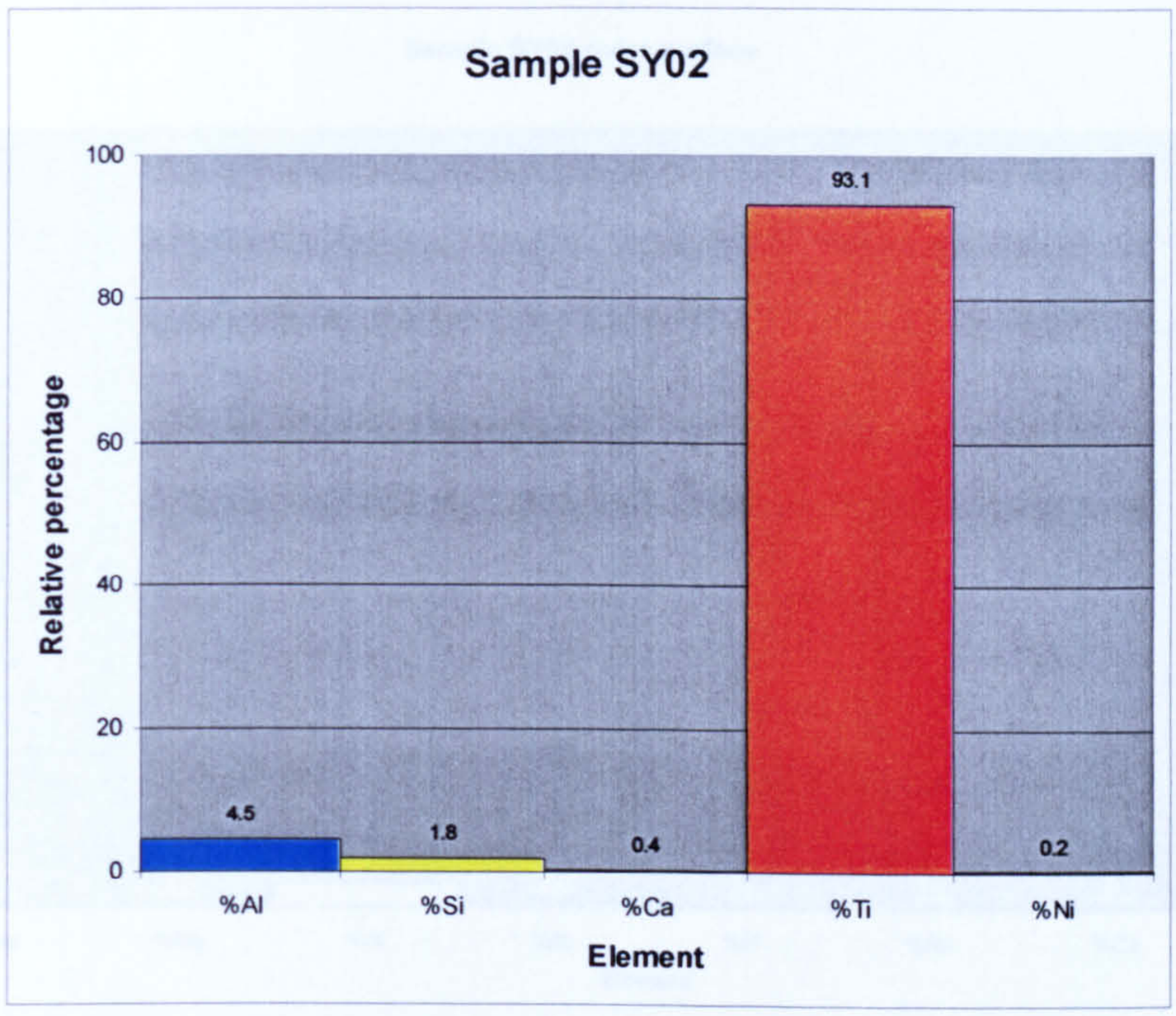

Figure 29: EDXA catalytic membrane SY02

The same analytical system was used to characterise SY04 after tests in the reactor. The results are shown in figure 30.

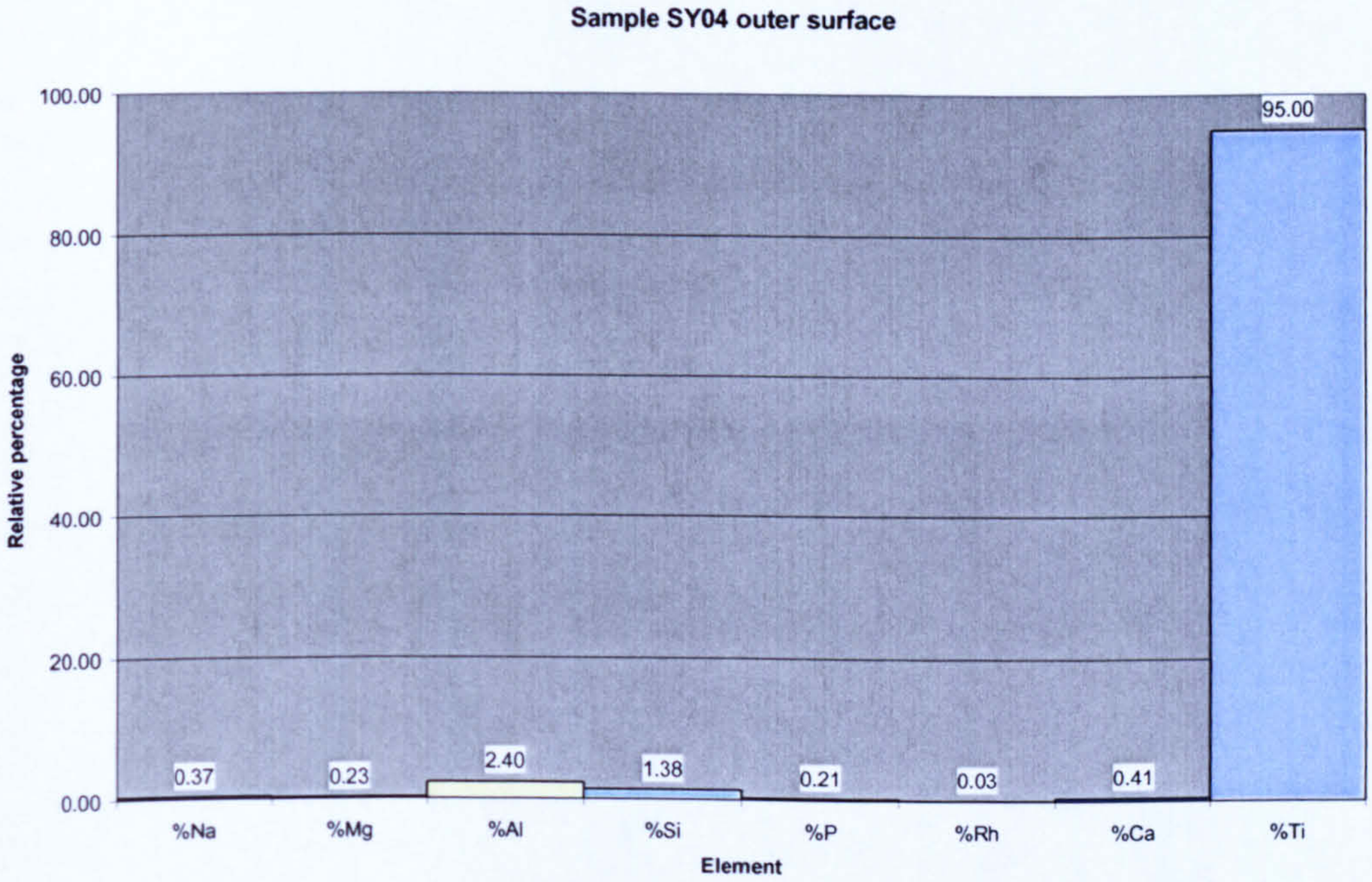

Figure 30: EDXA catalytic membrane SY04 (outer surface)

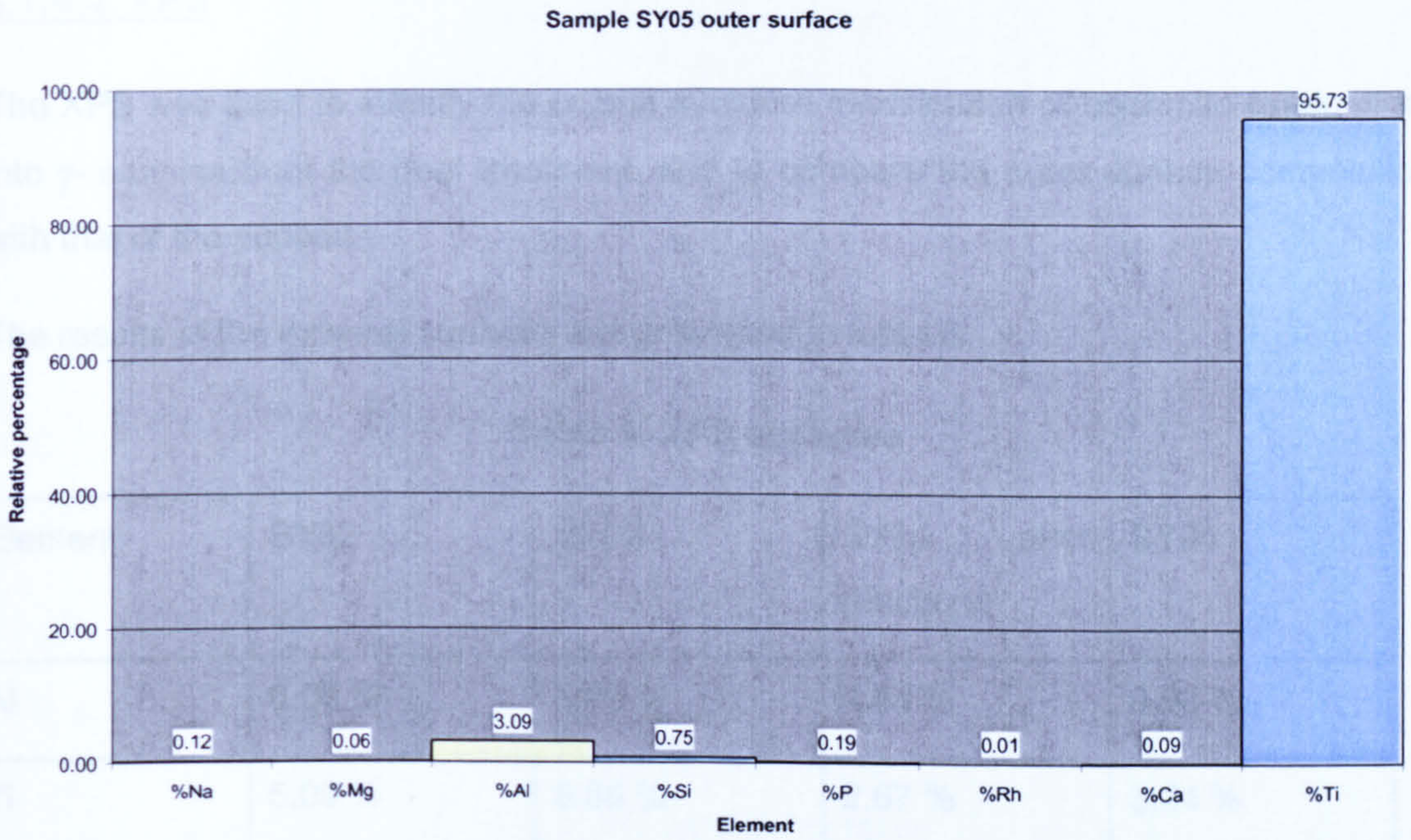

Figure 31: EDXA catalytic membrane SY05 (outer surface)

From Figure 29 can be observed that the nickel coating is not very effective for the catalytic membrane. From the 15% expected, only 0.2% was obtained.

3.7.4.4. XPS

The XPS was used to identify the crystal structure modification of boehmite (α-alumina) into γ- alumina from the heat treatment, and to compare the outer surface composition with that of the support.

The results of the external surfaces are presented in table 8.

Table 8: XPS analyses

Element	SY02	SY03	SY04 after reactions	SY05
Al	6.06 %	8.90 %	4.41 %	9.98 %
Ti	5.09 %	5.38 %	2.67 %	3.24 %
Si	12.74 %	4.94 %	4.44 %	0.43 %
Ca	0.60 %	1.34 %		0.19 %
C	19.40 %	24.57 %	58.36 %	21.69 %
P		1.09 %		
Rh		2.51 %	2.12 %	2.76 %
O	56.10 %	51.26 %	26.99 %	61.7 %

3.7.5. PRELIMINARY TEST RESULTS

Reaction tests were carried on with the rhodium based catalytic membrane SY04. These preliminary tests permitted the optimisation of the test rig. Figure 32 shows the concentrations of the reactants in the outlet stream.

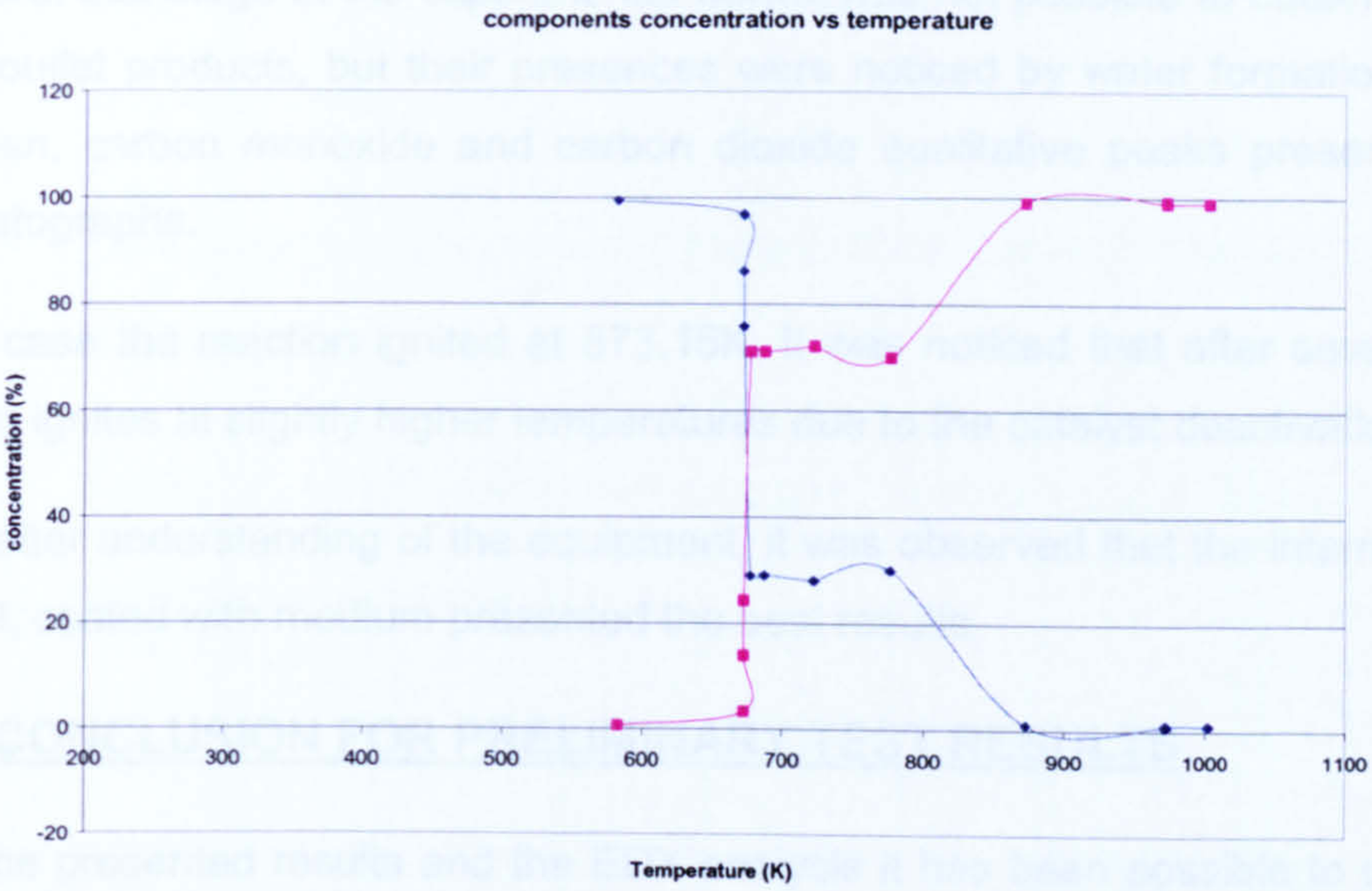

Figure 32: Screening tests

There are three distinct regions in the plot when the concentrations of the reactants at the reactor exit are plotted against the temperature.

Region 1 (473.15K-673.15K)

In this region there is very little reaction and the exit concentrations are constant.

Region 2 (673.15K-773.15K)

Above 673.15K, there is a decrease in the oxygen concentration at the reaction exit, indicating that chemical reaction is now taking place.

Region 3 (>773.15K)

Above 773.15K, the oxygen concentration decrease monotonically until complete conversion is observed at 873.15K. As expected the methane now shows an apparent increase since there is no oxygen.

3.7.6. DISCUSSION OF PRELIMINARY TEST RESULTS

Preliminary tests with Rhodium based catalytic membrane have shown that it is possible react methane and oxygen using the designed stainless steel reactor and the impregnated membrane.

In the first trial stage of the experimental work it was not possible to obtain the amounts of the outlet products, but their presences were noticed by water formation and by the hydrogen, carbon monoxide and carbon dioxide qualitative peaks present in the gas chromatographs.

In this case the reaction ignited at 873.15K. It was noticed that after several runs, the reaction ignites at slightly higher temperatures due to the catalyst deactivation effect.

After better understanding of the equipment, it was observed that the internally modified support, coated with rhodium presented the best results.

3.7.7. CONCLUSION FOR PRELIMINARY TEST RESULTS

From the presented results and the EDX analysis it has been possible to conclude that the nickel coating is not successful. Therefore, in subsequent experiments, the system was optimised as the reaction system was better understood and the analytical system was effectively calibrated.

3.8. KINETIC EXPERIMENTAL PROCEDURE

Kinetic experiments were carried out using the membrane giving the best results (SY05).

The variables under investigation were the feed ratio of methane and oxygen and consequently the total feed rate and the temperature of the reaction. A summary of the experimental variables and their range is presented in Table1.

The bulk of the experiments involved variation of the feed ratio and composition at predetermined temperature level and the variation of temperature at a selected feed ratio and composition. Kinetic studies were conducted under conditions of constant catalyst load.

A total of five kinetic runs were carried out altogether. They are summarised as it follows:

Run 1 – Flow rate is maintained constant, varying temperature. (6 measurements)

Run 2 – Temperature is maintained constant, varying oxygen feed flow rate (7 measurements)

Run 3 – Temperature is maintained constant, varying methane feed flow rate (6 measurements)

Run 4 – Temperature is maintained constant, adding nitrogen to the feed stream (5 measurements)

Run 5 – Temperature is maintained constant, adding carbon dioxide to the feed stream (5 measurements)

Table 9: Kinetic Runs

	Run 1	Run 2	Run 3	Run 4	Run 5
Temperature [K]	873.15-1083.15	1023.15	1023.15	1023.15	1023.15
O_2 feed flow rate [ml/min]	15	15-75	75	15	15
CH_4 feed flow rate [ml/min]	150	150	150-425	150	150
N_2 feed flow rate [ml/min]	-	-	-	0-60	-
CO_2 feed flow rate [ml/min]	-	-	-	-	5-60
Total feed flow rate [ml/min]	165	165-225	225-500	165-225	170-225

Kinetic runs were initiated after the catalyst calcination within the stainless steel reactor.

Standard gas was injected directly to the analytical system in order to check the equipment pre-calibration. If the retention times and compositions of the gases did not

match to the pre-calibration, normally due to different atmospheric conditions, a new calibration was done.

Once the analytical system was calibrated, the pre-determined feed flow rates were set in the mass flow controllers. Then, the heating of the reactor was turned on and the temperature was set at a pre-determined value by use of the power controller.

The feed delivery consisted of opening the on/off valves placed in front of the mass flow controllers in the feed system (Figures 3 and 4). Power supply to the heating tape was switched on and monitored by use of temperature display unit attached to the thermocouples located at different points over the entire length of the heated zone (see figure 8 and 9). The temperature in the reactor was monitored on a digital display unit (Figure 9).

The temperatures of the heating tapes were then allowed to stabilise. Steady temperature in the reactor was determined by constancy in several readings in the reactor over time.

Once the feed and reactor systems were stabilised, the analysis of the products would start by sending the products to the analytical system. Extended kinetic runs were carried out to asses the activity of the catalyst which decreased initially but attained a steady value after steady state has been reached as indicated by constancy in the experimental kinetic data.

For the tests involving variation of the feed composition, the temperature was allowed to stabilise; then the suitable adjustments to the feed flow rates in the mass flow controllers were made. Each different flow rate was sent to the analytical system.

Similarly for the tests involving the variation of reaction temperature, the feed rate was allowed to stabilise and suitable adjustment of the temperature was monitored by the heating system as described earlier.

All the different parameters were recorded and analysed by the analytical system. Once all the data was collected the oxygen feed system was closed by closing the cylinders and methane flow was maintained in order to purge the reactor until it reached room temperature. The reactor heating system was then switched off and the electronics of the analytical system also turned off. The detector oven and column oven of the gas

chromatograph was however kept active to maintain stability for subsequent experiments.

The needle valves of the reactor system were always maintained fully opened.

3.9. REACTOR DESIGN

3.9.1. INTERNAL DESIGN OF MEMBRANE

A cross-sectional view of the ceramic membrane is shown in figures 33 and 34. Pores are represented by cylindrical shapes for simplified analysis. The thickness of active porous layer and porous support layers are designated by t_1, t_2, t_3, t_4, and t_5, respectively, and r_1, r_2, r_3, r_4 and r_5 are the pore radii of their respective layers. Active support layers are formed of Rh impregnated α- and γ-alumina.

The materials selected must have similar thermal coefficients of expansion for adjacent layers. There is an advantage in selecting materials for the intermediate porous support layers, with expansion coefficients which gradually change from values near those for the active porous layer to values near those for the outer porous support layer. One way of achieving this, for instance, the porous support layer could contain 75% by weight of the material used in forming the active porous layer.

The above discussion does not exclude the use of identical materials in the active porous layer and the porous support layer. Such a material selection will eliminate chemical compatibility and differential thermal expansion problems but typically entails sacrifices in strength and material cost. The number of porous support layers will depend on the porous radius of the adjacent active porous layer, and will vary from a single layer for active porous layer with pore radii selected from the upper end of the specified range to as many as four for pore radii selected from the lower end of the specified range.

3.9.2. SYNGAS GENERATION PROCESS DESIGN

Figure 33 and 34 illustrate a composite membrane for syngas generation. An active porous layer is located at both sides facing the oxygen and methane containing gas, adjacent is a second active porous layer and is supported by layers with increasing pore radii, similar as before. Here the active porous layer on the bore side enhances the reaction between permeated oxygen and fuel species. Adjacent to the last porous

support layer is a layer of a reformer catalyst impregnated within the porous matrix. A process gas streams comprising a fuel, such as hydrocarbons and carbon monoxide, steam and recycle gas (H_2, CO, and CO_2) flows next to or through the catalyst impregnated layer. Since in this application fuel species have to diffuse to the bore side of the active layer and the adjacent porous layer, the gaseous environment at and near the bore of the active layer is less reducing than in the outer porous layers. As a result a complete or partial oxidation reaction will take place here with some reforming occurring as gas moves away from the active layers respectively. It is advantageous to coat pores of the last porous support layer with a reforming catalyst such as Rh to induce some endothermic reforming as combustion products flow through the porous support layer. This will assist in removing the heat of the exothermic oxidation reaction from the surface of the active porous layer. The gradient of oxygen activity in the porous layer will prevent damage to the active layers from exposure to very low oxygen partial pressures, thus permitting a greater degree of freedom in the selection of materials for these layers.

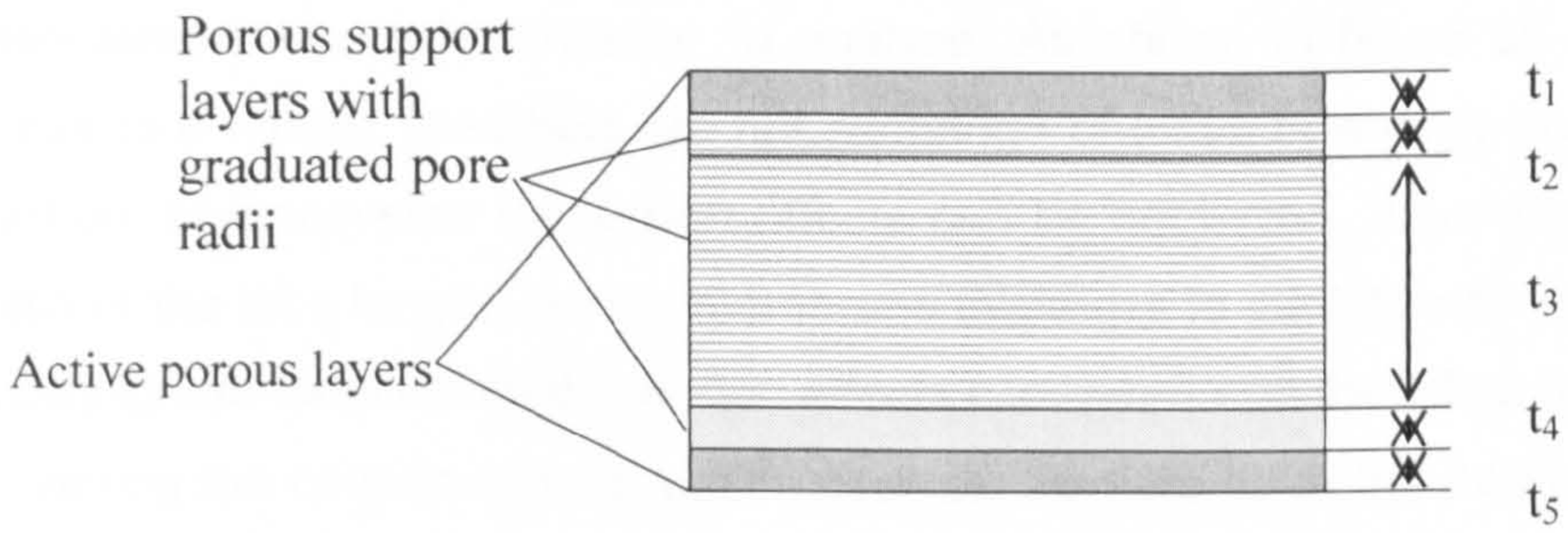

Figure 33: Cross-sectional view of ceramic membrane - thickness

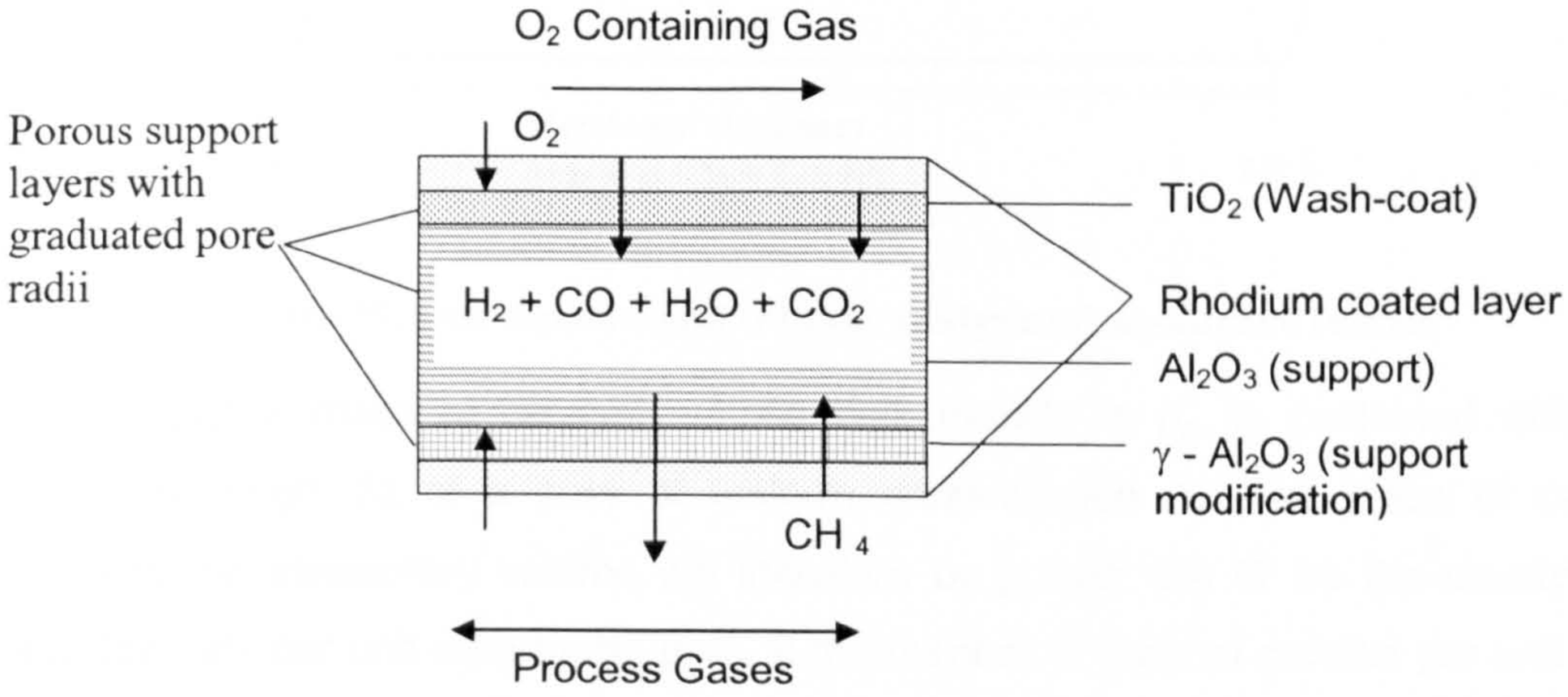

Figure 34: Cross-sectional view of ceramic membrane - reaction

3.9.3. MEMBRANE REACTOR DESIGN

The design equation for the isothermal fixed bed reactor with no longitudinal dispersion effects represents the simplest reactor to analyse. As shown in figure 35 each pore approximates to a tubular fixed bed. No net exchange of mass or energy occurs in the radial direction, so transverse dispersion effects can be neglected. If we also suppose that the ratio of the tube length, i.e. the membrane thickness to particle size is large then we can safely ignore longitudinal dispersion effects compared with the effect of bulk flow. Hence, in writing the conservation equation over an element δz of the thickness of the membrane (figure 35) may be considered that the fluid velocity u is independent of radial position. This implies a flat velocity profile (plug flow conditions) and ignores dispersion effects in the direction of flow.

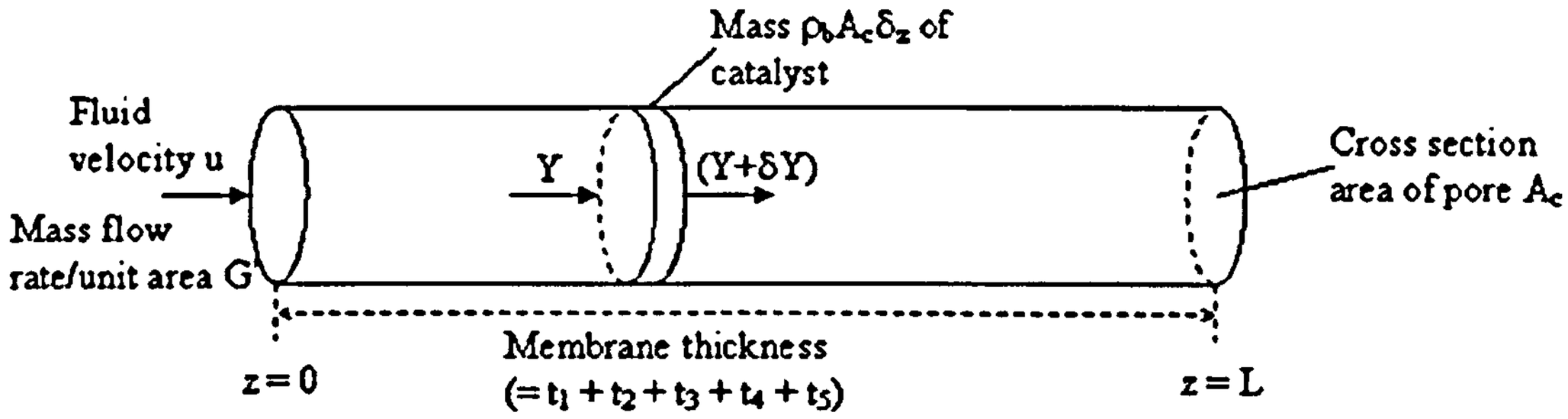

Figure 35: One dimensional tubular analysis of membrane reactor

Suppose that a mass of catalyst, whose bulk density is ρ_b, is contained within an elementary length δz of a pore of uniform cross-section A_c. The mass of catalyst occupying the elementary volume will therefore by $\rho_b A_c \delta z$. Let G' be the steady state mass flow rate per unit area to the pore. If the number of mols of product per unit mass of fluid entering the elementary section is Y and the amount emerging is (Y+δY), the net difference in mass flow per unit area across the element will be G'δY. In the steady state this will be balanced by the amount of product formed by chemical reaction within the element so:

$$G'\delta Y = \Re_Y^M \rho_b \delta_Z \qquad \textbf{Equation 1}$$

where the isothermal reaction rate $\Re_Y^M$ is expressed in units of mols per unit time per unit mass of catalyst. To calculate the length (please note that length in this case is the thickness of the membrane) of the reactor required to achieve a conversion corresponding to an exit concentration Y_L equation 1 is integrated from Y_0 to Y_L where the subscripts 0 and L refer to inlet and exit conditions respectively. Thus:

$$L = \frac{G'}{\rho_b} \int_{Y_0}^{Y_L} \frac{dY}{\Re_Y^M} \qquad \textbf{Equation 2}$$

The mass of catalyst *W* contained within this length will be $\rho_b L A_c$ while the residence time, clearly, will be $e\rho L/G'$ where ρ is the fluid density under the conditions of reaction. Replacing *L* by $W/\rho_b A_c$ it is possible to see that the residence time is $e\rho W/\rho_b G' A_c$, i.e. the void volume eW/ρ_b divided by the volumetric flow rate $G'A_c/\rho$, is equivalent to the quantity V/v for an unpacked tubular pore, where *V* is the pore volume and *v* the

volumetric flow rate. The reciprocal of the residence time $\rho_b G' A_c / e\rho W$ is the space velocity, useful for comparing reactor performance; the physical significance of this simply the rate of replacement of fluid within the void volume of the reactor.

When $\Re_Y$ is not a known function of Y an experimental programme to determine the chemical reaction rate is necessary. If the experimental reactor is operated in such a way that the conversion is sufficiently small – small enough that the flow of product can be considered to be an insignificant fraction of the total mass flow – the reactor is said to be operating differentially. Provided the small change in composition can be detected quantitatively, the reaction rate may be directly determined as a function of the mol fraction of reactants. On this basis a differential reactor only provides initial rate data. It is therefore important to carry out experiments in which products are added at the inlet, thereby determining the effect of any retardation by products. An investigation of this kind over a sufficiently wide range of conditions will yield the functional form of $\Re_Y$ and, by substitution in equation 2, the reactor size and catalyst mass can be estimated. If it is not possible to operate the reactor differentially conditions are chosen so that relatively high conversions are obtained and the reactor is now said to be an integral reactor. By operating the reactor in this way Y may be found as a function of W/G' and $\Re_Y$ determined, for any given Y, by evaluating the slope of the curve at various points.

4. RESULTS AND DISCUSSION

4.1. REACTOR CHARACTERISTICS/PERFORMANCE/STABILITY

Most reaction studies of partial oxidation of methane have been kinetic studies carried out using differential reactors. Because of the small dimensions of the catalyst beds employed, a reasonable approach to isothermal condition could be obtained. However, when higher conversions are sought, the amount of catalyst involved usually increases. The reactor used in this work can be considered isothermal due to the fact that the catalyst is contained only in a very small volume within the porous matrix of the membrane wall. The temperature is recorded by 5 different thermocouples placed along the 30cm of the reactor. However, methane partial oxidation is an exothermic process, with adiabatic temperature rises around 30K for every percentage point of increase in methane conversion [65]. It is therefore important to assess the magnitude of the temperature gradients in the bed when significant conversions are reached. The reaction zone is situated between 90cm and 275cm. Figure 36 shows the temperature profiles along the catalyst bed.

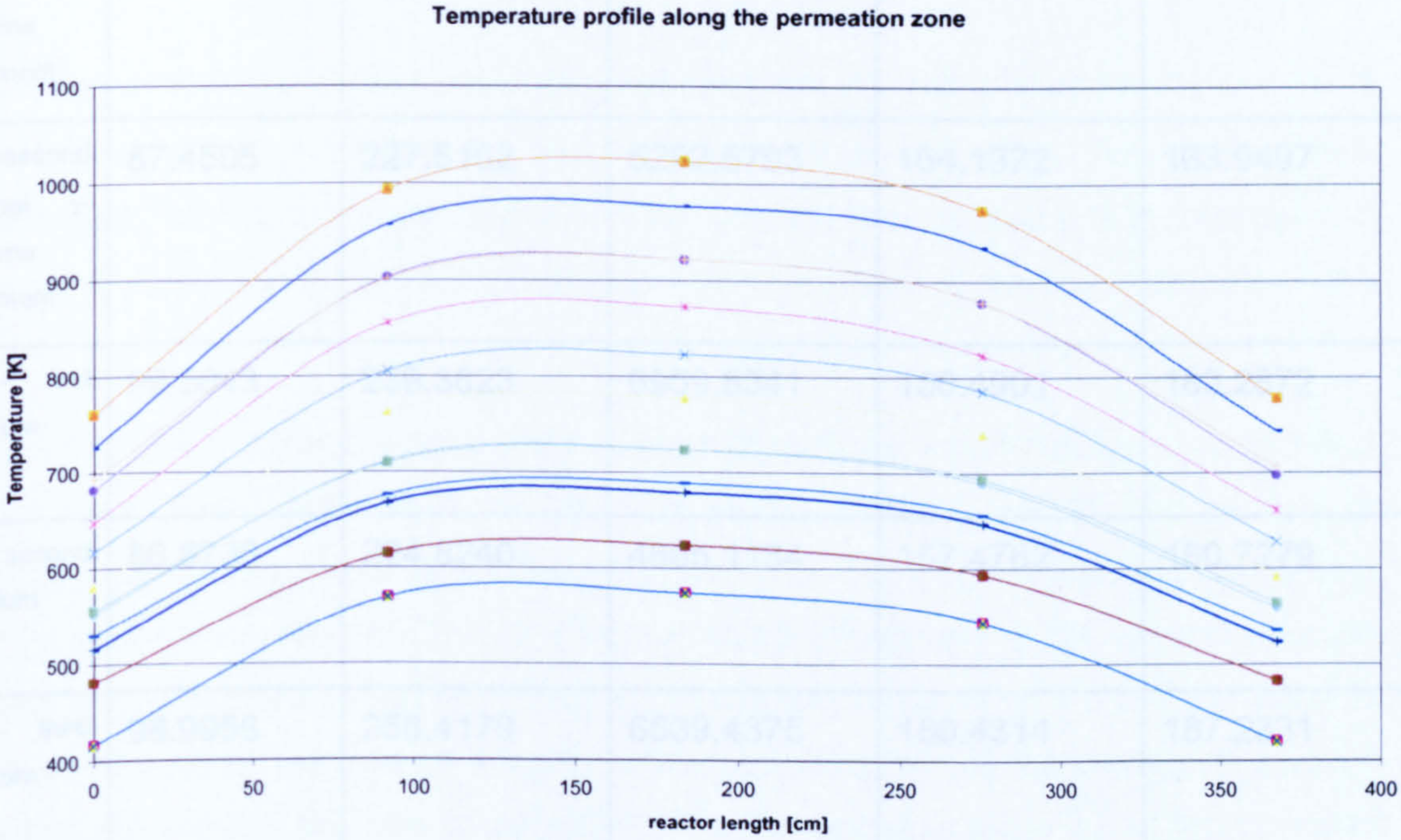

Figure 36: Reactor temperature profile

The temperature profile shows that over the length of the main reaction area, between the second and third thermocouple, the temperature is roughly constant. At both extremities, however the temperature is lower; this can be explained by the

limits of the heat insulation system and also by the heat exchange between the reactor and the exterior.

4.2. MEMBRANE CHARACTERISATION

4.2.1. ASAP

The surface area of the ceramic support considered for analysis (Table 10 and Figure 37) was determined on a single point (at P/Po 0.2), BET, Langmuir, BJH adsorption and BJH desorption, for cumulative surface area of pores between 1.7 and 300nm pore diameter.

Table 10: Surface area [m^2/g of sample]

Sample	Single Point	BET	Langmuir	BJH adsorption	BJH desorption
1 - row Support	99.6606	260.9962	7851.2779	181.4751	185.3435
2 - first internal γ-alumina treatment	86.7606	224.1342	4551.6301	173.0866	163.8798
3 – second internal γ-alumina treatment	87.4505	227.5162	5292.5793	164.1372	163.9497
4 – first rhodium coat	99.3643	259.3823	6959.8341	180.4901	183.2872
5 – second rhodium coat	86.8736	224.8240	4665.1134	157.4762	160.7279
4 – third rhodium coat	98.9956	258.4179	6539.4375	180.4314	187.2831
4 – fourth rhodium coat	86.7727	2243867	4534.7991	157.5856	161.1858
4 – after H_2 calcination	99.4755	261.4715	8763.9821	181.1238	169.7357

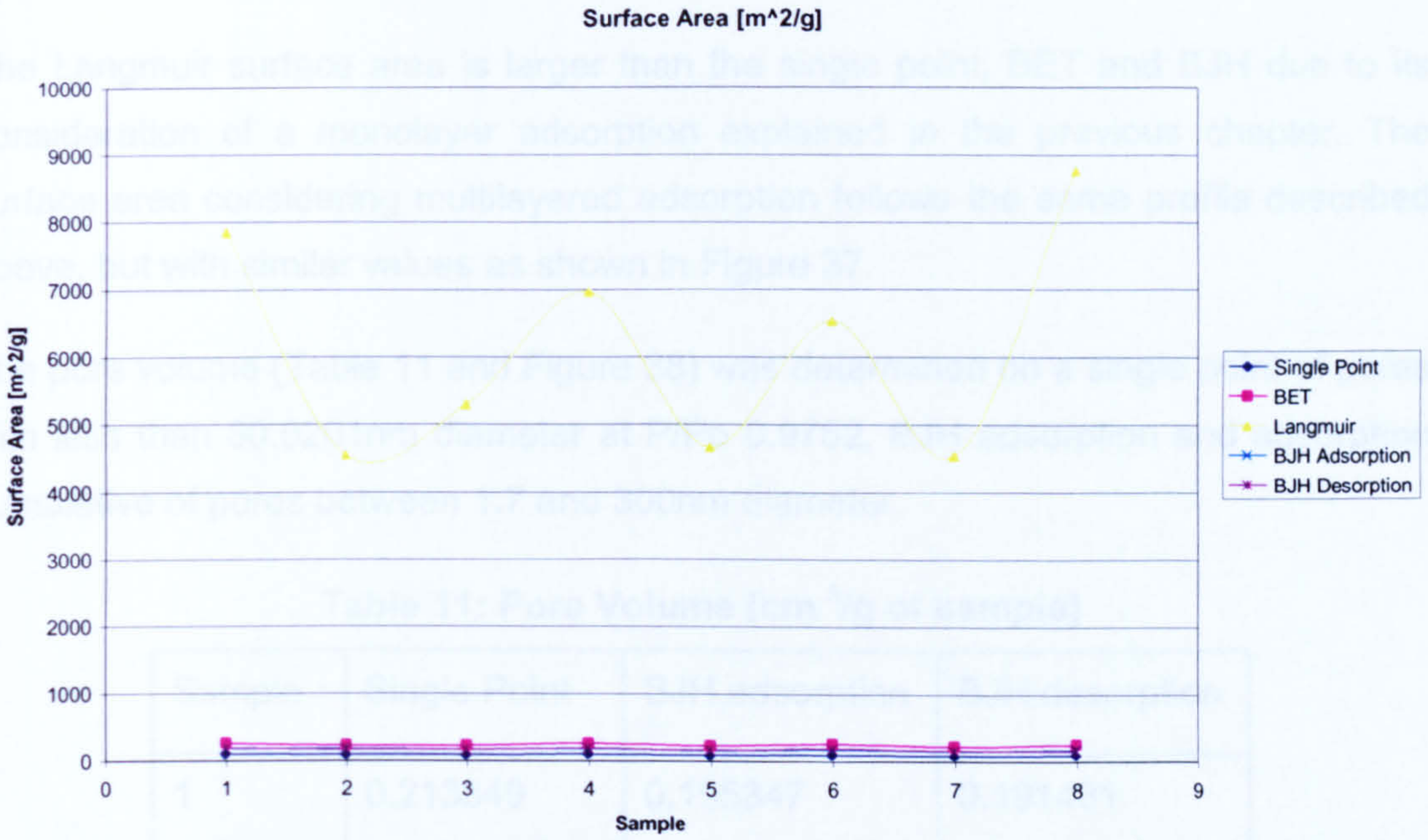

Figure 37: Effect of modifications on the surface area [m^2/g of sample]

The first γ-alumina modification shows the smallest surface area, probably due to its crystal structure, but after the second γ-alumina modification, the surface area increases, having a suitable value for the catalyst impregnation. It is important to remember that the γ-alumina modification occurred only in the inner surface of the tube.

After the first catalytic dip coating the surface area has a significant increase showing that by exposing both sides of the tube to the catalytic solution the catalyst is impregnated on the inner and outer tube surfaces. The second catalytic dip coating reduces the surface area. This can be due to the placement of the second catalytic layer on the top of the first layer and not inside the free pores. The trend is seen to occur throughout the third and fourth catalytic coating, where the third coat appears to occupy some of the free pores and the fourth coat sits on the top of the previous coated layers, thereby reducing the surface area.

After exposure of the prepared catalytic membrane to higher temperature in a hydrogen atmosphere, the rhodium chloride is reduced to its metallic form, and the crystals seem to be somehow rearranged. This rearrangement results in significant increase of the surface area. The final surface area is even larger than the ceramic

support surface area, optimising its surface/volume ratio and hence the catalytic activity of the membrane.

The Langmuir surface area is larger than the single point, BET and BJH due to its consideration of a monolayer adsorption explained in the previous chapter. The surface area considering multilayered adsorption follows the same profile described above, but with similar values as shown in Figure 37.

The pore volume (Table 11 and Figure 38) was determined on a single point of pores with less than 80.0201nm diameter at P/Po 0.9752, BJH adsorption and adsorption cumulative of pores between 1.7 and 300nm diameter.

Table 11: Pore Volume [cm ^{3}/g of sample]

Sample	Single Point	BJH adsorption	BJH desorption
1	0.213349	0.195347	0.191431
2	0.194703	0.180621	0.175126
3	0.199914	0.185261	0.185259
4	0.212418	0.193551	0.185821
5	0.184776	0.167976	0.160580
6	0.212508	0.194065	0.208827
7	0.185212	0.169191	0.161062
8	0.213523	0.195629	0.184523

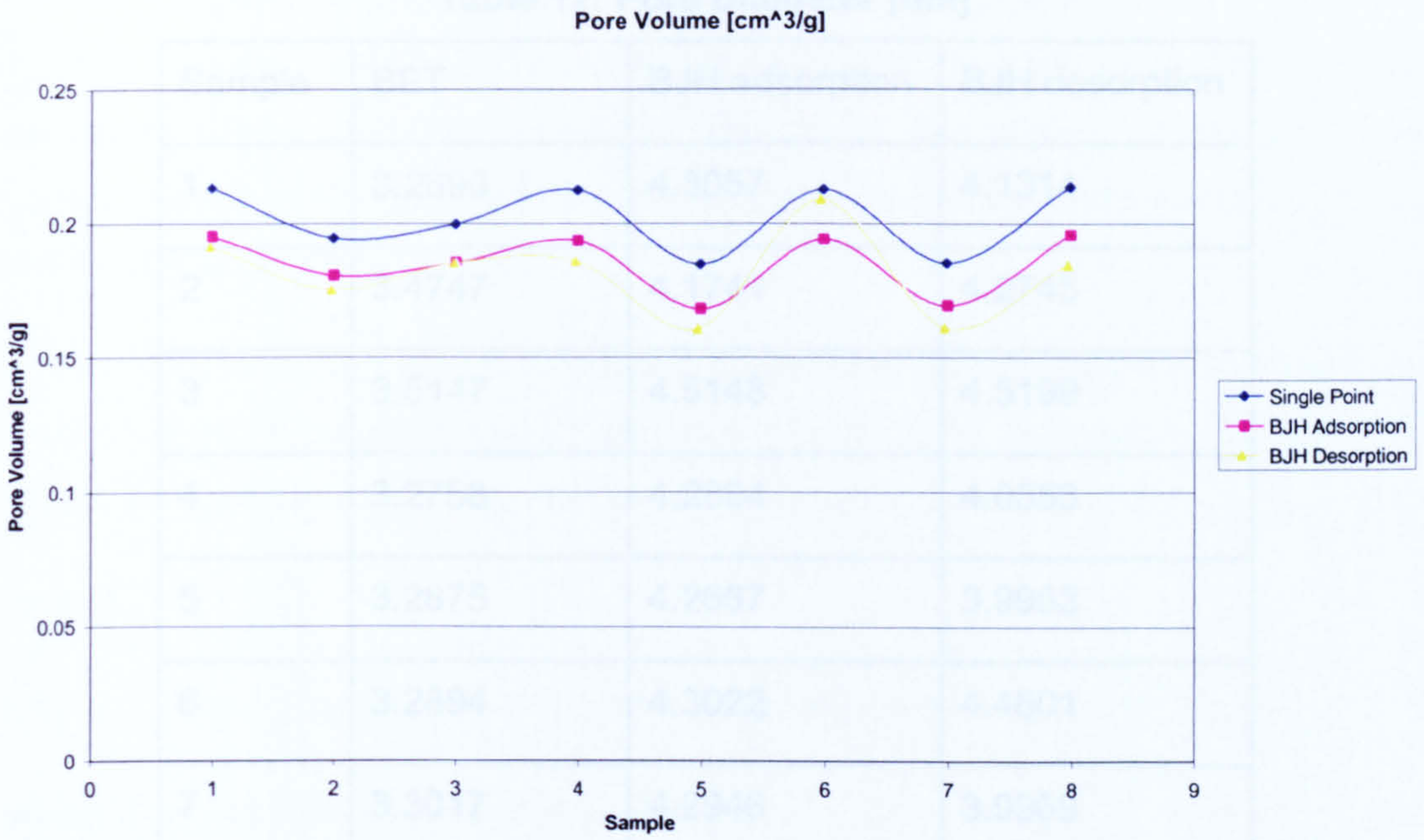

Figure 38: Effect of modifications on pore volume [cm^3/g of sample]

The pore volume also reflects the crystal structure. It can be observed that the first γ-alumina modification and heat treatment is not enough to affect the pore volume significantly, but after the second calcinations following the γ-alumina modification, the crystals appear to reorganise, as can be seen from the increase in pore volume and confirmed by the increase in pore diameter (Figures 38 and 39). The first catalytic coating takes place inside the pores of the modified support, as can be seen from the increase in pore volume and the decrease in pore diameter (Figures 38 and 39). This confirms that the third catalytic layer is deployed within the available free pores. The pore volume is slightly higher than the one for the first catalytic layer in a similar fashion to the increase in pore volume for the modified support to the first rhodium coating.

Calcinations with hydrogen activate the catalytic sites, increasing the pore volume. The deviation of the BJH desorption values can be explained by the possible entrapment of some nitrogen molecules inside the pores of the sample analysed.

As these values are related to the weight of the samples, some possible variation on the values specified need to be considered. The scale used was a digital scale with only one decimal number of accuracy.

The pore size (Table 12 and Figure 39) was determined by the average of pore diameter (4V/A by BET) and BJH adsorption and desorption average pore diameter.

Table 12: Pore Diameter [nm]

Sample	BET	BJH adsorption	BJH desorption
1	3.2698	4.3057	4.1314
2	3.4747	4.1741	4.2745
3	3.5147	4.5148	4.5199
4	3.2758	4.2894	4.0553
5	3.2875	4.2667	3.9963
6	3.2894	4.3022	4.4601
7	3.3017	4.2946	3.9969
8	3.2665	4.3203	4.3485

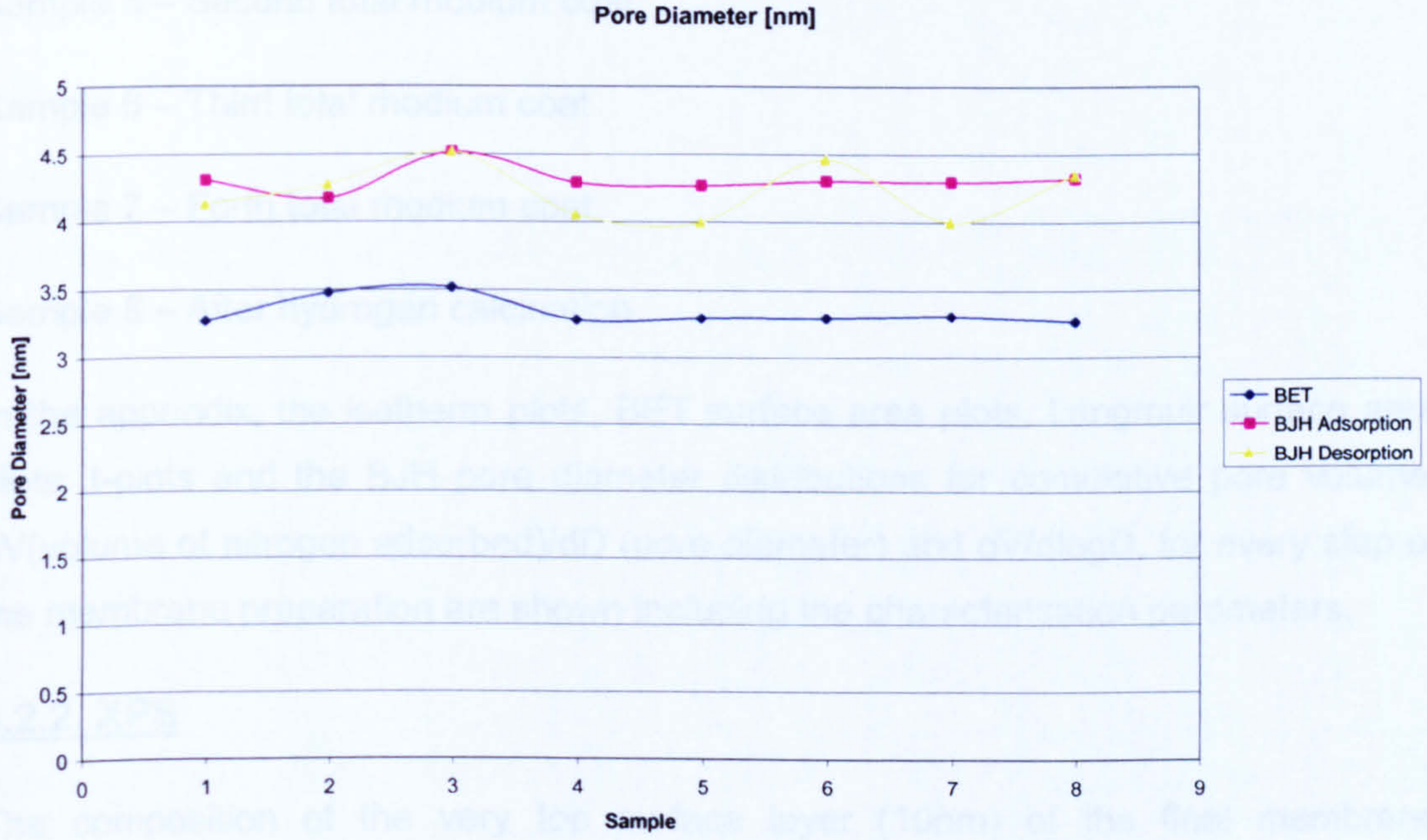

Figure 39: Pore Diameter [nm]

For monolayer adsorption, the characteristics of the samples as shown by the BET pore diameter increases with the γ-alumina support modification. This can be explained by impurities possibly present in the smaller pores of the raw support which after being submitted to an γ-alumina solution and heat treatment were

removed. Subsequent evidences (XPS and EDX analysis) confirm the presence of impurities in the samples. The same curve profile is noticed in the nitrogen desorption, where probably instead of impurities, the nitrogen molecules were trapped in the smaller pores of the raw support. This effect does not occur in the multilayered adsorption.

For the catalytic coating the pore diameter does not show any significant change, but it can be seen in the multilayered analysis that after the hydrogen calcination the catalyst is exposed as was indicated by the increase in pore diameter.

Where:

Sample 1 – Row support (α-alumina tube externally wash coated with titania)

Sample 2 – First internal γ-alumina treatment

Sample 3 – Second internal γ-alumina treatment

Sample 4 – First total rhodium coat

Sample 5 – Second total rhodium coat

Sample 6 – Third total rhodium coat

Sample 7 – Forth total rhodium coat

Sample 8 – After hydrogen calcination

In the appendix, the isotherm plots, BET surface area plots, Langmuir surface area plots, t-plots and the BJH pore diameter distributions for cumulative pore volume, dV(volume of nitrogen adsorbed)/dD (pore diameter) and dV/dlogD, for every step of the membrane preparation are shown including the characterisation parameters.

4.2.2. XPS

The composition of the very top surface layer (10nm) of the final membrane preparation steps was examined and the results are shown in tables 13 and 14.

As opposed to EDX, which gives information on the bulk material, the surface composition analysis can sometimes be misleading because of the possibility of surface contamination.

It is clear that the XPS results vary from the bulk composition data (EDX analysis 4.2. 4.). This is further discussed at the end of this section.

Table 13: XPS analysis – tube side

Sample	% Al	% Si	% Rh	% Ca	%Ti	% O	% C	% Cl	% F
1	10.36	8.17	0	2.15	8.71	47.29	23.32	0	0
2	10.53	3.1	0.1	0.67	10.44	51.95	23.21	0	0
3	15.5	2.47	0.62	0.72	9.91	54.7	16.09	0	0
4	13.08	2.55	1.14	0.14	9.59	50.64	22.85	0	0
5	12.39	3.07	1.17	0.18	8.65	52.21	21.94	0.4	0
6	16.23	3.02	0.15	0.05	8.14	53.13	19.42	0	0
7	14.91	2.66	0.14	0.13	9.7	53.34	19.11	0	0
8	16.07	2.83	0	0.04	7.22	54.23	19.6	0	0

Table 14: XPS analysis – shell side

Sample	% Al	% Si	% Rh	% Ca	%Ti	% O	% C	% Cl	% F
1	10.36	8.17	0	2.15	8.71	47.29	23.32	0	0
2	8.96	8.55	2.33	1.75	5.85	51.51	21.05	0	0
3	9.47	6.73	0.96	1.31	6.88	51.65	23	0	0
4	6.29	6.33	2.62	0.67	5.3	46.61	32.18	0	0
5	5.83	5.5	1.47	0.27	6.62	43.44	25.85	0.97	10.04
6	3.96	8.1	2.15	0.52	4.15	44.63	32.89	4.01	0
7	5.3	7.42	0.97	0.27	6.32	47.27	29.64	0	2.82
8	9.98	0.43	2.76	0.19	3.24	61.7	21.69	0	0

4.2.3. SEM

Scanning electron microscopy (SEM) confirms the observations from the nitrogen adsorption characterisation, presenting in a pictorial view the modifications to the crystal structures in the various steps during the membrane preparation.

γ-alumina modification is clearly visible on the inner pore structure. The increase in pore diameter is clear, confirming the ASAP for monolayer analysis (BET).

The effectiveness of the first two rhodium impregnations can also be observed, and no major modification occurred on the surface following subsequent impregnations. The decrease in pore diameter and rhodium deposition is also evident from the SEMs.

Rhodium depositions can be observed on the SEMs and a very clean surface is shown on figure 55 for the sample after the heat treatment in hydrogen atmosphere.

SEMs with different magnifications are shown in Figures 40-55. The outer surface micrographs show the non-homogeneity of the surface, for example the support has a flat area that can be simply structural modification during its extrusion in the manufacturing process. The non-homogeneity is less evident after the heating for the γ-alumina modification.

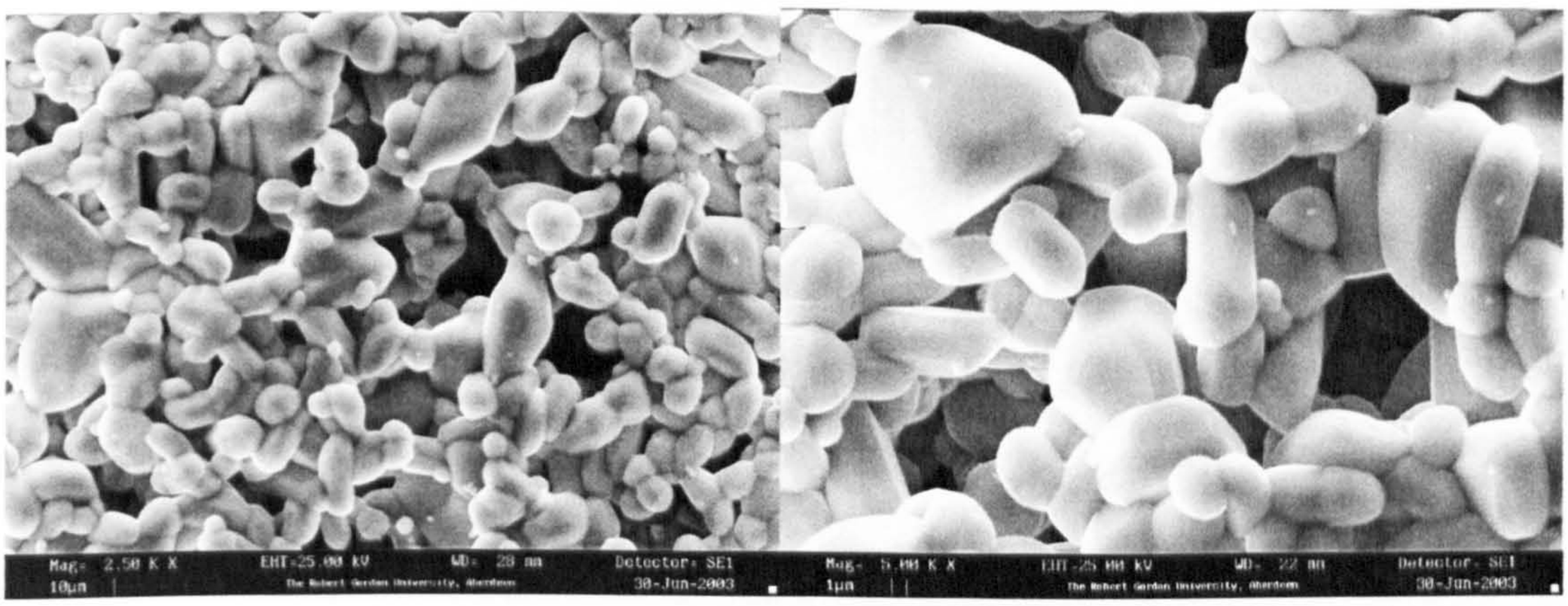

Figure 40: Sample 1 inner surface

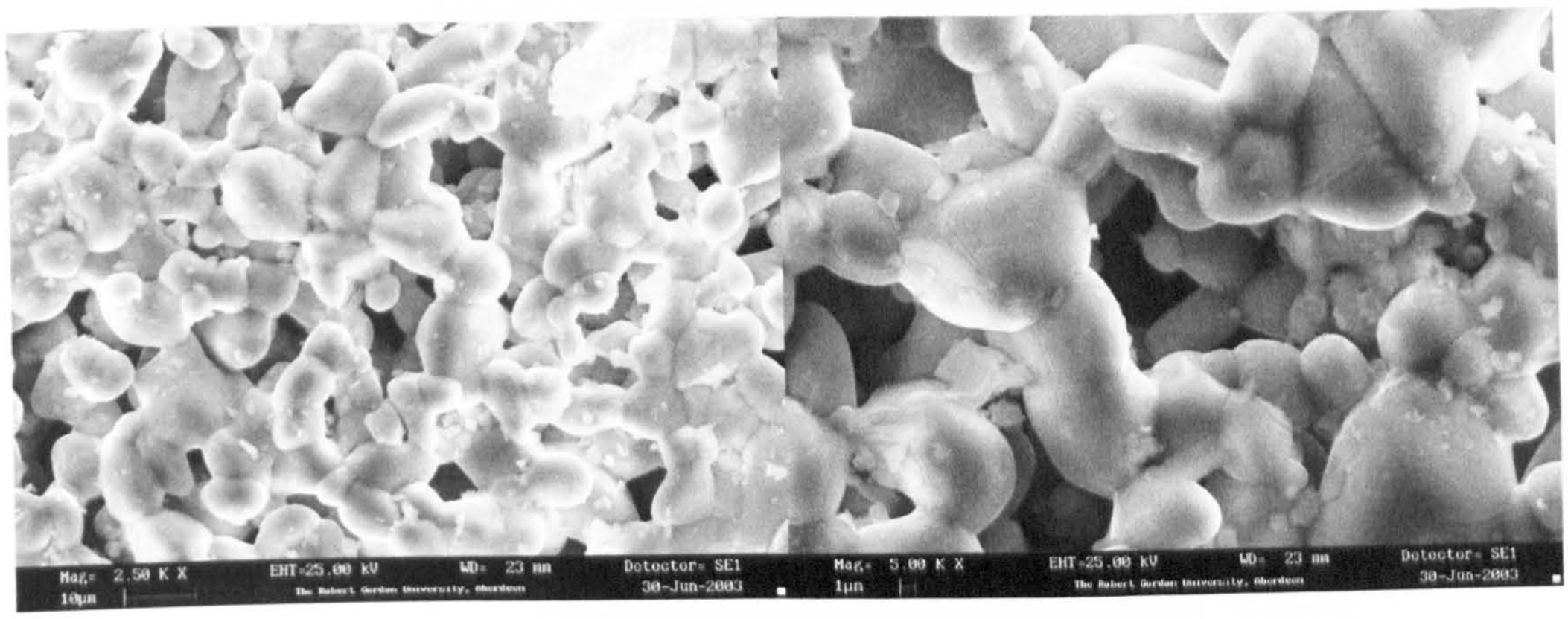

Figure 41: Sample 2 inner surface

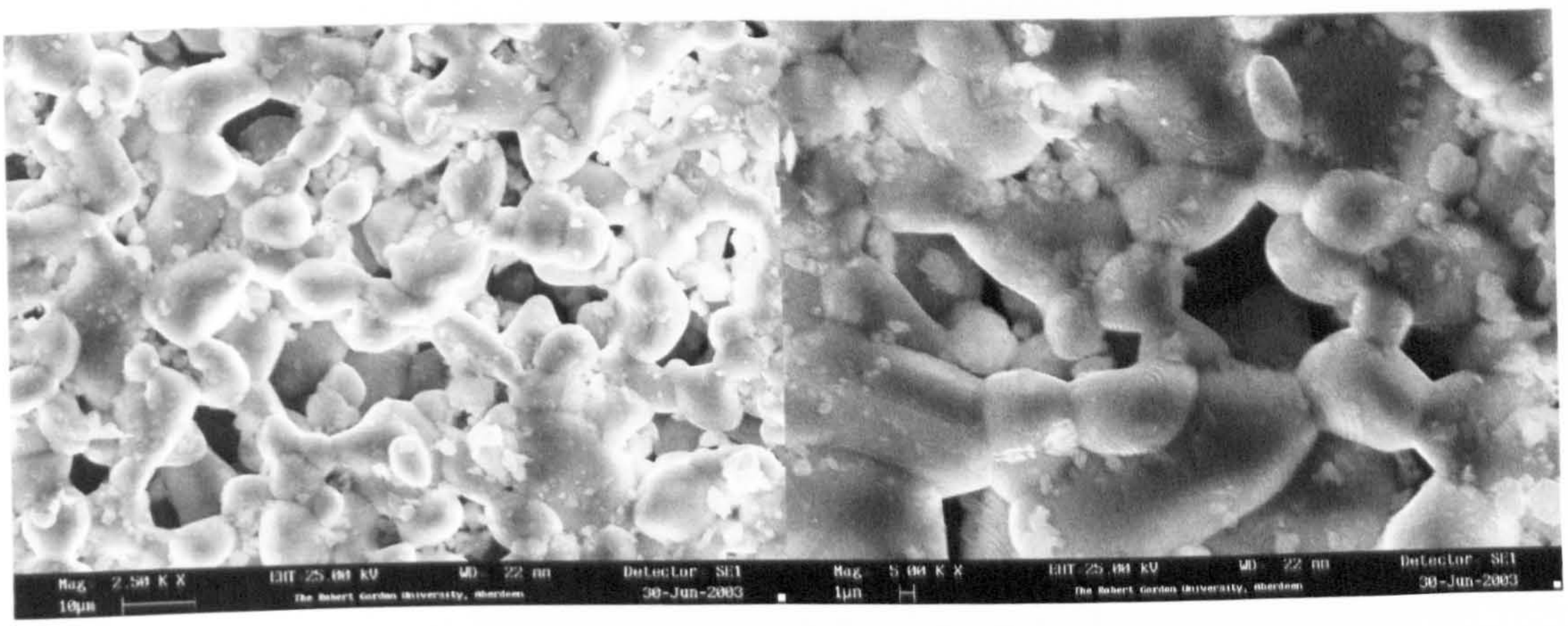

Figure 42: Sample 3 inner surface

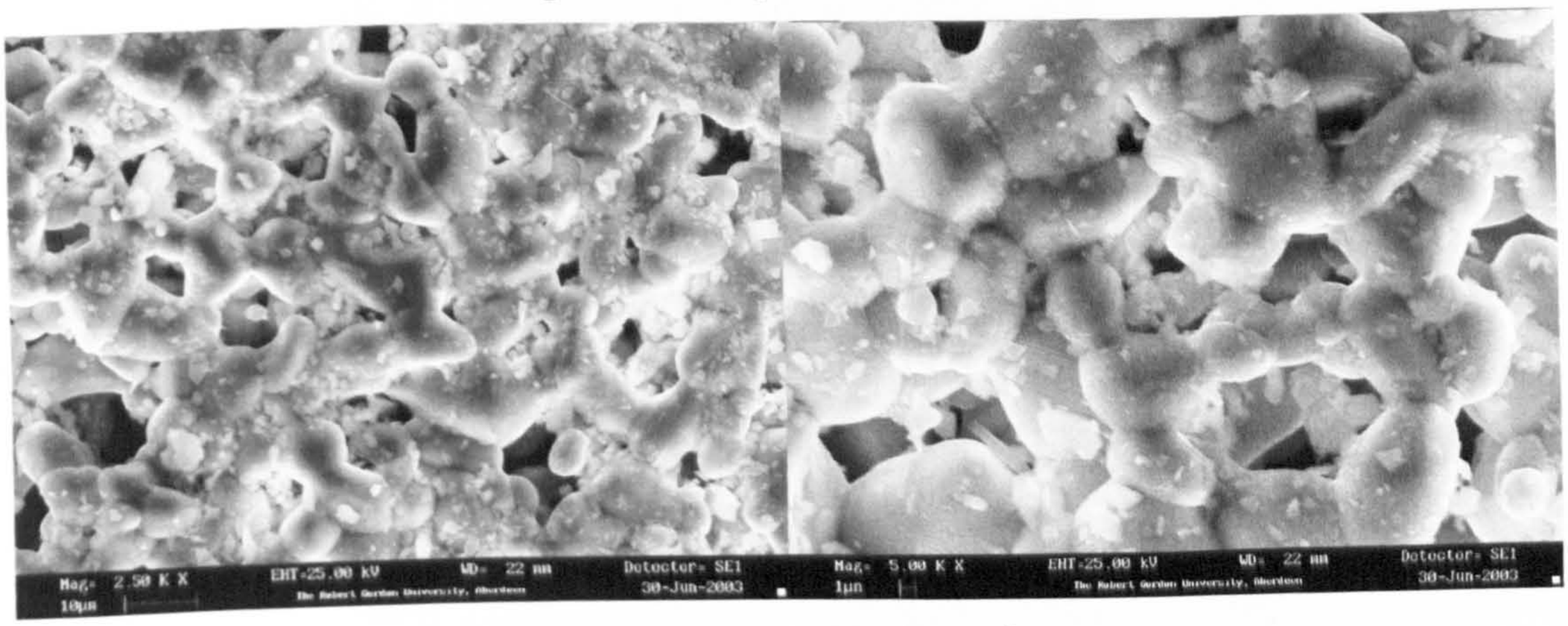

Figure 43: Sample 4 inner surface

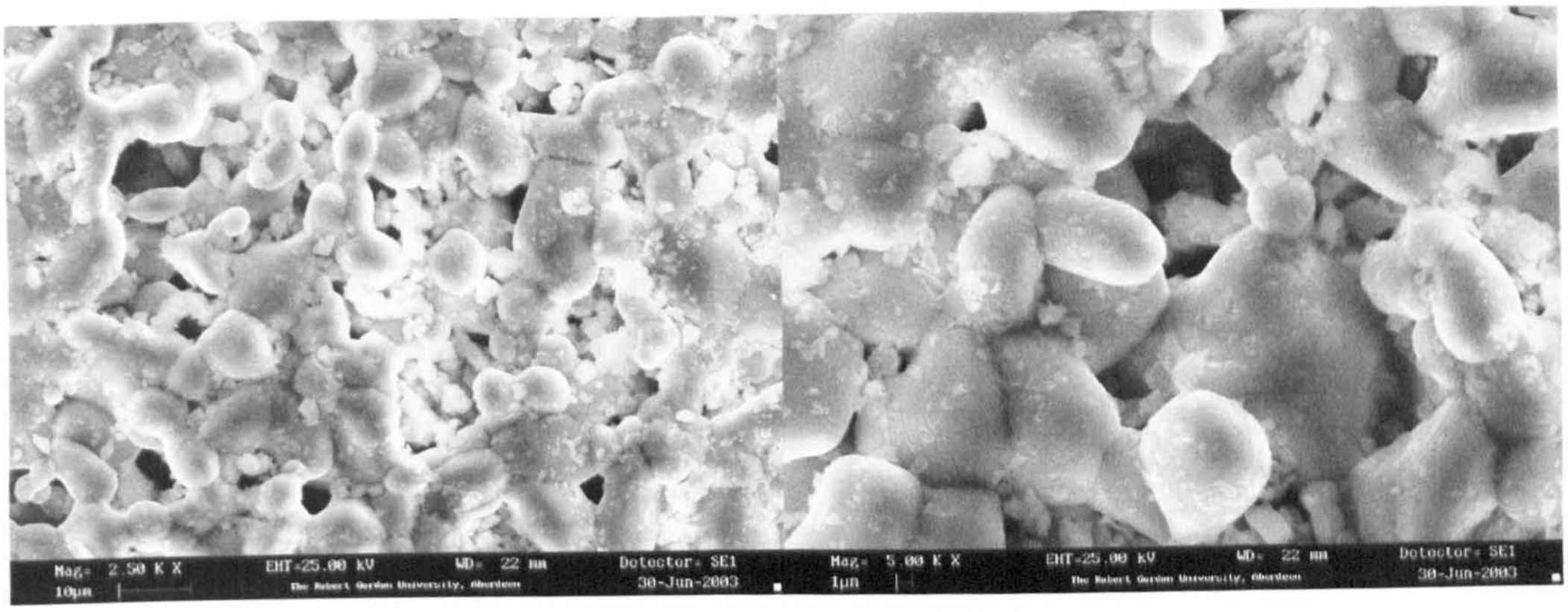

Figure 44: Sample 5 inner surface

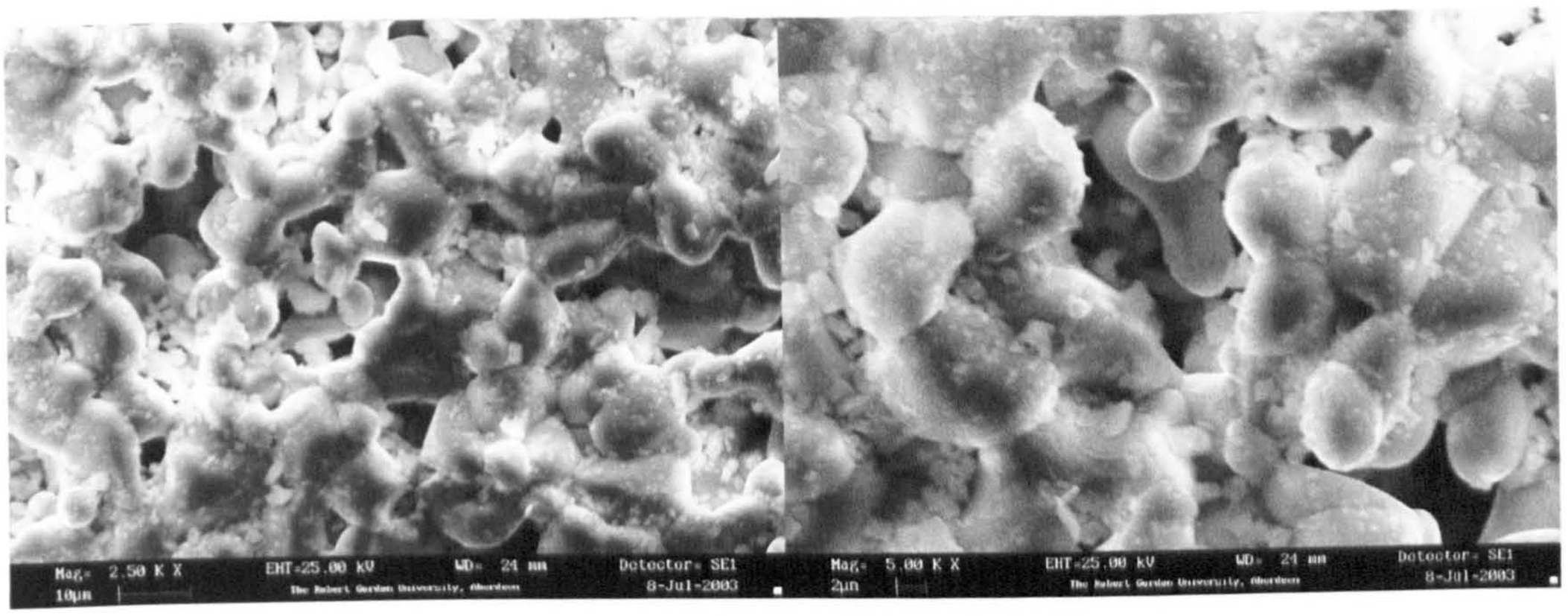

Figure 45: Sample 6 inner surface

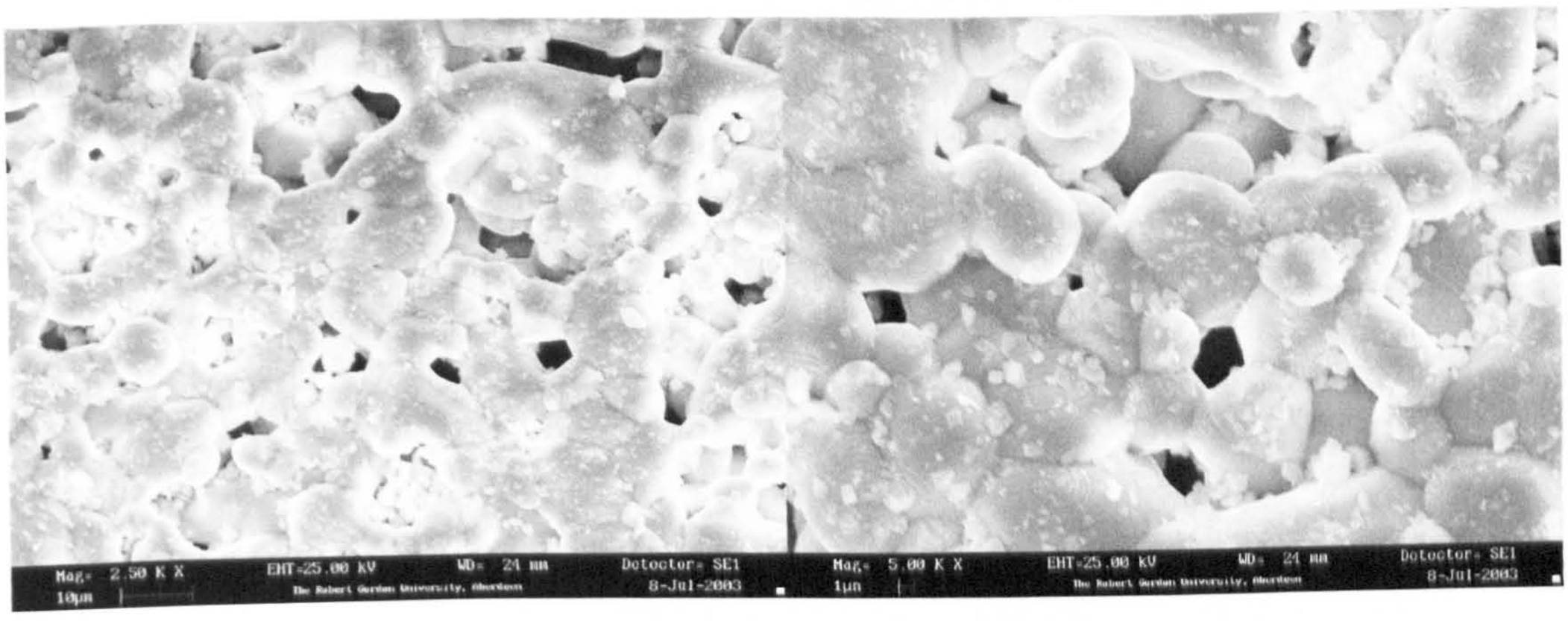

Figure 46: Sample 7 inner surface

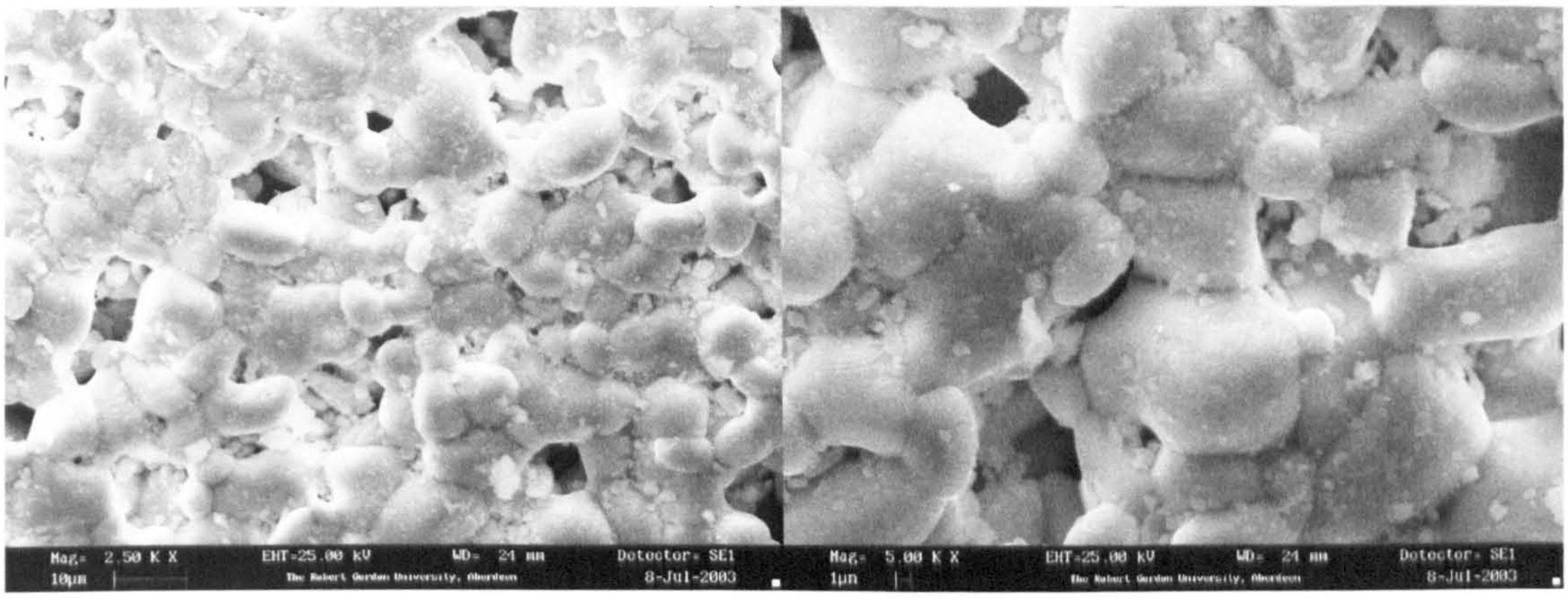

Figure 47: Sample 8 inner surface

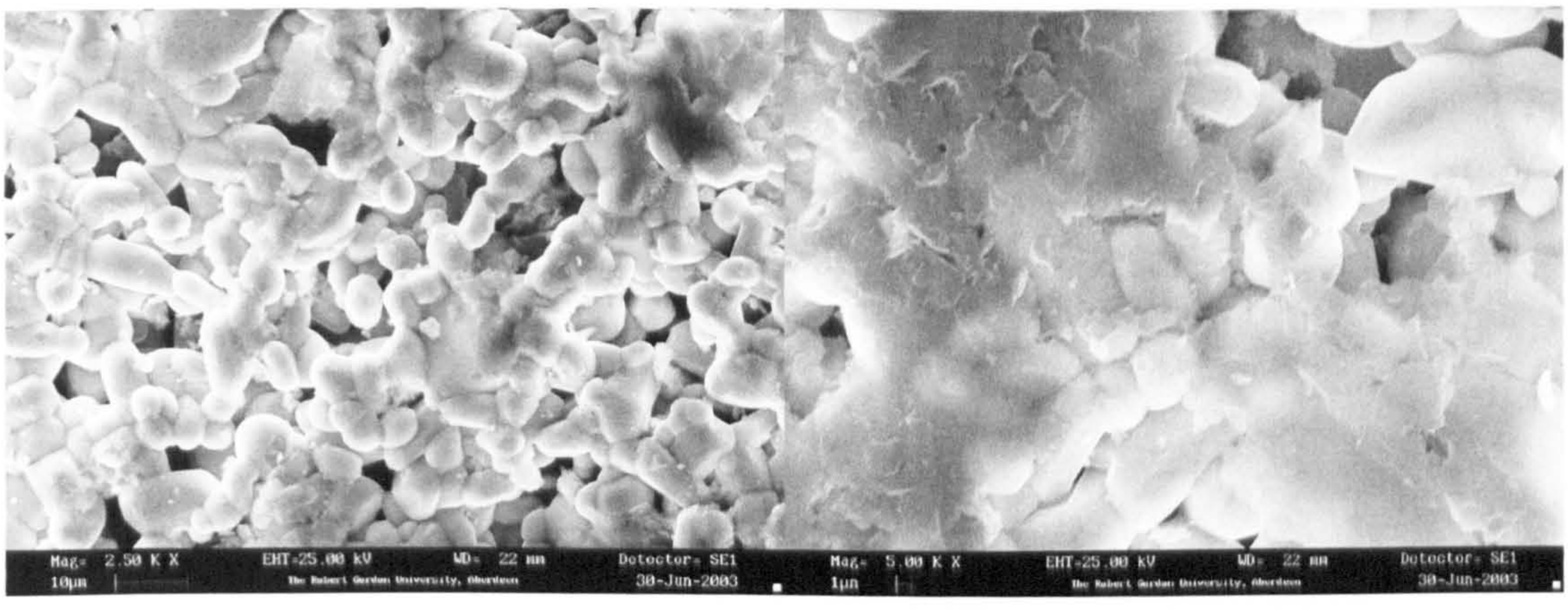

Figure 48: Sample 1 outer surface

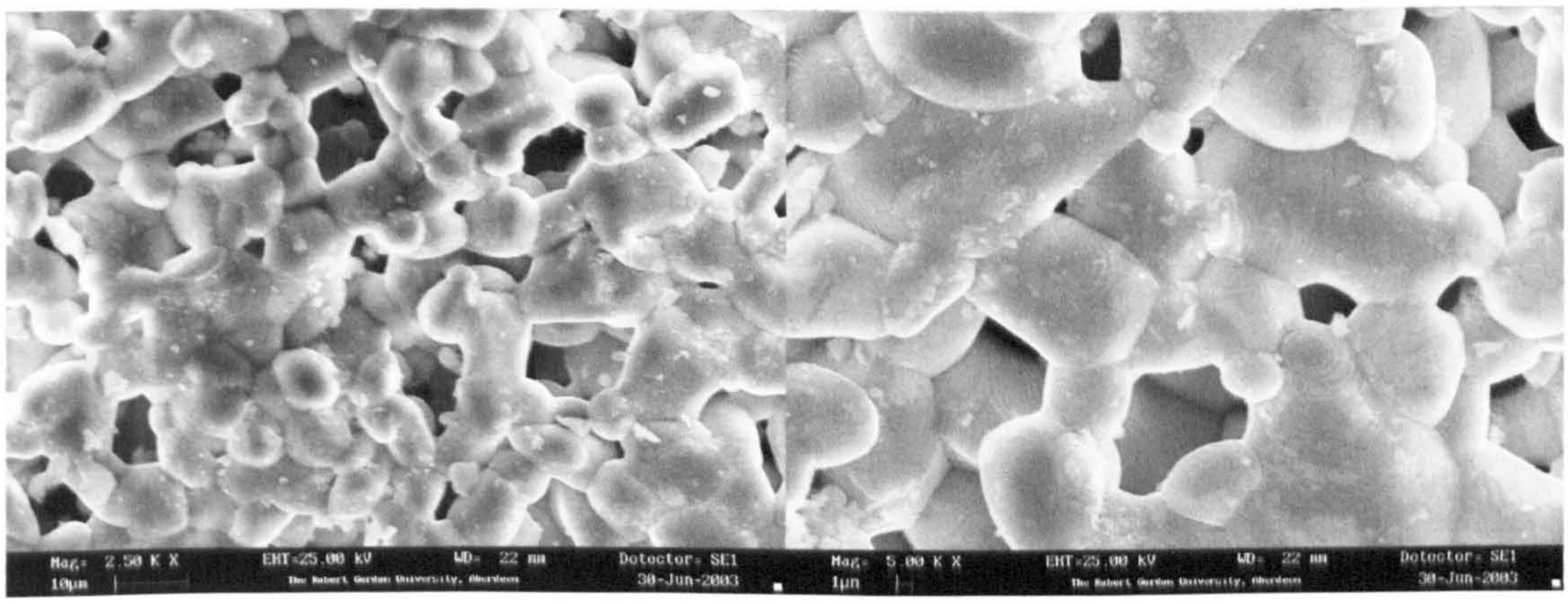

Figure 49: Sample 2 outer surface

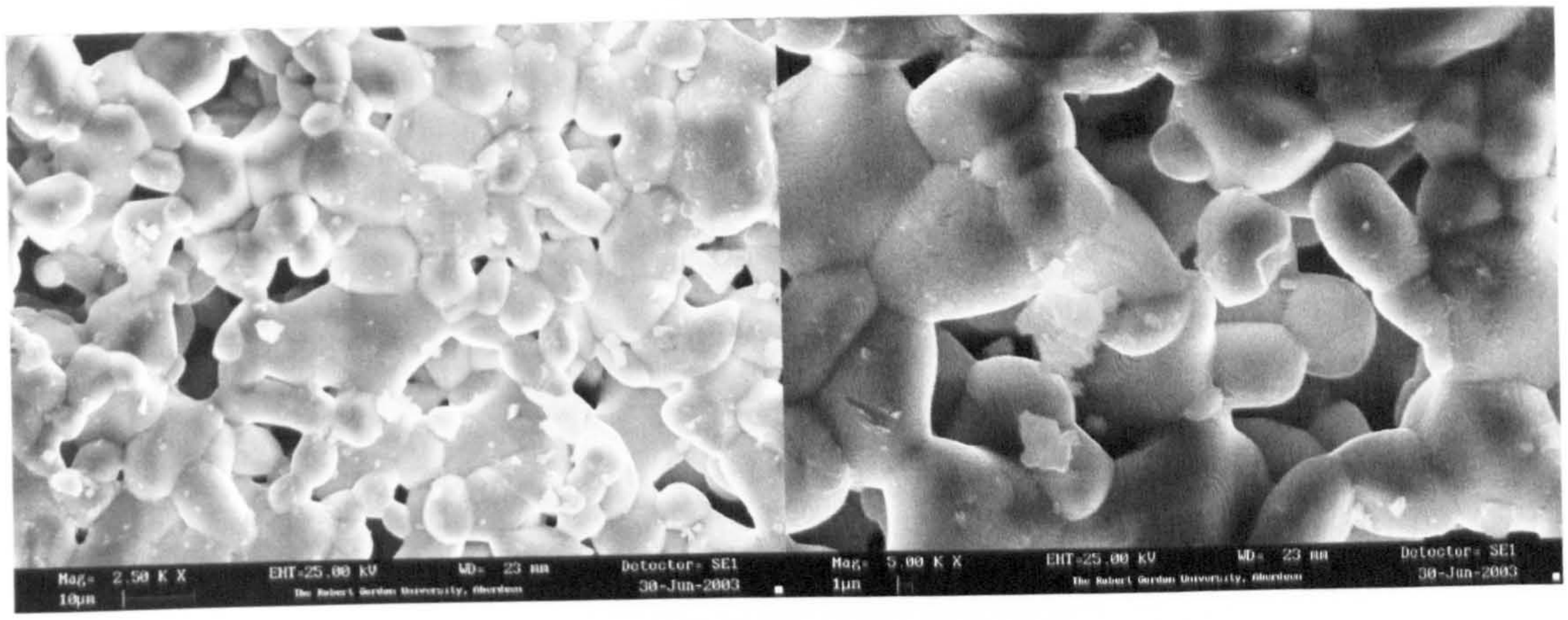

Figure 50: Sample 3 outer surface

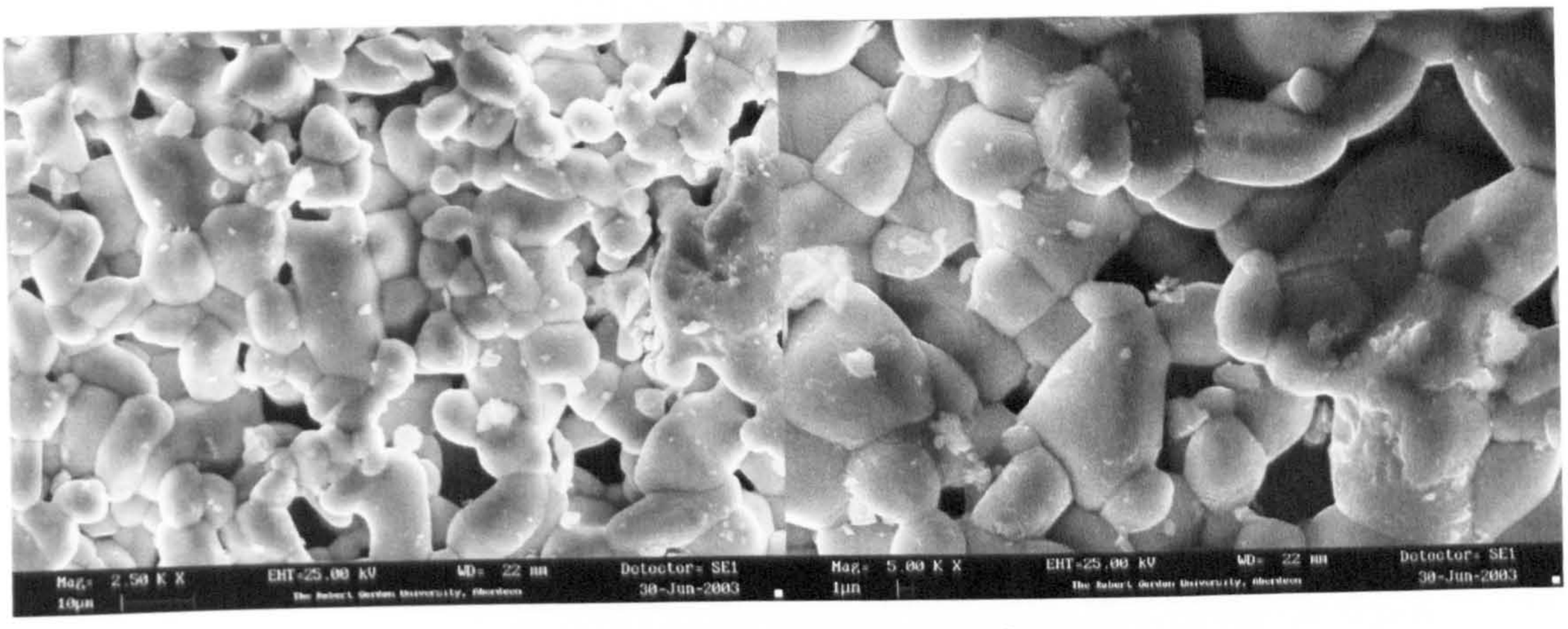

Figure 51: Sample 4 outer surface

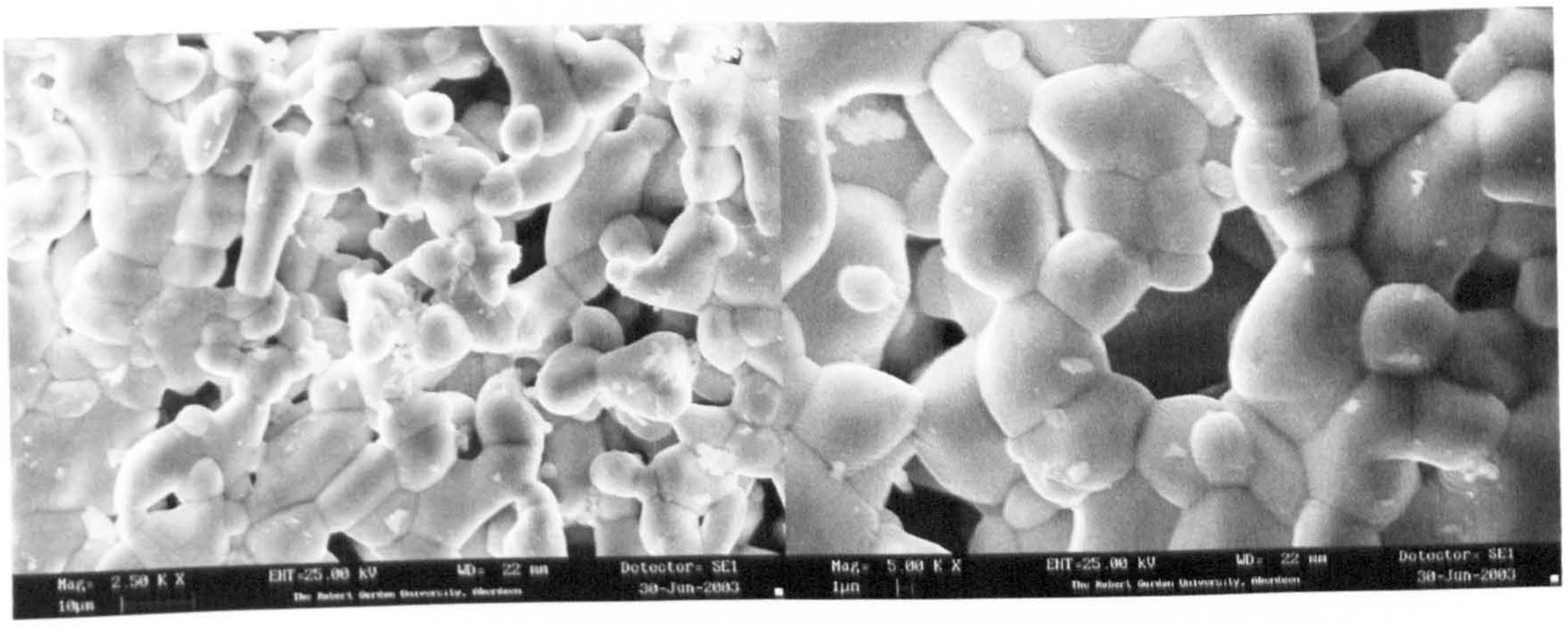

Figure 52: Sample 5 outer surface

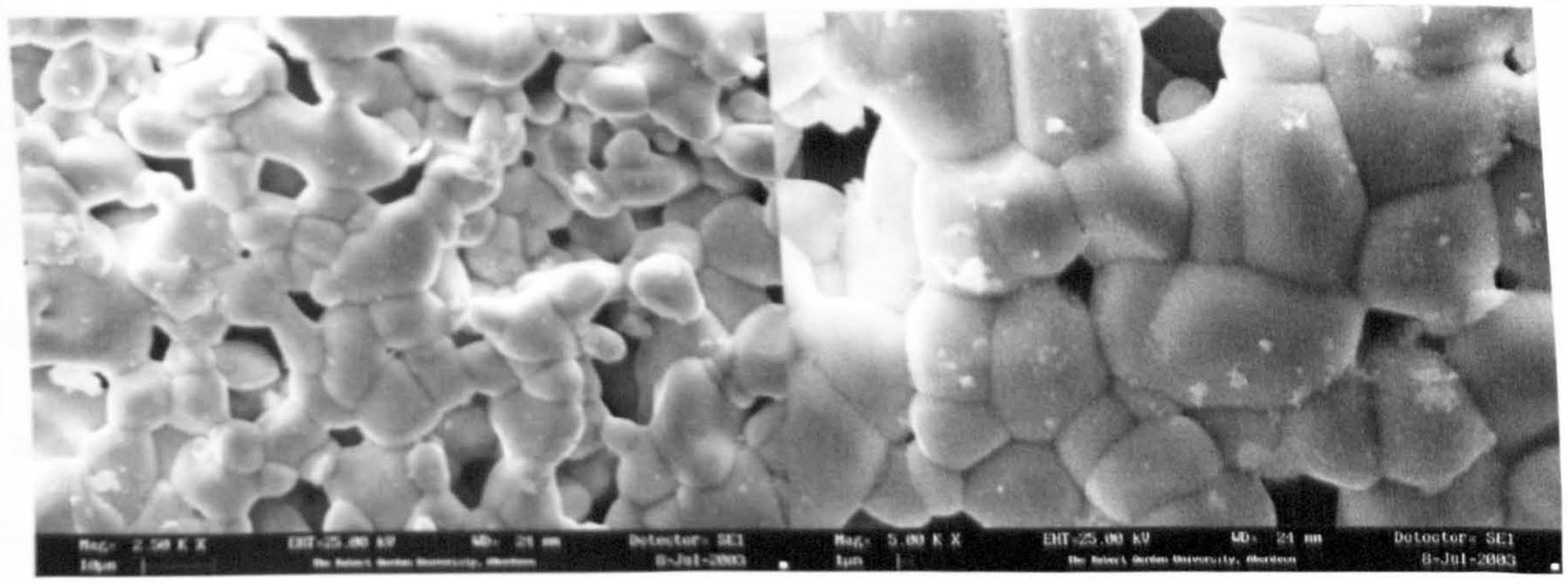

Figure 53: Sample 6 outer surface

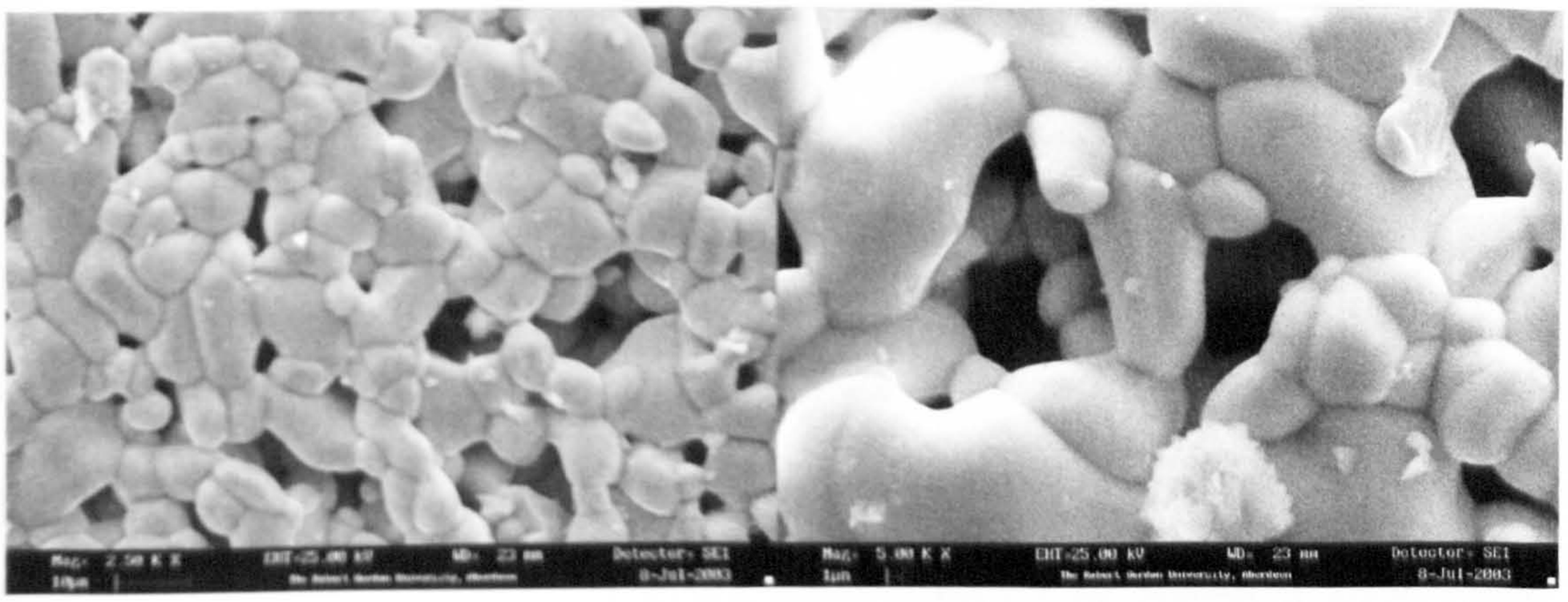

Figure 54: Sample 7 outer surface

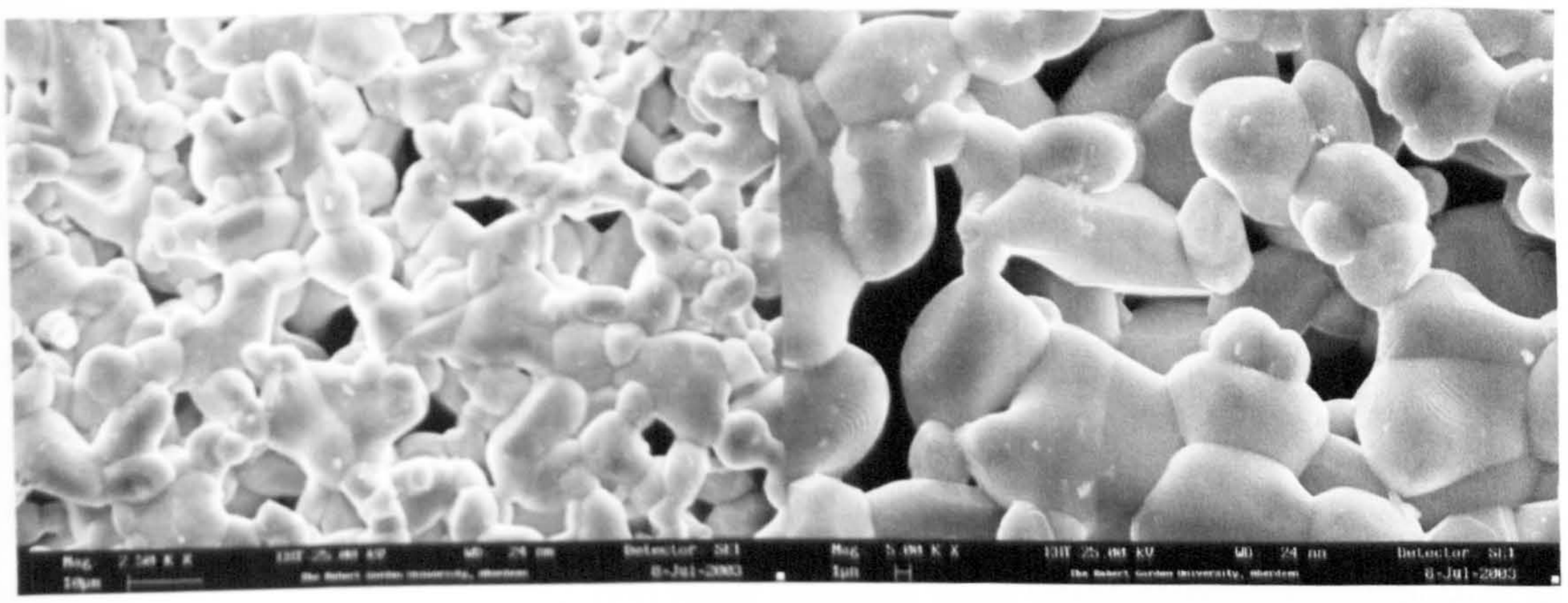

Figure 55: Sample 8 outer surface

Where again:

Sample 1 – Row support (α-alumina tube externally wash coated with titania)

Sample 2 – First internal γ-alumina treatment

Sample 3 – Second internal γ-alumina treatment

Sample 4 – First total rhodium coat

Sample 5 – Second total rhodium coat

Sample 6 – Third total rhodium coat

Sample 7 – Forth total rhodium coat

Sample 8 – After hydrogen calcination

This also applies for the EDXA sampling numbers.

4.2.4. EDXA

The samples used for SEM and EDXA were obtained by cutting a small piece (~5mm^2) from the membrane itself. The pieces were analysed by SEM followed by EDXA. The EDXA was analysed in five different points on the surface of the 5mm^2 piece and the average of the results was considered(Tables 15 and 16).

From the energy dispersion x-ray analysis it appears that even with great care, it was impossible to avoid contamination. The source of contamination can be water used to dissolve the chemicals, the way that the samples were handled, the oven tray or some other chemicals impregnated on the measuring cylinders or any other laboratorial equipment used.

The shell side (Table 15) is the one most affected from these contaminations, due to its exposure, whereas the tube side (Table 16) usually suffers contaminations from the water in lower concentrations.

Sodium, magnesium, phosphorus and calcium are typical examples of impurities contained in the water.

The elements to be analysed are aluminium and titanium from the support and rhodium in order to evaluate the degree of catalyst impregnation.

The outer surface (Table 15), which was wash coated with titanium, shows a decrease in titanium concentration and increase in aluminium concentration for the first internal γ-alumina deposition. Simultaneously sodium concentration increases, indicating that the surface was contaminated, most likely from the water. As γ-alumina modification involves heat treatment, some of the other impurities were cleaned at high temperatures.

After the second internal γ-alumina deposition and heat treatment, the outer surface was again cleaned by the high temperature, exposing its titanium composition and it was again slightly impregnated with aluminium from the excess of γ-alumina in the inner tube.

The first rhodium coating was effective in impregnating rhodium on the outer surface and the second impregnation slightly increased the rhodium concentration, but further depositions proved not to enhance rhodium concentration on the tube outer surface. The concentration of impurities significantly increased during the rhodium deposition.

The calcination in hydrogen atmosphere at 673.15K removed some of the impurities.

As expected, for the inner surface (Table 16) the handling-caused impurities were not as considerable as on the outer surface. The titanium concentration shows that the wash coat also affected the inner surface.

The significant increase in aluminium concentration on the inner surface, indicates the effectiveness of the γ-alumina modification, increasing by 10% in the first modification and doubling in the second.

The rhodium concentration values again confirm the assumption made for the outer surface. The first and second impregnations were effective, but further coatings did not improve the rhodium concentration in the inner surface. After the calcination in hydrogen atmosphere, the rhodium concentration does not change.

Tables 15 and 16 show detailed variations of the element concentrations.

Table 15: Outer surface (shell side) EDX analysis

Sample	%Na	%Mg	%Al	%Si	%P	%Rh	%Ca	%Ti
1	0.00	0.22	2.75	1.08	0.30	0.04	0.28	95.44
2	0.81	0.06	3.94	1.15	0.14	0.01	0.27	93.65
3	0.52	0.05	3.97	0.57	0.14	0.01	0.14	94.60
4	0.32	0.33	7.10	1.18	0.14	0.04	0.16	90.77
5	1.38	0.10	5.59	1.24	0.16	0.05	0.14	91.38
6	0.51	0.01	6.13	2.6	0.23	0.04	0.25	87.61
7	0.92	0.16	5.01	1.01	0.2	0.03	0.09	93.23
8	0.12	0.06	3.09	0.75	0.19	0.01	0.09	95.73
Average %	0.57	0.12	4.70	1.20	0.19	0.03	0.18	92.80

Table 16: Inner surface (tube side) EDX analysis

Sample	%Na	%Mg	%Al	%Si	%P	%Rh	%Ca	%Ti
1	0.06	0.10	1.36	0.30	0.08	0.03	0.01	98.20
2	0.28	0.10	11.27	0.17	0.04	0.00	0.05	88.16
3	0.19	0.06	23.02	0.19	0.07	0.01	0.04	76.49
4	0.06	0.13	21.22	0.26	0.04	0.02	0.05	78.25
5	0.15	0.09	24.47	0.19	0.00	0.02	0.05	75.11
6	0	0.18	22.66	0.34	0.01	0.02	0.03	76.98
7	0.28	0.04	20.95	0.3	0.13	0.01	0.01	78.35
8	0.11	0.08	22.88	0.23	0.07	0.01	0.05	76.62
Average %	0.14	0.10	18.48	0.25	0.06	0.02	0.04	81.02

Rh is the active catalyst for the proposed reaction of methane and oxygen to generate the syngas. It is therefore useful to compare the Rh concentration observed for XPS and EDX analysis, which have been presented in Tables 13-16.

Since XPS analyses only the top layer surface, it can be observed from table 13 that the Rh concentration for sample 1 is zero. However, the concentration of Rh in the inner surface increases for samples 2 to 5. A decrease is observed on samples 6, 7 and 8 where it again attains zero. For the EDXA (Table 16) shows that concentration of Rh on the sample 1 is 0.03% which reduces to zero in sample 2. However, subsequent samples show a greater stability in Rh concentration then in the case of the XPS. This is attributed to the fact that while the XPS sees only the top 10nm of the top layer thickness, the EDXA is able to penetrate more deeply and thus provide more of the bulk concentration within the sample. A similar trend occurs when the analysis is carried out on shell-side samples, but the Rh concentration of sample 8 does not decrease down to zero.

4.3. PRODUCT DISTRIBUTION, REACTION AND STOICHIOMETRY

4.3.1. DEFINITION OF TERMS

Terms used in this chapter to express the experimental parameters are presented in this section.

The parameters obtained from the experimental rig were (at NTP):

Volumetric feed flow rate – v_i [ml/min]

Reactor pressures – P_n [bar]

Room temperature – T_{room} [K]

Reactor temperatures - T_n [K]

Molar fraction of the outlet stream - y_i [-]

Where the subscripts:

i – reactants (methane and oxygen) or any other species of interest.

n – is the position in the reactor

The parameters calculated:

Molar flow rates: $$F\left[\frac{mol}{\min}\right] = v\left[\frac{ml}{\min}\right] \Big/ 22400\left[\frac{ml}{mol}\right]$$ **Equation 3**

For a flow system, the concentration C_i at a given point can be determined from F_i and the total volumetric flow rate *v* at that point.

Molar concentrations: $$C_i\left[\frac{mol}{ml}\right] = \frac{F_i}{v}\left[\frac{mol/\min}{ml/\min}\right]$$ **Equation 4**

or in case where the volumetric flow rate *v* is not known, an approximated value can be obtained from the multiplication of the total concentration by the molar fraction y_i at that point.

Conversion of component i, X_i is the amount of the methane or oxygen fed into the reactor which is converted into products in passing through the reactor.

$$X_i = \frac{\text{concentration of the reactant in feed} - \text{concentration of the reactant in product}}{\text{concentration of the reactant in feed}}$$

Equation 5

Yield is the fractional conversion of methane to the product

$$Y_i = \frac{\text{molar concentration of particular product}}{\text{molar concentration of methane in feed}} x \left(\frac{\text{number of carbon atoms in the product}}{\text{number of carbon atoms in the feed}}\right)$$

Equation 6

Selectivity is defined as the molar percentage of methane converted that reacts to produce the desired product.

$$S_i = \frac{\text{molar concentration of particular product}}{\text{molar concentration of methane consumed}} x \left(\frac{\text{number of carbon atoms in the product}}{\text{number of carbon atoms in the feed}}\right)$$ **Equation 7**

The relationship between selectivity and yield based on the above definitions is as described in equation below:

$$S_i = \frac{Y_i}{X_{methane}} x \left(\frac{\text{number of carbon atoms in the product}}{\text{number of carbon atoms in the feed}}\right)$$ **Equation 8**

The feed ratio is the ratio of the volumetric flow rate of methane to that of oxygen entering the reactor.

The syngas ratio is the ratio of the molar fraction of hydrogen to that of carbon monoxide.

The vol% of nitrogen in the oxygen feed is the percentage of nitrogen in the oxygen volumetric feed flow stream.

The vol% of carbon dioxide in the methane feed is the percentage of carbon dioxide in the methane volumetric feed flow stream.

The temperature T is the set point temperature in the middle of the reactor. It is shown in the reactor characterisation to be the point with highest temperature in the reactor.

4.3.2. RESULTS FOR PRODUCTS DISTRIBUTION, REACTION & STOICHIOMETRY

Before presenting the experimental results, a brief description of the essential roles of stoichiometry and thermodynamics in this system has been evaluated.

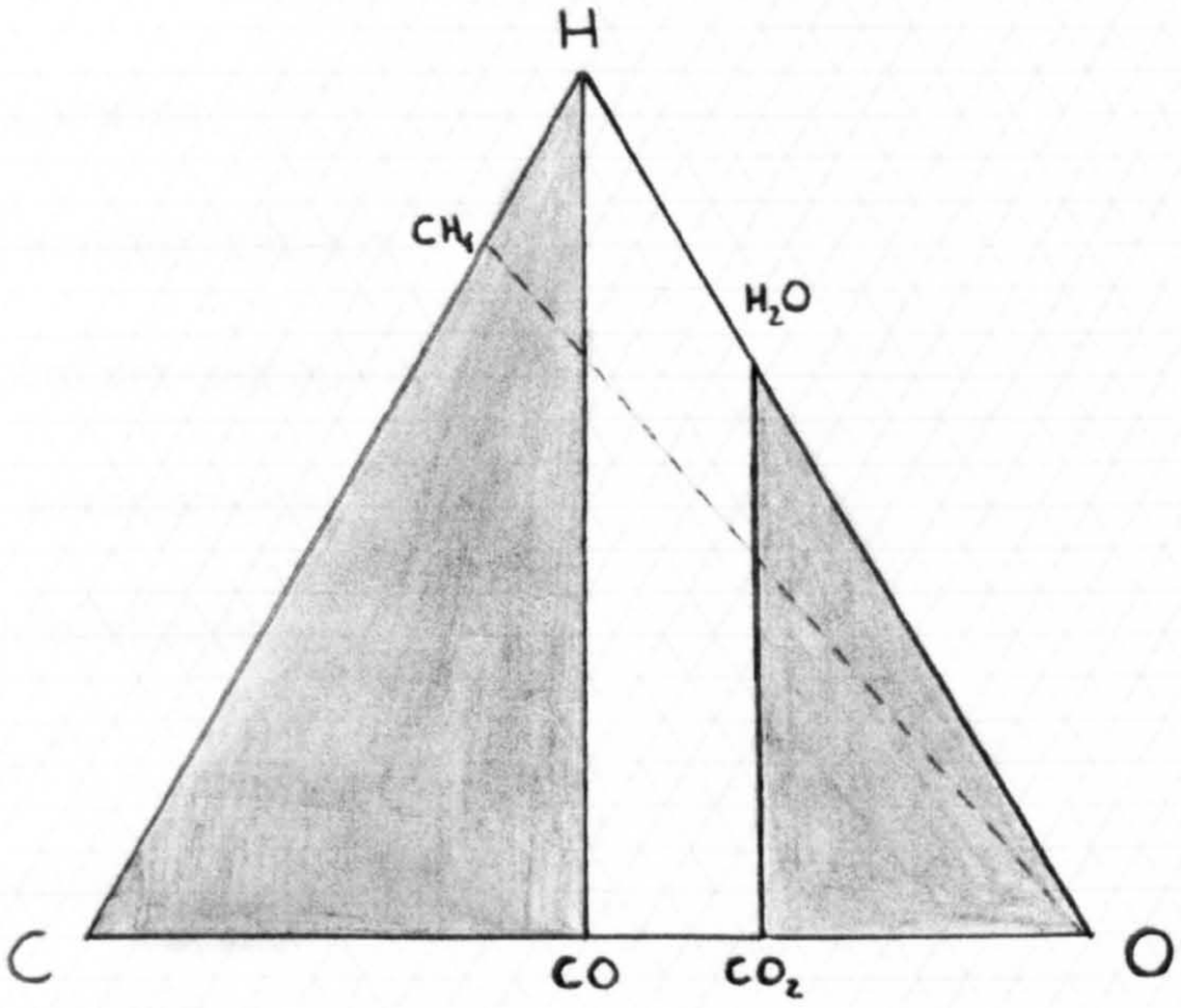

Figure 56: A ternary composition diagram of the C-H-O system

The ternary plot of Figure 56 illustrates the role of stoichiometry in this system. For any reaction where CH_4 and O_2 are the only reactant species in the feed, the atomic composition of the mixture is represented by a point located on the reactant line shown in figure 56 as a dashed line [30].

The unshaded area represents the accessible region of H_2, H_2O, CO, and CO_2 compositions. The lightly shaded region indicates the inaccessible compositions for this feed composition.

The "composition" of any point plotted on a ternary diagram can be determined (or any point can be plotted). Percentage values for atomic **H** are read from zero along the basal line (axis) at the bottom of the diagram to 100% at the vertex of the triangle. Similarly, values for atomic **O** are read from zero along the upper left axis, to 100% at the lower right vertex. And finally, values for atomic **C** are read from zero along the upper right axis to 100% at the lower left vertex.

Obviously, the stoichiometry of the direct methane partial oxidation to syngas production, $CH_4 + ½\ O_2 \longrightarrow 2\ H_2 + CO$ suggests that the ideal synthesis gas reactor (i.e. 100% selectivity to carbon monoxide and hydrogen) should operate at a CH_4/O_2 mole ratio of 2/1 if total conversion of the reactants occurs [30].

Factors that mitigate against ideal performance are:

1) Side reactions

2) Reactor configuration

    a. Mass transfer limitation

    b. Temperature distribution

    c. Flow characteristics

3) Flammability constraints

4) Feed delivery

    a. Co-feeding

    b. Separate feeding

5) Kinetics of reaction

    a. Exothermic

    b. Endothermic

When a membrane reactor is used, these non-ideal factors can be minimised as follows:

- Side reactions are reduced because the reactant (oxygen) concentration can be controlled.

- Catalyst is impregnated within the walls of the membrane and this reduces mass transfer limitation due to a wider distribution of reactants residential times and also facilitates temperature distribution. The hydrodynamic characteristics of the reactor are also enhanced due to absence of a tightly packed bed of catalytic material.

- A wide range of oxygen and methane concentrations can now be used since the reactants are fed separately.

4.3.2.1. Effect of Methane Conversion on Yield and Selectivity

In the present investigation, only hydrogen, carbon monoxide, carbon dioxide and water were produced in any detectable amounts. The distribution of these products will now be examined.

The variants analysed were temperature and volumetric feed flow rate.

Results were obtained for varying temperature using constant feed flow rates of 150 ml/min of methane and 15 ml/min of oxygen.

The experimental chapter gives more details on the procedure of the data collection.

Results for varying feed flow rate in order to obtain a wide range of methane conversion readings with constant temperature of 1023.15K are shown in figures 57, 58, 60 and 61. Methane conversions with constant feed flow rate (165ml/min), varying temperature are shown in figures 59 and 62.

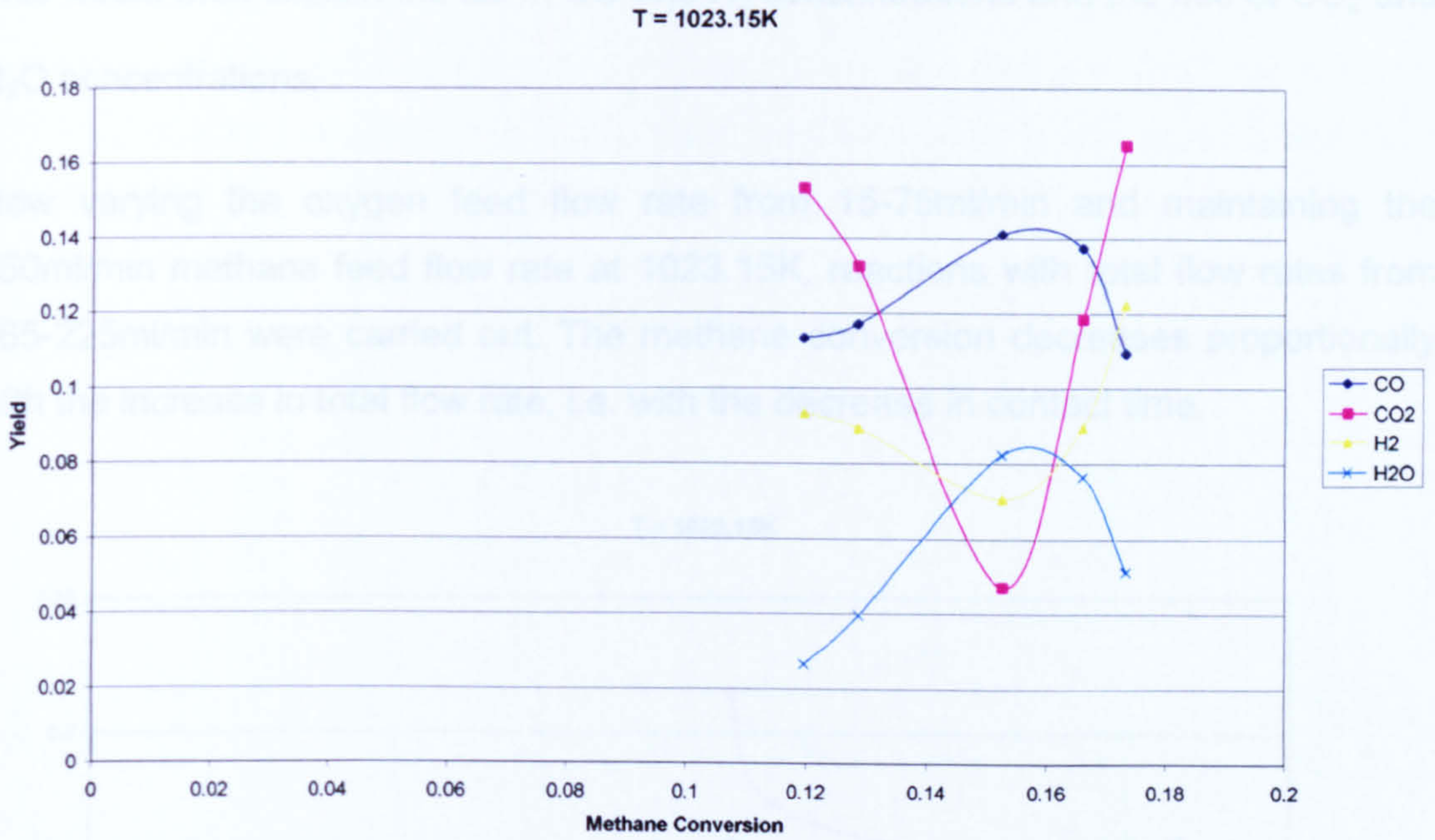

Figure 57: Yield vs. low methane conversion at 1023K – Run 3

In order to achieve low methane conversions, experiments were carried out with constant oxygen feed flow rate of 75ml/min and varying methane feed flow rate from 150 to 425ml/min, giving a range of total feed flow rates from 225 to 500ml/min. The higher total feed flow rate decreases the contact time of the reactants with the catalyst, decreasing methane conversion.

Figure 57 shows the effect of methane conversion (<18%) on the yield of carbon monoxide (CO), carbon dioxide (CO_2), hydrogen (H_2) and water (H_2O) respectively. Both CO and H_2O pass through a maximum while CO_2 and H_2 pass through a minimum at a methane conversion of 15.4%. Between methane conversions of 12-15.4%, methane reacts with oxygen to form CO_2, H_2, H_2O and CO via a parallel kinetic scheme:

$$CH_4 + O_2 \longrightarrow CO + H_2 + H_2O$$
$$\searrow\ CO_2$$

As the methane conversion increases, CO_2 reacts with H_2 while CO reacts with H_2O through the water-gas-shift:

$$CO_2 + H_2 \rightarrow H_2O + CO$$

$$CO + H_2O \rightarrow CO_2 + H_2$$

This would then explain the fall in CO and H_2 concentrations and the rise of CO_2 and H_2O concentrations.

Now varying the oxygen feed flow rate from 15-75ml/min and maintaining the 150ml/min methane feed flow rate at 1023.15K, reactions with total flow rates from 165-225ml/min were carried out. The methane conversion decreases proportionally with the increase in total flow rate, i.e. with the decrease in contact time.

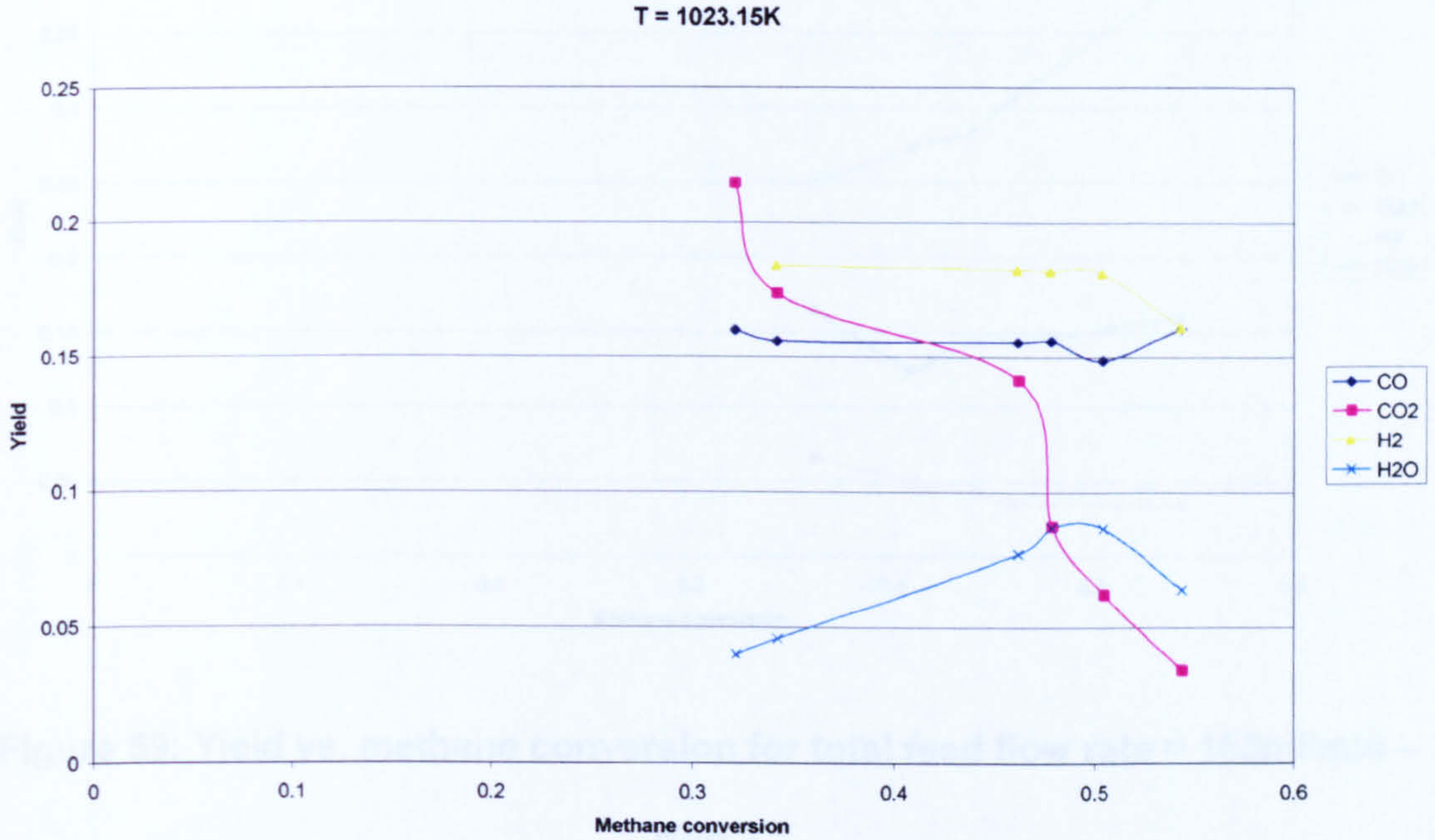

Figure 58: Yield vs. methane conversion at 1023K – Run 2

Figure 58 shows the effect of methane conversion (>30%) on the yield of CO, CO_2, H_2 and H_2O respectively. The behaviour is significantly different from that at lower conversions disclosed in figure 57. Here, the yields of CO and H_2 are more constant with conversions up to about 46%. Above this value, the CO yield increases while the yield to H_2 falls. The CO_2 yield falls continuously and passes through a point of inflexion at 46% methane conversion. The yield profile for H_2O is more or less similar to that discussed in figure 57 and it increases and passes through a maximum at high methane conversion. These observations have led to the kinetic scheme at high methane conversion:

$$CH_4 + O_2 \longrightarrow CO + H_2 + H_2O$$
$$\searrow \quad CO_2$$

$$H_2O + CO_2 + H_2 \rightarrow CH_4 + CO$$

Therefore an increase in contact time provides high yields of hydrogen and carbon monoxide and low yields of water and carbon dioxide and methane conversion above 50%. To obtain this contact time the total feed flow rate needs to be lower than 185ml/min for this load of catalyst and temperature of 1023.15K.

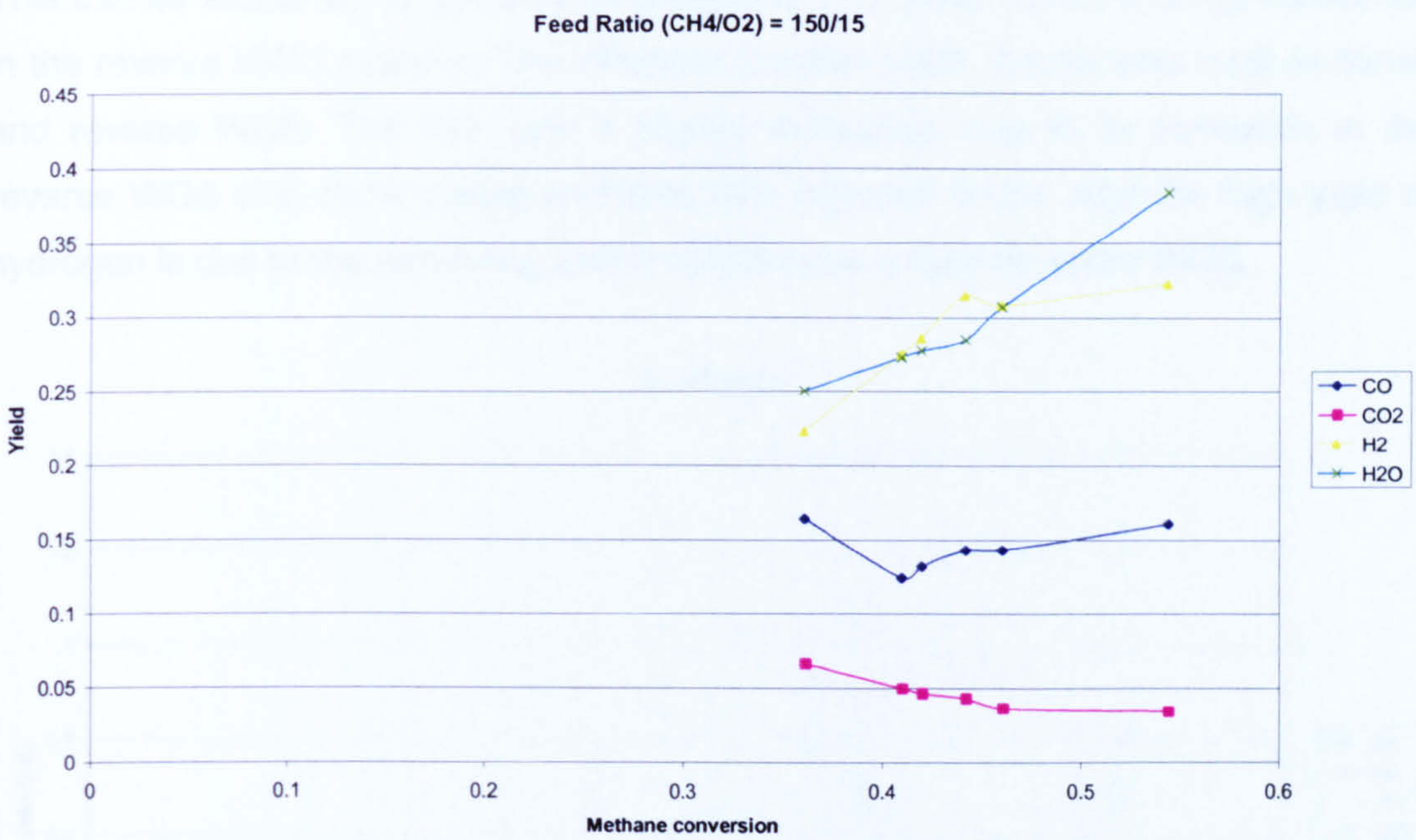

Figure 59: Yield vs. methane conversion for total feed flow rate = 165ml/min – Run 1

Figure 59 shows the influence of temperature on methane conversion and products yields for a total feed flow rate of 165ml/min (constant contact time), 150ml/min of methane and 15ml/min of oxygen. As the temperature rises the methane conversion increases. This occurs for temperatures from 873.15K to 1023.15K, but methane conversion has a considerable fall at temperature above 1083.15K. The first values observed in figure 59 represent values for 1083.15K. The other points follow the assumption that increasing temperature, methane conversion also increases.

It is observed that as methane conversion increases, more water is formed and the yield of CO increases slightly and CO_2 yield decreases a little.

It is possible to assume that as the temperature increases, the reaction tends to go towards a total oxidation route followed by a reverse water gas shift reaction, but some remaining partial oxidation and WGS reaction also need to be considered.

$$CH_4 + O_2 \rightarrow CO + H_2O + H_2$$
$$\searrow CO_2$$

$$CO_2 + CH_4 \rightarrow H_2O + CO$$

This can be explained by the small decrease in CO_2 yield, which is being consumed in the reverse WGS reaction. The increase in water yield, results from total oxidation and reverse WGS. The CO yield a slightly increases, due to its formation in the reverse WGS and some partial oxidation that may still occur. And the high yield of hydrogen is due to the remaining partial oxidation and may be some WGS.

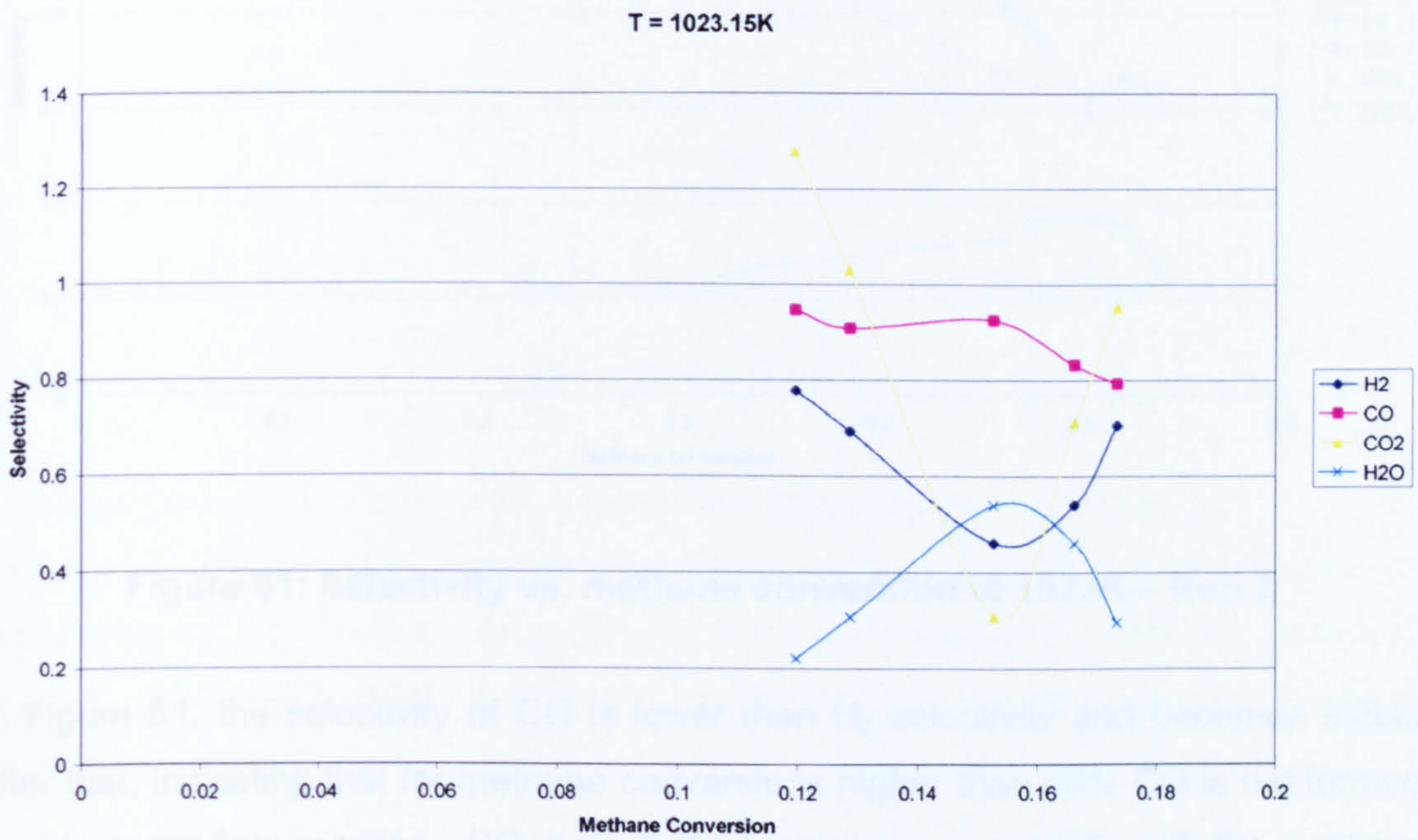

Figure 60: Selectivity vs. low methane conversion at 1023K – Run 3

Figure 60 shows the high CO_2 selectivity for low methane conversion. This means that the CO_2 is formed from some secondary reactions for low methane conversion. The CO selectivity remains almost constant with values around 0.09. It is possible this is an indication of the absence of secondary reactions involving CO in low methane conversions. Hydrogen selectivity decreases for methane conversions lower than 15%, and increases for higher conversions, reaching values close to those for CO at methane conversions above 0.17. Water selectivity profile follows a mirror image of hydrogen selectivity, increasing for conversions up to 15% and decreasing for higher conversions.

For higher values of methane conversion (Figure 60) water selectivity falls, suggesting consumption of water probably via the steam methane reforming reaction. Hydrogen selectivity decreases significantly for methane conversions up to 50%, increasing slightly after that.

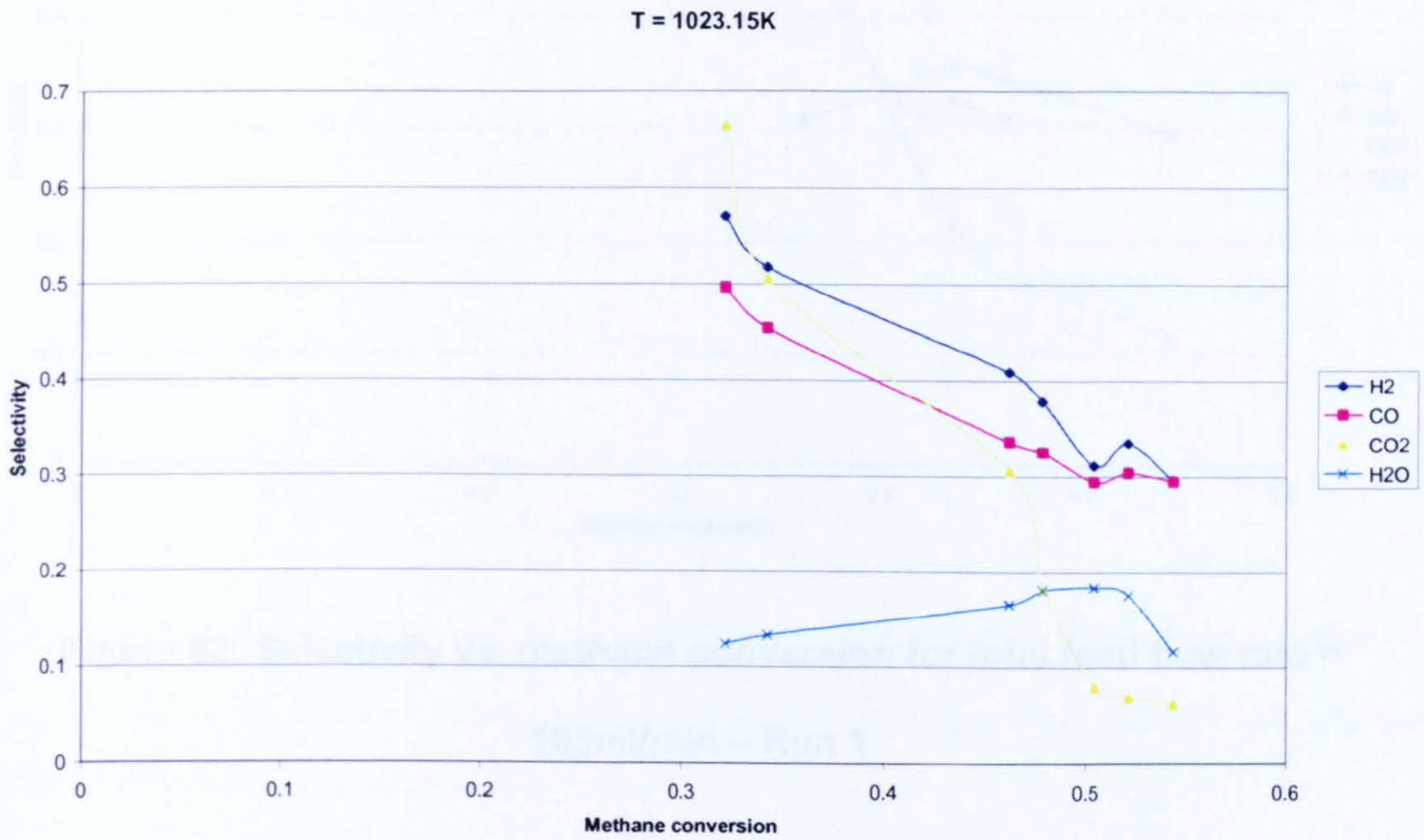

Figure 61: Selectivity vs. methane conversion at 1023K – Run 2

In Figure 61, the selectivity of CO is lower than H_2 selectivity and becomes stable after that, indicating that for methane conversions higher than 46% CO is not formed by any secondary reaction. CO_2 selectivity decreases very rapidly with the increase of methane conversion, being the less selective gas formed in this reaction since total oxidation reaction is minimized.

It is important to note that the above mentioned experimental data (Figure 61) were taken for varying contact times, which can have an influence on the selectivity values. Data for constant contact time, but varying temperature values are shown in figure 62.

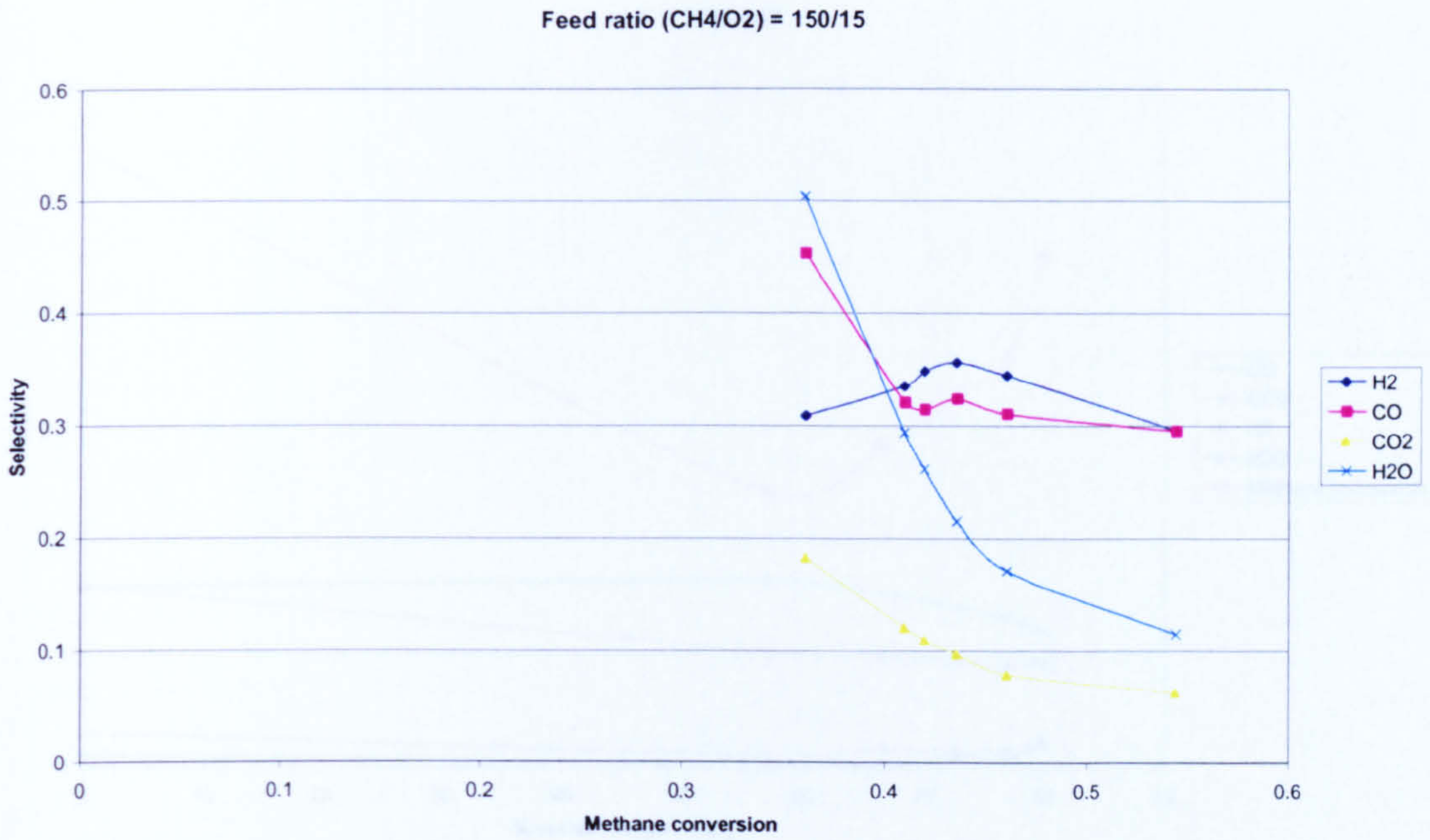

Figure 62: Selectivity vs. methane conversion for total feed flow rate = 165ml/min – Run 1

The hydrogen and CO selectivities pass through a maximum value at 45% methane conversion. The increase can be due to an optimisation on the parameters of temperature of the reaction. For methane conversions below 40%, the CO selectivity value is significantly higher than the H_2 selectivity suggesting a reaction between methane and carbon dioxide.

Water and CO_2 selectivities decrease monotonically to lower values than CO and H_2, giving optimised results for the syngas generation reaction.

4.3.2.2. Effect of Feed Dilution on Conversion, Yield and Selectivity

If nitrogen is added to the feed, in such a manner as to simulate air composition, the results are as shown in figures 63 and 65.

If carbon dioxide is added to the feed, the results are as shown in figure 64 and 66.

The yields for the variation of nitrogen and carbon dioxide concentrations on the volumetric feed flow rate are shown in figures 63 and 64.

The selectivity to the products for the variation of nitrogen and carbon dioxide concentrations on the volumetric feed flow rate are shown in figures 65 and 66.

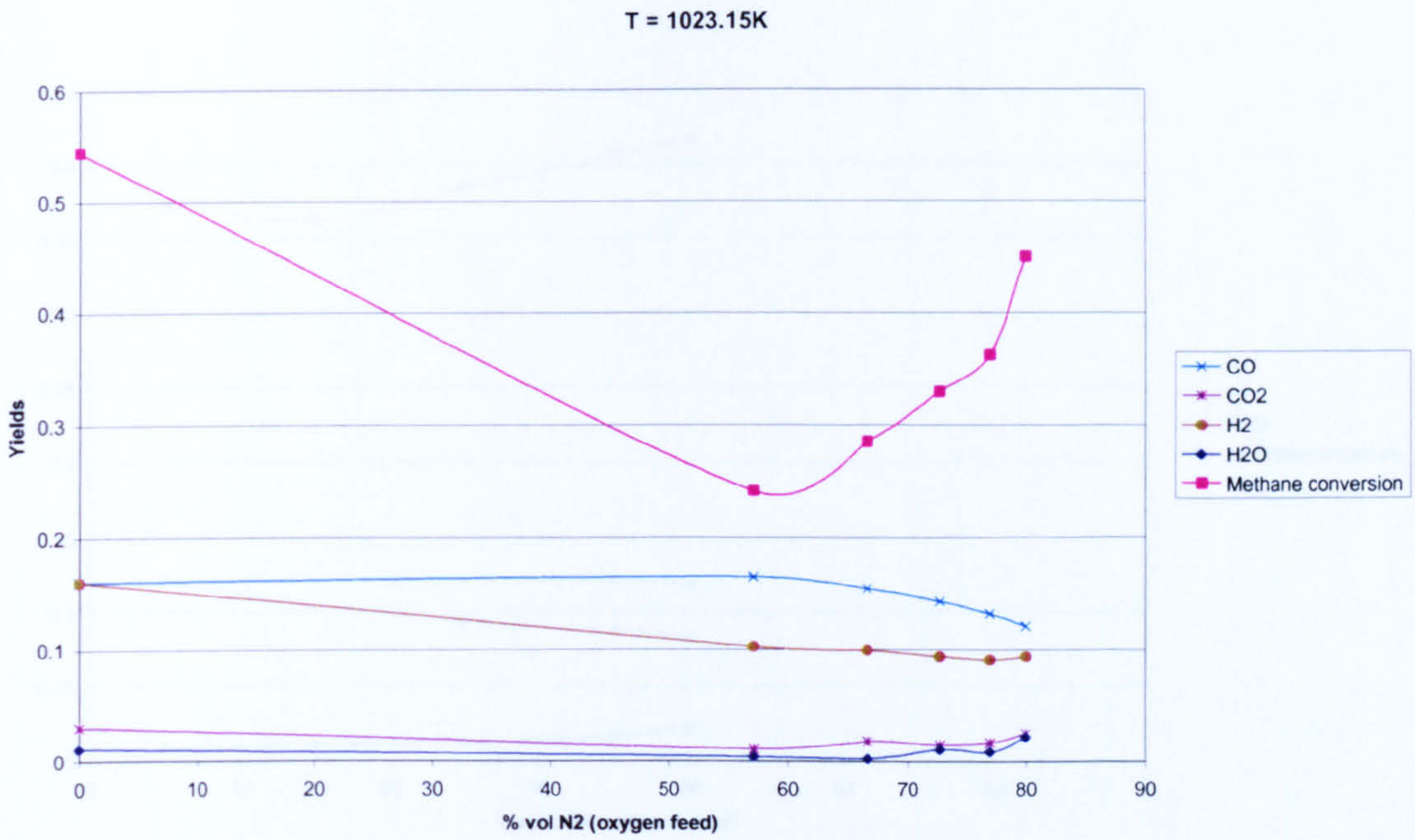

Figure 63: Yield vs. nitrogen concentration in the oxygen feed stream – Run 4

The addition of nitrogen to the system basically influences the contact time of the reactants with respect to products formation.

It is possible to observe that water and CO_2 yield values do not show any significant change compared to those with no addition of nitrogen.

CO yields fall steadily with the addition of nitrogen to the system.

Hydrogen yield values decrease initially with N_2 addition but then remain constant after 50%vol of nitrogen in the oxygen feed.

However, above around 66.5%vol N_2 (oxygen feed) the yields of CO_2 and H_2O (total oxidation products) show an increase as methane conversion increases. This suggests that reaction 9 becomes dominant at these conditions.

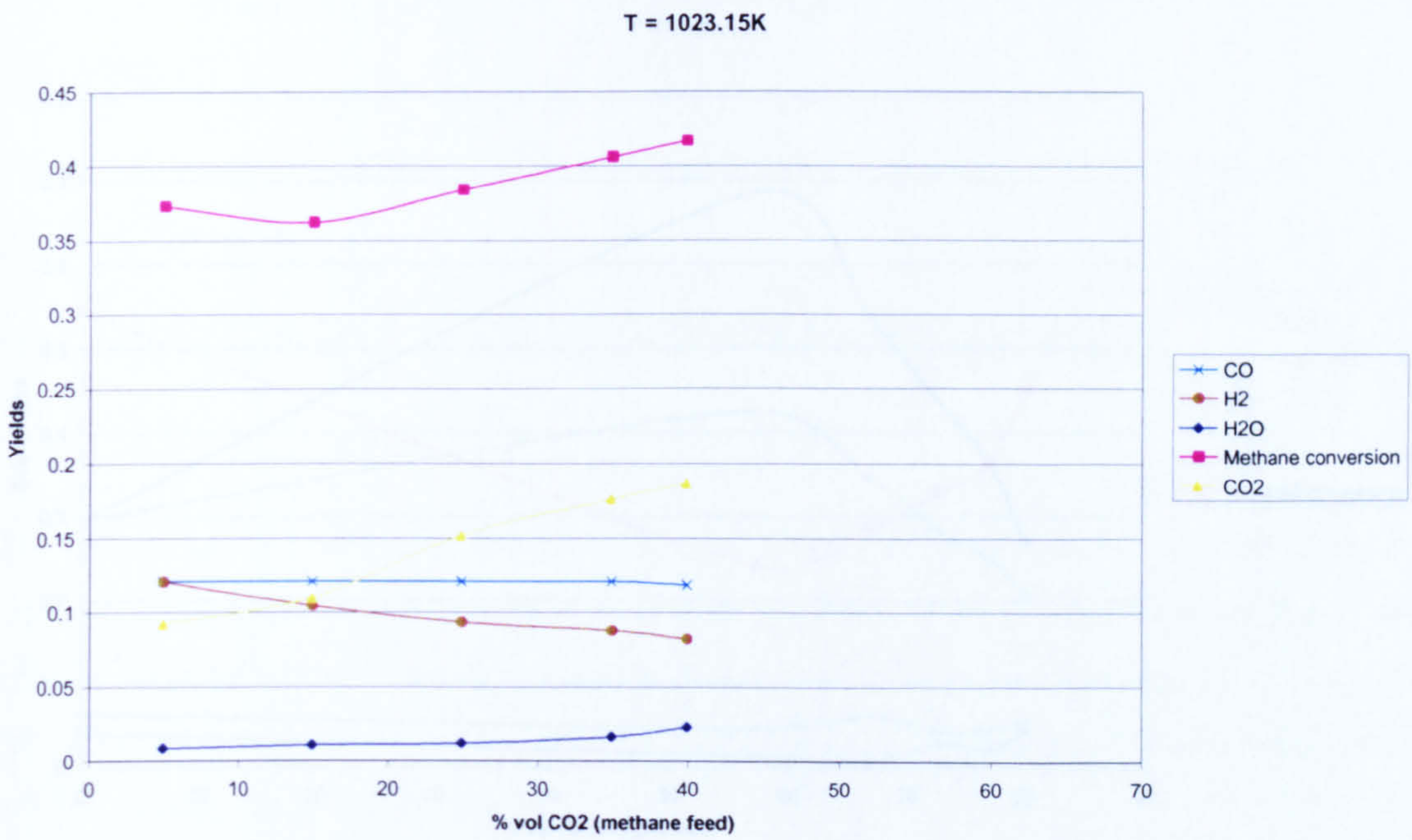

Figure 64: Yield vs. carbon dioxide concentration in the methane feed stream – Run 5

In contrast to nitrogen, the addition of CO_2 in the feed does not influence CO yield, but reduces hydrogen yield as it increases H_2O yield. Thus it is possible to observe that CO_2 addition in the system facilitates water formation and inhibits hydrogen formation.

The effect of addition of CO_2 to the feed is shown in figure 64. Increasing the CO_2 concentration increases the conversion of methane. While the CO yield is unaffected the H_2 yield falls and the H_2O yield increases. The methane seems to be converted to H_2O and CO_2. But the CO_2 further reacts with H_2 to form CO and H_2O via the water-gas-shift reaction pathway.

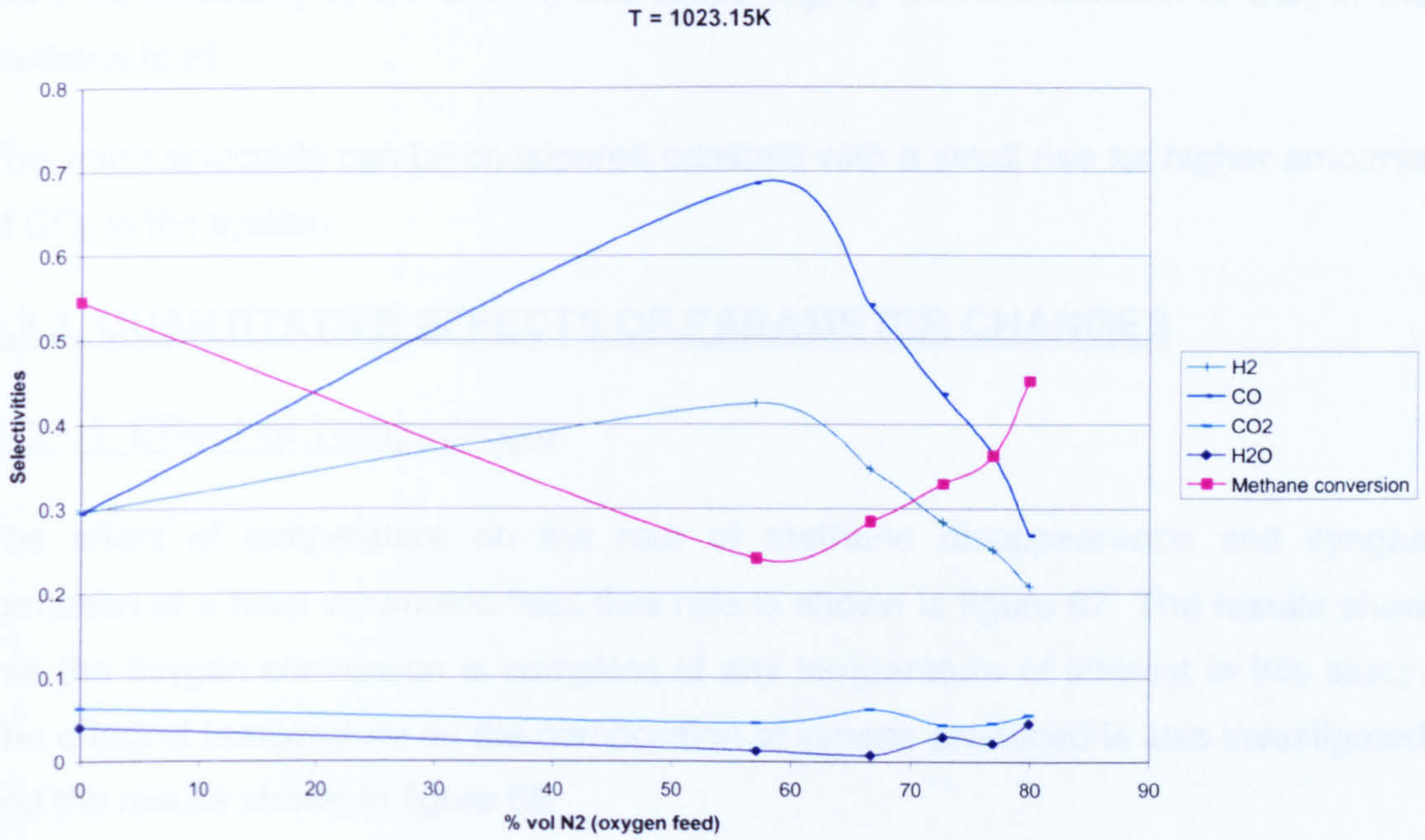

Figure 65: Selectivity vs. nitrogen concentration in the oxygen feed stream – Run 4

The selectivity of carbon dioxide and water as shown in the yield chart is not affected by the addition of nitrogen to the system. But carbon monoxide and hydrogen selectivities show a continuous drop after a peak at around 57.5%vol of nitrogen.

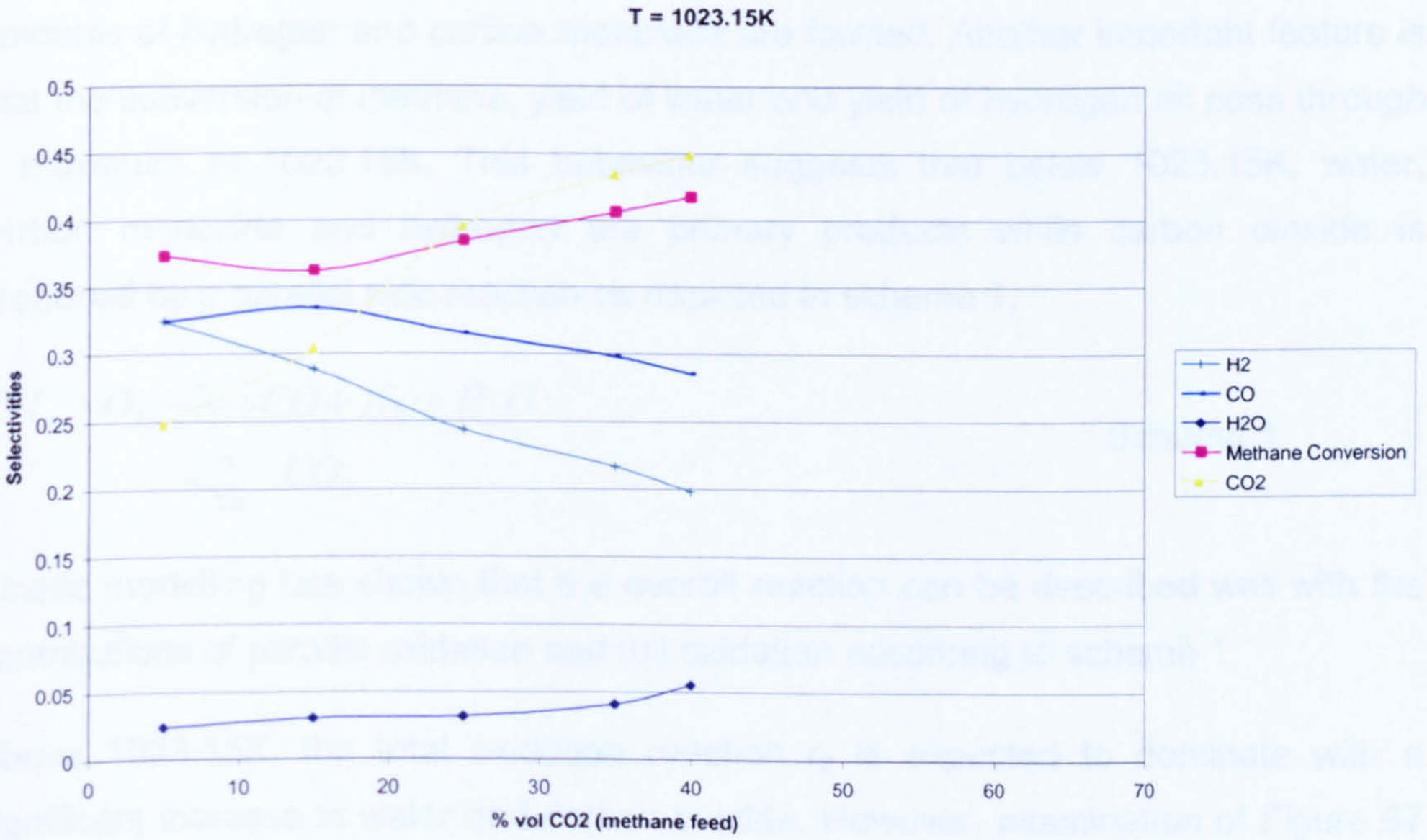

Figure 66: Selectivity vs. carbon dioxide concentration in the methane feed stream – Run 5

Here the selectivity to CO and H_2 decreases slightly with the addition of CO_2 in the methane feed.

The water selectivity can be considered constant with a small rise for higher amounts of CO_2 in the system

4.3.3. QUANTITATIVE EFFECTS OF PARAMETER CHANGES

4.3.3.1. Effect of Temperature

The effect of temperature on the rate of methane disappearance and syngas formation at a fixed volumetric feed flow rate is shown is figure 67. The results show that the oxygen conversion is complete at any temperature of interest in this study. The effect of temperature on the composition of syngas produced is also investigated and the results shown in figure 68.

It is well recognised that the partial oxidation of methane may occur via two distinct mechanisms, i.e., direct partial oxidation or total oxidation followed by reforming reactions [32]. In order to elucidate the mechanism for the catalytic membrane reactor used in this study, the effect of the temperature on the methane conversion and product yields was studied.

The results of the analysis are presented in Figures 67 and 68 respectively.

Figure 67 shows that all the oxygen is consumed. This occurs before significant amounts of hydrogen and carbon monoxide are formed. Another important feature is that the conversion of methane, yield of water and yield of hydrogen all pass through a maximum at 1023.15K. This behaviour suggests that below 1023.15K, water, carbon monoxide and hydrogen are primary products while carbon dioxide is produced by a parallel side reaction as depicted in scheme 1.

$$CH_4 + O_2 \xrightarrow{r_1} CO + H_2 + H_2O$$
$$\searrow^{r_2} \; CO_2$$

Scheme 1

Kinetic modelling has shown that the overall reaction can be described well with the contributions of parallel oxidation and full oxidation according to scheme 1.

Above 1023.15K, the total oxidation reaction r_2 is expected to dominate with a significant increase in water and carbon dioxide. However, examination of Figure 67 shows that the carbon dioxide yield shows only a modest increase above 1023.15K, while the yields for water and hydrogen fall above this temperature. This suggests

that hydrogen, carbon dioxide and water are being consumed accordingly to scheme 2.

$$CO_2 + H_2O + H_2 \xrightarrow{r_3} CH_4 + CO$$ Scheme 2

Scheme 2 will help to explain the fall in the water and hydrogen yields, the modest CO_2 yield increase and the fall in methane conversion at temperatures above 1023.15K.

An important aspect in the conversion of synthesis gas to liquids is the hydrogen/carbon monoxide ratio. A ratio of 2/1 is optimum for this conversion. Figure 69 shows a plot of the H_2/CO over the temperature range studied. The optimum for gas-to-liquids conversion is obtained at a temperature of 1023.15K. Above this temperature, a ratio below 2.0 is attained while below 1023.15K, a value above 2.0 is obtained.

The hydrogen/carbon monoxide ratio varies with temperature. It is observed from Figure 68 that for temperatures up to 973.15K the ratio is constant, but with a further increase of 50K it falls to the specific value of 2, suitable for F-T reactions. It falls even more at higher temperatures.

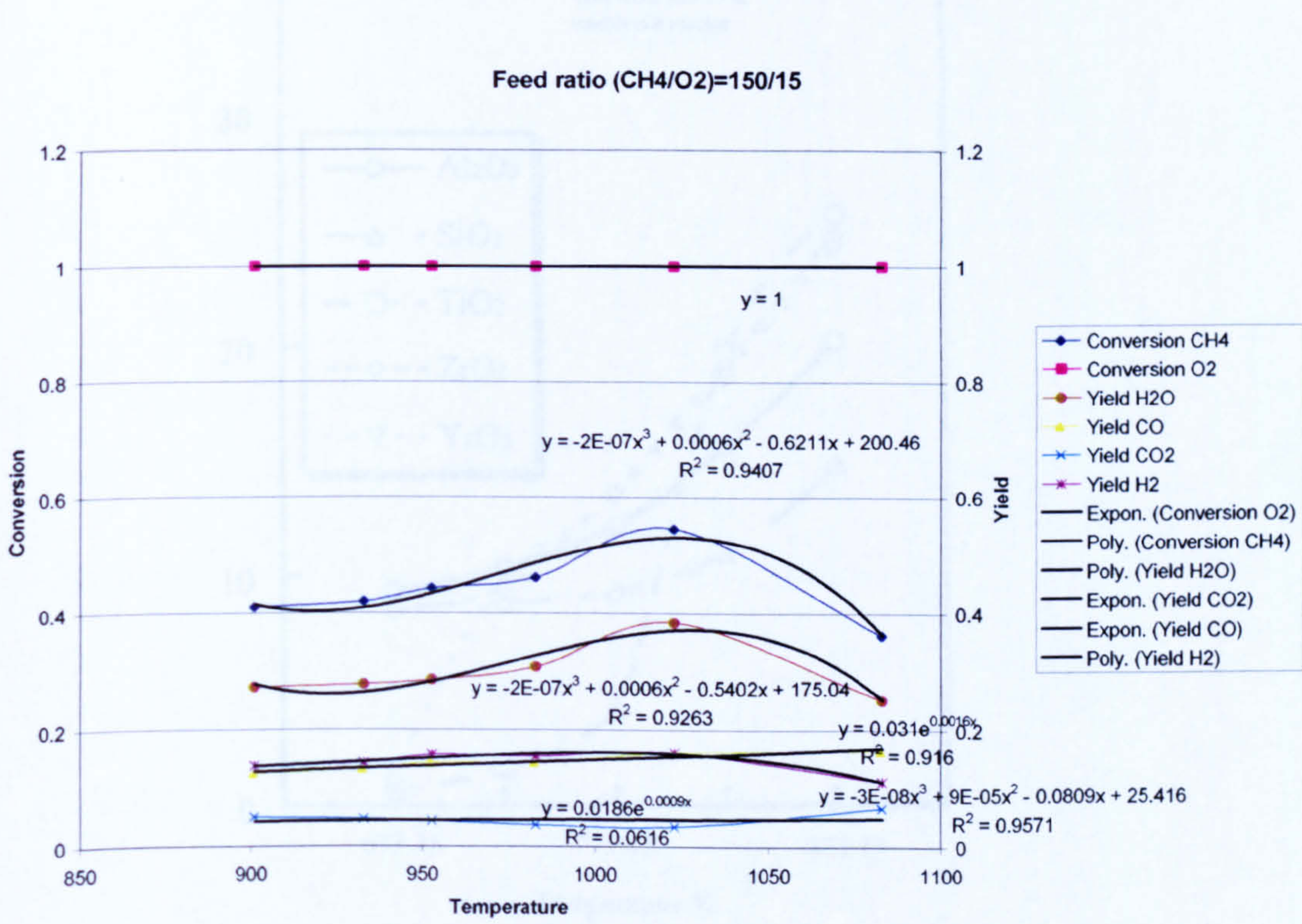

Figure 67: Effect of temperature on methane conversion – Run 1

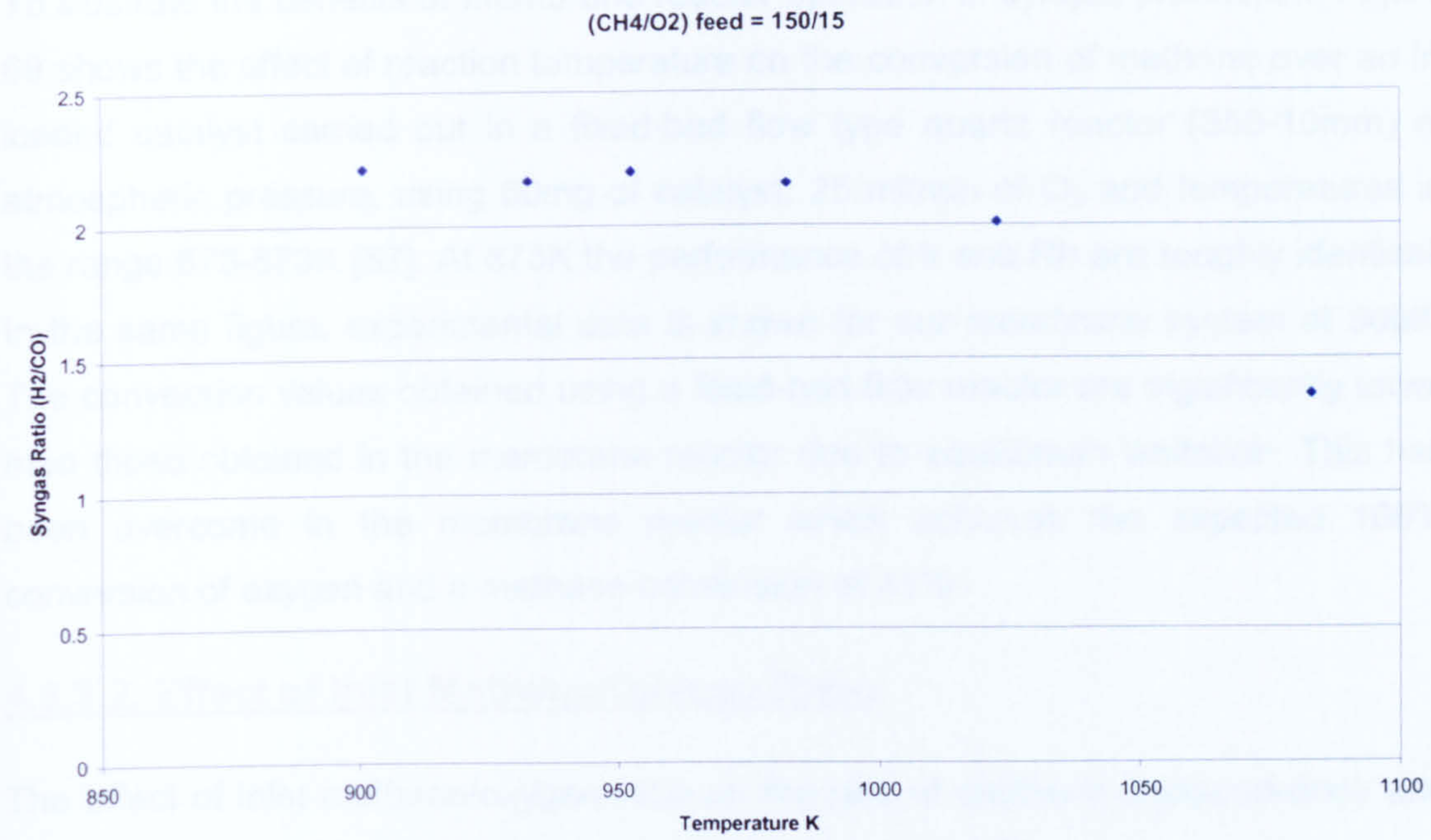

Figure 68: Effect of temperature on syngas ratio – Run 1

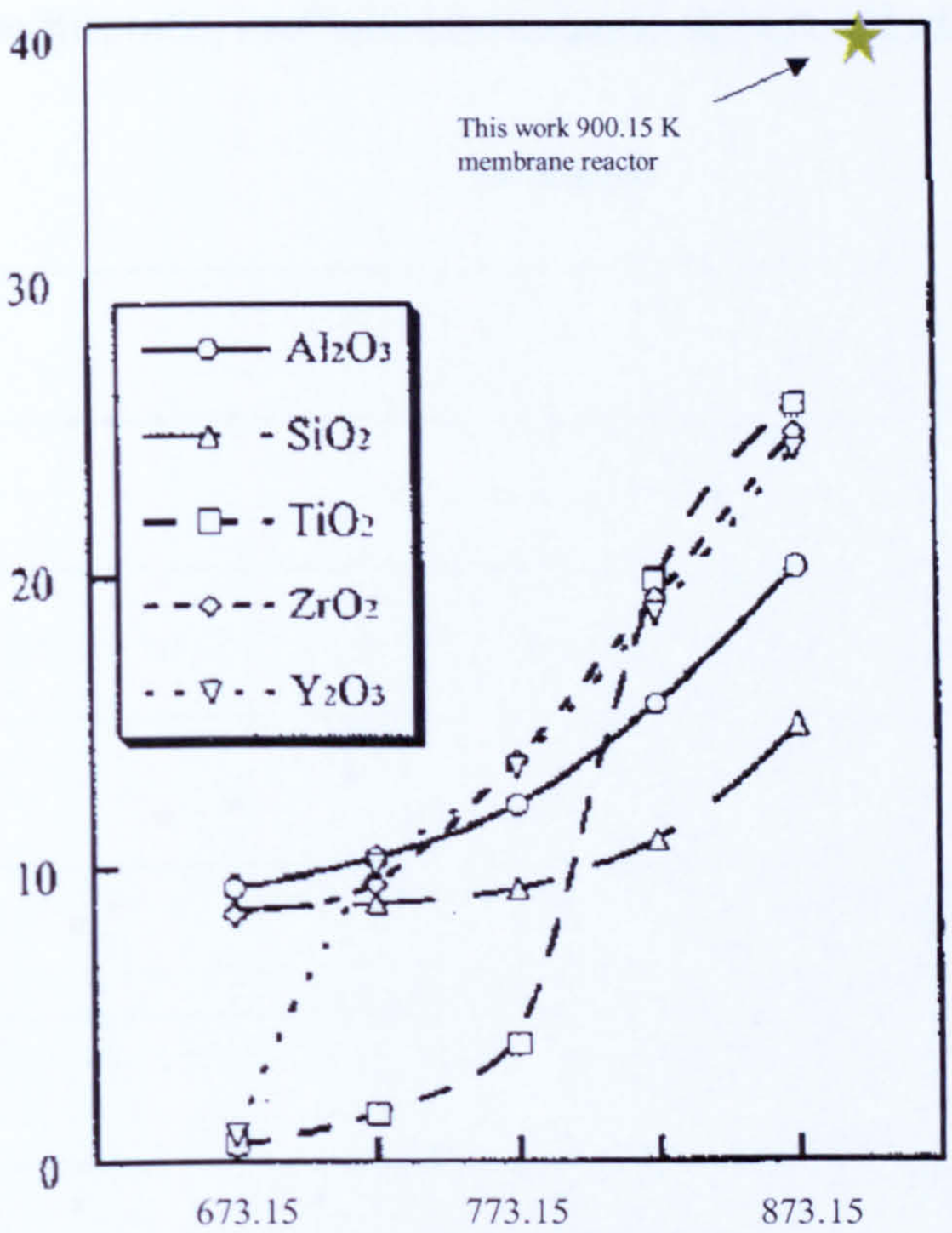

Figure 69: Effect of reaction temperature on the conversion of methane for fixed-bed and membrane reactor [87]

To illustrate the benefits of membrane reactor operation in syngas production, Figure 69 shows the effect of reaction temperature on the conversion of methane over an Ir-loaded catalyst carried out in a fixed-bed flow type quartz reactor (350-10mm) at atmospheric pressure, using 60mg of catalyst, 25 ml/min of O_2 and temperatures in the range 673-873K [87]. At 873K the performance of Ir and Rh are roughly identical. In the same figure, experimental data is shown for our membrane system at 900K. The conversion values obtained using a fixed-bed flow reactor are significantly lower than those obtained in the membrane reactor due to equilibrium limitation. This has been overcome in the membrane reactor which achieves the expected 100% conversion of oxygen and a methane conversion of 41%.

4.3.3.2. Effect of Inlet Methane/Oxygen Ratio

The effect of inlet methane/oxygen ratio on the rate of methane disappearance and syngas formation at a fixed temperature is shown is figure 70.

The results show that, while the oxygen conversion is always total, the methane conversion increases linearly with methane/oxygen ratio up to a methane/oxygen ratio of 4. Above this ratio, methane conversions remain virtually constant.

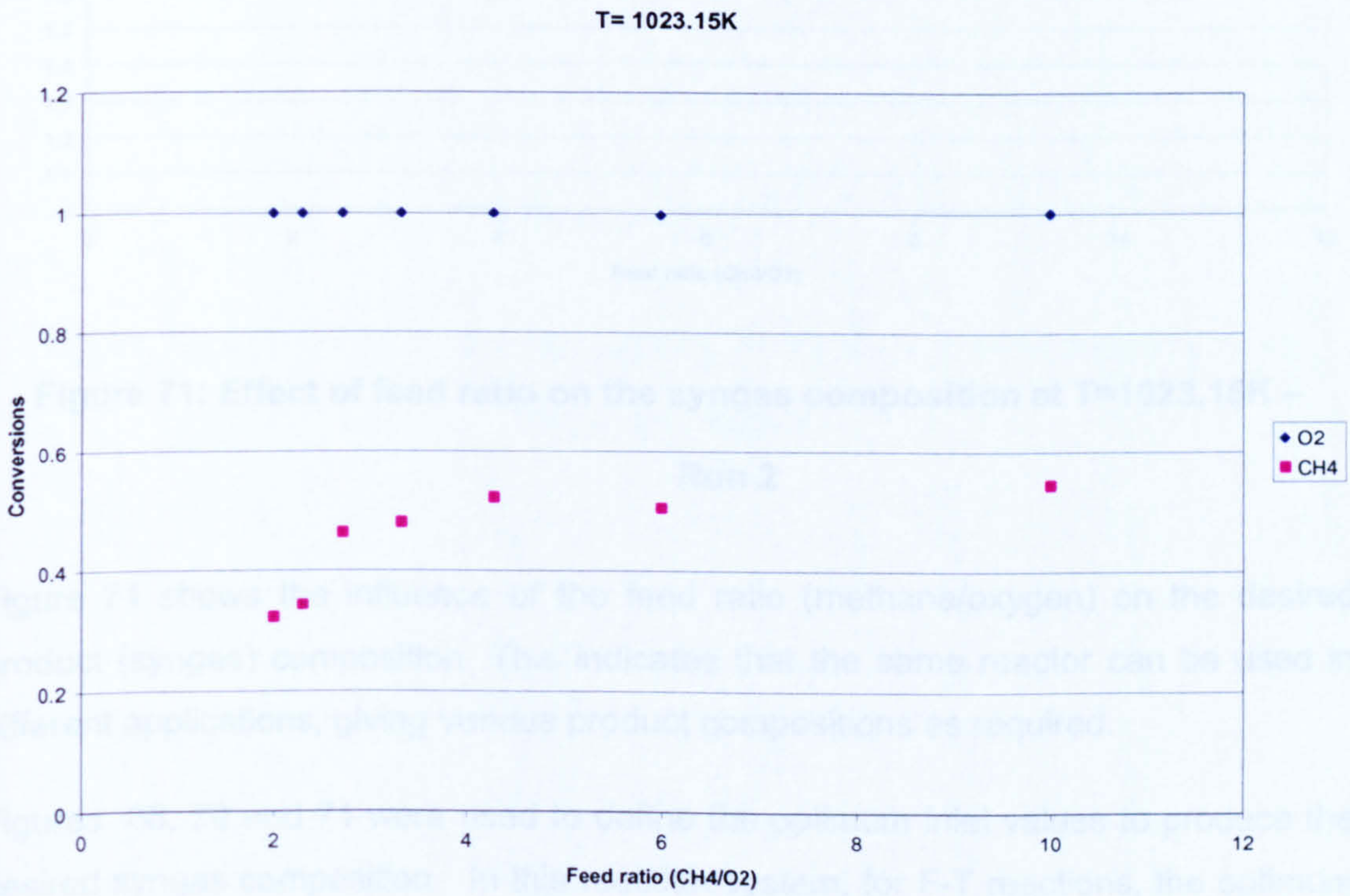

Figure 70: Effect of feed ration on the reactant conversion at T=1023.15K – Run 2

As mentioned earlier, the reaction occurs with 100% of oxygen conversion. From figure 70 it is observed that methane conversion increases steadily up to a feed ratio of 4. Above this value methane conversion remains constant. This could be attributed to the limitation in the area of contact of methane and the membrane. Increasing the membrane length will enable more methane to be activated resulting in higher conversions. Another possibility is to increase the number of tubes for the same reactor length. This will increase the reaction surface area and lead to enhanced methane conversions.

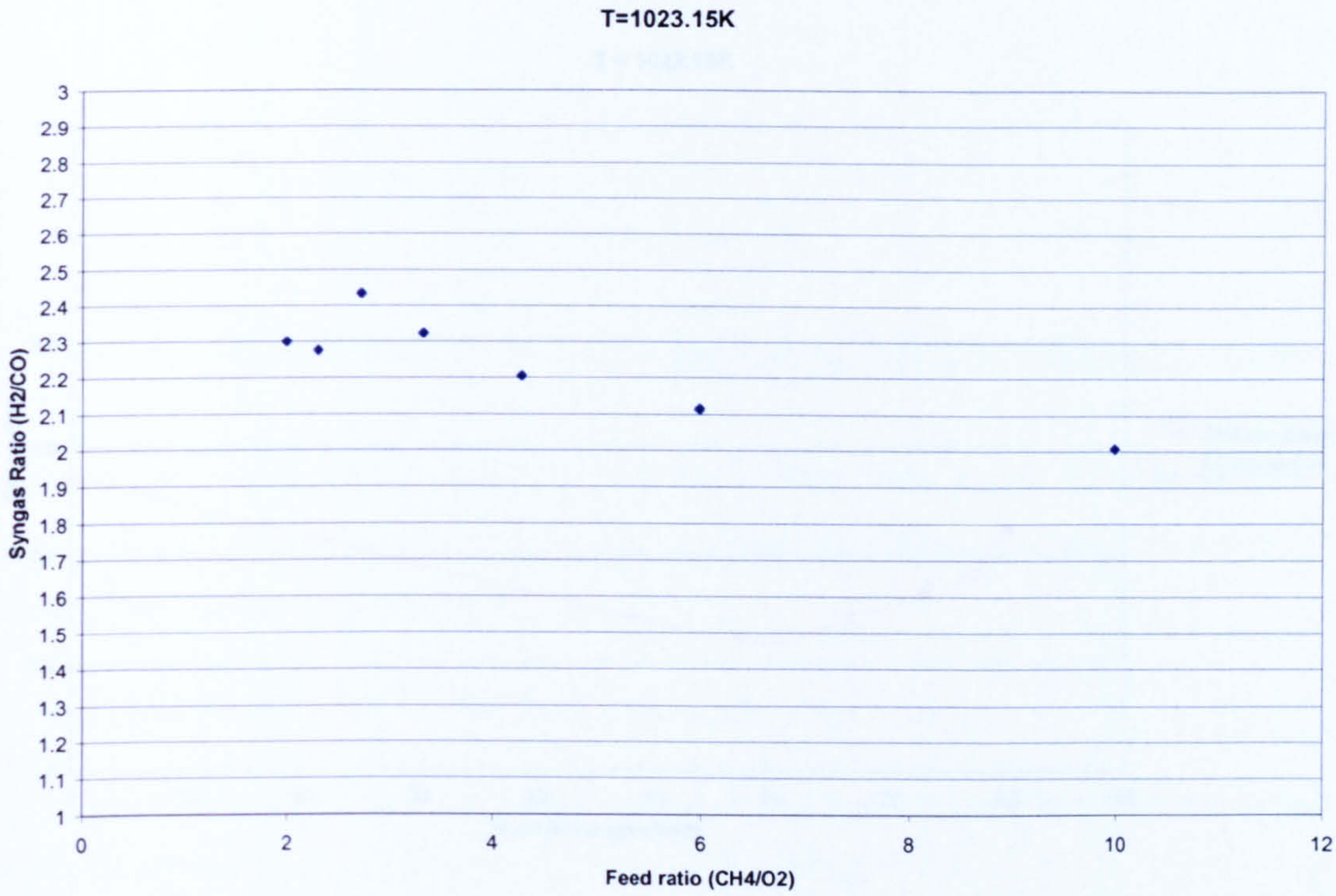

Figure 71: Effect of feed ratio on the syngas composition at T=1023.15K – Run 2

Figure 71 shows the influence of the feed ratio (methane/oxygen) on the desired product (syngas) composition. This indicates that the same reactor can be used in different applications, giving various product compositions as required.

Figures 68, 70 and 71 were used to define the optimum inlet values to produce the desired syngas composition. In this reaction system, for F-T reactions, the optimum feed composition of methane/oxygen is 10 at temperature of 1023.15K. This will give (for this size of reactor and this specific load of catalyst) a methane conversion of almost 60% and syngas ratio of 2.

4.3.3.3. Effect of Inlet Nitrogen Concentration

The effect of nitrogen concentration on the rate of methane disappearance and syngas formation at a fixed temperature is shown is figure 72.

The results show that the methane conversion decreases at concentrations around 50vol% N_2, increasing with the %vol. of N_2 inlet concentration.

The effect of nitrogen concentration on the type of syngas produced is showed in figure 73.

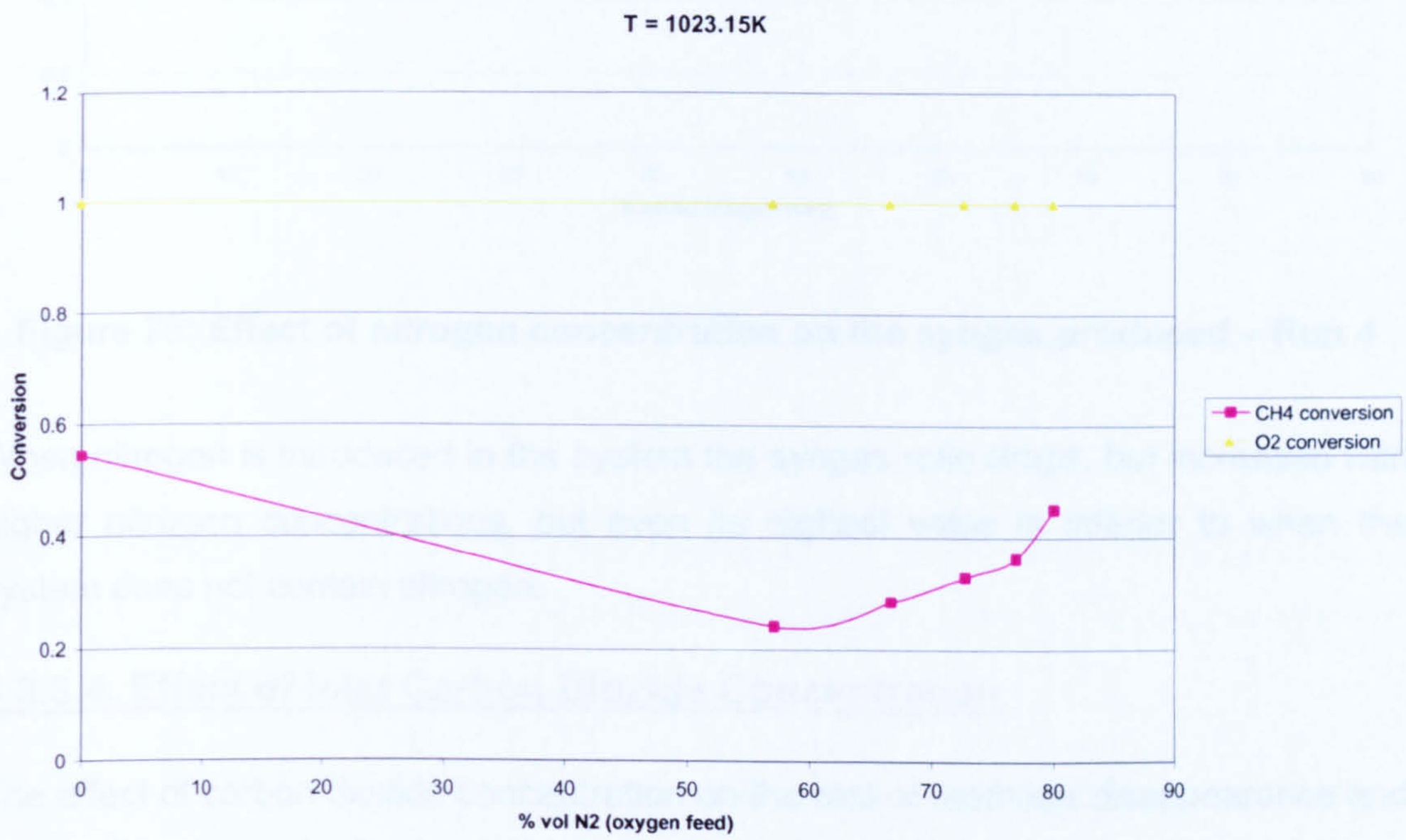

Figure 72: Effect of nitrogen concentration on the reactant conversion at T=1023K – Run 4

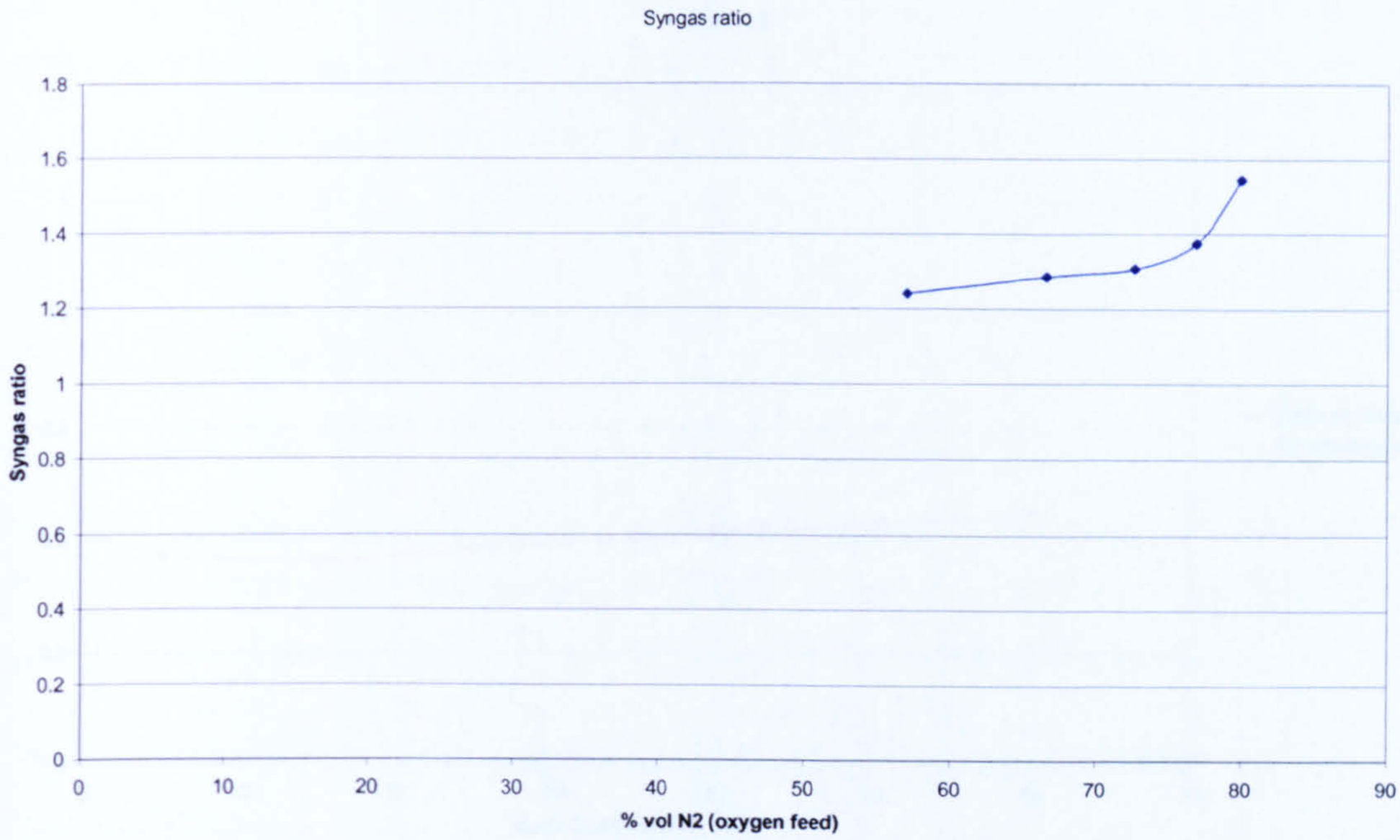

Figure 73: Effect of nitrogen concentration on the syngas produced – Run 4

When nitrogen is introduced in the system the syngas ratio drops, but increased with higher nitrogen concentrations, but even its highest value is inferior to when the system does not contain nitrogen.

4.3.3.4. Effect of Inlet Carbon Dioxide Concentration

The effect of carbon dioxide concentration on the rate of methane disappearance and syngas formation at a fixed temperature is shown is figure 74.

The results show that the conversion of methane varies slightly, increasing with higher concentrations of carbon dioxide inlet concentrations.

The effect of carbon dioxide concentration on the type of syngas produced is showed in figure 75.

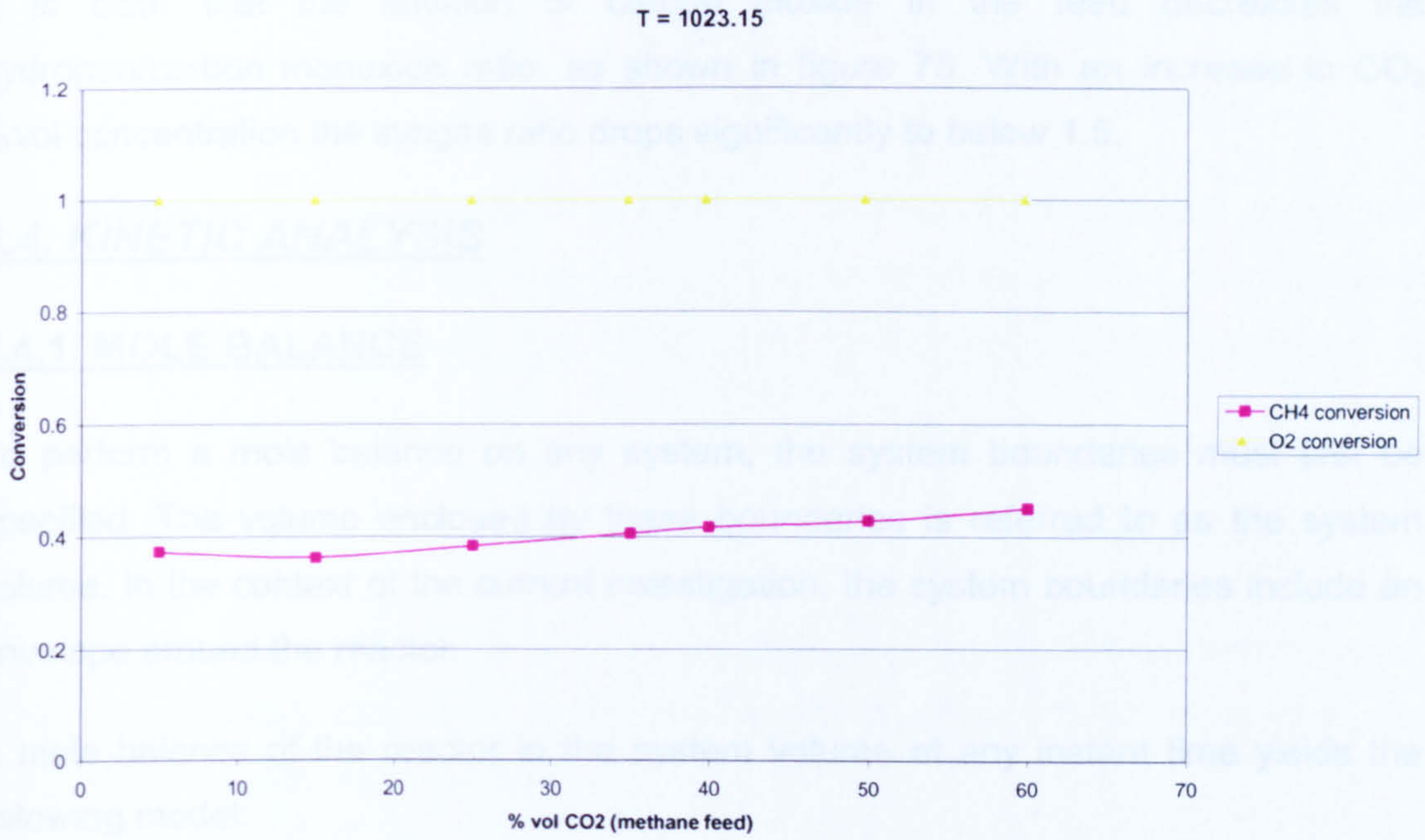

Figure 74: Effect of carbon dioxide concentration on the reactant conversion – Run 5

The conversion of methane is lower but relatively constant for operations which contain carbon dioxide in the feed, increasing slightly for higher CO_2 concentrations at constant temperature.

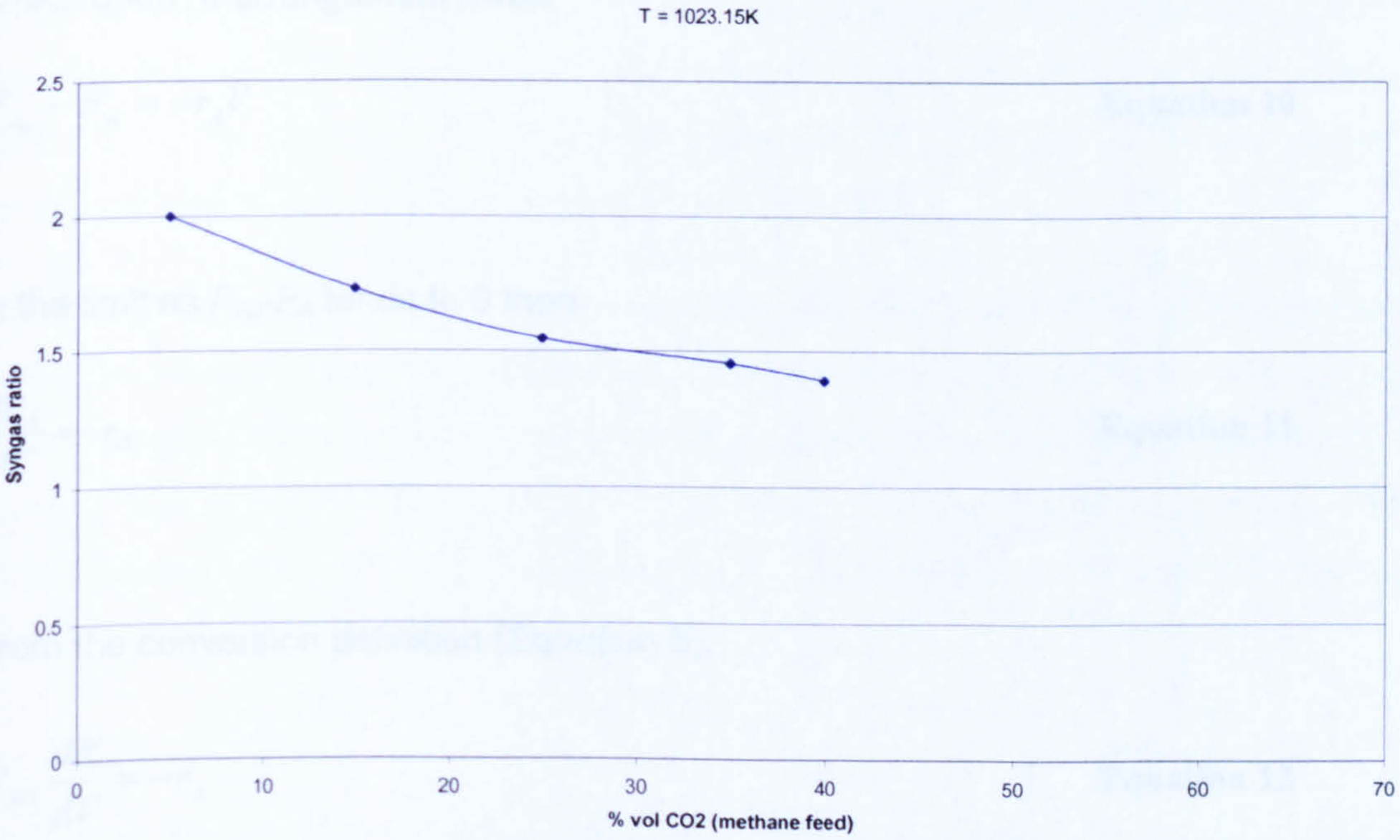

Figure 75: Effect of carbon dioxide concentration on the syngas produced at T=1023.15K – Run 5

It is clear that the addition of carbon dioxide in the feed decreases the hydrogen/carbon monoxide ratio, as shown in figure 75. With an increase in CO_2 %vol concentration the syngas ratio drops significantly to below 1.5.

4.4. KINETIC ANALYSIS

4.4.1. MOLE BALANCE

To perform a mole balance on any system, the system boundaries must first be specified. The volume enclosed by these boundaries is referred to as the system volume. In the context of the current investigation, the system boundaries include an envelope around the reactor.

A mole balance of the reactor in the system volume at any instant time yields the following model:

in+ generation-out=accumulation

From the mole balance for tubular reactors working at steady state, the reaction rate of the reacting species A can be calculated by [88]:

$$F_{A_0} + r_A V - F_A = 0 \qquad \textbf{Equation 9}$$

Which upon re-arrangement gives

$$F_{A_0} - F_A = -r_A V \qquad \textbf{Equation 10}$$

In the limit as F_{A0}-F_A tends to 0 then

$$\frac{dF_A}{dV} = -r_A \qquad \textbf{Equation 11}$$

From the conversion definition (Equation 5);

$$F_{A0}\frac{dX}{dV} = -r_A \qquad \textbf{Equation 12}$$

Which upon integration yields

$$F_{A0}\int_{x=0}^{x} dX = -\int_{0}^{V} r_A dV \qquad \textbf{Equation 13}$$

The volume of the reaction considered is the volume of the catalytic membrane assuming a highly disperse catalyst on its surface, resulting in a homogeneous surface reaction on the whole length of the membrane. Therefore equation 10 can be written:

$$\frac{F_{A0}X}{V} = -r_A \qquad \textbf{Equation 14}$$

Equation 14 was used to calculate the reaction rate from the experimental data, where the reaction volume V, is assumed as the membrane volume available for reaction. This is calculated as follows:

$$V = \pi \ x \ membrane\ thickness^2 \ x \ reactor\ length$$

$$V = \pi(1.875-1.25)^2 35$$

$$V = 43cm^3$$

4.4.2. RATE LAW

The rate of disappearance of the reactants depends on temperature and compositions. For many reactions it can be written as the product of a reaction rate constant *k* and a function of the concentrations (activities) of the various species involved in the reaction. The algebraic equation that relates $-r_A$ to the species concentrations is called the kinetic expression or rate law.

The dependence of the reaction rate $-r_A$ on the concentrations of the species present is almost without exception determined by experimental observation. Although the functional dependence may be postulated from theory, experiments are necessary to confirm the proposed form. One of the most common general forms of this dependence is the product concentration of the individual reacting species, each of which is raised to a power, for example:

$$-r_A = k_A C_A^{\ m} C_B^{\ n} \qquad \textbf{Equation 15}$$

Where in this case C_B could be the oxygen concentration and C_A the methane concentration.

The exponents of the concentrations in equation 15 above lead to a concept of *reaction order.* The order of a reaction refers to the powers to which the concentrations is raised in the kinetic law. The overall order of the reaction, is the sum of the reaction orders of the individual reactants.

In this work, as soon as the reaction ignites, the oxygen conversion is 100% for all the different parameters studied, thus it is feasible to assume that the oxygen concentration in the product stream does not affect the reaction rate to any significant extent.

Since $n = 0 \qquad C_B^{\,n} = 1$

Therefore, equation 15 can be written as:

$$-r_A = k_A C_A^{\,m} \qquad \textbf{Equation 16}$$

Where species A is methane.

Combining reaction rate values obtained from the mole balance (Equation 10) with the rate law (Equation 12) enable us to evaluate *m* and the values for the reaction constant for each run.

Equation 12 can be linearized as follows:

$$\ln(-r_A) = \ln k_A + m \ln C_A \qquad \textbf{Equation 17}$$

The reaction rate constant *k* is independent of the concentration of the species involved in the reaction [88]. The quantity *k* is also referred to as the specific reaction rate (constant). It almost always strongly dependent on the temperature. In gas-phase reactions, it depends on the catalyst and may be a function of total pressure. In liquid systems it can also be a function of total pressure, and in addition can depend on other parameters, such as ionic strength and choice of solvent. These other variables normally exhibit much less effect on the specific reaction rate than does temperature, so for the purpose of the material presented here it will be assumed that k_A depends only on temperature. This assumption is valid in most laboratory and industrial reactions and seems to work quite well. [88]

Table 17 shows the values of k for different temperatures.

Table 17: *k* value – Run 1

Temperature K	K
873.15	2.30491×10^{-10}
901.15	2.29871×10^{-10}
933.15	2.30766×10^{-10}
953.15	2.32025×10^{-10}
983.15	2.3231×10^{-10}
1023.15	2.25016×10^{-10}
1083.15	2.22511×10^{-10}

From Equation 13, it was possible to plot *ln k vs. ln* C_A in order to obtain the order of the reaction and the constant of the reaction value for each of the constant temperature runs. Run 1 is not included because it was carried out for different temperatures and run 3 gave different profile due to the very low methane conversion, also not included on this plot.

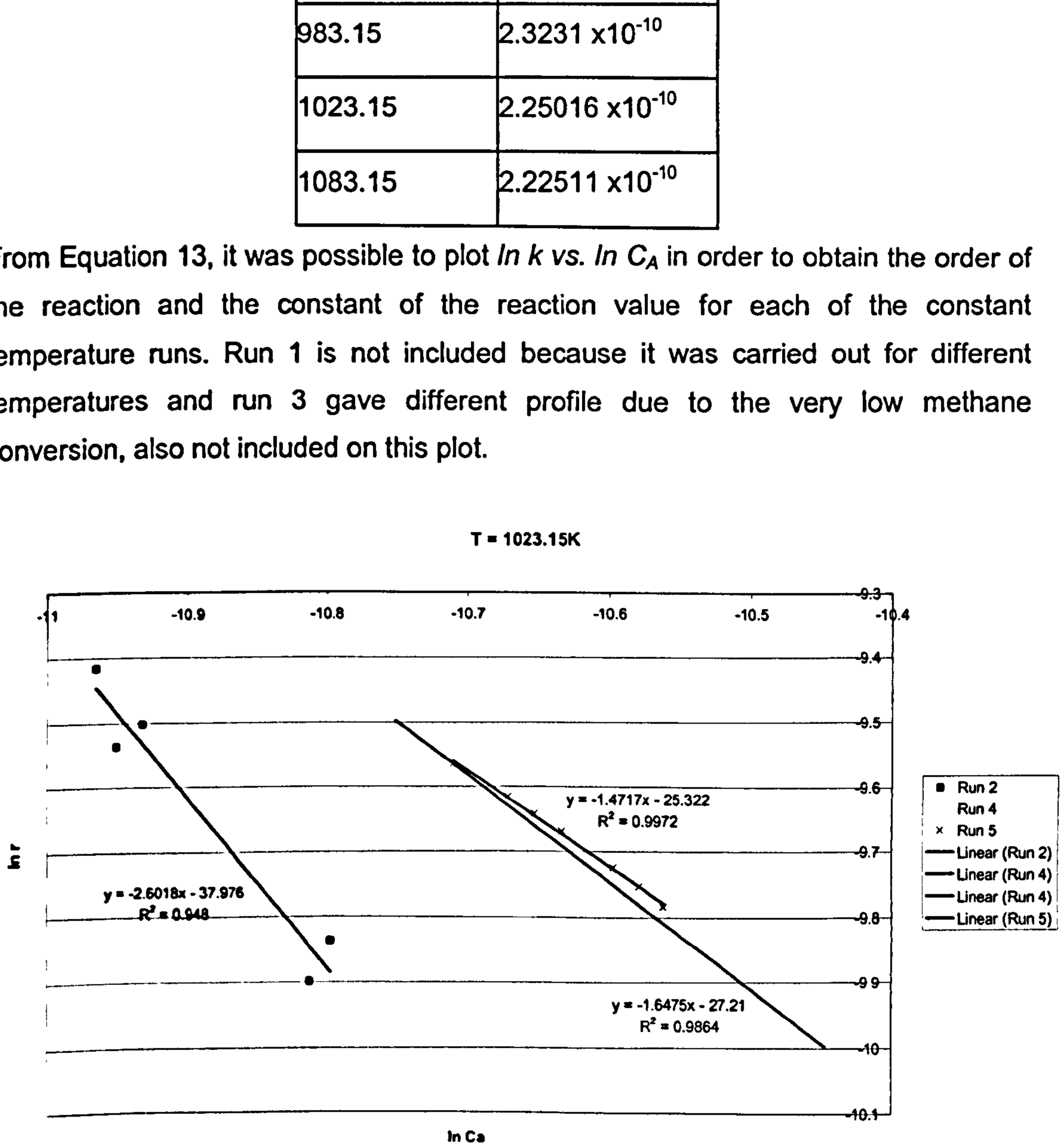

Figure 76: *ln* r_A *vs. ln* C_A – all runs

Table 18 summarises the *k* and *m* values for the different parameters evaluated.

Table 18: Summary of the reaction orders and constants

Run	K	m
2	3.215×10^{-17}	-2.6018
4	1.52×10^{-12}	-1.6475
5	1×10^{-11}	-1.4717

4.4.3. ACTIVATION ENERGY

It was the Swedish chemist Arrhenius who first suggested that the temperature dependence of the specific reaction rate, k_A, could be correlated by an equation of the type

$$k_A(T) = Ae^{-E/RT}$$ Arrhenius equation

where A = preexponential factor or frequency factor

E = activation energy, J/mol or cal/mol

R = gas constant = 8.314 J/mol K (= 1.987 cal/mol K)

T = absolute temperature, K

The Arrhenius equation has been verified empirically to give the temperature behaviour of most reaction rate constants within experimental accuracy over fairly large temperature ranges.

The activation energy *E* has been equated with a minimum energy that must be possessed by reacting molecules before the reaction will occur. From the kinetic theory of gases, the factor $e^{-E/RT}$ gives the fraction of the collisions between molecules that together have this minimum energy *E*. Although this might be an acceptable elementary explanation, some suggested that *E* is nothing more than an empirical parameter correlating the specific reaction rate to temperature.

The activation energy is determined experimentally by carrying out the reaction at several different temperatures. After taking the natural logarithm of the Arrhenius equation:

$$\ln k_A = \ln A - \frac{E}{R}\left(\frac{1}{T}\right) \qquad \textbf{Equation 18}$$

The nature of Equation 18 suggests that a plot of ln k_A versus 1/T should be a straight line whose slope is proportional to the ratio of the activation energy and the gas constant. Such a plot for run 1 is shown in Figure 77.

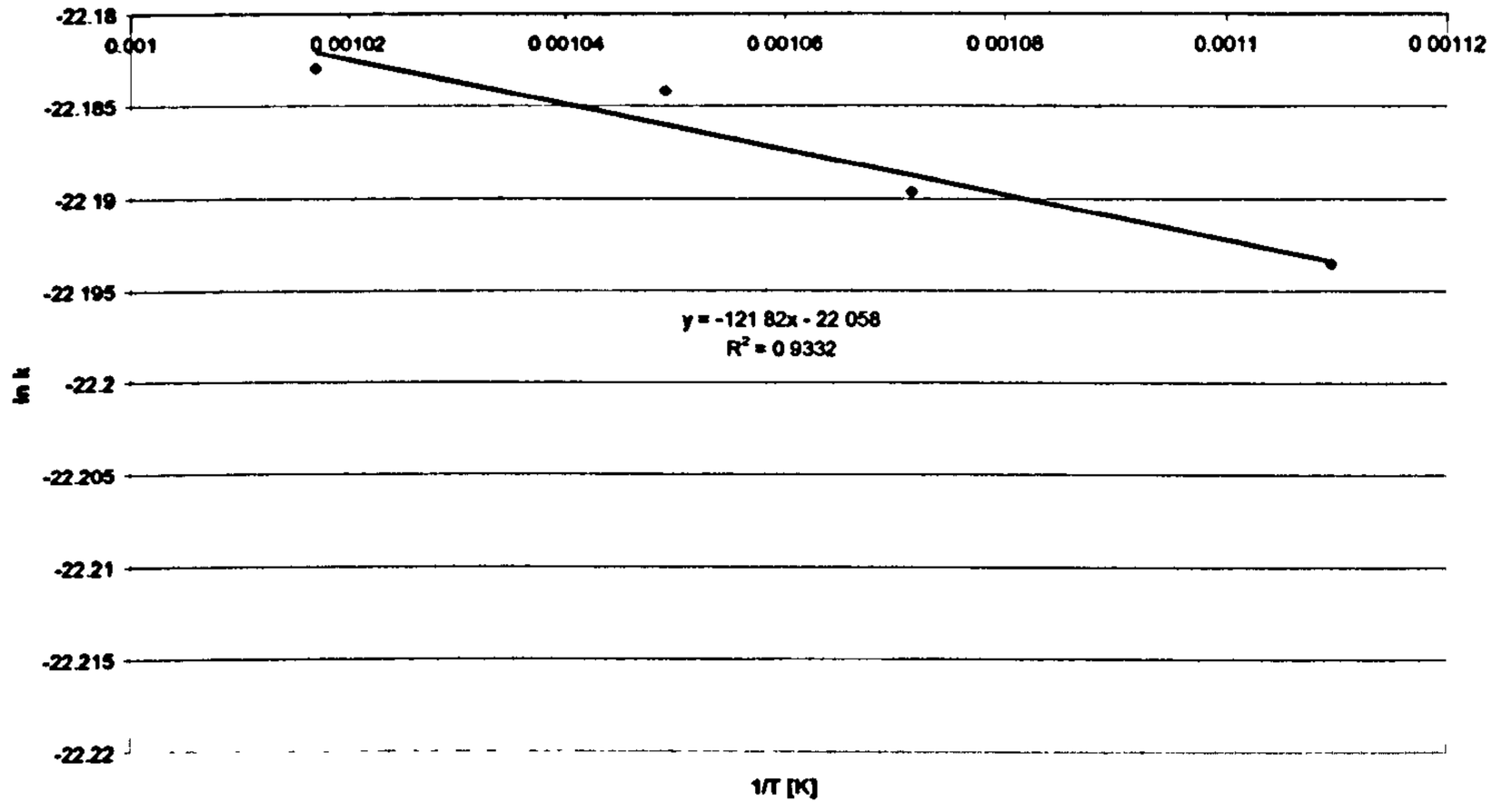

Figure 77: Plot of *ln k_A vs. 1/T* – Run 1

From the slope the activation energy was also evaluated

$\frac{E}{R} = -121.82$, therefore

E = -1.012 kJ/mol K or E = -0.24 kcal/mol K

The preexponential factor or frequency factor A was evaluated

ln A = 22.058, therefore A = 2.6×10^{-10}

The partial oxidation reaction itself is highly exothermic. The activation energy value obtained of –1.012kJ/mol K suggests that the reaction is only slightly exothermic. This is consistent with the fact that since there is significant water production, under adequate conditions some methane reacts with steam via steam reforming. Also, under suitable conditions carbon dioxide reacts with methane. These two reactions are endothermic, and as a result the combined reactions create a thermo neutral system.

5. CONCLUSION AND SIGNIFICANCE

Partial oxidation is an interesting, highly versatile and promising approach to generating synthesis gas from methane and oxygen or air, which can provide the hydrogen to carbon monoxide ratios suitable for methanol and gas-to-liquids processes. This investigation has extended the envelope of applicability by utilising a membrane-catalyst that is non-selective to oxygen but nevertheless results in complete oxygen conversion. Based on the experimental results obtained, the following conclusions can be drawn:

A methodology of modifying commercially available ceramic membranes and incorporating catalytic material with the porous matrix framework has been developed. The membranes have been characterised using scanning electron microscopy, energy dispersive x-ray analysis, x-ray photoelectron spectroscopy and cryogenic nitrogen adsorption respectively. These show a porous structure with highly dispersed catalytic material within its framework.

This study has designed and constructed a novel membrane-catalyst for the efficient contact of methane and oxygen so as to overcome the flammability constraints inherent in co-fed flow reactor systems.

A screening test involving a number of catalysts revealed that rhodium was the most effective and selective catalyst for syngas production from methane.

In the novel membrane reactor, the active porous layer is located at both sides facing the oxygen and methane containing gas, adjacent is a second active porous layer and is supported by layers with increasing pore radii. Here, active porous layer on the bore side enhances the reaction between permeated oxygen and fuel species.

A process gas stream comprising a fuel, such as hydrocarbons and carbon monoxide, steam and recycle gas (H_2, CO, and CO_2) flows next to or through the catalyst impregnated layer. Since in this application fuel species have to diffuse to the bore side of the active layer and the adjacent porous layer, the gaseous environment at and near the bore of the active layer is less reducing than in the outer porous layers. As a result a complete or partial oxidation reaction takes place with some reforming occurring as gas moves away from the active layers respectively. It is advantageous to coat pores of the last porous support layer with a reforming catalyst such as Rh to induce some endothermic reforming as combustion products flow through the porous support layer. This will assist in removing the heat of the

exothermic oxidation reaction from the surface of the active porous layer. The gradient of oxygen activity in the porous layer will prevent damage to the active layers from exposure to very low oxygen partial pressures, thus permitting a greater degree of freedom in the selection of materials for these layers.

The result of this model of catalyst/reactant contact is the non-triangular reaction kinetic scheme; $CH_4 + O_2 \xrightarrow{k_1} CO + H_2 + H_2O$ (with k_2 to CO_2) at temperatures below 1023.15K.

A reactor design model which assumes a flow through an isothermal cylindrical pore incorporating the catalyst has been developed in conjunction with the power rate law to obtain kinetic design parameters for the reaction.

An optimum reactor operating temperature of 1023.15K has been observed. Above this temperature, total oxidation products comprising carbon dioxide and water predominate resulting in lower synthesis gas generation.

The reaction takes place within the membrane support. This is justified by the fact that the composition of the reaction products exiting the tube side and the shell side are identical.

A mathematical expression relating methane conversion and the respective products yields with reactor temperature has been established. This would be helpful in reactor optimisation.

The investigation has also revealed that for this reactor, there is an optimum methane/oxygen ratio of 10.0 at which point the syngas ratio was 2 and methane conversion was constant. This has been attributed to the limitation in the active area of contact between the methane and catalyst. One possible solution is to increase the membrane length or to increase the number of tubes while maintaining the same reactor length. This will increase the reaction surface area and lead to enhanced methane conversion.

The investigation has also shown the effect of the presence of diluents including nitrogen and carbon dioxide. In the CO_2 instances case the diluent concentration reduces the syngas ratio while for nitrogen, the ration increased but was below the required value of 2.0.

Reforming of natural gas with CO_2 is not only important in industry for CO production, but also attracts interest as a CO_2 consuming reaction, which is a greenhouse gas.

This reaction is of interest because the lower H_2/CO ratio in the product gas is used in the industrial manufacture of oxo-alcohols, where carbon monoxide is combined with hydrogen in a 1:1 ratio to form an aldehyde. This aldehyde is then reacted with pure hydrogen to form the desired oxo-alcohol product.

In the commercial production of Fischer-Tropsch gas-to-liquids, the syngas generation process is very expensive due to the need for an oxygen separation stage. In the current reactor system, this separation is not necessary since the oxygen conversion is 100%. However, nitrogen will be present in the feedstock to the Fischer-Tropsch reactors. The presence of nitrogen can only be problematic if there is a recycle stream. We envisage a process where all the methane is consumed which means there is no need for a recycle stream. Therefore our estimate indicate that the absence of an air separation stage will cut the syngas generation cost by 40% resulting in a highly competitive process.

Further Industrial Significance

The syngas ceramic membrane reactor is a highly flexible technology and can be used to produce many syngas compositions by adjusting the oxygen transmembrane pressure and methane flowrate independently. The final choice depends on the operating costs and investments. In current industrial practice, it is more cost effective to adjust the syngas ratio in the gas purification section to get the required syngas and side stream product, e.g. an oxogas (H_2/CO=1.0) and a separate H_2 product.

In the porous ceramic membrane process, optimisation of H_2 production can be obtained by suitably adjusting the CH_4/O_2 ratio and reaction temperature. At CH_4/O_2 feed ratio below 4.0, higher H_2/CO ratios are attained while above CH_4/O_2 feed ratio of 4.0 the H_2/CO ratio falls monotonically. Also, at a fixed CH_4/O_2 feed ratio, temperatures below 1023.15K produce a H_2/CO ratio higher than 2.0 while at temperatures above 1023.15K, the H_2/CO ratio falls significantly below 2.0.

Operating cost for traditional oxygen-consuming syngas technologies are sensitive to oxygen price. Therefore, low-oxygen consumption and high methane conversion are essential. In the ceramic membrane reactor, experiments conducted with air have confirmed that total oxygen conversion can still be attained and there will be no need for an oxygen separation plant. This avoids the need for high pressure operation. High-preheat temperatures can also be avoided since there is no need to reduce oxygen consumption. The investment for a ceramic membrane reactor plant

producing e.g. H_2/CO = 1.5 to 2.0, is lower than other syngas technologies. Operating costs will also be significantly lower since there is no need for an oxygen separating plant.

Current activity in industrial gas-to-liquids plants

Royal Dutch/Shell Group just inked a deal with the small Middle Eastern nation of Qatar that could spark new markets for natural gas. If Shell's roughly $5 billion investment to build one of the world's largest gas-to-liquids (GTL) plants is successful, the transportation fuel substitute would ease demand on crude oil as well as find productive uses for stranded natural gas globally [89].

Japan's Institute of Energy Economics, declares that the demand for GTL in Asia alone is about 5 million barrels a day [4].

Qatar Petroleum and Shell signed the deal in October 2003 that would convert natural gas from Qatar's North Field into clean burning diesel fuel. The goal is to produce 140,000 barrels of GTL a day by 2009—a mission that is not just environmentally friendly but also one that is competitively priced with that of oil. Qatar, which ranks behind Russia and Iran in terms of total natural gas reserves and is also loyal to the United States, is aggressively opening its reserves to GTL development [89].

If the cost to produce GTL can support going forward, market demand appears to be strong: In Europe, sulphur emissions from road fuels are to be cut dramatically by 2005 while new EPA regulations call for reducing the sulphur content in diesel fuel by 97 percent by 2010. Shell already has a GTL pilot plant in Malaysia that has been producing 12,000 barrels a day [3].

GTL has been on the radar since the mid 1990s, when Exxon and Qatar Petroleum first talked about making productive use of Qatar's gas reserves. The negotiations infused hope that GTL would fast become a reality. But that has not happened, although others have invested and shown a keen interest in the technology. Beside Exxon and Shell, Marathon Oil, ChevronTexaco, ConocoPhillips and South Africa's Sasol have deals in the works for GTL projects in Qatar. If all goes according to plan, within a decade Qatar says that it can generate 700,000 barrels a day of GTL [3].

Meanwhile, Russian conglomerates Gazprom and Yukos are working with American developer Syntroleum to find ways to monetize the gas reserves, or turn them into

cash. Syntroleum is performing feasibility studies in Siberia as well looking at 12 potential GTL sites across Russia [89].

Finally, BP is working on a GTL project. The long-term goal is to bring stranded gas from Alaska's North Slope to the Lower 48, about 35 tcf of known reserves. In late July 2003, BP started harnessing its Nikiski project, which is cranking out about 100 barrels a day of a clear liquid called synthetic crude oil. While the number of barrels will rise to about 250 barrels a day, the plant will be dismantled after about 18 months. That's because BP is only out to prove the viability of the technology—not mass produce GTL because it is not yet cost effective [89].

GTL, while a newer concept than LNG, has key advantages in that it can use the same transportation system as that of crude oil. At the same time, the prices for a barrel of GTL and oil are competitive. The difference, however, is that GTL emits no sulphur and is generally a cleaner burning fuel. As new ways are found to produce GTL more efficiently and as environmental regulations tighten, the investments made by the major oil companies in GTL could pay off—not just for shareholders but for everyone else too [3].

6. RECOMMENDATIONS FOR FUTURE WORK

A mathematical model should be developed capable of predicting the optimum membrane area and feed conversion at any given flow rate and syngas composition. This will enable the determination of key parameter values for optimum reactor performance.

A pilot plant unit should be constructed and tested in conjunction with the model to enhance the commercialisation of the technology.

It is recommended that long-term stability tests be conducted on the pilot plant unit to confirm the suitability of the catalysts and membrane in industrial practice.

It is recommended an extensive secondary market study be carried out to ascertain the market size to this process.

REFERENCES

1. **Basile, A., L. Paturzo, and A. Vazzana, *Membrane reactor for the production of hydrogen and higher hydrocarbons from methane over Ru/Al_2O_3 catalyst.* Chemical Engineering Journal, 2002. 4045: p. 1-9.**
2. **Macdonald, B., *Syngas - not just a load of hot air.* ECN Chemscope, 1999: p. 24-25.**
3. **Wang, H.Y. and E. Ruckenstein, *Partial oxidation of methane to synthesis gas over MgO- and SiO_2-supported rhodium catalysts.* Journal of Catalysis, 1999. 186: p. 181-187.**
4. **Fischer, P. A., *Natural Gas: Part 8: Monetising Stranded Gas.* World Oil, Nov. 2001. p. 72-80.**
5. ***World LNG/GTL Review.* Zeus Development Corp., 2001.**
6. **Jess, A., R. Popp, and K. Hedden, *Fischer-Tropsch-synthesis with nitrogen-rich syngas; Fundamentals and reactor design aspects.* Applied Catalysis A: General, 1999. 186(1-2): p. 321-342.**
7. **Wilhelm, D.J., et al., *Syngas production for gas-to-liquids applications: technologies, issues and outlook.* Fuel Processing Technology, 2001. 71(1-3): p. 139-148.**
8. **Newsome, D.S. and B.G. Mandelik, *Kirk-Othmer Encyclopedia of Chemical Technology.* 3rd ed. Vol. 12. 1981, New York: Wiley-Interscience.**
9. **Haggin, J., Chemical Engineering News, 1992. 70: p. 33.**
10. **Michel, S., Hydrocarbon Processing, 1989. 68(4): p. 37.**
11. **Solbakken, A., Studies in Surface Science and Catalysis, 1991. 61: p. 447.**
12. **Pena, M.A., J.P. Gomez, and J.L.G. Fierro, *New catalytic routes for syngas and hydrogen production.* Applied Catalysis A: General, 1996. 144(1-2): p. 7-57.**
13. **Nielsen, J.R., I. Dibkjaer, and L.J. Christiansen, *NATO ASI Chemical Reactor Technology for Environmentaly Safe Reactors and Products.* 1992 ed, ed. H.d. Lasa. 1992: Dordrecht. 249.**
14. **Satterfield, C.N., *Heterogeneous Catalysis in Industrial Practice.* 1991, New York: McGraw-Hill.**
15. **Rostrup-Nielsen, J.R., *Production of synthesis gas.* Catalysis Today, 1993. 18(4): p. 305-324.**
16. **Rostrup-Nielsen, J.R., J.R. Anderson, and B. M., Catalysis Science and Technology, 1984. 5: p. 1.**
17. **Gobina, E., *Inorganic membranes tackle oxo-alcohol synthesis gas production in a fluidised-bed reactor.* Membrane Technology, 2000. 2000(125): p. 4-8.**
18. **Richardson, J.T. and S.A. Paripatyadar, *Carbon dioxide reforming of methane with supported rhodium.* Applied Catalysis, 1990. 61(1): p. 293-309.**
19. **Bodrov, I.M. and L.O. Apel'baum, Kinet. Katal., 1967. 8: p. 379.**

20. **Rostrupnielsen J. R. and Hansen J. H. B., *CO2-Reforming of Methane over Transition Metals.* Journal of Catalysis, 1993. 144(1): p. 38-49.**

21. **Vernon, P.D.F., et al., *Partial oxidation of methane to synthesis gas, and carbon dioxide as an oxidising agent for methane conversion.* Catalysis Today, 1992. 13(2-3): p. 417-426.**

22. **Perera, J.S.H.Q., et al., Catalysis Letters, 1991. 11: p. 219.**

23. **Rostrup-Nielsen, J.R., Journal of Catalysis, 1984. 85: p. 31.**

24. **Rostrup-Nielsen, J.R., Studies in Surface Science and Catalysis, 1991. 68: p. 85.**

25. **Pinto, A., *Steam Reforming.* 1988, Imperial Chemical Industries PLC (London, GB2): US.**

26. **Goetsch, D.A. and G.R. Say, *Synthesis gas preparation and catalyst therefor.* 1991, Exxon Research and Engineering Company (Florham Park, NJ): US.**

27. **Supp, E., Hydrocarbon Processing, 1984. 63(7): p. 34c.**

28. **Fujitani; Yoshiyasu (Nagoya, J. and J. Muraki; Hideaki (Nagoya, *Process for partially oxidizing hydrocarbons.* 1976, Kabushiki Kaisha Toyota Chuo Kenkyusho (JA): US.**

29. **Hwang, H.-S., R.M. Heck, and R.M. Yarrington, *Fuel cell electric power production.* 1984, Engelhard Corporation (Iselin, NJ): US.**

30. **Hickman, D.A. and L.D. Schmidt, *Synthesis Gas Formation by Direct Oxidation of Methane over Pt Monoliths.* Journal of Catalysis, 1992. 138: p. 267-282.**

31. **Hickman, D.A. and L.D. Schmidt, *Steps in CH4 Oxidation on Pt and Rh Surfaces: High-Temperature Reactor Simulations.* AIChE Journal, 1993. 39(7): p. 1164-1177.**

32. **Prettre, M., C. Eichner, and M. Perrin, Trans. Faraday Society, 1946. 43: p. 335.**

33. **Huszar, K., G. Racs, and Szekely, Acta Chim. Acad. Sci. Hung., 1971. 70: p. 287.**

34. **Gavalas, G.R., C. Phichticul, and G.E. Voecks, Journal of Catalysis, 1984. 88: p. 54.**

35. **Lafarga, D., J. Santamaria, and M. Menendez, *Methane Oxidative Coupling Using Porous Ceramic Membrane Reactors - I. Reactor Development.* Chemical Engineering Science, 1994. 49(12): p. 2005-2013.**

36. **Blanks, R.F., T.S. Wittrig, and D.A. Peterson, *Bidirectional adiabatic synthesis gas generator.* Chemical Engineering Science, 1990. 45(8): p. 2407-2413.**

37. **Ashcroft, A.T., et al., Nature, 1990. 344: p. 319.**

38. **Ashcroft, A.T., et al., Nature, 1991. 352: p. 225.**

39. **Poirier, M.G., G. Jean, and M.P. Poirier, Studies in Surface Science and Catalysis, 1992. 73: p. 359.**

40. **Vermeiren, W.J.M., E. Blomsma, and P.A. Jacobs, *Catalytic and thermodynamic approach of the oxyreforming reaction of methane.* Catalysis Today, 1992. 13(2-3): p. 427-436.**

41. **Dissanayake, D., et al., Journal of Catalysis, 1991. 132: p. 117.**

42. **Choudhary V. R., Rajput A. M., and Prabhakar B., *Nonequilibrium Oxidative Conversion of Methane to CO and H2 with High Selectivity and Productivity over Ni/Al2O3 at Low Temperatures.* Journal of Catalysis, 1993. 139(1): p. 326-328.**

43. **Dissanayake, D., M.P. Rosynek, and J.H. Lunsford, Journal of Physics and Chemistry, 1993. 97: p. 3644.**

44. **Hayakawa, T., et al., Catalysis Letters, 1993. 22: p. 307.**

45. **Alqahtani, H., D. Eng, and M. Stoukides, J. Eletrochem. Soc., 1993. 140: p. 1677.**

46. **Nakamura, J., et al., J. Jpn. Petrol. Inst., 1993. 36(2): p. 97.**

47. **Lapszewicz, J. and X. Jiang, Amerrican Chem. Soc., 1992. 37(1): p. 252.**

48. **Buyevskaya, O.V., D. Wolf, and M. Baerns, Catalysis Letters, 1994. 29: p. 249.**

49. **Walter, K., et al., Catalysis Letters, 1994. 29: p. 261.**

50. **Mallens, E.P.J., J.H.B.J. Hoebink, and C.B. Marin, Catalysis Letters, 1995. 33: p. 291.**

51. **Peuckert, M. and H.P. Bonzel, *Characterization of oxidized platinum surfaces by X-ray photoelectron spectroscopy*. Surface Science, 1984. 145(1): p. 239-259.**

52. **Niehus, H. and G. Comsa, *Surface and subsurface oxygen adsorbed on Pt(111)*. Surface Science, 1980. 93(2-3): p. L147-L150.**

53. **Bosch, H. and F. Janssen, *Formation and control of nitrogen oxides*. Catalysis Today, 1988. 2(4): p. 369-379.**

54. **Korchnak, J.D., M. Dunster, and A. English. Patent no. WO90/06282, 1990.**

55. **Hochmuth, J.K., Applied Catalysis B, 1992. 100: p. 89.**

56. **Torniainen, P., X. Chu, and L.D. Schmidt, Journal of Catalysis, 1994. 146(1): p. 1.**

57. **Gomez, J.P., et al. in *4th International Natural Gas Conversion Simposium*. 1995. South Africa.**

58. **Brophy, J.H. and F.J. Weinberg., Patent no. WO/85/04647, British Petroleum Company. 1985**

59. **Brophy, J.H. and C.D. Telford. Patent no. WO85/05094, British Petroleum Company, 1985.**

60. **Sie, S.T., Patent no. US5186859, Shell Oil CO (US), 1993.**

61. **Bharadwaj, S.S. and L.D. Schmidt, Journal of Catalysis, 1994. 146(1): p. 1L.**

62. **Alibrando, M. and E.E. Wolf. *Partial Oxidation of Methane to Synthesis Gas in a Fast Flow Membrane Reactor*. in *3rd World Congress on Oxidation Catalysis*: Elsevier Science B. V.**

63. **Wang, H., Y. Cong, and W. Yang, *Partial oxidation of ethane to syngas in an oxygen-permeable membrane reactor*. Journal of Membrane Science, 2002. 209(1): p. 143-152.**

64. **Jin, W., et al., *Experimental and simulation study on a catalyst packed tubular dense membrane reactor for partial oxidation of methane to syngas*. Chemical Engineering Science, 2000. 55(14): p. 2617-2625.**

65. **Coronas, J., M. Menendez, and J. Santamaria, *Methane Oxidative Coupling Using Porous Ceramic Membrane Reactors - II Reaction Studies*. Chemical Engineering Science, 1994. 49(00): p. 00-010.**

66. **A., F.G. and J.A. Lapszewicz. Catalysis. Vol. 11. 1994, London: The Royal Society of Chemistry. 412.**

67. **Lahn, G.C., et al.** ***Section A1: Syngas production and conversion.*** **in** ***Eurogas 92.*** **1992.**

68. **Jean, F. P. and Bonifai, R., Patent No US4620940, Institut Francais du Petrole, 1991.**

69. **Scott, K. and J. Lobato,** ***Mass transfer characteristics of cross-corrugated membranes*1.*** **Desalination, 2002. 146(1-3 SU -): p. 255-258.**

70. **Bredesen, R.** ***Key points in the development of catalytic membrane reactors.*** **in** ***13th International Congress of Chemical and Process Engineering.*** **1998. Praha, Czech Republic: SINTEF Materials Technology.**

71. **Koops, G.H.,** ***Nomenclature and Symbols in Membrane Science and Technology.*** **European Society of Membrane Science and Technology, 1995.**

72. **Soria, R.,** ***Overview on industrial membranes.*** **Catalysis Today, 1995. 25(3-4): p. 285-290.**

73. **Keizer, K., et al.,** ***Microstructural properties of non-supported microporous ceramic membrane top-layers obtained by the sol-gel process.*** **Journal of Non-Crystalline Solids, 1996. 195(3): p. 203-217.**

74. **Dyer, P.N. and C.M. Chen.** ***Engineering development of ceramic membrane reactor systems for converting natural gas to hydrogen and synthesis gas for liquid transportation fuels.*** **in** ***2000 Hydrogen program review.*** **2000: Air products and chemicals inc.**

75. **Bredesen, R.** ***A technical and economic assessment of membrane reactors for hydrogen and syngas production.*** **in** ***United nations - economic commission for europe seminar.*** **1996. Cetraro, Calabria (Italy).**

76. **Gobina, E.,** ***Membrane technology allows high yields of syngas at reduced temperatures.*** **Remote gas strategies, 2000: p. 4-5.**

77. **Galuszka, J., R.N. Pandey, and S. Ahmed,** ***Methane conversion to syngas in a palladium membrane reactor.*** **Catalysis Today, 1998. 46(2-3): p. 83-89.**

78. **Lewis, R.J.,** ***SAX'S Dangerour Prorpieties,*** **ed. E. edition.**

79. **Brunauer, S., P.H. Emmet, and E. Teller,** ***Adsorption of gases in multimolecular layers.*** **Journal of American Chemical Society, 1938. 60: p. 309-319.**

80. **Barret, E.P., L.G. Joyner, and P.P. Halenda,** ***The determination of pore volume and area distribution in porous substances. I. Computations from nitrogen isotherms.*** **Journal of American Chemical Society, 1951. 73: p. 373-380.**

81. **Lippens, B.C. and J.H.d. Boer,** ***Studies on pore systems in catalyst v. the t method.*** **Journal of Catalysis, 1965. 4: p. 319-323.**

82. **Lindlar, B., et al.,** ***Chemical modification of high-quality large-pore M41S materials.*** **Journal of Materials Chemistry, 2002. 12: p. 528-533.**

83. **Briggs, D., M.P. Seah, and Wiley,** ***Practical surface analysis.*** **Auger and x-ray photoelectron spectroscopy. Vol. Vol 1.**

84. **Tough, I.,** ***An Introduction to the Scanning Electron Microscope.*** **2001. Class notes. Department of Applied Science – The Robert Gordon University.**

85. **Tough, I.** ***Quantitative X-ray Analysis Using the Scanning Electron Microscope.*** **2001. Class notes. Department of Applied Science – The Robert Gordon University.**

86. **Li, S., et al.,** ***Partial oxidation of methane to carbon monoxide and hydrogen over NiO/La2O3/[gamma]-Al2O3 catalyst.*** **Applied Catalysis A: General, 1996. 134(1): p. 67-80.**

87. **Nakagawa, K., et al.,** ***Partial Oxidation of Methane to Synthesis Gas with Iridium-loaded Titania Catalyst.*** **Chemistry Letters, 1996: p. 1029-1030.**

88. **Fogler, H.S.,** ***Elements of Chemical Reaction Engineering.*** **Third Edition ed, ed. P.H.I.S.I.t.P.a.C.E. Sciences. 1999.**

89. **Silverstein, K.** ***Gas-to-liquids Investments Sets Off Sparks.*** **UtiliPoint International, Inc. Oct. 2003.**

APPENDIX

EXPLORATORY TABLE FROM LITERATURE REVIEW

Reference	Process	Membrane	Min Temp	CH4 conversion	O2 conversion	CO select	H2 select	Feed rate
Wolf, E. E.; Alibrando, M.	POM	porous	320	70%	100%	90%	82%	750cc/min
Bodke, A. S.; Bharadwaj, S. S.; Schmict, L. D.	POM	non membrane	1000	99%	N/A	94%	95%	N/A
Wang, H. Y.; Ruckenstein, E.	POM	non membrane	750	80%	N/A	92%	96%	N/A
Dyer, Paul N.; Chen, C.M.	POM/ATR	ITM	900	90%	70%	96%		N/A
Praxair technology	POM/ATR	OTM	800	N/A	N/A	N/A		N/A
Diskin, A. M.; Cunningham, R. H.; Ormerod, R. M.	ATR	non membrane	750	N/A	N/A	85%		N/A
Kilner, J.; Benson, S.; Lane, J.; Waller, D.	POM	dense, Pd	350	20%	N/A	20%	18%	N/A
Choudhary, V. R.; Mamman, A. S.	ATR	non membrane	700	>80%	N/A	N/A		N/A
Chu, Y.; Li, S.; Lin, J.; Gu, J.; Yang, Y.	POM	non membrane	500	94.60%	100%	92.40%	100%	N/A
Basile, A.; Paturzo, L.; Lagana, F.	POM	dense membrane	250-550	56.20%	N/A	N/A	58.80%	N/A

Reference	feed ratio	catal load	pressure	catalyst	reaction t
Wolf, E. E.; Alibrando, M.	1/1 - 3/1	50-60mg	N/A	Rh/TiO2	N/A
Bodke, A. S.; Bharadwaj, S. S.; Schmict, L. D.	1.5 - 2.1	N/A	N/A	nobel met	N/A
Wang, H. Y.; Ruckenstein, E.	2.1/1	N/A	1 atm	Rh/MgO	20 hours
Dyer, Paul N.; Chen, C.M.	1.8 - 2	Ni	1 atm	LaSrCoFl	700 hours
Praxair technology	N/A	N/A	N/A	N/A	N/A
Diskin, A. M.; Cunningham, R. H.; Ormerod, R. M.	N/A	1.09mg	N/A	N/A	N/A
Kilner, J.; Benson, S.; Lane, J.; Waller, D.	N/A	N/A	N/A	N/A	N/A
Choudhary, V. R.; Mamman, A. S.	1.8 - 8	N/A	N/A	N/A	N/A
Chu, Y.; Li, S.; Lin, J.; Gu, J.; Yang, Y.	2.0/1	N/A	1 atm	La/Ni	N/A
Basile, A.; Paturzo, L.; Lagana, F.	2.0/1	3.15g	0.6bar	Palladium	N/A

ISOTHERM PLOT

Sample:	Support
Operator:	Susi Olsen
Submitter:	
File Name:	C:\ASAP2010\DATA\SY0501.SMP

Started:	22/05/03 09:26:19	Analysis Adsorptive:	N2
Completed:	22/05/03 20:51:26	Analysis Bath:	77.35 K
Report Time:	23/05/03 11:00:05	Thermal Correction:	No
Sample Weight:	0.3000 g	Smoothed Pressures:	No
Warm Freespace:	16.0000 cm³	Cold Freespace:	45.0000 cm³
Equil. Interval:	45 secs	Low Pressure Dose:	None

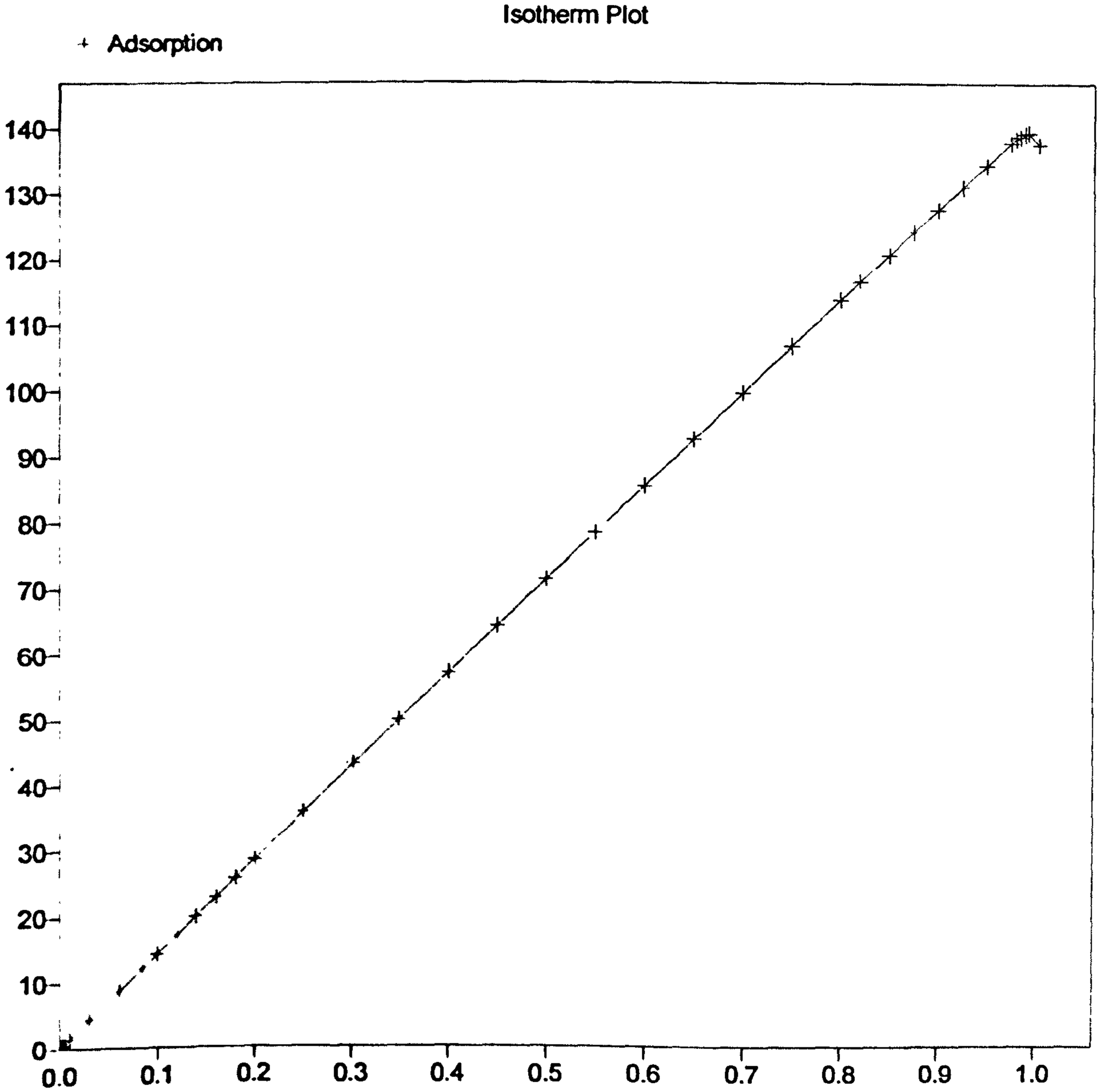

SY05 02 - First internal gamma alumina

Sample: First internal gamma alumina
Operator: Susi Olsen
Submitter:
File Name: C:\ASAP2010\DATA\SY0502.SMP

Started:	21/05/03 10:15:22	Analysis Adsorptive:	N2
Completed:	21/05/03 21:25:24	Analysis Bath:	77.35 K
Report Time:	21/05/03 21:25:24	Thermal Correction:	No
Sample Weight:	0.3000 g	Smoothed Pressures:	No
Warm Freespace:	16.0000 cm³	Cold Freespace:	45.0000 cm³
Equil. Interval:	45 secs	Low Pressure Dose:	None

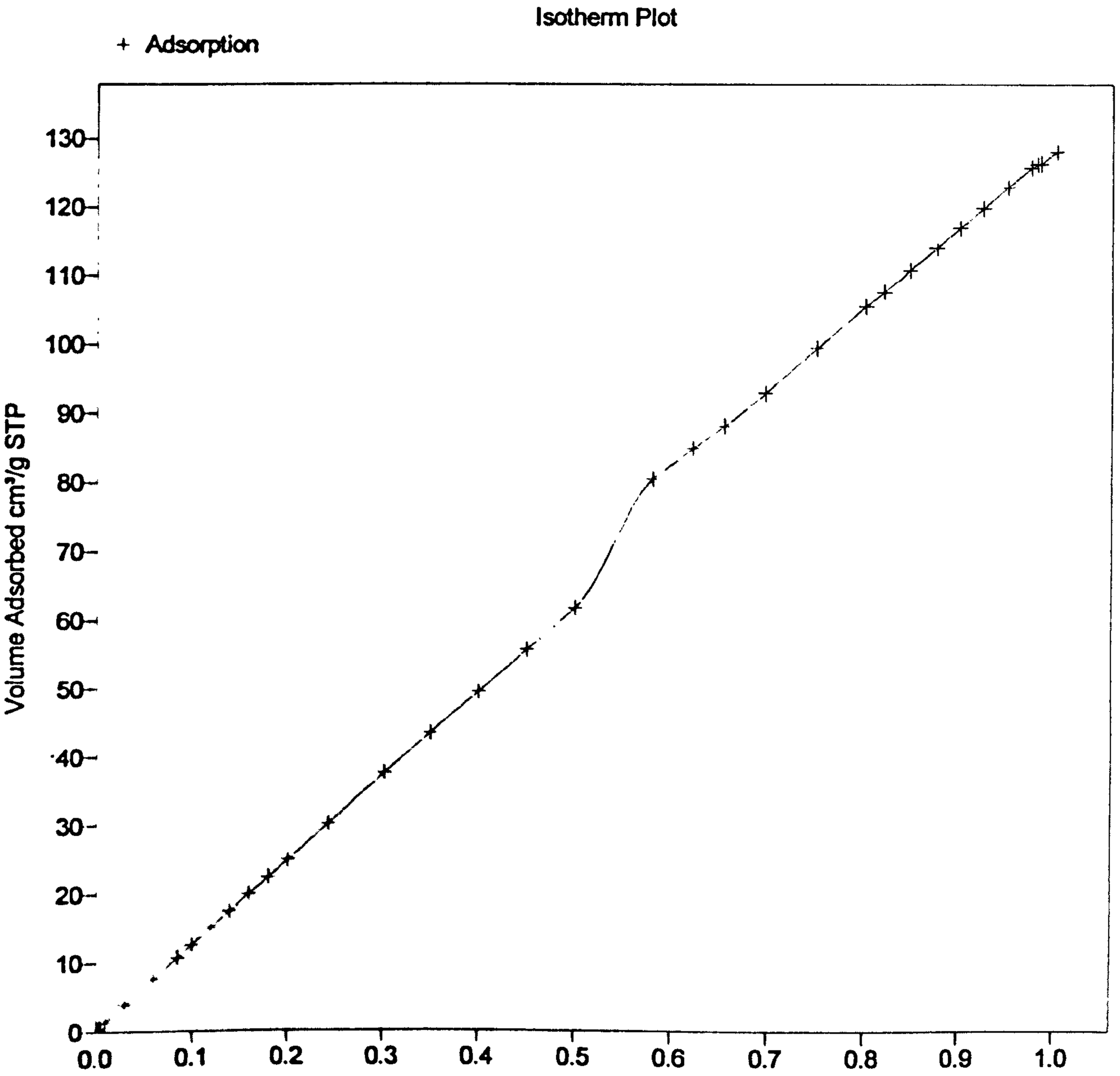

Sample: second internal gamma alumina coating
Operator: Susi Olsen
Submitter:
File Name: C:\ASAP2010\DATA\SY0503.SMP

Started:	27/05/03 09:24:51	Analysis Adsorptive:	N2
Completed:	27/05/03 20:06:51	Analysis Bath:	77.35 K
Report Time:	27/05/03 20:06:51	Thermal Correction:	No
Sample Weight:	0.3000 g	Smoothed Pressures:	No
Warm Freespace:	16.0000 cm³	Cold Freespace:	45.0000 cm³
Equil. Interval:	45 secs	Low Pressure Dose:	None

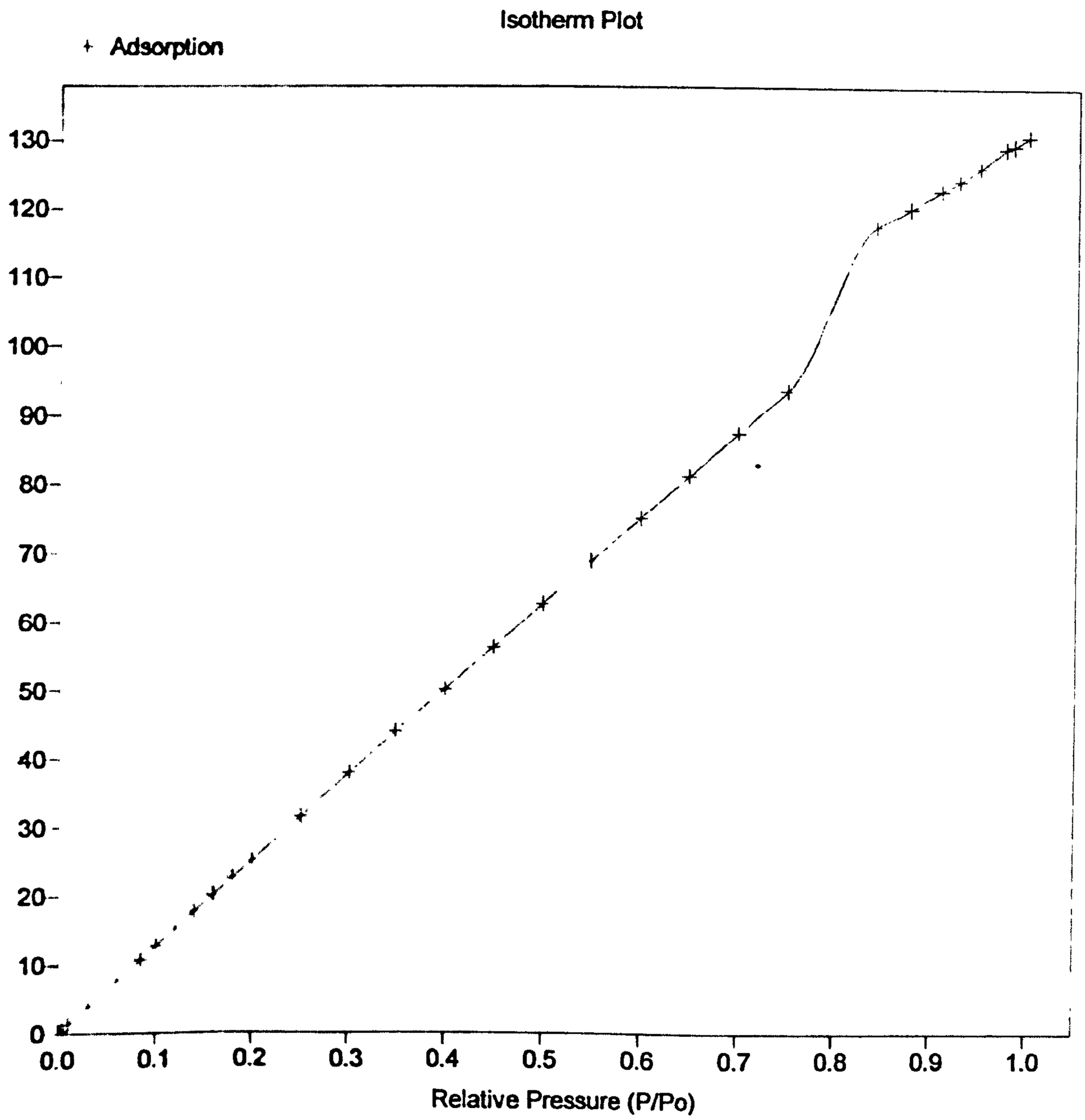

Sample: First Rhodium coating
Operator: Susi Olsen
Submitter:
File Name: C:\ASAP2010\DATA\SY0504.SMP

Started: 28/05/03 09:33:43
Completed: 28/05/03 20:47:16
Report Time: 28/05/03 20:47:16
Sample Weight: 0.3000 g
Warm Freespace: 16.0000 cm³
Equil. Interval: 45 secs

Analysis Adsorptive: N2
Analysis Bath: 77.35 K
Thermal Correction: No
Smoothed Pressures: No
Cold Freespace: 45.0000 cm³
Low Pressure Dose: None

Isotherm Plot

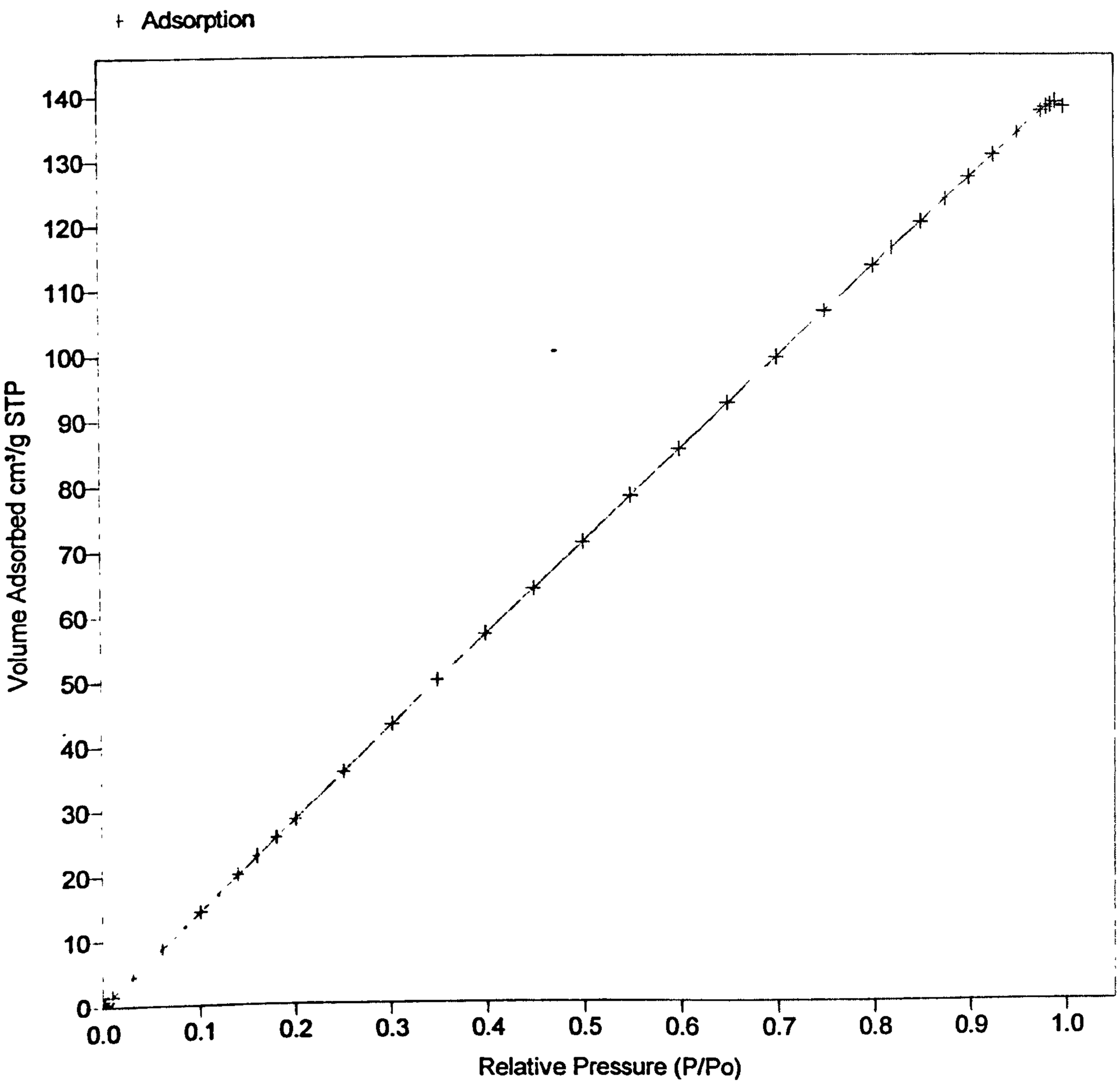

SY05 05 - Second Rhodium coating

Sample:	Second Rhodium coating		
Operator:	Susi Olsen		
Submitter:			
File Name:	C:\ASAP2010\DATA\SY0505.SMP		
Started:	29/05/03 09:30:16	Analysis Adsorptive:	N2
Completed:	29/05/03 20:51:43	Analysis Bath:	77.35 K
Report Time:	29/05/03 20:51:43	Thermal Correction:	No
Sample Weight:	0.3000 g	Smoothed Pressures:	No
Warm Freespace:	16.0000 cm³	Cold Freespace:	45.0000 cm³
Equil. Interval:	45 secs	Low Pressure Dose:	None

Isotherm Plot

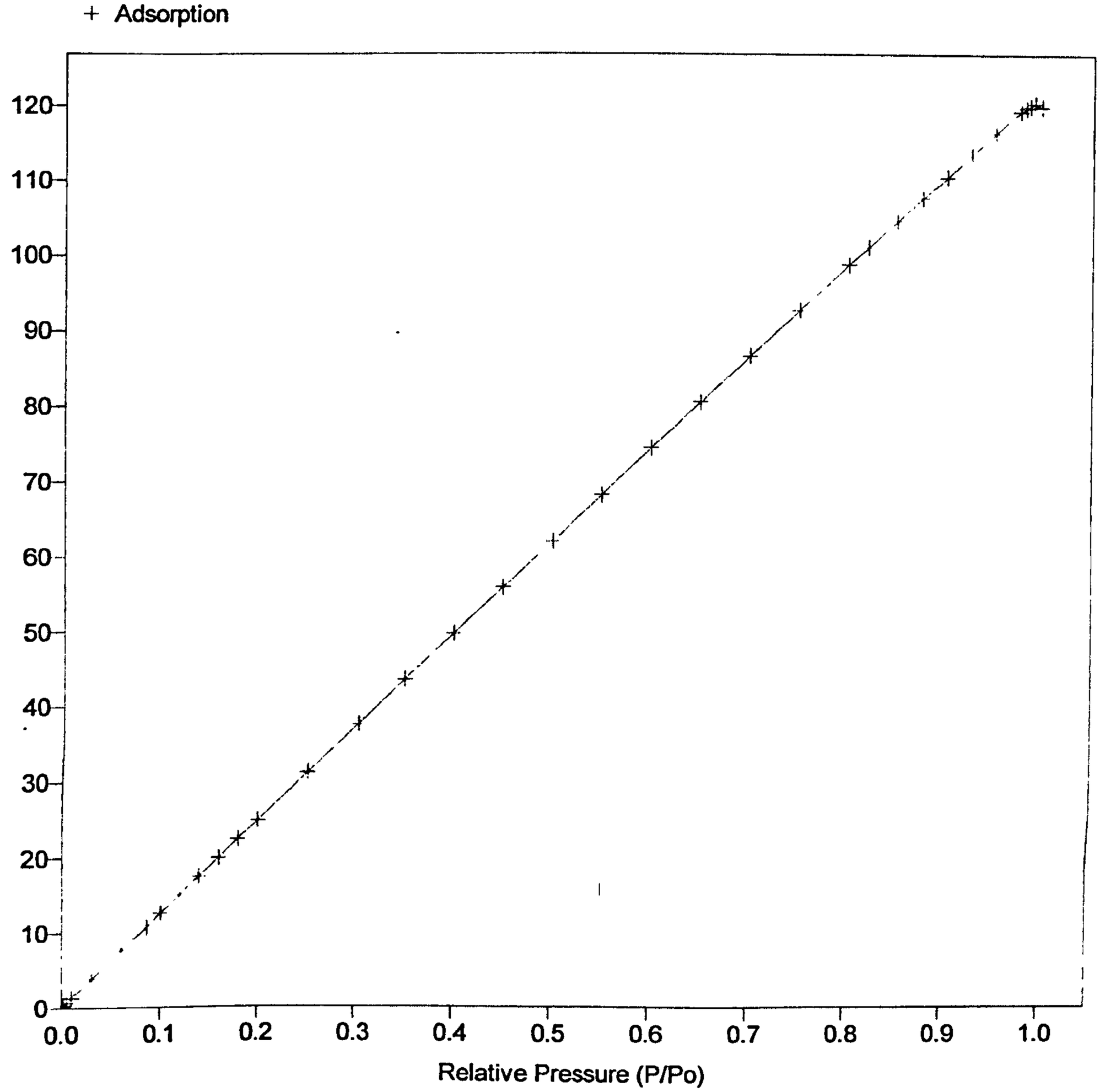

Sample: Third Rhodium coating
Operator: Susi Olsen
Submitter:
File Name: C:\ASAP2010\DATA\SY0506.SMP

Started: 30/05/03 09:06:26
Completed: 30/05/03 20:03:33
Report Time: 30/05/03 20:03:34
Sample Weight: 0.3000 g
Warm Freespace: 16.0000 cm³
Equil. Interval: 45 secs

Analysis Adsorptive: N2
Analysis Bath: 77.35 K
Thermal Correction: No
Smoothed Pressures: No
Cold Freespace: 45.0000 cm³
Low Pressure Dose: None

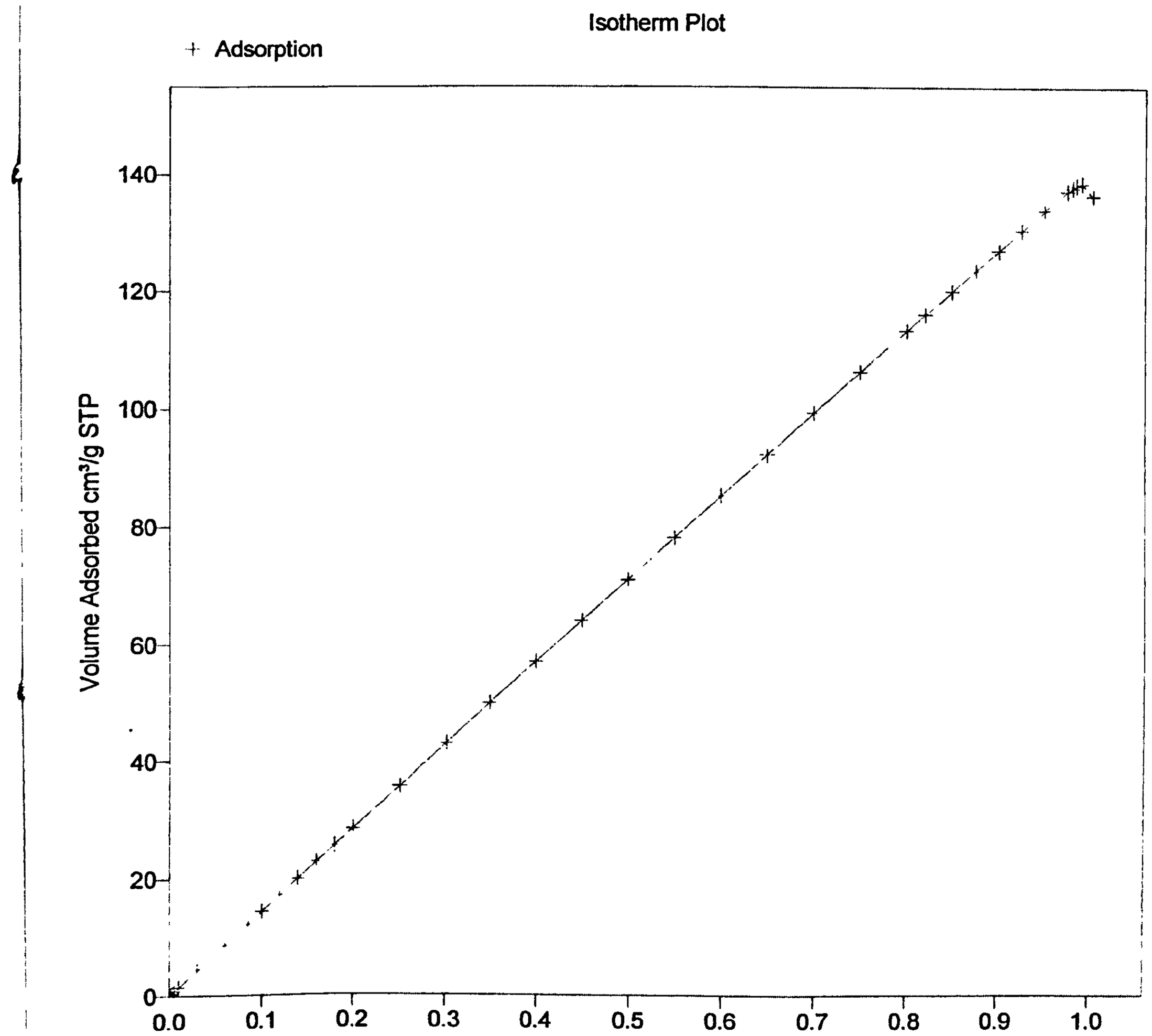

Sample: Forth Rhodium coating
Operator: Susi Olsen
Submitter:
File Name: C:\ASAP2010\DATA\SY0507.SMP

Started: 03/06/03 08:55:36
Completed: 03/06/03 20:23:40
Report Time: 03/06/03 20:23:40
Sample Weight: 0.3000 g
Warm Freespace: 16.0000 cm³
Equil. Interval: 45 secs

Analysis Adsorptive: N2
Analysis Bath: 77.35 K
Thermal Correction: No
Smoothed Pressures: No
Cold Freespace: 45.0000 cm³
Low Pressure Dose: None

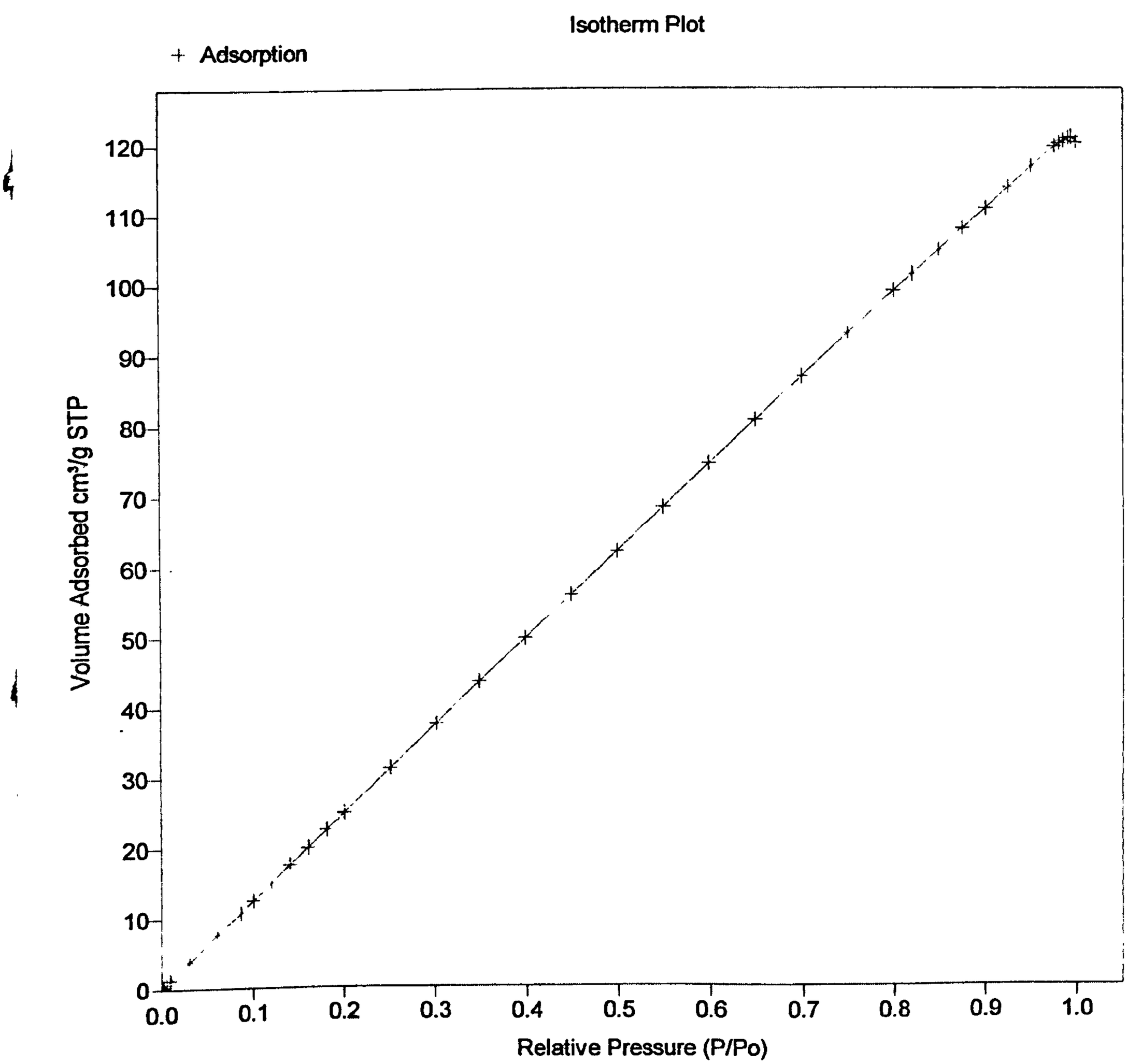

Sample: Forth Rhodium coating after H2 calcination
Operator: Susi Olsen
Submitter:
File Name: C:\ASAP2010\DATA\SY0508.SMP

Started: 04/06/03 10:23:00
Completed: 04/06/03 22:04:16
Report Time: 04/06/03 22:04:17
Sample Weight: 0.3000 g
Warm Freespace: 16.0000 cm³
Equil. Interval: 45 secs

Analysis Adsorptive: N2
Analysis Bath: 77.35 K
Thermal Correction: No
Smoothed Pressures: No
Cold Freespace: 45.0000 cm³
Low Pressure Dose: None

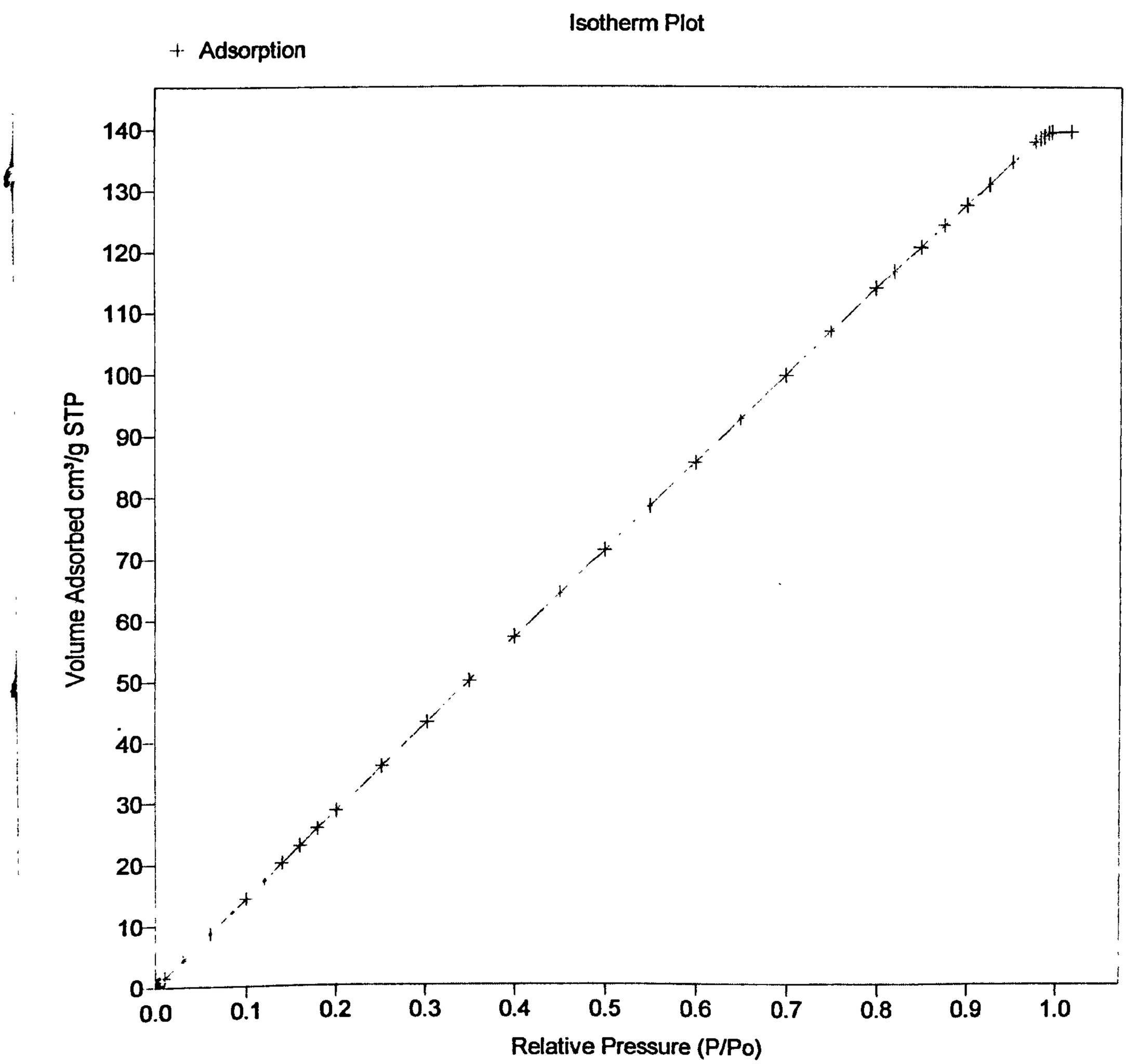

BET SURFACE AREA PLOT

Sample:	Support
Operator:	Susi Olsen
Submitter:	
File Name:	C:\ASAP2010\DATA\SY0501.SMP
Started:	22/05/03 09:26:19
Completed:	22/05/03 20:51:26
Report Time:	23/05/03 11:00:05
Sample Weight:	0.3000 g
Warm Freespace:	16.0000 cm³
Equil. Interval:	45 secs
Analysis Adsorptive:	N2
Analysis Bath:	77.35 K
Thermal Correction:	No
Smoothed Pressures:	No
Cold Freespace:	45.0000 cm³
Low Pressure Dose:	None

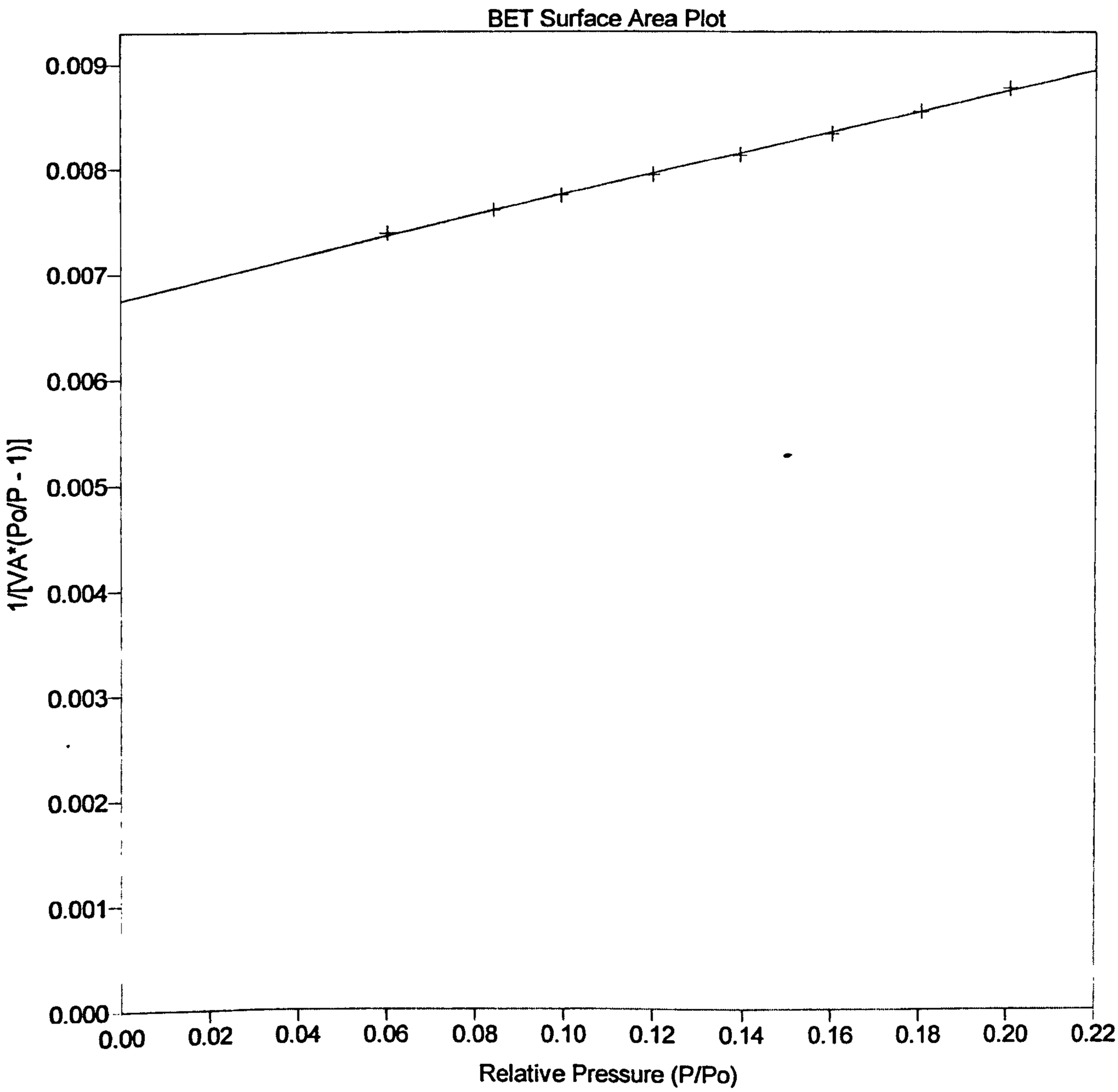

SY05 02 - First internal gamma alumina

Sample:	First internal gamma alumina		
Operator:	Susi Olsen		
Submitter:			
File Name:	C:\ASAP2010\DATA\SY0502.SMP		
Started:	21/05/03 10:15:22	Analysis Adsorptive:	N2
Completed:	21/05/03 21:25:24	Analysis Bath:	77.35 K
Report Time:	21/05/03 21:25:24	Thermal Correction:	No
Sample Weight:	0.3000 g	Smoothed Pressures:	No
Warm Freespace:	16.0000 cm³	Cold Freespace:	45.0000 cm³
Equil. Interval:	45 secs	Low Pressure Dose:	None

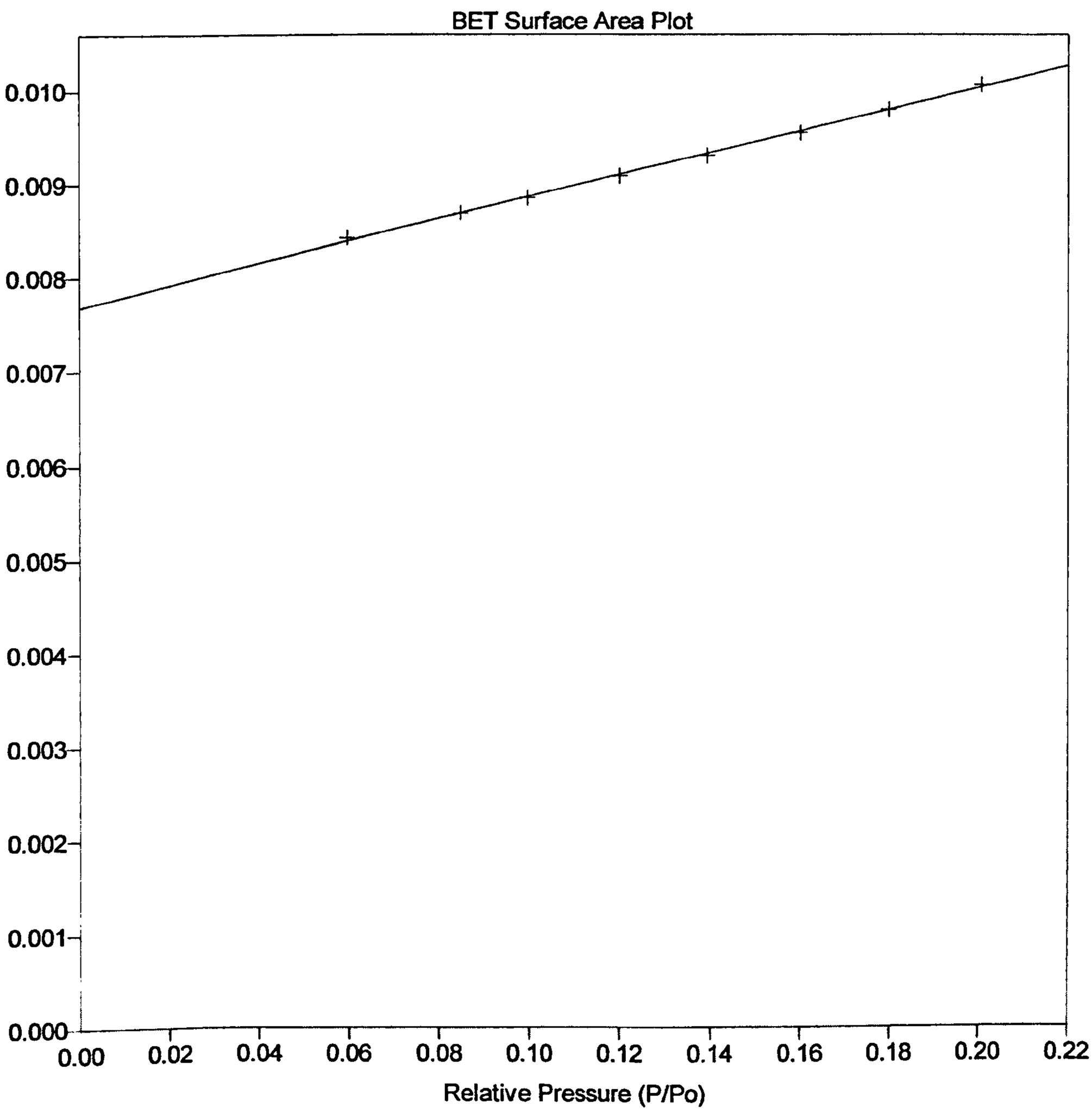

Sample: second internal gamma alumina coating
Operator: Susi Olsen
Submitter:
File Name: C:\ASAP2010\DATA\SY0503.SMP

Started:	27/05/03 09:24:51	Analysis Adsorptive:	N2
Completed:	27/05/03 20:06:51	Analysis Bath:	77.35 K
Report Time:	27/05/03 20:06:51	Thermal Correction:	No
Sample Weight:	0.3000 g	Smoothed Pressures:	No
Warm Freespace:	16.0000 cm³	Cold Freespace:	45.0000 cm³
Equil. Interval:	45 secs	Low Pressure Dose:	None

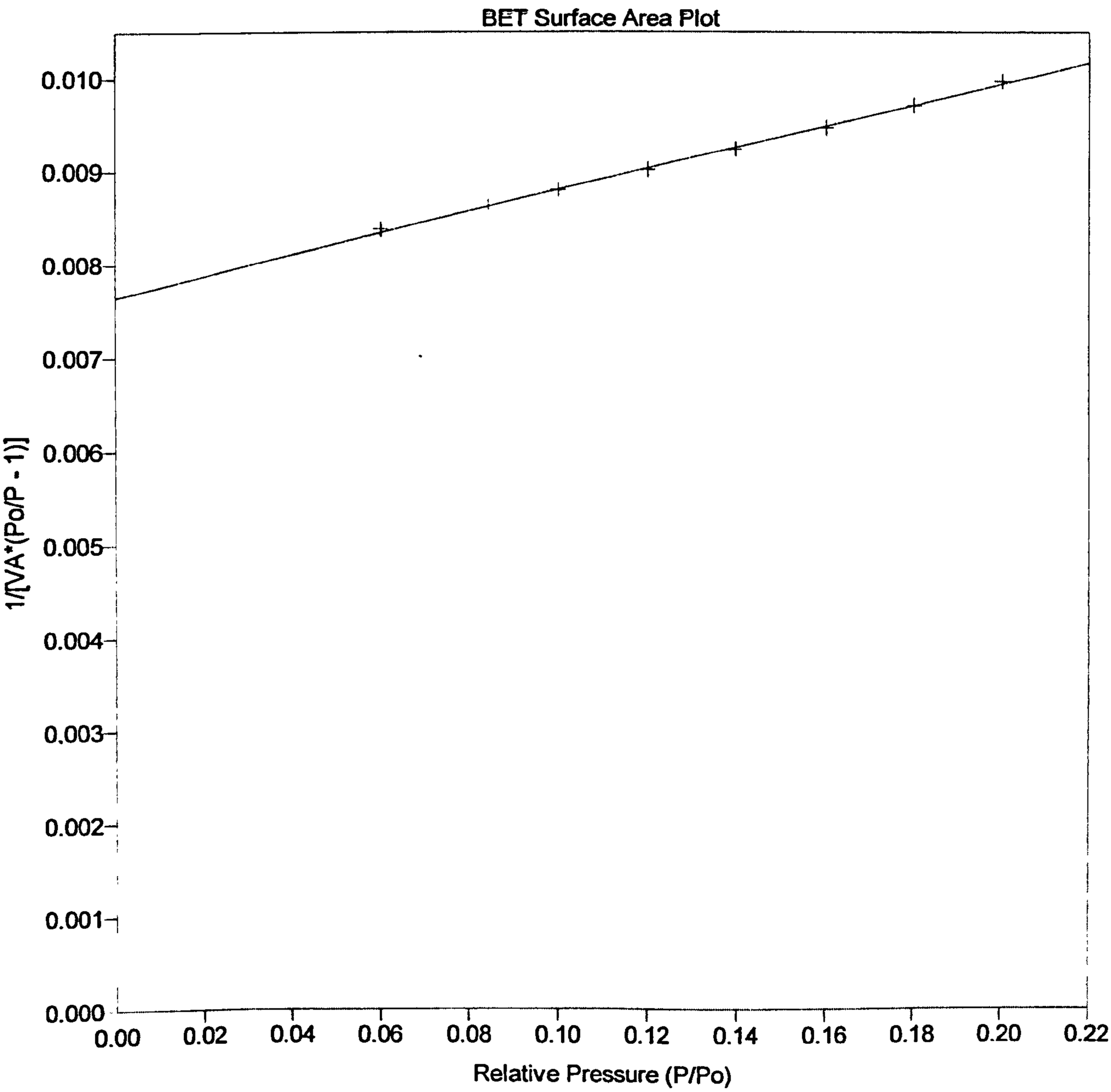

SY05 04 - First Rhodium coating

Sample:	First Rhodium coating
Operator:	Susi Olsen
Submitter:	
File Name:	C:\ASAP2010\DATA\SY0504.SMP

Started:	28/05/03 09:33:43	Analysis Adsorptive:	N2
Completed:	28/05/03 20:47:16	Analysis Bath:	77.35 K
Report Time:	28/05/03 20:47:16	Thermal Correction:	No
Sample Weight:	0.3000 g	Smoothed Pressures:	No
Warm Freespace:	16.0000 cm³	Cold Freespace:	45.0000 cm³
Equil. Interval:	45 secs	Low Pressure Dose:	None

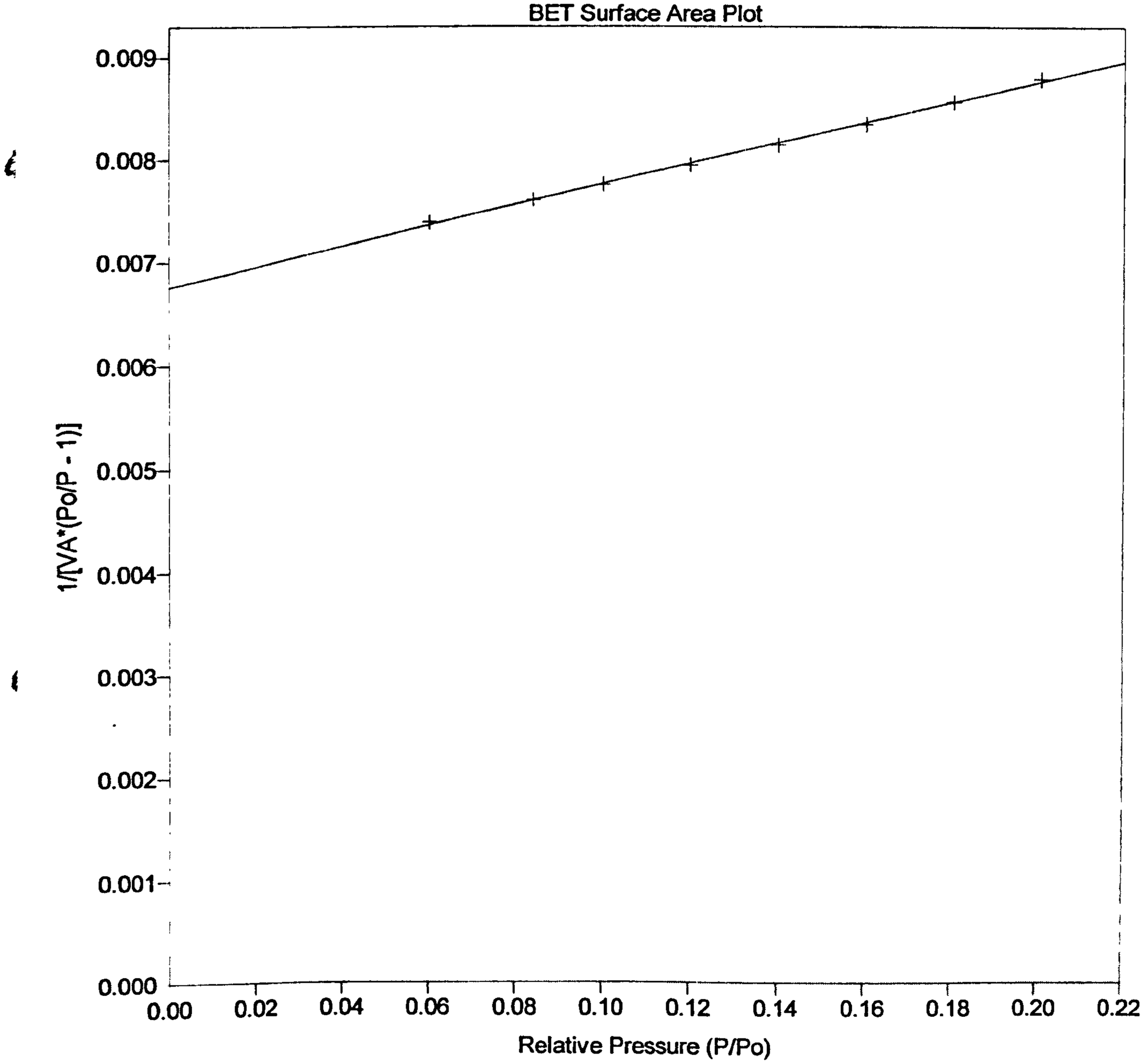

SY05 05 - Second Rhodium coating

Sample:	Second Rhodium coating		
Operator:	Susi Olsen		
Submitter:			
File Name:	C:\ASAP2010\DATA\SY0505.SMP		
Started:	29/05/03 09:30:16	Analysis Adsorptive:	N2
Completed:	29/05/03 20:51:43	Analysis Bath:	77.35 K
Report Time:	29/05/03 20:51:43	Thermal Correction:	No
Sample Weight:	0.3000 g	Smoothed Pressures:	No
Warm Freespace:	16.0000 cm³	Cold Freespace:	45.0000 cm³
Equil. Interval:	45 secs	Low Pressure Dose:	None

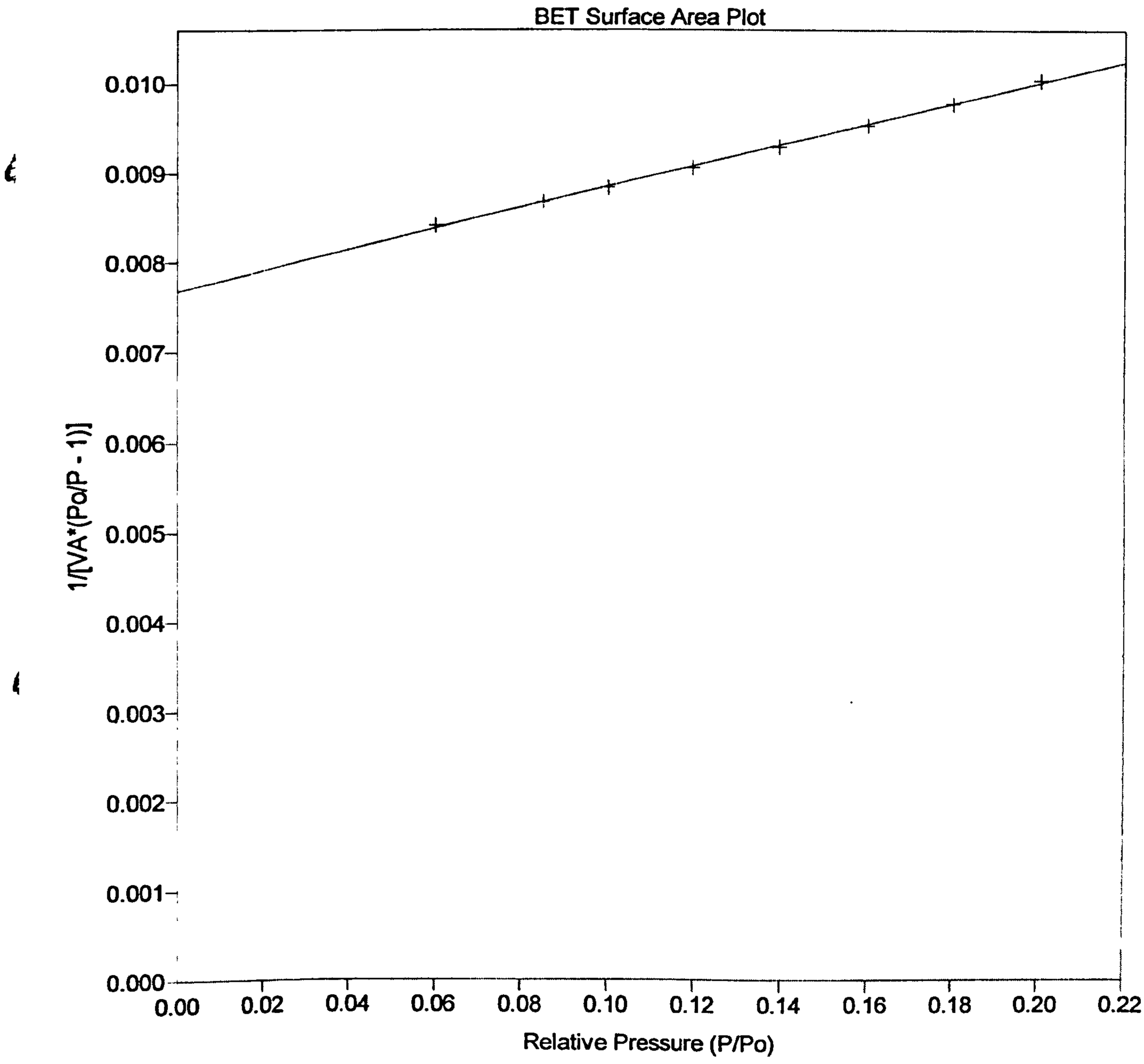

SY05 06 - Third Rhodium coating

Sample: Third Rhodium coating
Operator: Susi Olsen
Submitter:
File Name: C:\ASAP2010\DATA\SY0506.SMP

Started: 30/05/03 09:06:26
Completed: 30/05/03 20:03:33
Report Time: 30/05/03 20:03:34
Sample Weight: 0.3000 g
Warm Freespace: 16.0000 cm³
Equil. Interval: 45 secs

Analysis Adsorptive: N2
Analysis Bath: 77.35 K
Thermal Correction: No
Smoothed Pressures: No
Cold Freespace: 45.0000 cm³
Low Pressure Dose: None

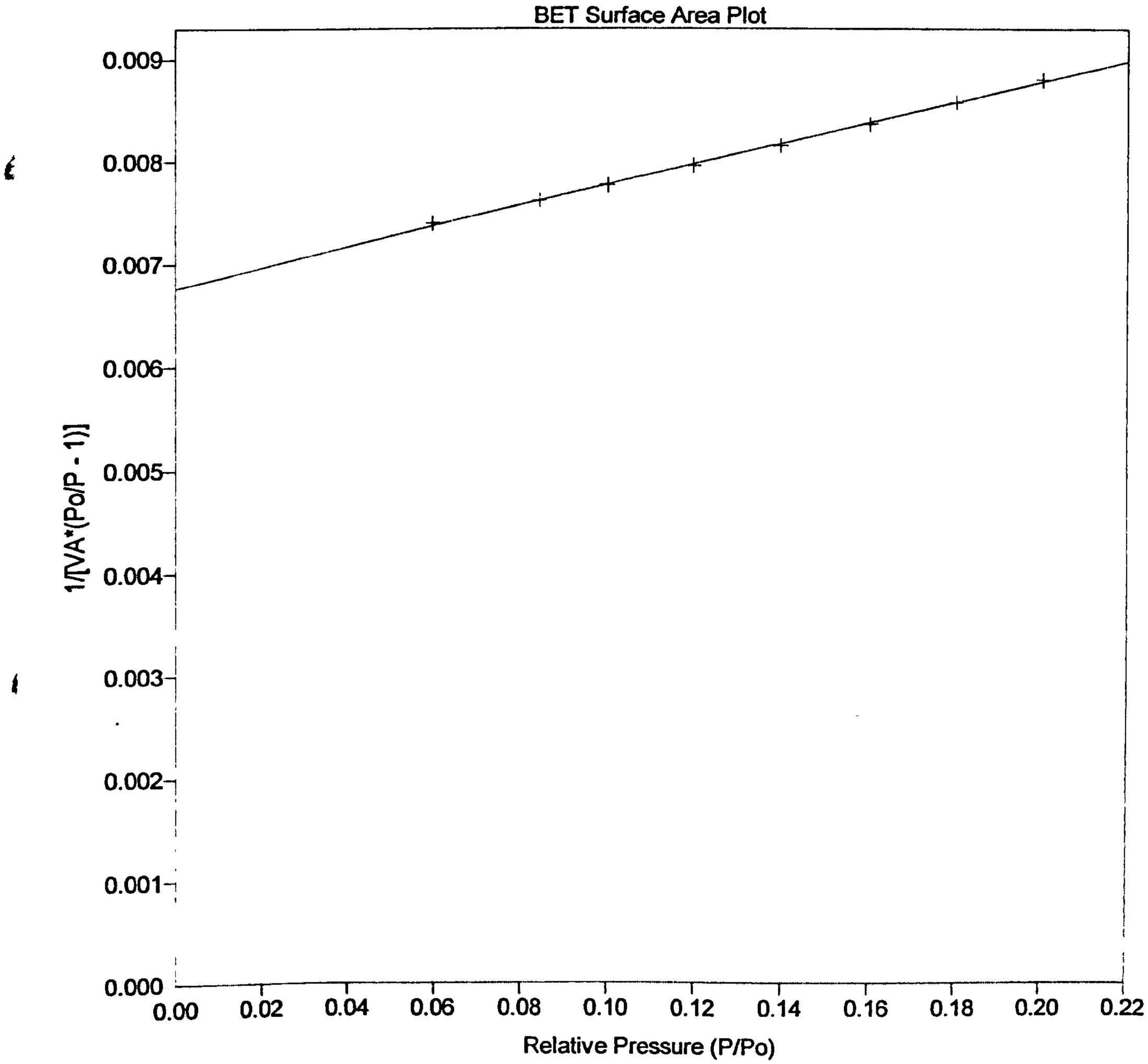

Sample: Forth Rhodium coating
Operator: Susi Olsen
Submitter:
File Name: C:\ASAP2010\DATA\SY0507.SMP

Started: 03/06/03 08:55:36
Completed: 03/06/03 20:23:40
Report Time: 03/06/03 20:23:40
Sample Weight: 0.3000 g
Warm Freespace: 16.0000 cm³
Equil. Interval: 45 secs

Analysis Adsorptive: N2
Analysis Bath: 77.35 K
Thermal Correction: No
Smoothed Pressures: No
Cold Freespace: 45.0000 cm³
Low Pressure Dose: None

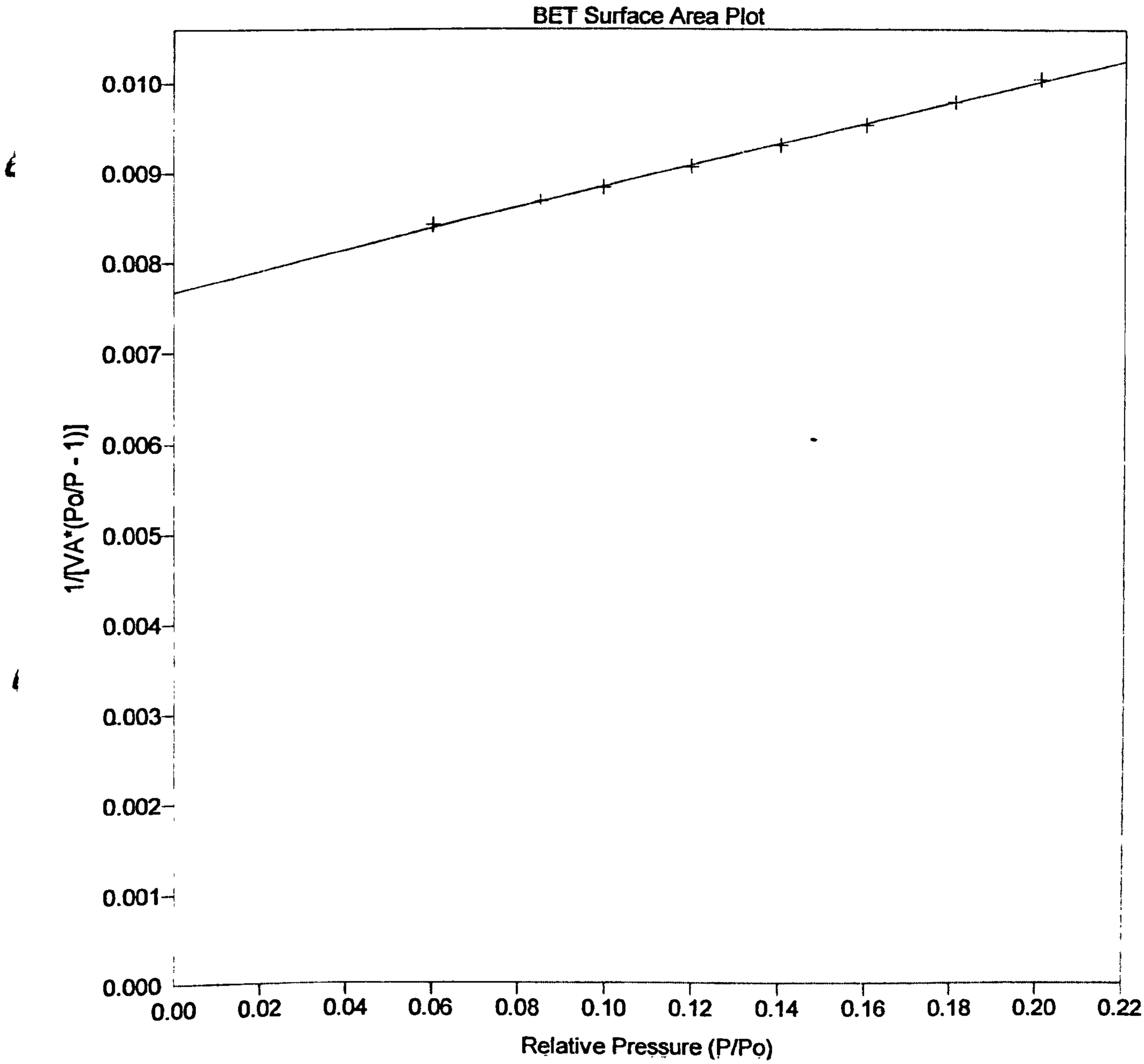

Sample: Forth Rhodium coating after H2 calcination
Operator: Susi Olsen
Submitter:
File Name: C:\ASAP2010\DATA\SY0508.SMP

Started: 04/06/03 10:23:00
Completed: 04/06/03 22:04:16
Report Time: 04/06/03 22:04:17
Sample Weight: 0.3000 g
Warm Freespace: 16.0000 cm³
Equil. Interval: 45 secs

Analysis Adsorptive: N2
Analysis Bath: 77.35 K
Thermal Correction: No
Smoothed Pressures: No
Cold Freespace: 45.0000 cm³
Low Pressure Dose: None

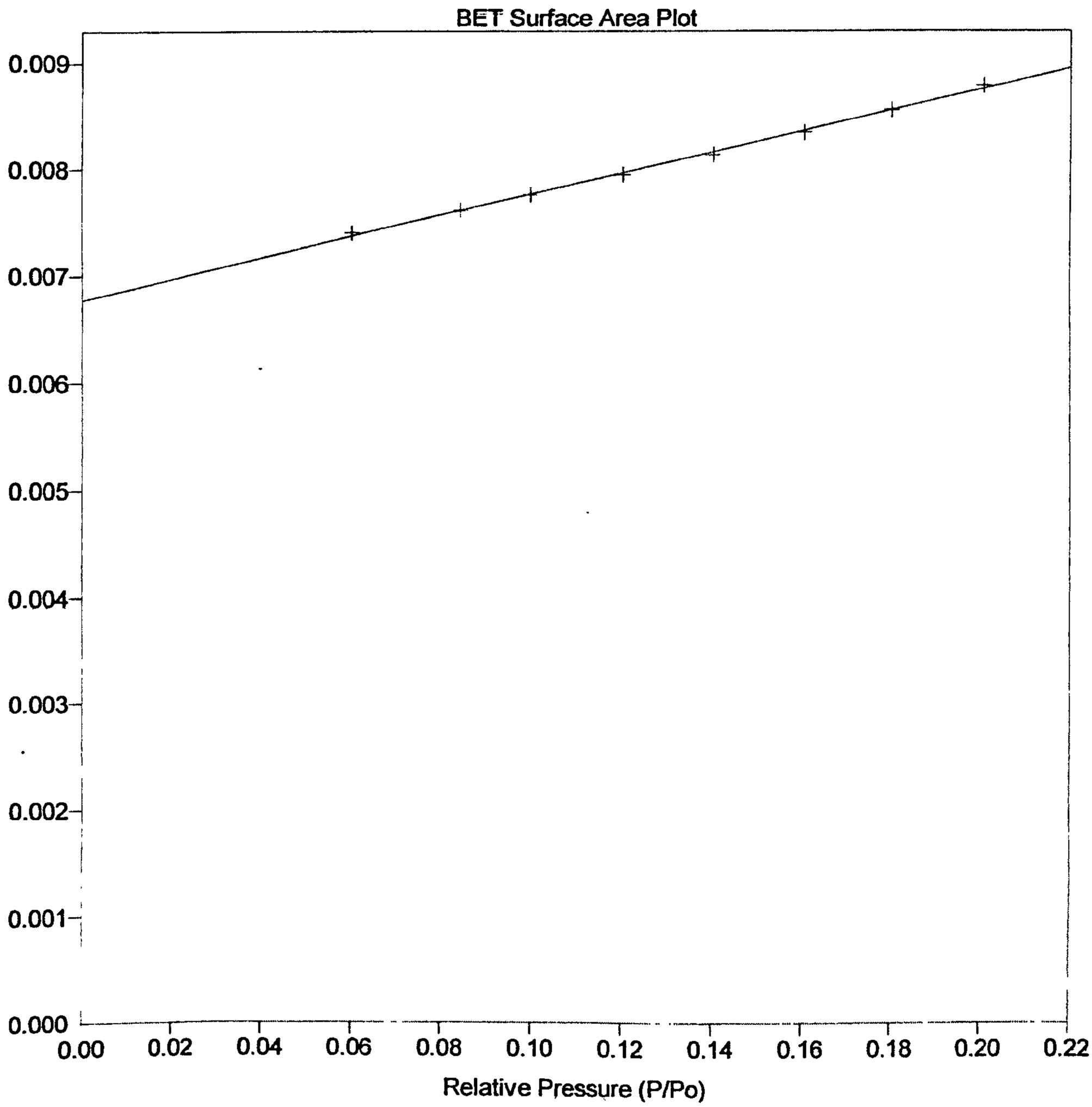

LANGMUIR SURFACE AREA PLOT

Sample: Support
Operator: Susi Olsen
Submitter:
File Name: C:\ASAP2010\DATA\SY0501.SMP

Started:	22/05/03 09:26:19	Analysis Adsorptive:	N2
Completed:	22/05/03 20:51:26	Analysis Bath:	77.35 K
Report Time:	23/05/03 11:00:05	Thermal Correction:	No
Sample Weight:	0.3000 g	Smoothed Pressures:	No
Warm Freespace:	16.0000 cm³	Cold Freespace:	45.0000 cm³
Equil. Interval:	45 secs	Low Pressure Dose:	None

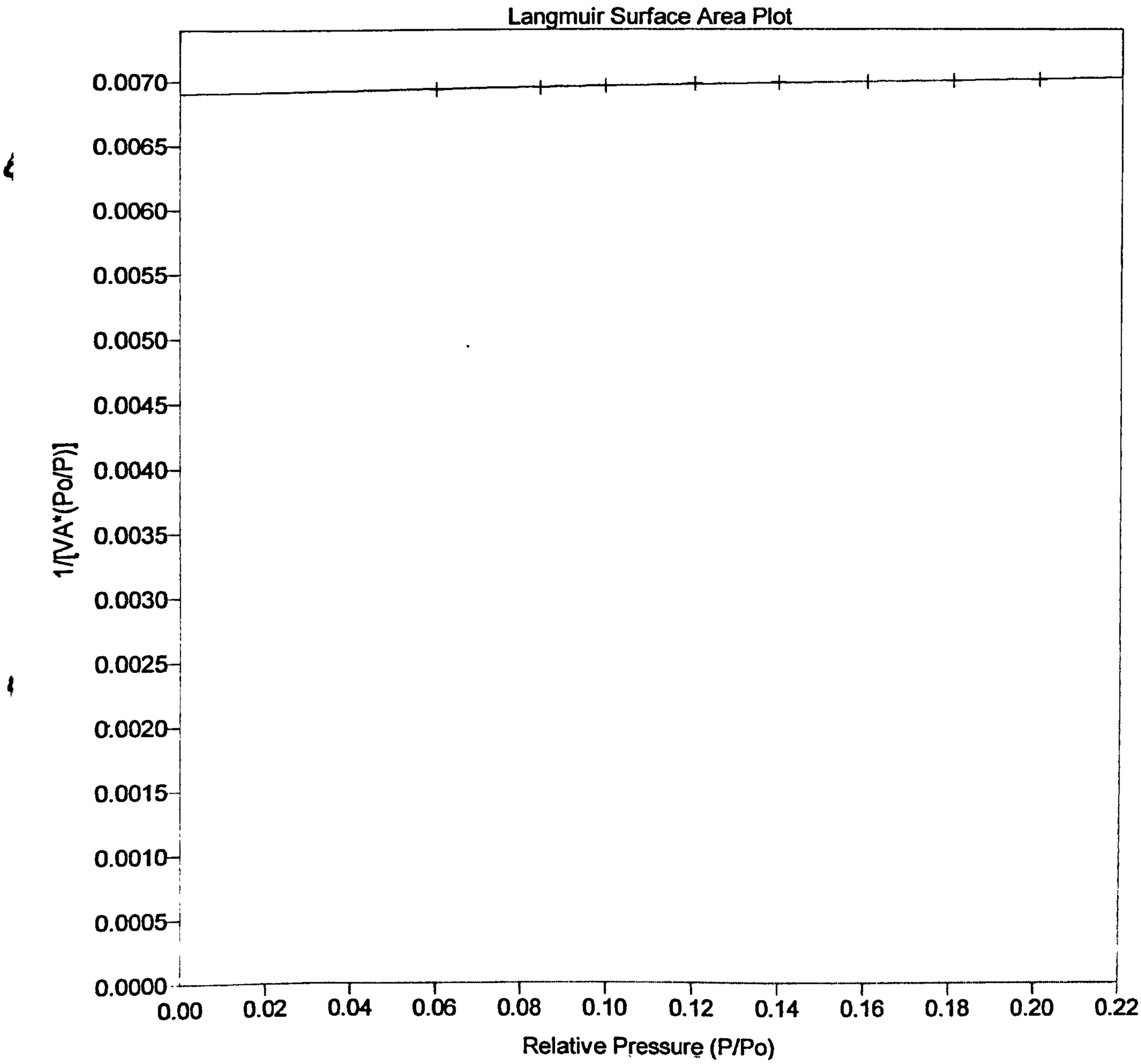

SY05 02 - First internal gamma alumina

Sample:	First internal gamma alumina		
Operator:	Susi Olsen		
Submitter:			
File Name:	C:\ASAP2010\DATA\SY0502.SMP		
Started:	21/05/03 10:15:22	Analysis Adsorptive:	N2
Completed:	21/05/03 21:25:24	Analysis Bath:	77.35 K
Report Time:	21/05/03 21:25:24	Thermal Correction:	No
Sample Weight:	0.3000 g	Smoothed Pressures:	No
Warm Freespace:	16.0000 cm³	Cold Freespace:	45.0000 cm³
Equil. Interval:	45 secs	Low Pressure Dose:	None

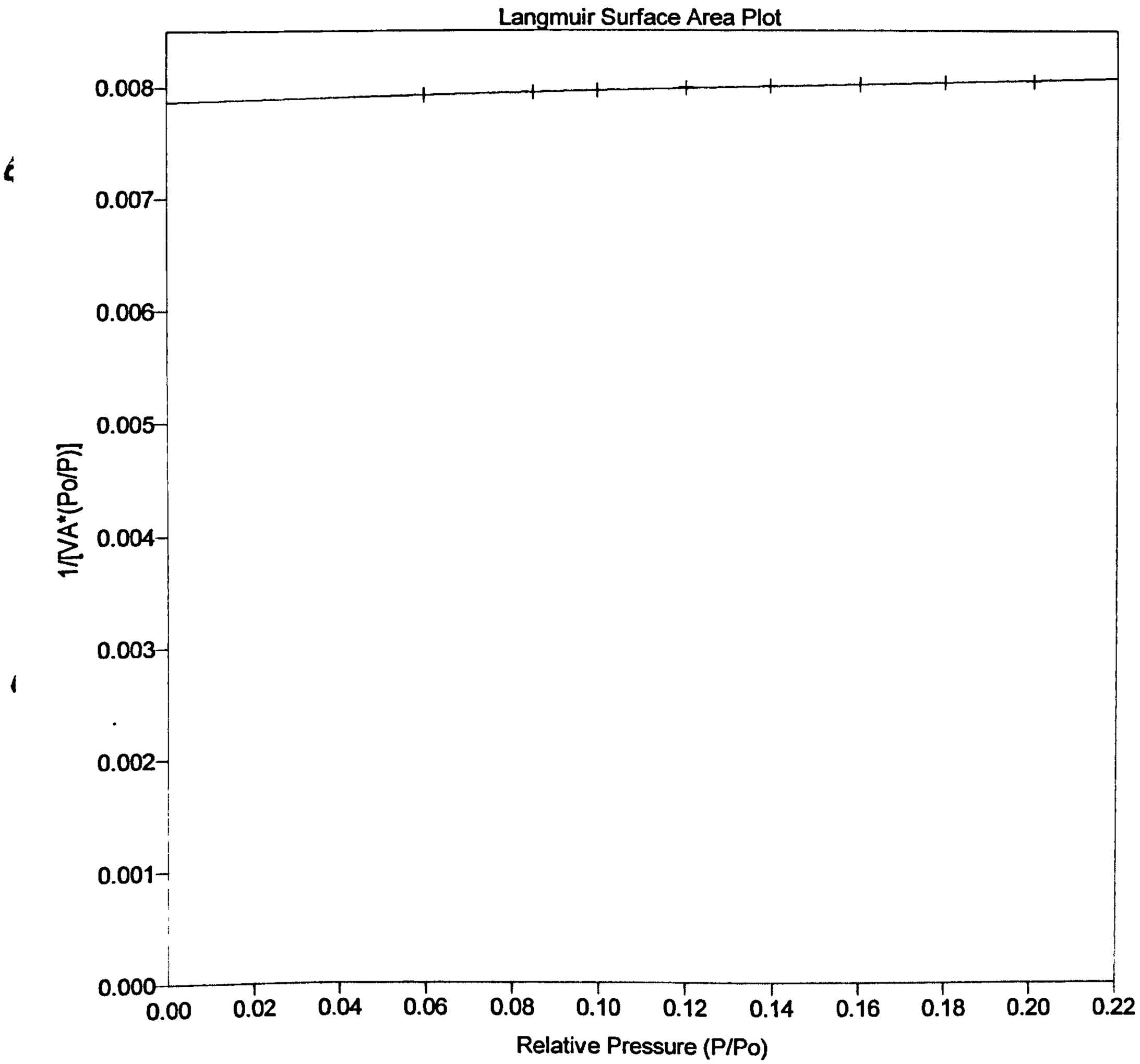

SY05 01 - Second internal gamma alumina coating

Sample:	second internal gamma alumina coating		
Operator:	Susi Olsen		
Submitter:			
File Name:	C:\ASAP2010\DATA\SY0503.SMP		
Started:	27/05/03 09:24:51	Analysis Adsorptive:	N2
Completed:	27/05/03 20:06:51	Analysis Bath:	77.35 K
Report Time:	27/05/03 20:06:51	Thermal Correction:	No
Sample Weight:	0.3000 g	Smoothed Pressures:	No
Warm Freespace:	16.0000 cm³	Cold Freespace:	45.0000 cm³
Equil. Interval:	45 secs	Low Pressure Dose:	None

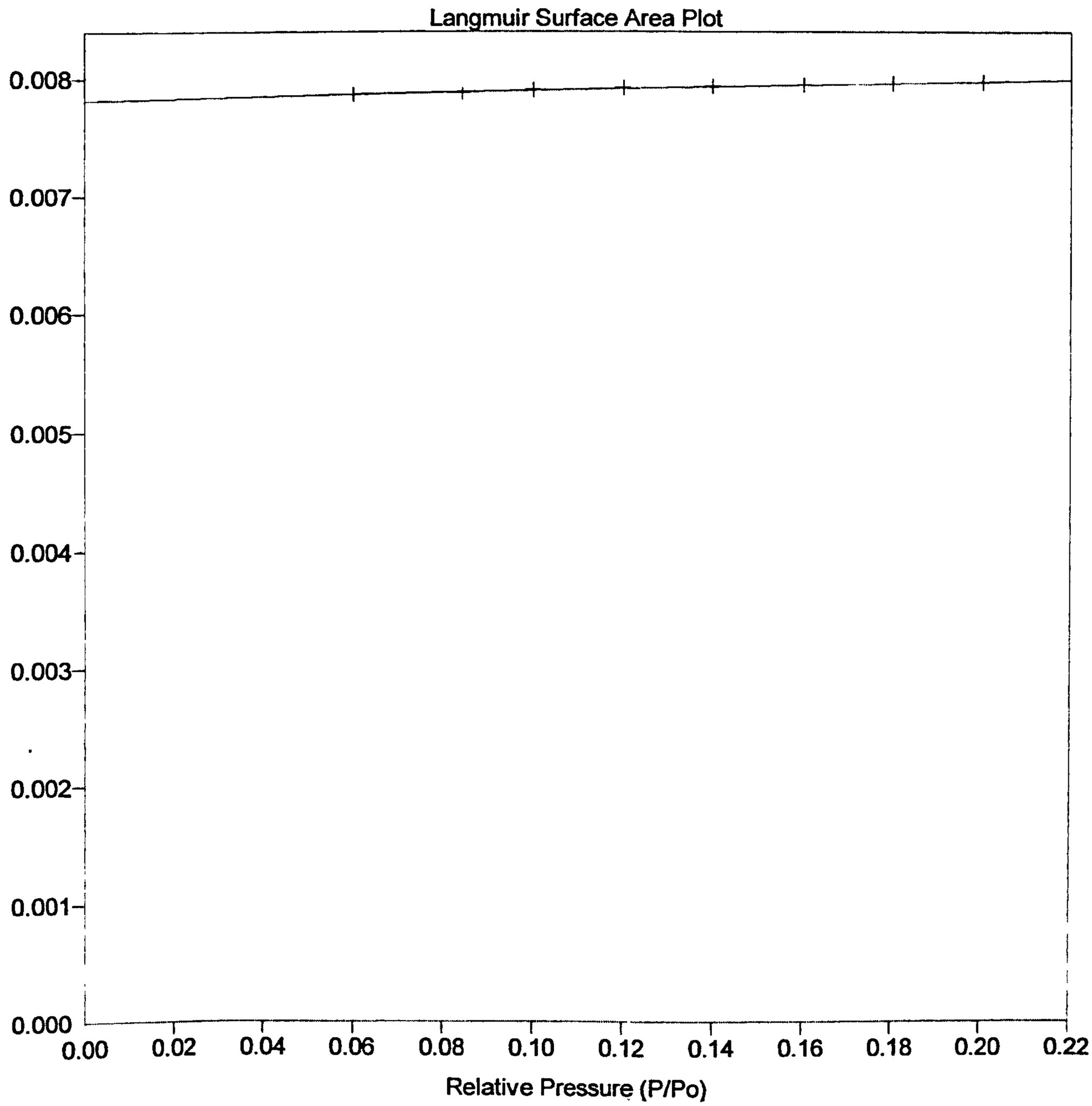

Sample:	First Rhodium coating		
Operator:	Susi Olsen		
Submitter:			
File Name:	C:\ASAP2010\DATA\SY0504.SMP		
Started:	28/05/03 09:33:43	Analysis Adsorptive:	N2
Completed:	28/05/03 20:47:16	Analysis Bath:	77.35 K
Report Time:	28/05/03 20:47:16	Thermal Correction:	No
Sample Weight:	0.3000 g	Smoothed Pressures:	No
Warm Freespace:	16.0000 cm³	Cold Freespace:	45.0000 cm³
Equil. Interval:	45 secs	Low Pressure Dose:	None

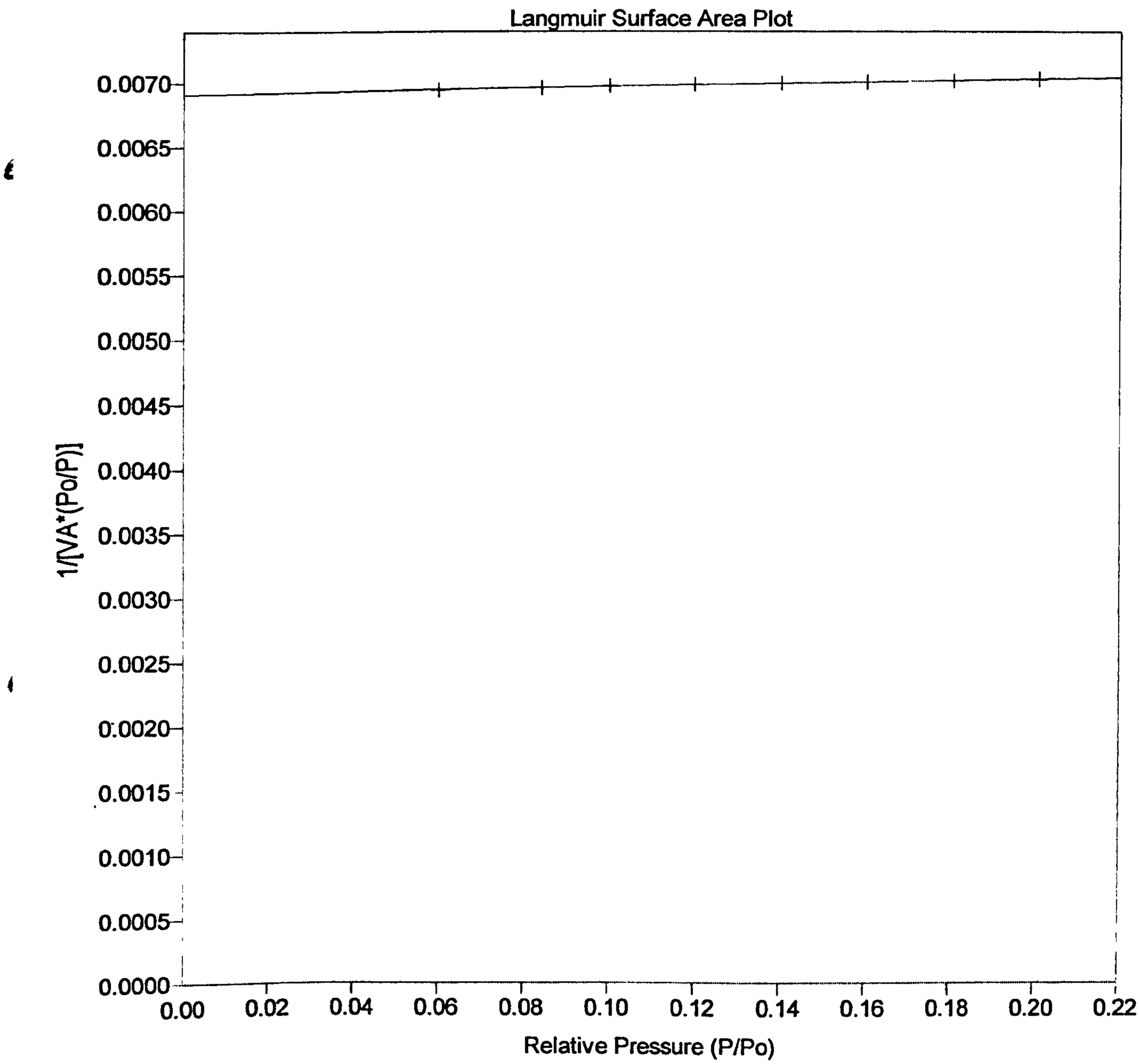

Sample: Second Rhodium coating
Operator: Susi Olsen
Submitter:
File Name: C:\ASAP2010\DATA\SY0505.SMP

Started: 29/05/03 09:30:16
Completed: 29/05/03 20:51:43
Report Time: 29/05/03 20:51:43
Sample Weight: 0.3000 g
Warm Freespace: 16.0000 cm³
Equil. Interval: 45 secs
Analysis Adsorptive: N2
Analysis Bath: 77.35 K
Thermal Correction: No
Smoothed Pressures: No
Cold Freespace: 45.0000 cm³
Low Pressure Dose: None

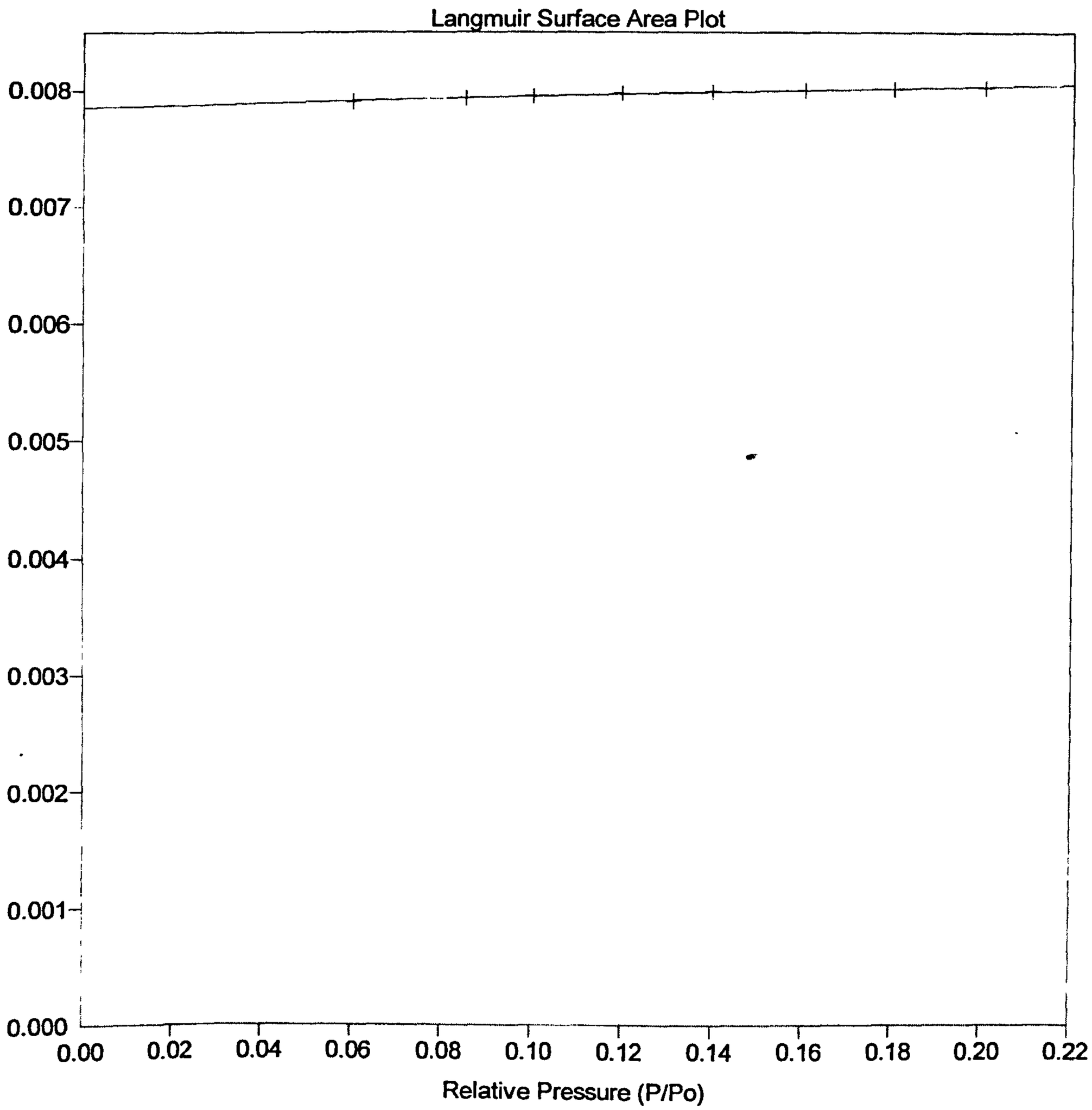

Sample:	Third Rhodium coating		
Operator:	Susi Olsen		
Submitter:			
File Name:	C:\ASAP2010\DATA\SY0506.SMP		
Started:	30/05/03 09:06:26	Analysis Adsorptive:	N2
Completed:	30/05/03 20:03:33	Analysis Bath:	77.35 K
Report Time:	30/05/03 20:03:34	Thermal Correction:	No
Sample Weight:	0.3000 g	Smoothed Pressures:	No
Warm Freespace:	16.0000 cm³	Cold Freespace:	45.0000 cm³
Equil. Interval:	45 secs	Low Pressure Dose:	None

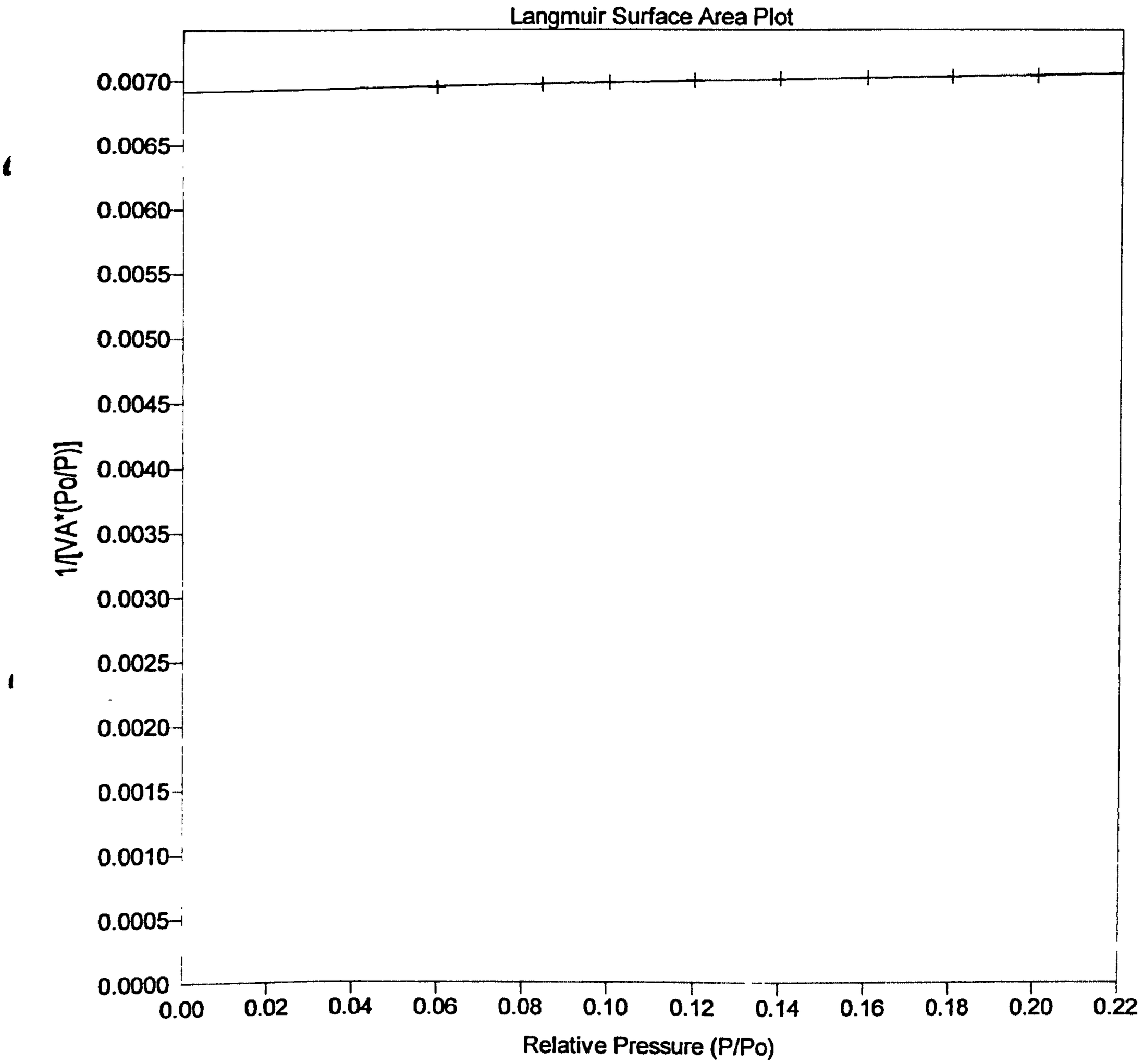

Sample: Forth Rhodium coating
Operator: Susi Olsen
Submitter:
File Name: C:\ASAP2010\DATA\SY0507.SMP

Started:	03/06/03 08:55:36	Analysis Adsorptive:	N2
Completed:	03/06/03 20:23:40	Analysis Bath:	77.35 K
Report Time:	03/06/03 20:23:40	Thermal Correction:	No
Sample Weight:	0.3000 g	Smoothed Pressures:	No
Warm Freespace:	16.0000 cm³	Cold Freespace:	45.0000 cm³
Equil. Interval:	45 secs	Low Pressure Dose:	None

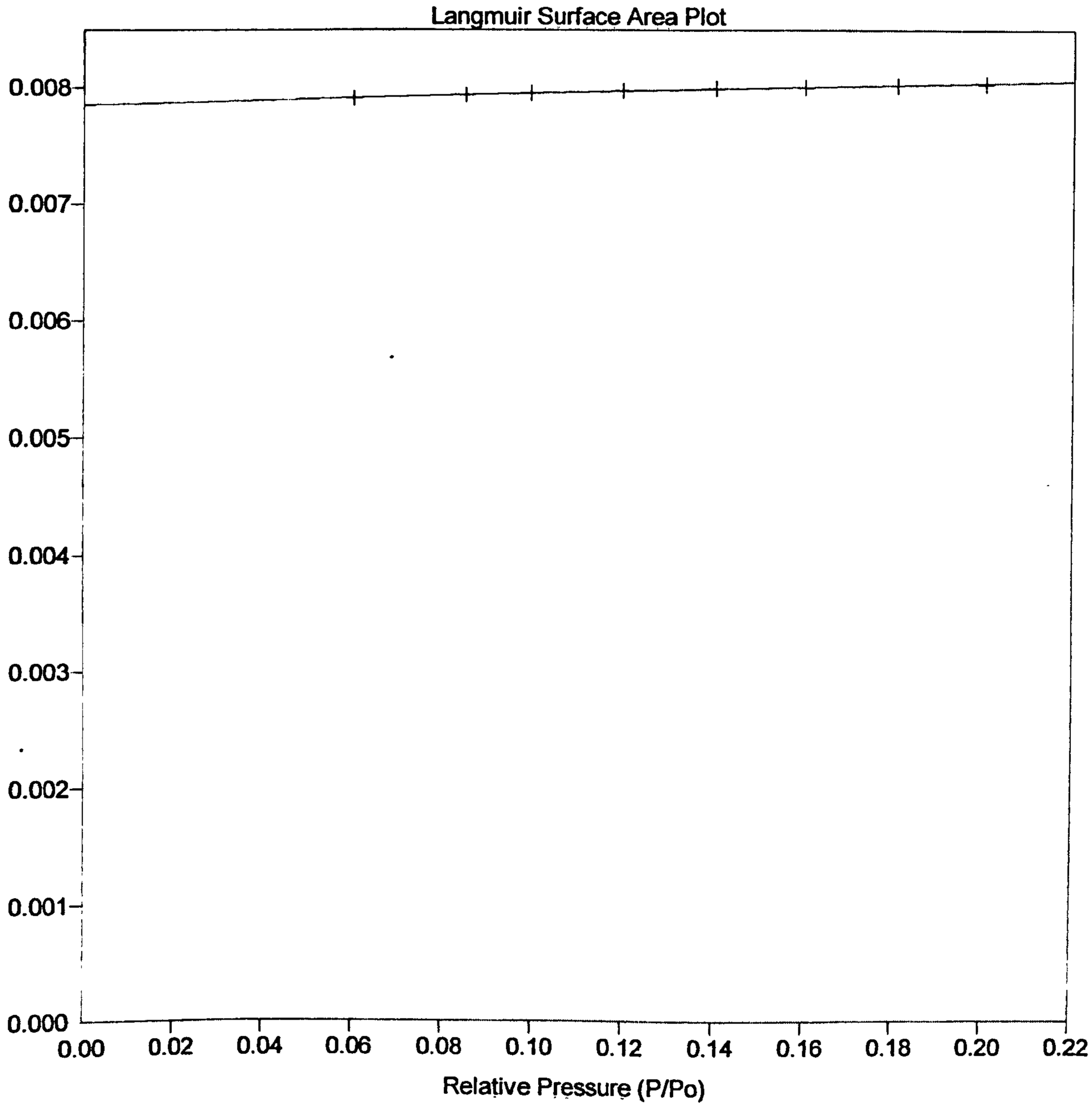

Sample: Forth Rhodium coating after H2 calcination
Operator: Susi Olsen
Submitter:
File Name: C:\ASAP2010\DATA\SY0508.SMP

Started: 04/06/03 10:23:00
Completed: 04/06/03 22:04:16
Report Time: 04/06/03 22:04:17
Sample Weight: 0.3000 g
Warm Freespace: 16.0000 cm³
Equil. Interval: 45 secs

Analysis Adsorptive: N2
Analysis Bath: 77.35 K
Thermal Correction: No
Smoothed Pressures: No
Cold Freespace: 45.0000 cm³
Low Pressure Dose: None

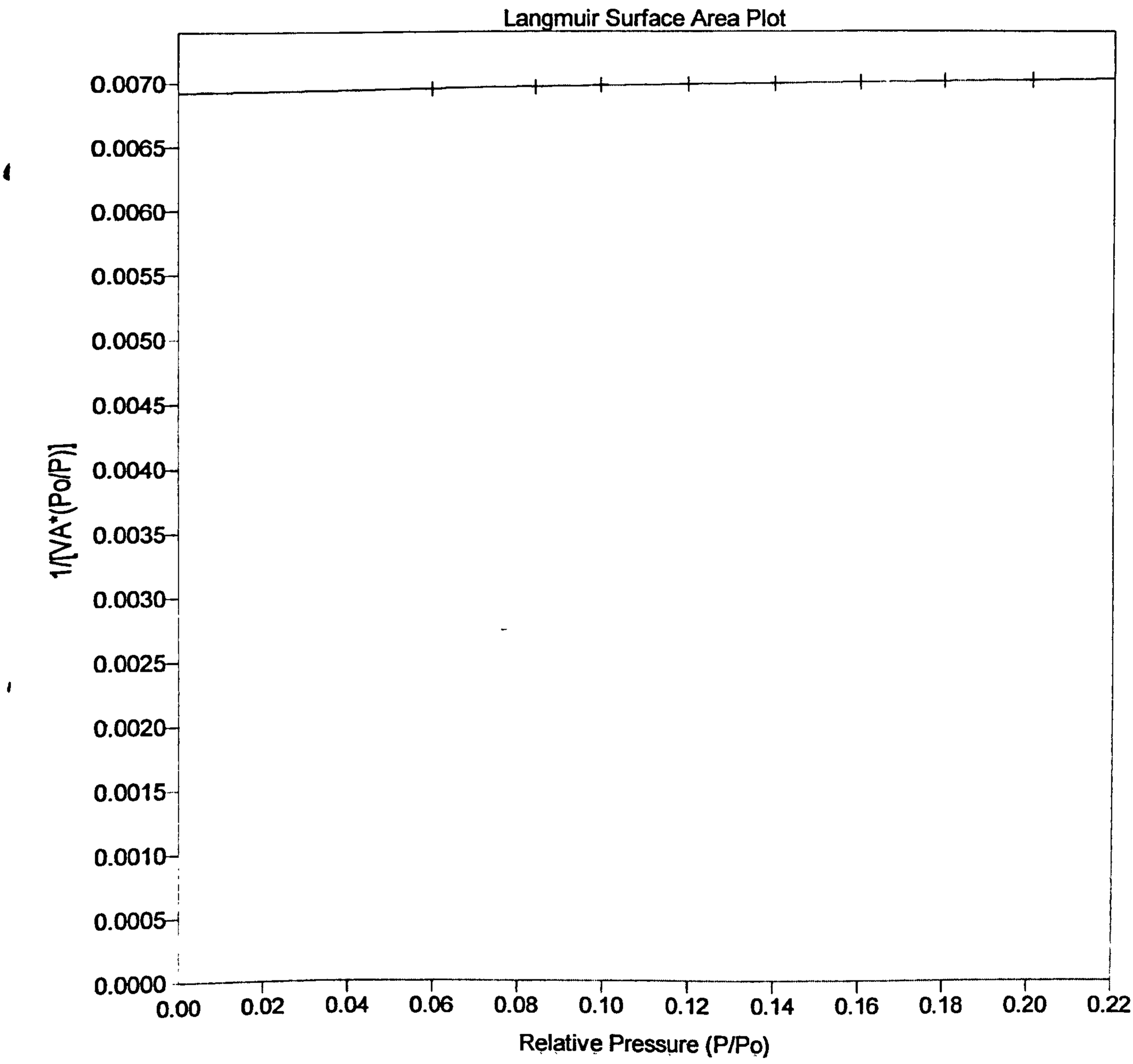

T – PLOT

Sample: Support
Operator: Susi Olsen
Submitter:
File Name: C:\ASAP2010\DATA\SY0501.SMP

Started: 22/05/03 09:26:19
Completed: 22/05/03 20:51:26
Report Time: 23/05/03 11:00:05
Sample Weight: 0.3000 g
Warm Freespace: 16.0000 cm³
Equil. Interval: 45 secs
Analysis Adsorptive: N2
Analysis Bath: 77.35 K
Thermal Correction: No
Smoothed Pressures: No
Cold Freespace: 45.0000 cm³
Low Pressure Dose: None

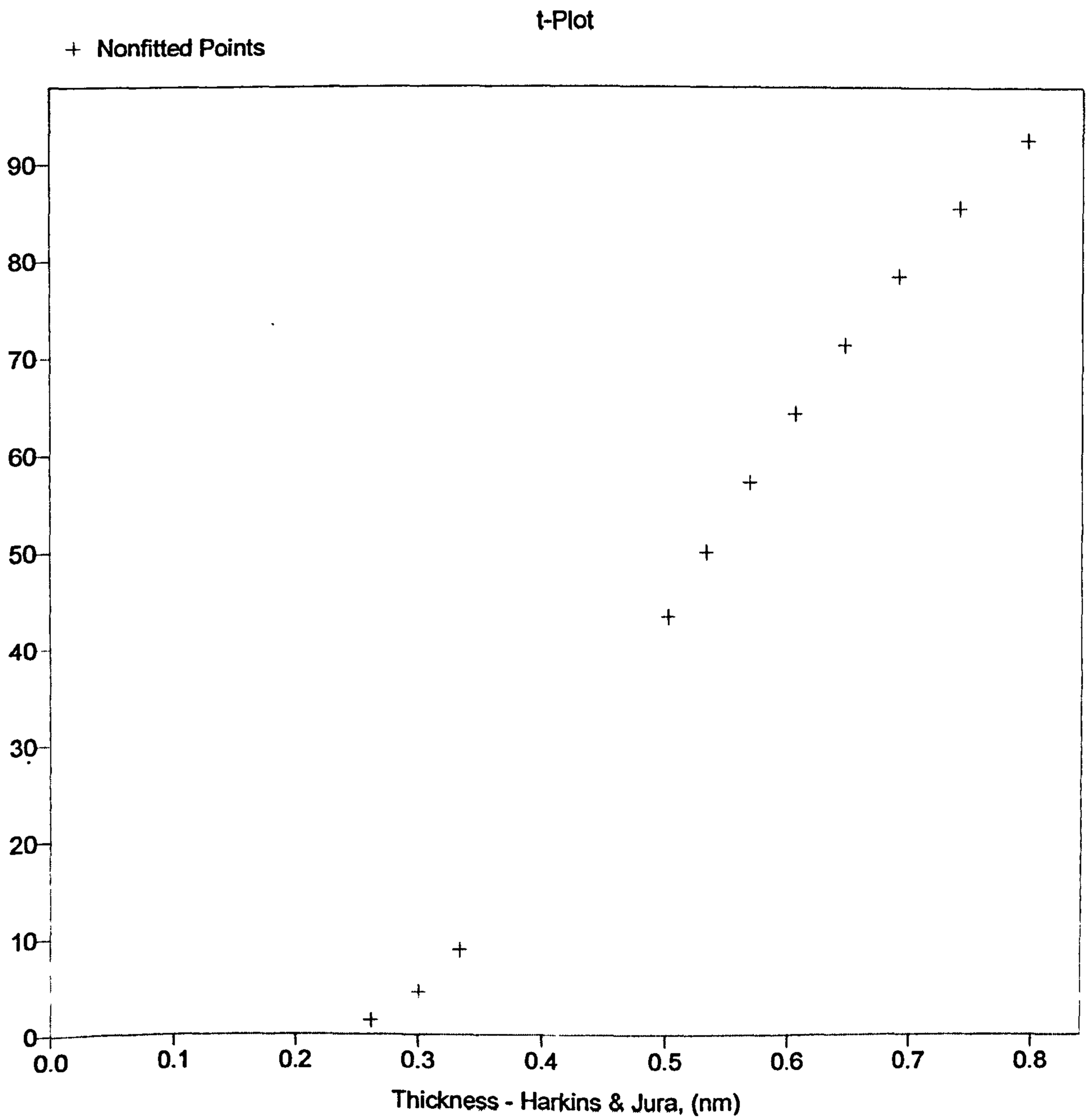

Sample: First internal gamma alumina
Operator: Susi Olsen
Submitter:
File Name: C:\ASAP2010\DATA\SY0502.SMP

Started: 21/05/03 10:15:22
Completed: 21/05/03 21:25:24
Report Time: 21/05/03 21:25:24
Sample Weight: 0.3000 g
Warm Freespace: 16.0000 cm³
Equil. Interval: 45 secs

Analysis Adsorptive: N2
Analysis Bath: 77.35 K
Thermal Correction: No
Smoothed Pressures: No
Cold Freespace: 45.0000 cm³
Low Pressure Dose: None

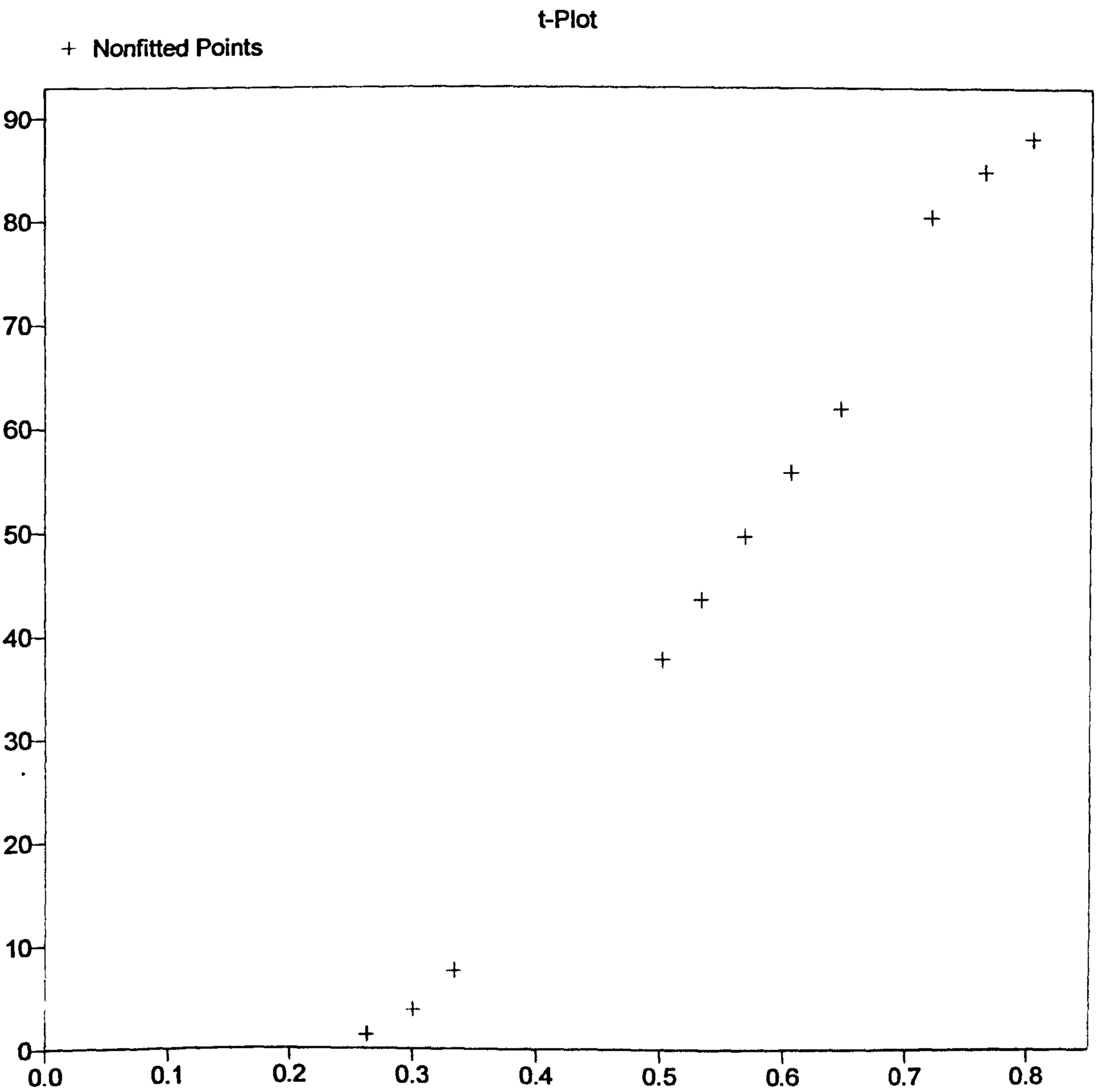

SY05 01 - Second internal gamma alumina coating

Sample: second internal gamma alumina coating
Operator: Susi Olsen
Submitter:
File Name: C:\ASAP2010\DATA\SY0503.SMP

Started: 27/05/03 09:24:51
Completed: 27/05/03 20:06:51
Report Time: 27/05/03 20:06:51
Sample Weight: 0.3000 g
Warm Freespace: 16.0000 cm³
Equil. Interval: 45 secs

Analysis Adsorptive: N2
Analysis Bath: 77.35 K
Thermal Correction: No
Smoothed Pressures: No
Cold Freespace: 45.0000 cm³
Low Pressure Dose: None

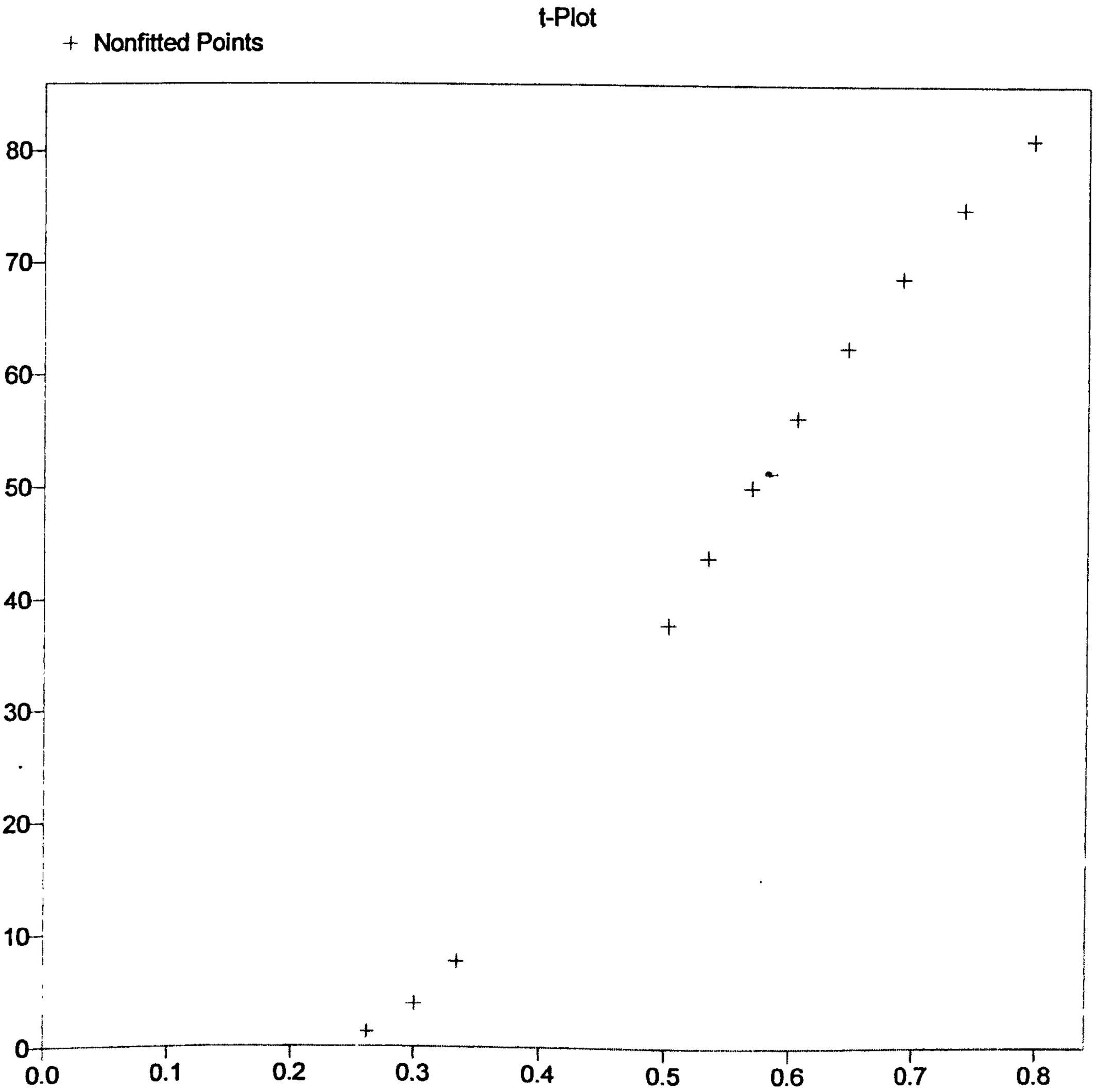

Sample: First Rhodium coating
Operator: Susi Olsen
Submitter:
File Name: C:\ASAP2010\DATA\SY0504.SMP

Started:	28/05/03 09:33:43	Analysis Adsorptive:	N2
Completed:	28/05/03 20:47:16	Analysis Bath:	77.35 K
Report Time:	28/05/03 20:47:16	Thermal Correction:	No
Sample Weight:	0.3000 g	Smoothed Pressures:	No
Warm Freespace:	16.0000 cm³	Cold Freespace:	45.0000 cm³
Equil. Interval:	45 secs	Low Pressure Dose:	None

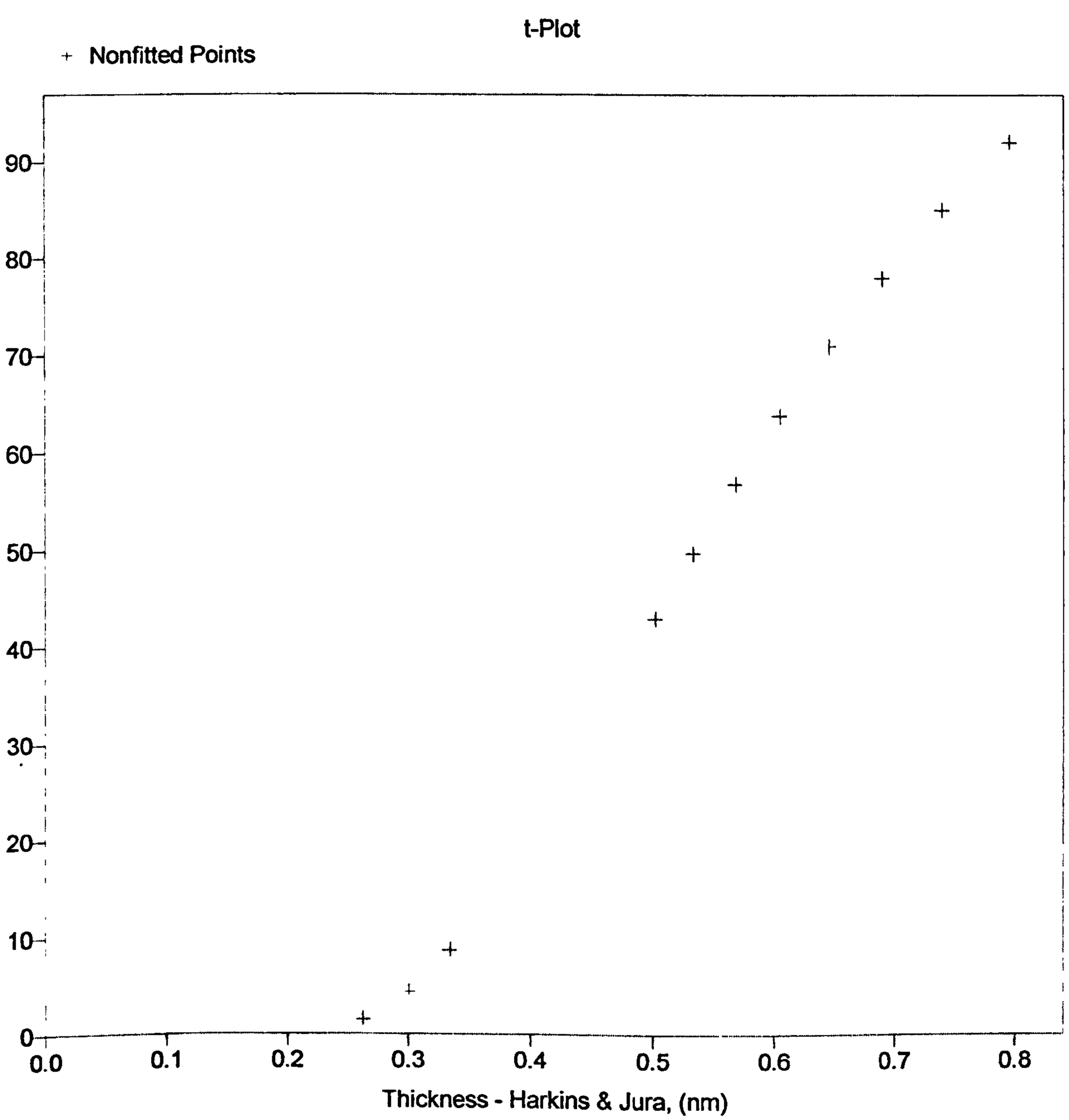

Sample: Second Rhodium coating
Operator: Susi Olsen
Submitter:
File Name: C:\ASAP2010\DATA\SY0505.SMP

Started: 29/05/03 09:30:16
Completed: 29/05/03 20:51:43
Report Time: 29/05/03 20:51:43
Sample Weight: 0.3000 g
Warm Freespace: 16.0000 cm³
Equil. Interval: 45 secs

Analysis Adsorptive: N2
Analysis Bath: 77.35 K
Thermal Correction: No
Smoothed Pressures: No
Cold Freespace: 45.0000 cm³
Low Pressure Dose: None

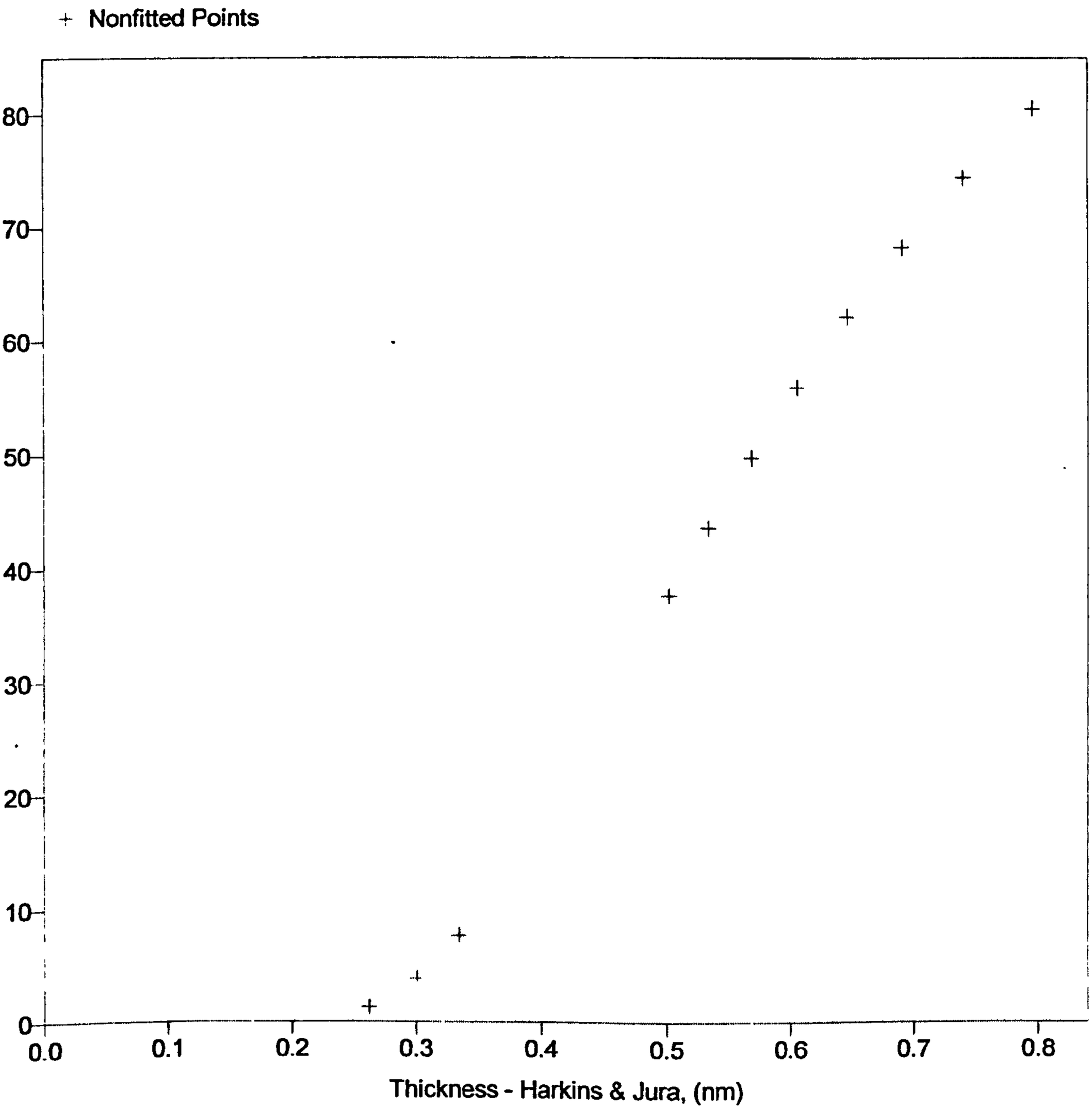

Sample:	Third Rhodium coating		
Operator:	Susi Olsen		
Submitter:			
File Name:	C:\ASAP2010\DATA\SY0506.SMP		
Started:	30/05/03 09:06:26	Analysis Adsorptive:	N2
Completed:	30/05/03 20:03:33	Analysis Bath:	77.35 K
Report Time:	30/05/03 20:03:34	Thermal Correction:	No
Sample Weight:	0.3000 g	Smoothed Pressures:	No
Warm Freespace:	16.0000 cm³	Cold Freespace:	45.0000 cm³
Equil. Interval:	45 secs	Low Pressure Dose:	None

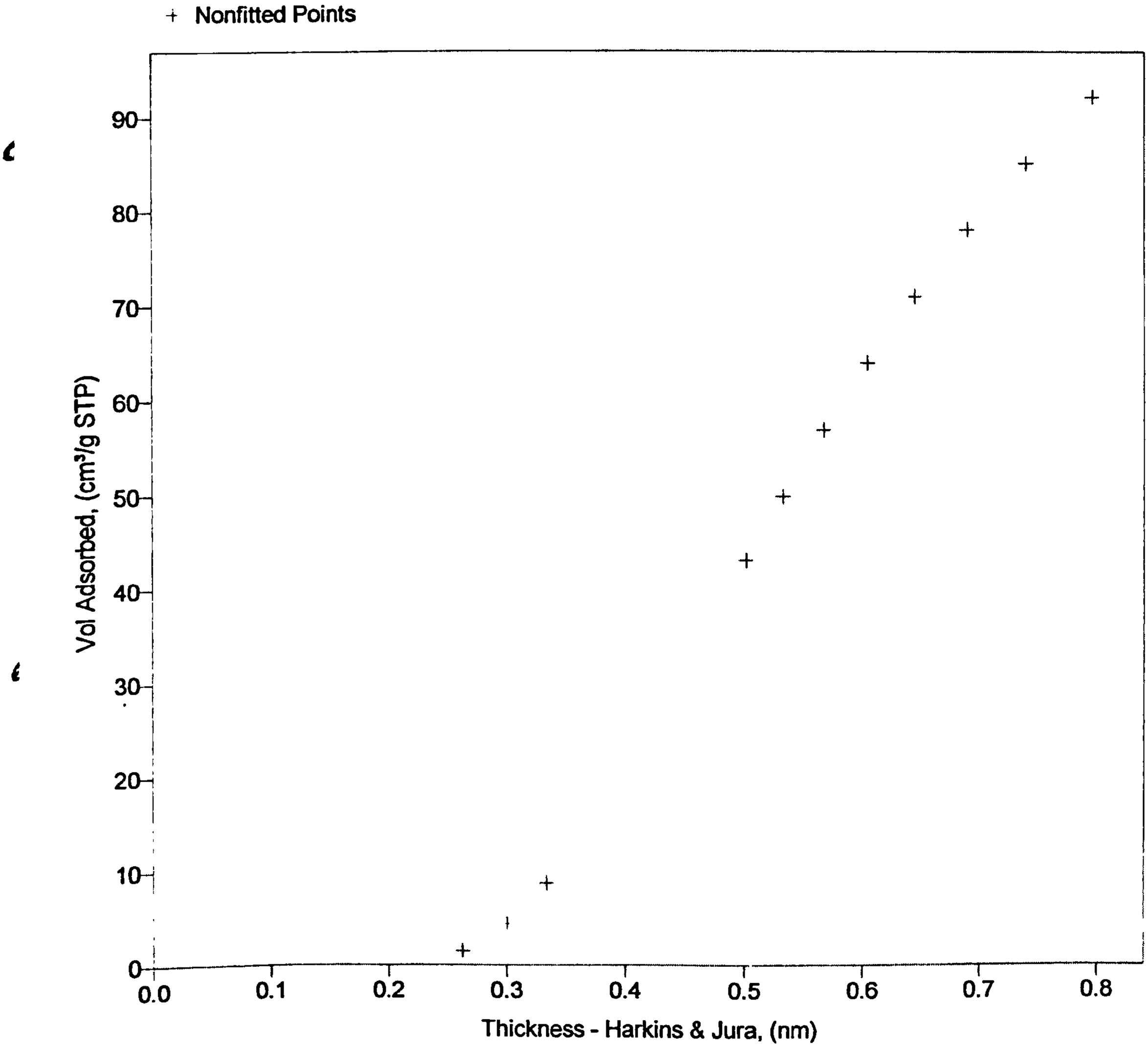

Sample: Forth Rhodium coating
Operator: Susi Olsen
Submitter:
File Name: C:\ASAP2010\DATA\SY0507.SMP

Started: 03/06/03 08:55:36
Completed: 03/06/03 20:23:40
Report Time: 03/06/03 20:23:40
Sample Weight: 0.3000 g
Warm Freespace: 16.0000 cm³
Equil. Interval: 45 secs

Analysis Adsorptive: N2
Analysis Bath: 77.35 K
Thermal Correction: No
Smoothed Pressures: No
Cold Freespace: 45.0000 cm³
Low Pressure Dose: None

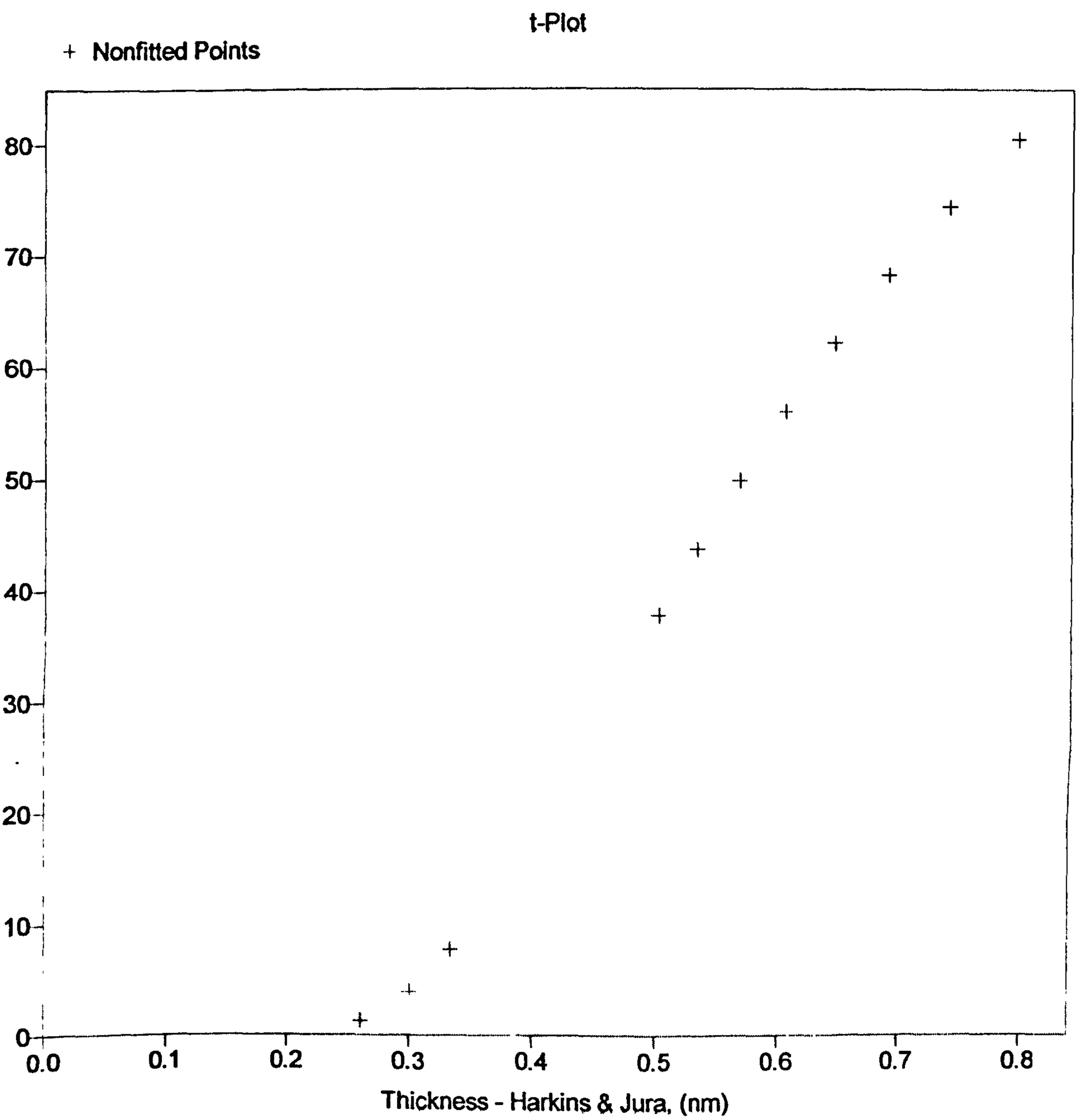

Sample: Forth Rhodium coating after H2 calcination
Operator: Susi Olsen
Submitter:
File Name: C:\ASAP2010\DATA\SY0508.SMP

Started: 04/06/03 10:23:00
Completed: 04/06/03 22:04:16
Report Time: 04/06/03 22:04:17
Sample Weight: 0.3000 g
Warm Freespace: 16.0000 cm³
Equil. Interval: 45 secs

Analysis Adsorptive: N2
Analysis Bath: 77.35 K
Thermal Correction: No
Smoothed Pressures: No
Cold Freespace: 45.0000 cm³
Low Pressure Dose: None

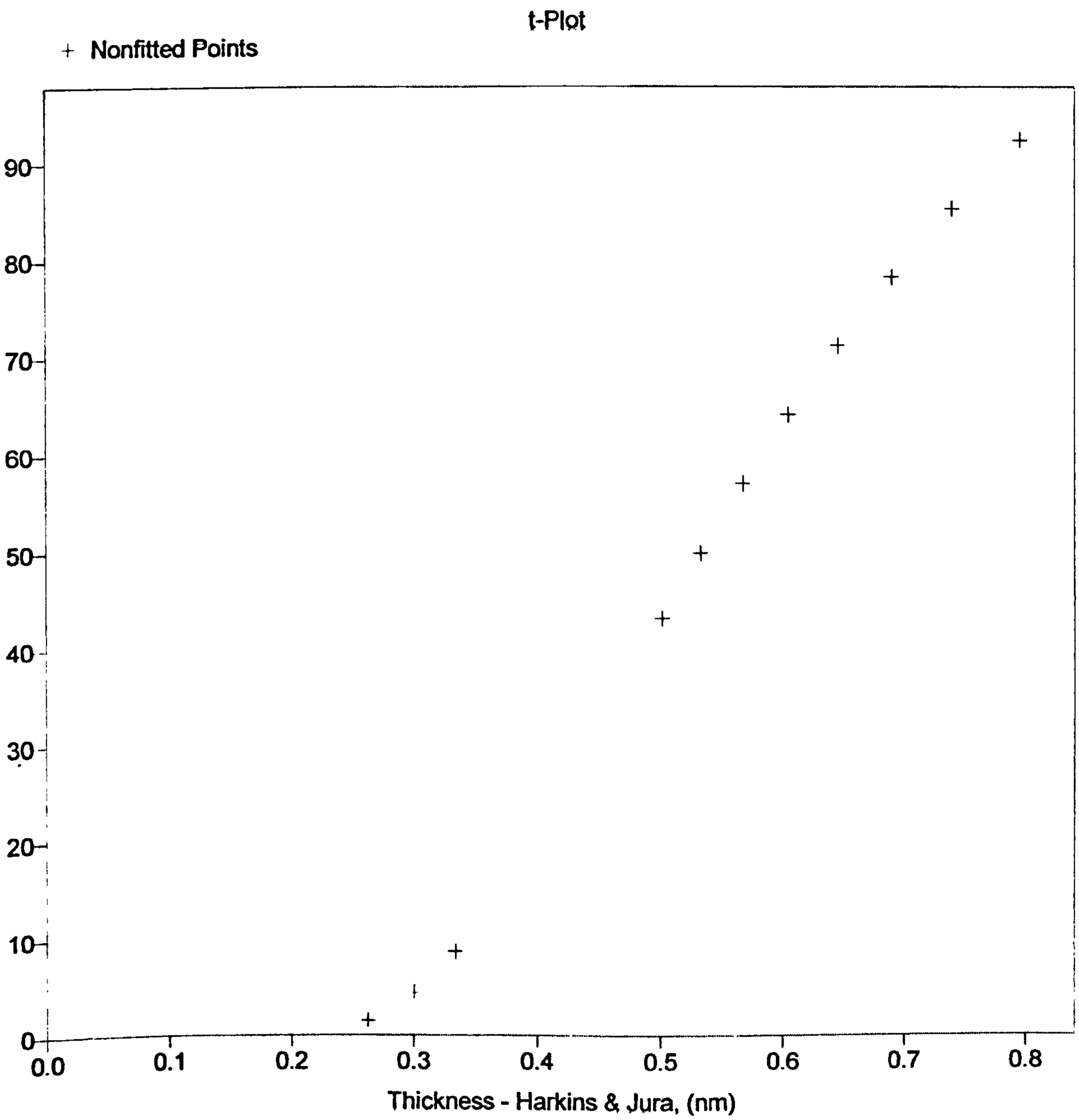

BJH DESORPTION CUMULATIVE PORE VOLUME

Sample: Support
Operator: Susi Olsen
Submitter:
File Name: C:\ASAP2010\DATA\SY0501.SMP

Started: 22/05/03 09:26:19
Completed: 22/05/03 20:51:26
Report Time: 23/05/03 11:00:05
Sample Weight: 0.3000 g
Warm Freespace: 16.0000 cm³
Equil. Interval: 45 secs

Analysis Adsorptive: N2
Analysis Bath: 77.35 K
Thermal Correction: No
Smoothed Pressures: No
Cold Freespace: 45.0000 cm³
Low Pressure Dose: None

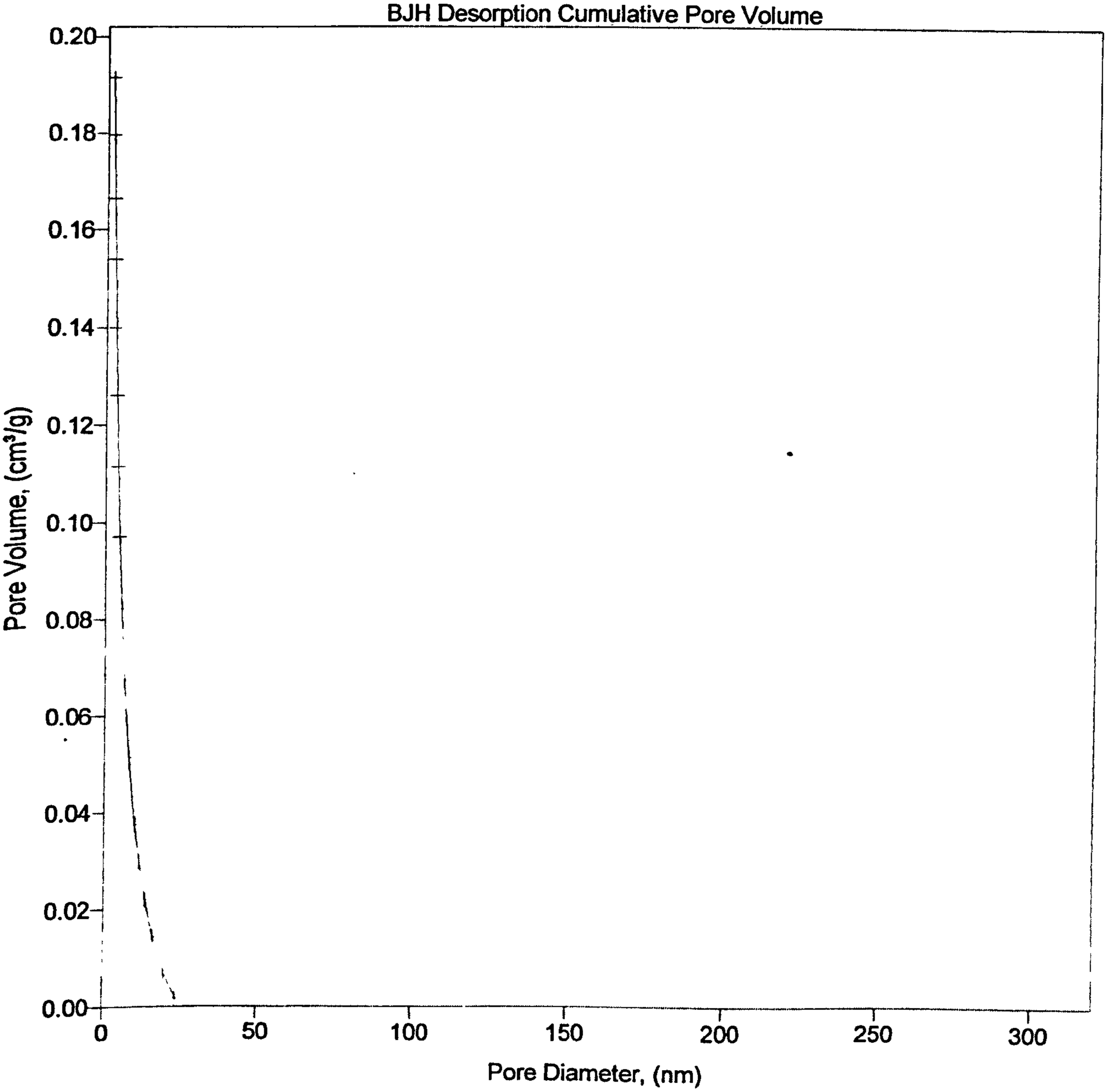

Sample: First internal gamma alumina
Operator: Susi Olsen
Submitter:
File Name: C:\ASAP2010\DATA\SY0502.SMP

Started: 21/05/03 10:15:22
Completed: 21/05/03 21:25:24
Report Time: 21/05/03 21:25:24
Sample Weight: 0.3000 g
Warm Freespace: 16.0000 cm³
Equil. Interval: 45 secs

Analysis Adsorptive: N2
Analysis Bath: 77.35 K
Thermal Correction: No
Smoothed Pressures: No
Cold Freespace: 45.0000 cm³
Low Pressure Dose: None

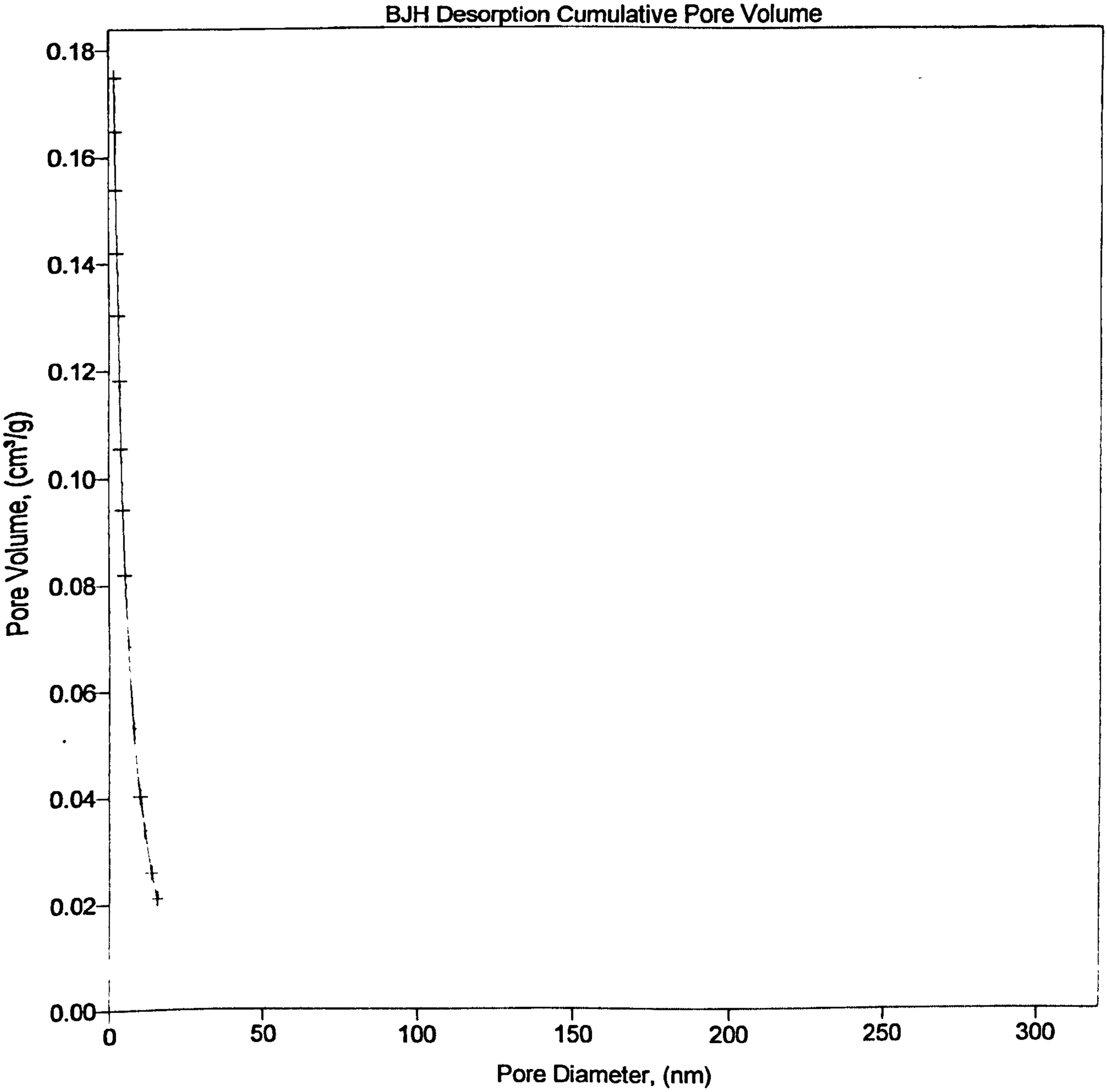

Sample: second internal gamma alumina coating
Operator: Susi Olsen
Submitter:
File Name: C:\ASAP2010\DATA\SY0503.SMP

Started: 27/05/03 09:24:51
Completed: 27/05/03 20:06:51
Report Time: 27/05/03 20:06:51
Sample Weight: 0.3000 g
Warm Freespace: 16.0000 cm³
Equil. Interval: 45 secs

Analysis Adsorptive: N2
Analysis Bath: 77.35 K
Thermal Correction: No
Smoothed Pressures: No
Cold Freespace: 45.0000 cm³
Low Pressure Dose: None

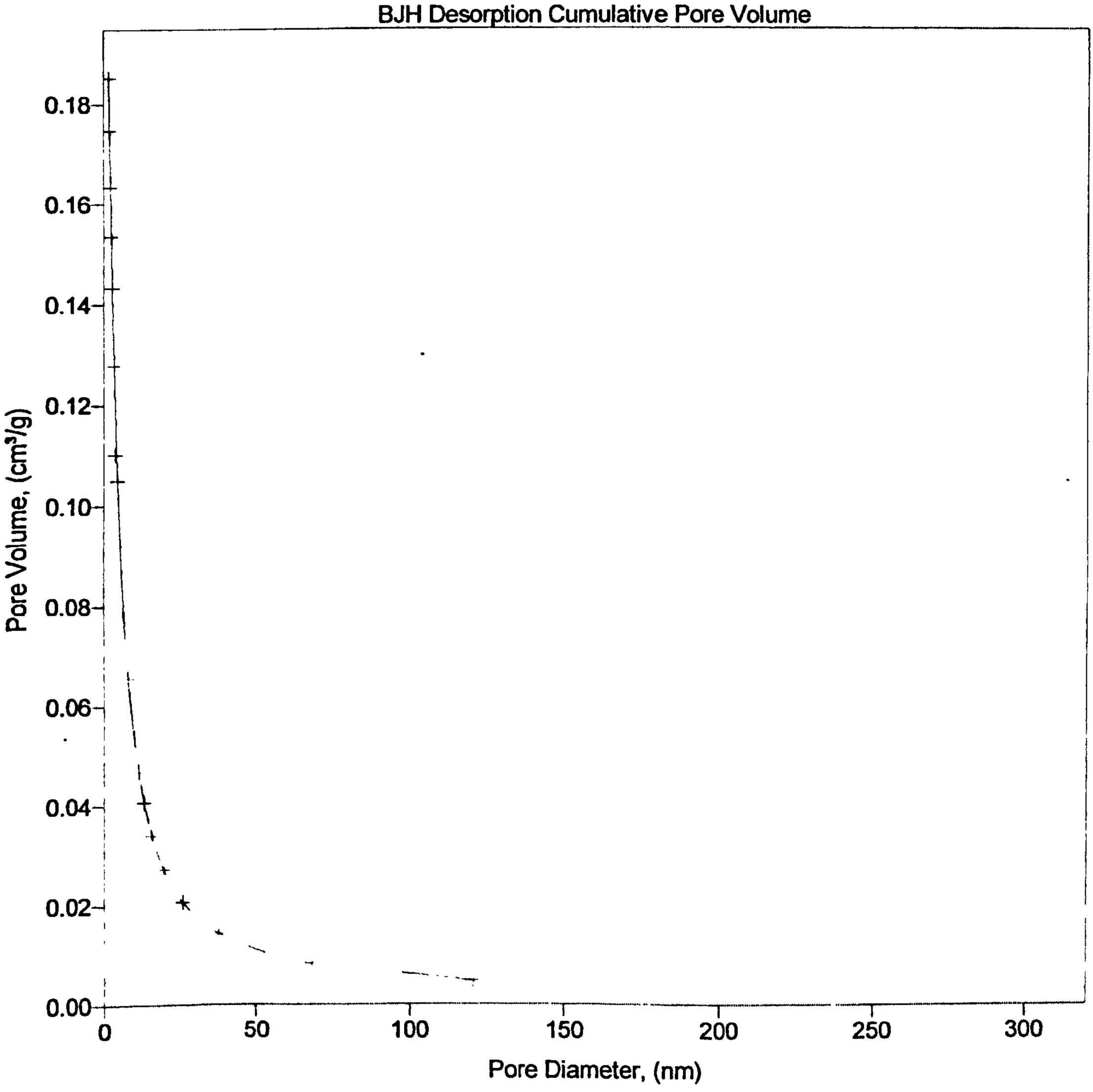

Sample:	First Rhodium coating
Operator:	Susi Olsen
Submitter:	
File Name:	C:\ASAP2010\DATA\SY0504.SMP

Started:	28/05/03 09:33:43	Analysis Adsorptive:	N2
Completed:	28/05/03 20:47:16	Analysis Bath:	77.35 K
Report Time:	28/05/03 20:47:16	Thermal Correction:	No
Sample Weight:	0.3000 g	Smoothed Pressures:	No
Warm Freespace:	16.0000 cm³	Cold Freespace:	45.0000 cm³
Equil. Interval:	45 secs	Low Pressure Dose:	None

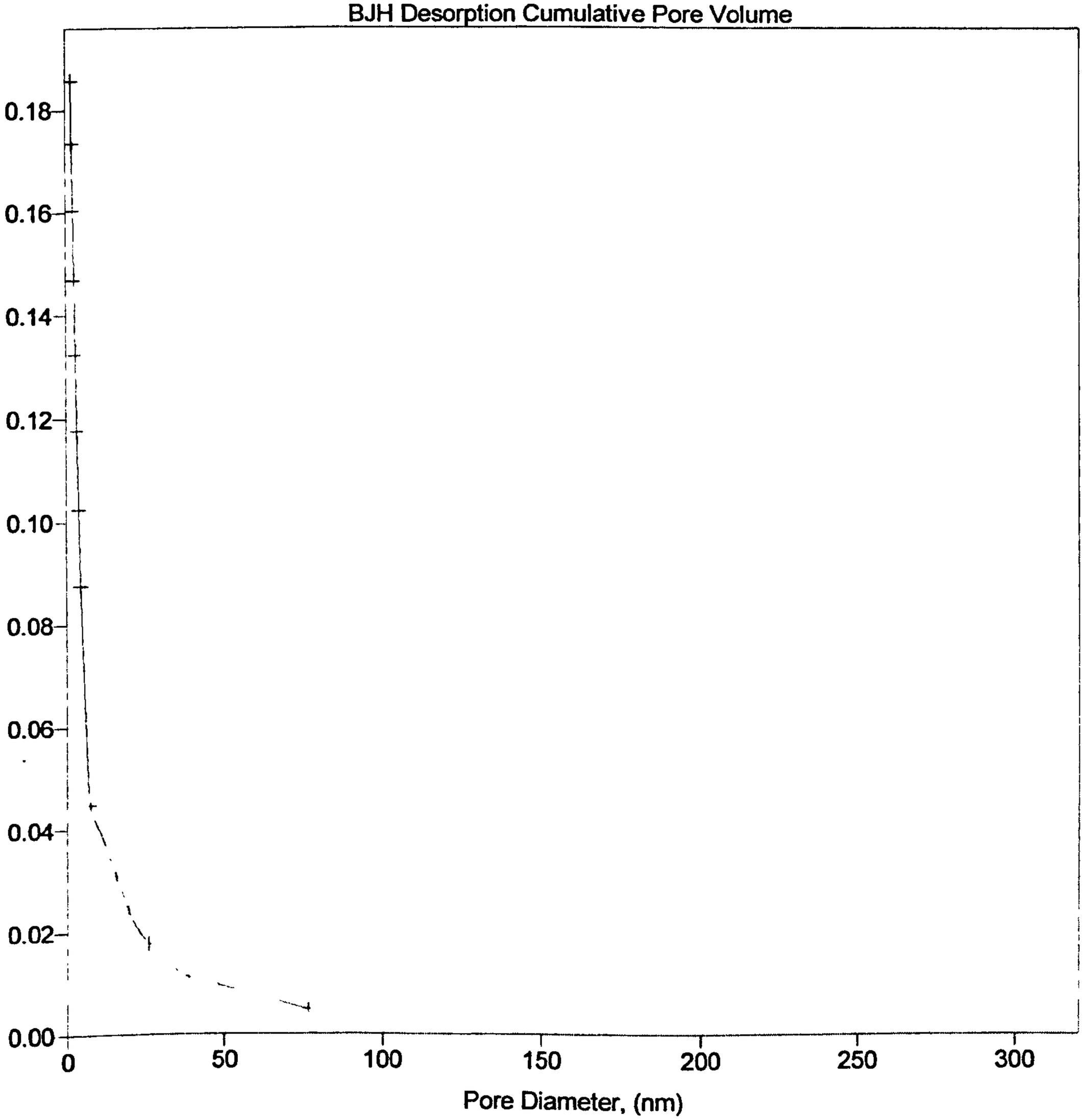

Sample: Second Rhodium coating
Operator: Susi Olsen
Submitter:
File Name: C:\ASAP2010\DATA\SY0505.SMP

Started: 29/05/03 09:30:16
Completed: 29/05/03 20:51:43
Report Time: 29/05/03 20:51:43
Sample Weight: 0.3000 g
Warm Freespace: 16.0000 cm³
Equil. Interval: 45 secs

Analysis Adsorptive: N2
Analysis Bath: 77.35 K
Thermal Correction: No
Smoothed Pressures: No
Cold Freespace: 45.0000 cm³
Low Pressure Dose: None

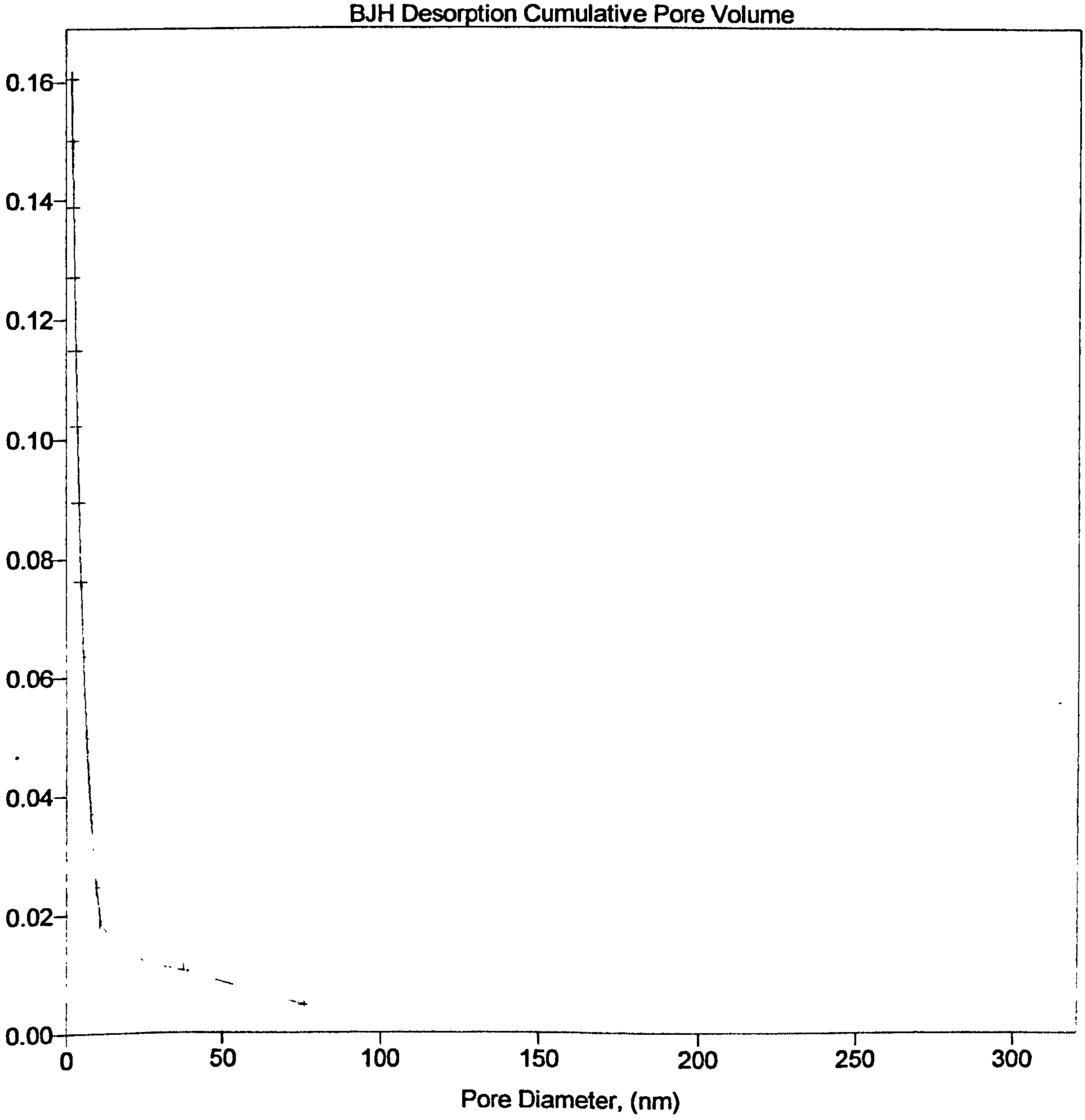

SY05 06 - Third Rhodium coating

Sample: Third Rhodium coating
Operator: Susi Olsen
Submitter:
File Name: C:\ASAP2010\DATA\SY0506.SMP

Started: 30/05/03 09:06:26
Completed: 30/05/03 20:03:33
Report Time: 30/05/03 20:03:34
Sample Weight: 0.3000 g
Warm Freespace: 16.0000 cm³
Equil. Interval: 45 secs

Analysis Adsorptive: N2
Analysis Bath: 77.35 K
Thermal Correction: No
Smoothed Pressures: No
Cold Freespace: 45.0000 cm³
Low Pressure Dose: None

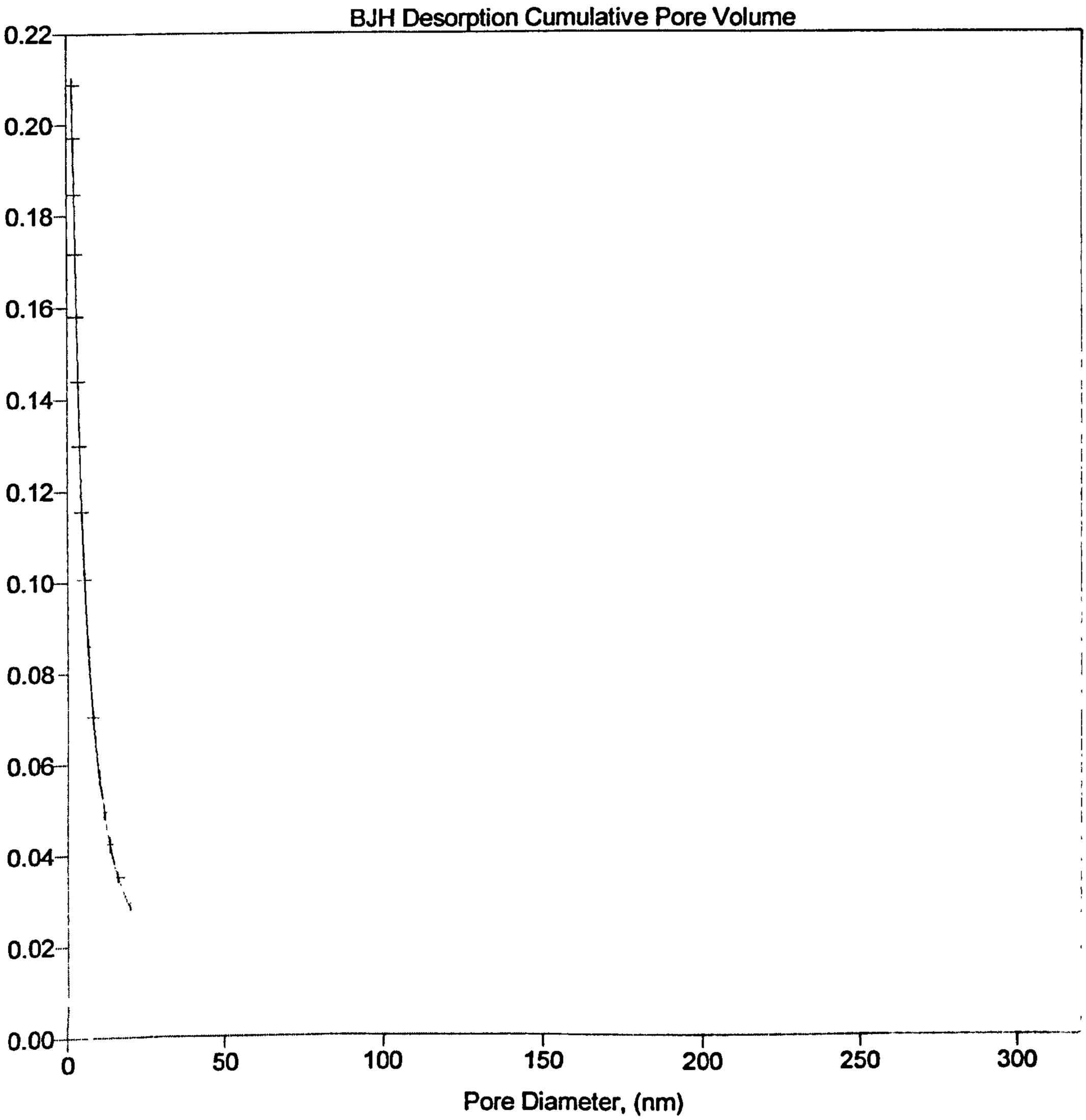

Sample: Forth Rhodium coating
Operator: Susi Olsen
Submitter:
File Name: C:\ASAP2010\DATA\SY0507.SMP

Started: 03/06/03 08:55:36
Completed: 03/06/03 20:23:40
Report Time: 03/06/03 20:23:40
Sample Weight: 0.3000 g
Warm Freespace: 16.0000 cm³
Equil. Interval: 45 secs

Analysis Adsorptive: N2
Analysis Bath: 77.35 K
Thermal Correction: No
Smoothed Pressures: No
Cold Freespace: 45.0000 cm³
Low Pressure Dose: None

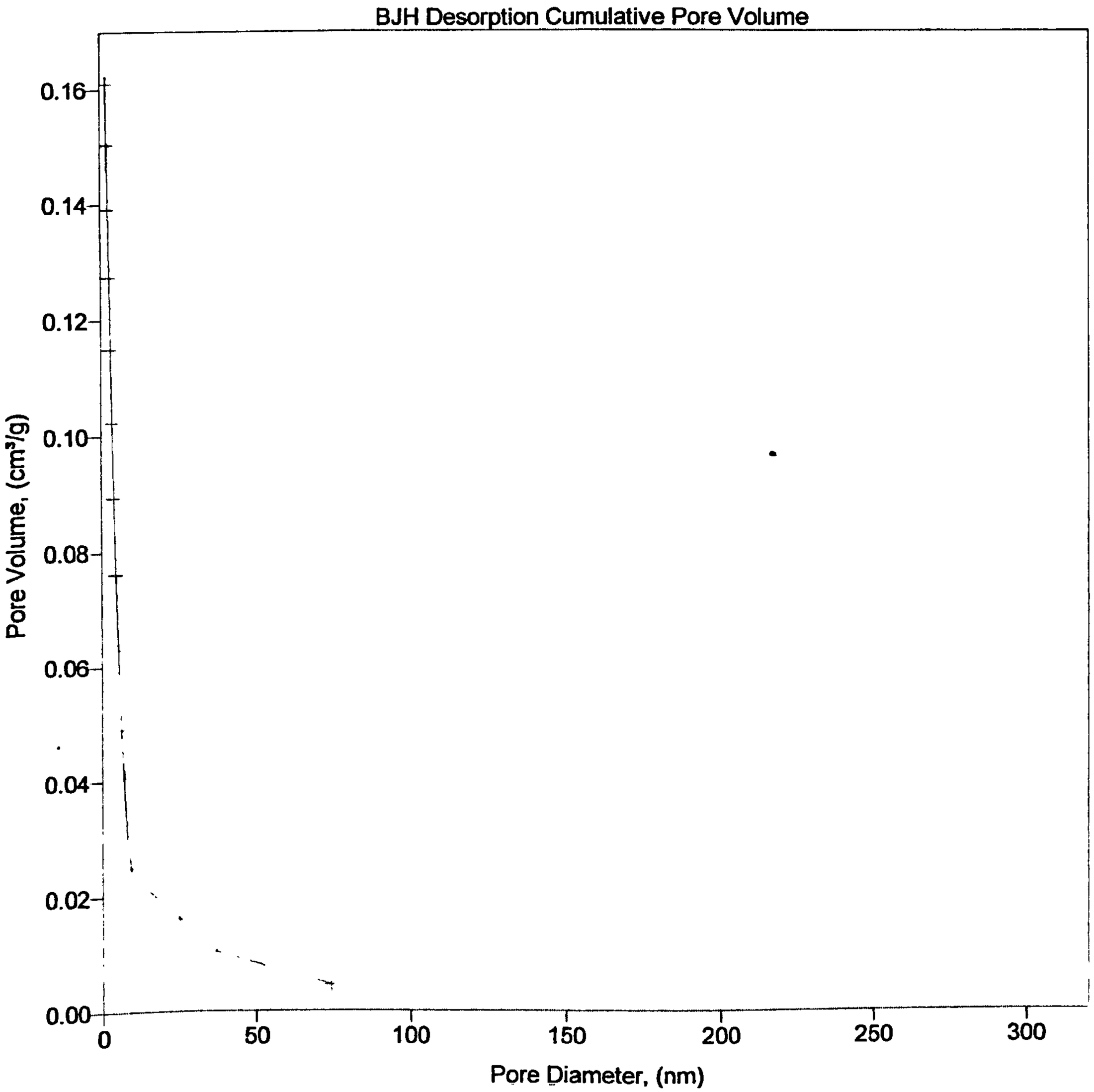

Sample: Forth Rhodium coating after H2 calcination
Operator: Susi Olsen
Submitter:
File Name: C:\ASAP2010\DATA\SY0508.SMP

Started: 04/06/03 10:23:00
Completed: 04/06/03 22:04:16
Report Time: 04/06/03 22:04:17
Sample Weight: 0.3000 g
Warm Freespace: 16.0000 cm³
Equil. Interval: 45 secs

Analysis Adsorptive: N2
Analysis Bath: 77.35 K
Thermal Correction: No
Smoothed Pressures: No
Cold Freespace: 45.0000 cm³
Low Pressure Dose: None

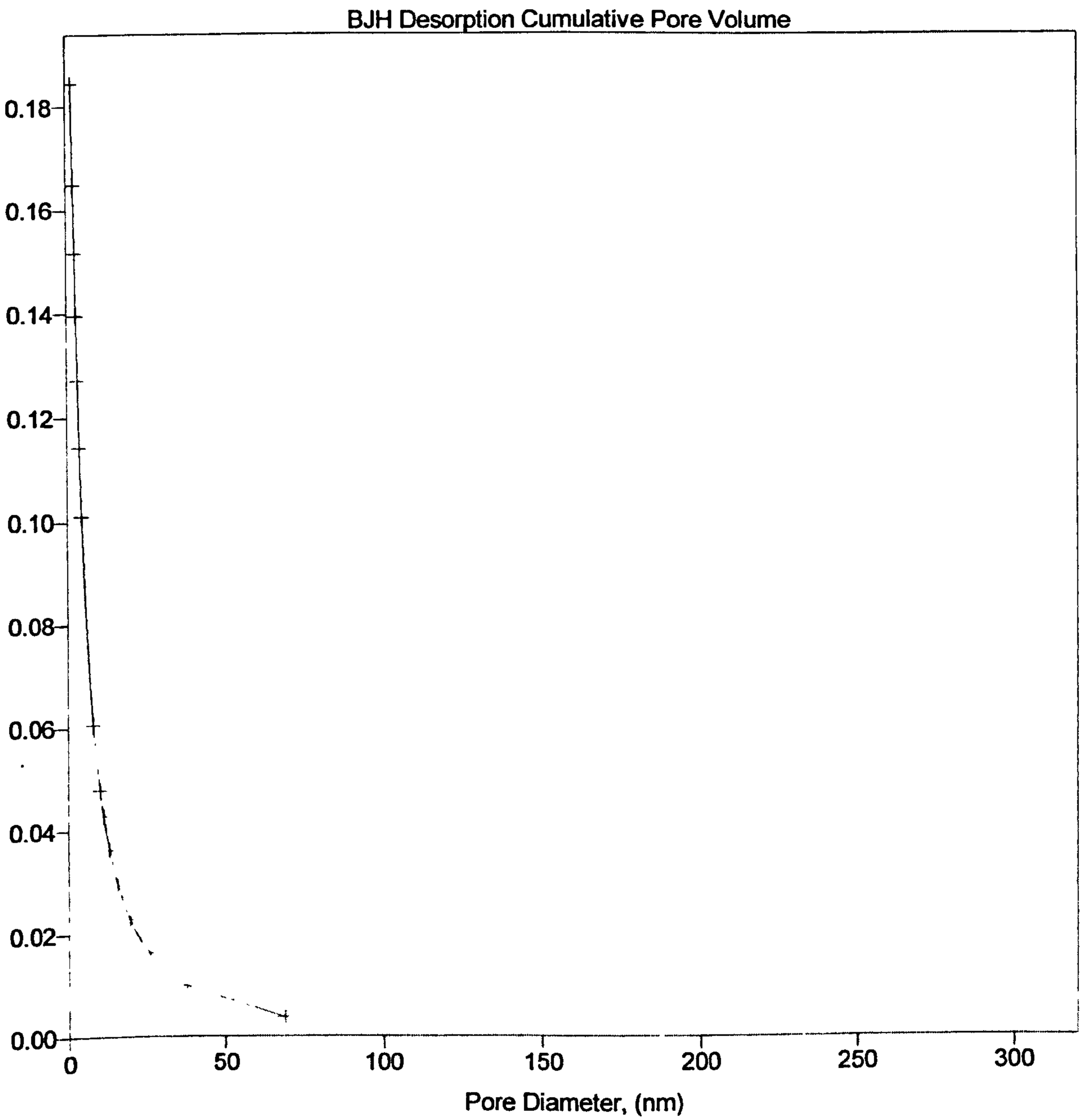

BJH DESORPTION dV / dD PORE VOLUME

Sample: Support
Operator: Susi Olsen
Submitter:
File Name: C:\ASAP2010\DATA\SY0501.SMP

Started: 22/05/03 09:26:19
Completed: 22/05/03 20:51:26
Report Time: 23/05/03 11:00:05
Sample Weight: 0.3000 g
Warm Freespace: 16.0000 cm³
Equil. Interval: 45 secs

Analysis Adsorptive: N2
Analysis Bath: 77.35 K
Thermal Correction: No
Smoothed Pressures: No
Cold Freespace: 45.0000 cm³
Low Pressure Dose: None

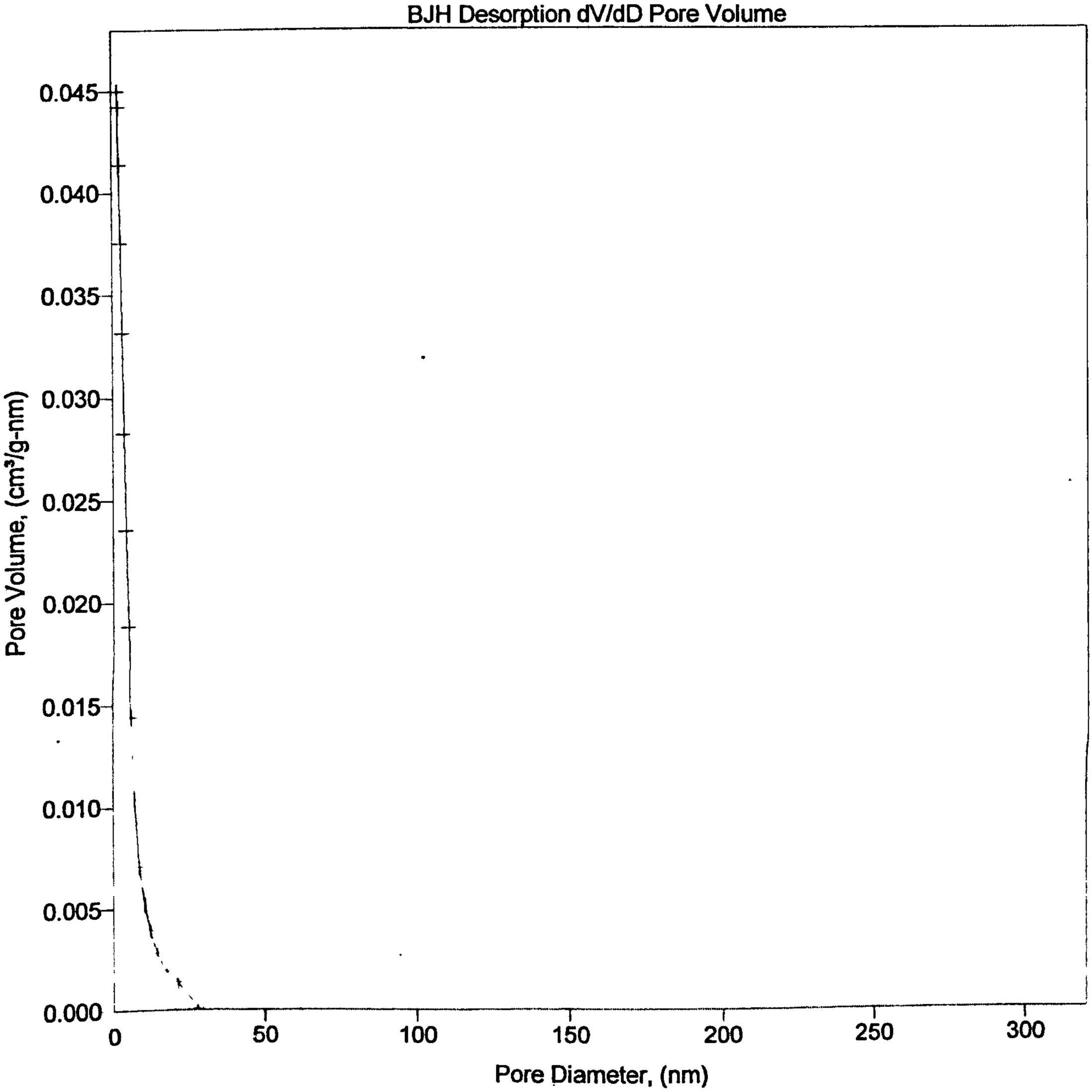

Sample: First internal gamma alumina
Operator: Susi Olsen
Submitter:
File Name: C:\ASAP2010\DATA\SY0502.SMP

Started:	21/05/03 10:15:22	Analysis Adsorptive:	N2
Completed:	21/05/03 21:25:24	Analysis Bath:	77.35 K
Report Time:	21/05/03 21:25:24	Thermal Correction:	No
Sample Weight:	0.3000 g	Smoothed Pressures:	No
Warm Freespace:	16.0000 cm³	Cold Freespace:	45.0000 cm³
Equil. Interval:	45 secs	Low Pressure Dose:	None

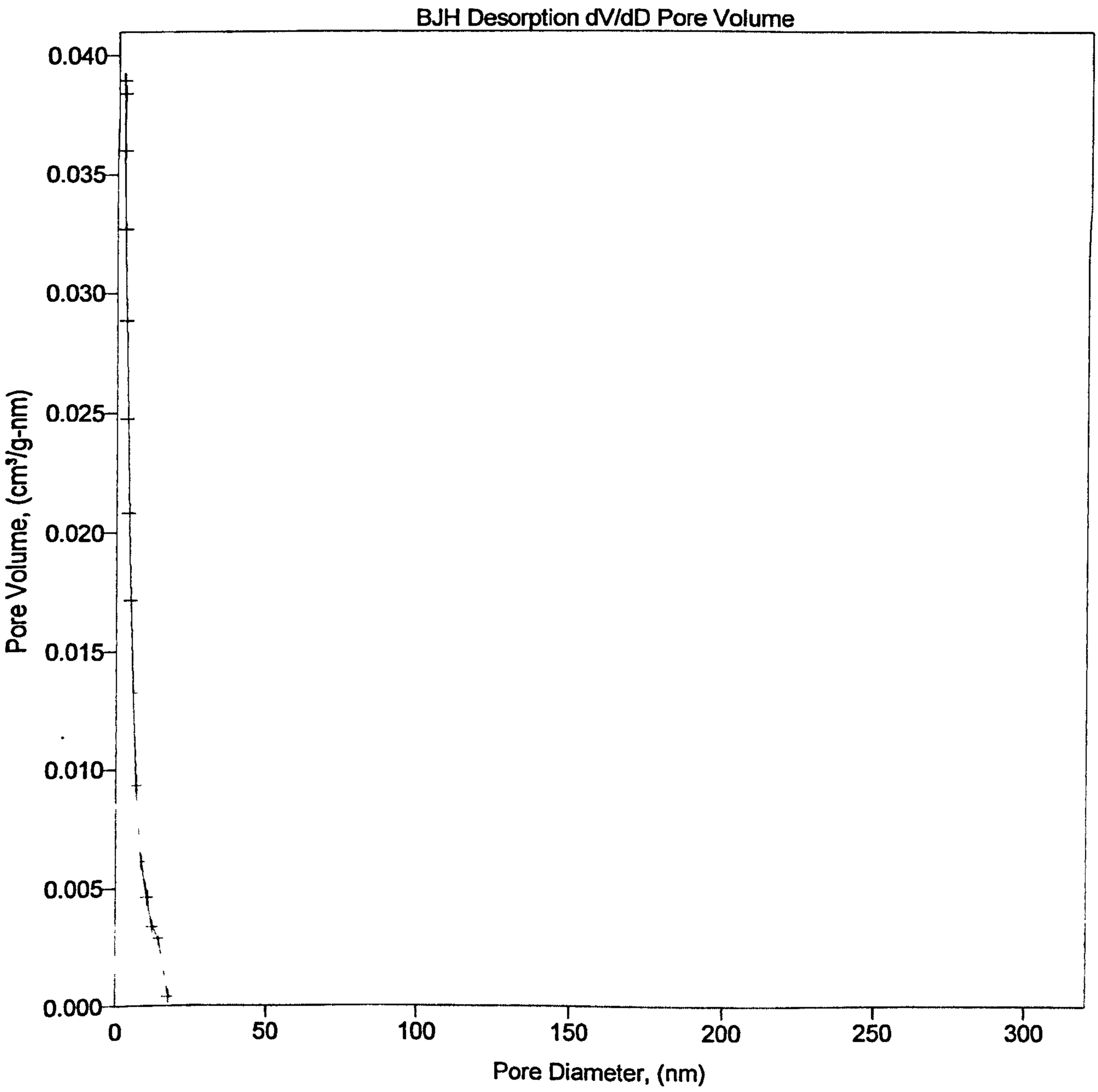

Sample: second internal gamma alumina coating
Operator: Susi Olsen
Submitter:
File Name: C:\ASAP2010\DATA\SY0503.SMP

Started: 27/05/03 09:24:51
Completed: 27/05/03 20:06:51
Report Time: 27/05/03 20:06:51
Sample Weight: 0.3000 g
Warm Freespace: 16.0000 cm³
Equil. Interval: 45 secs

Analysis Adsorptive: N2
Analysis Bath: 77.35 K
Thermal Correction: No
Smoothed Pressures: No
Cold Freespace: 45.0000 cm³
Low Pressure Dose: None

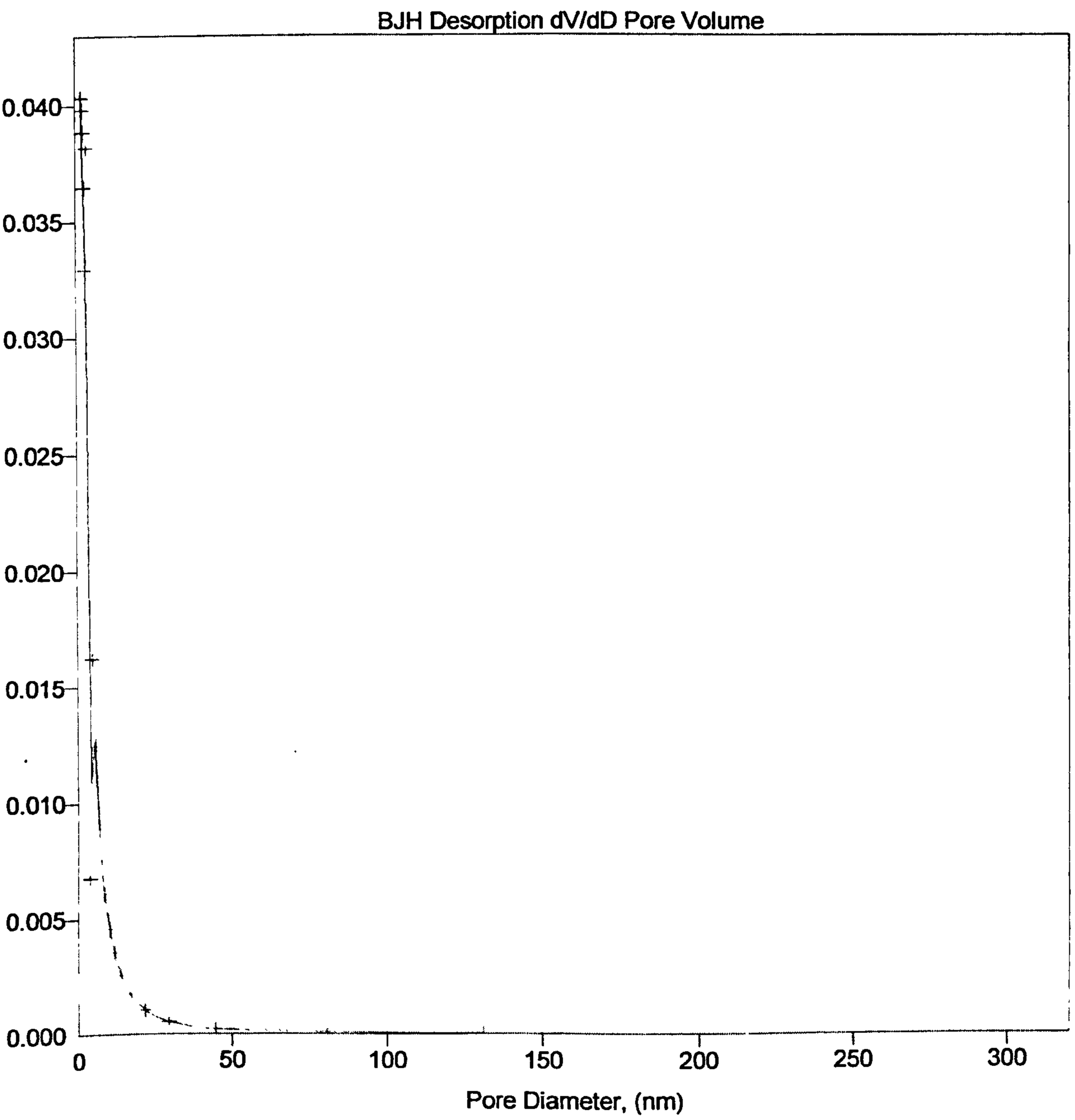

Sample: First Rhodium coating
Operator: Susi Olsen
Submitter:
File Name: C:\ASAP2010\DATA\SY0504.SMP

Started: 28/05/03 09:33:43
Completed: 28/05/03 20:47:16
Report Time: 28/05/03 20:47:16
Sample Weight: 0.3000 g
Warm Freespace: 16.0000 cm³
Equil. Interval: 45 secs

Analysis Adsorptive: N2
Analysis Bath: 77.35 K
Thermal Correction: No
Smoothed Pressures: No
Cold Freespace: 45.0000 cm³
Low Pressure Dose: None

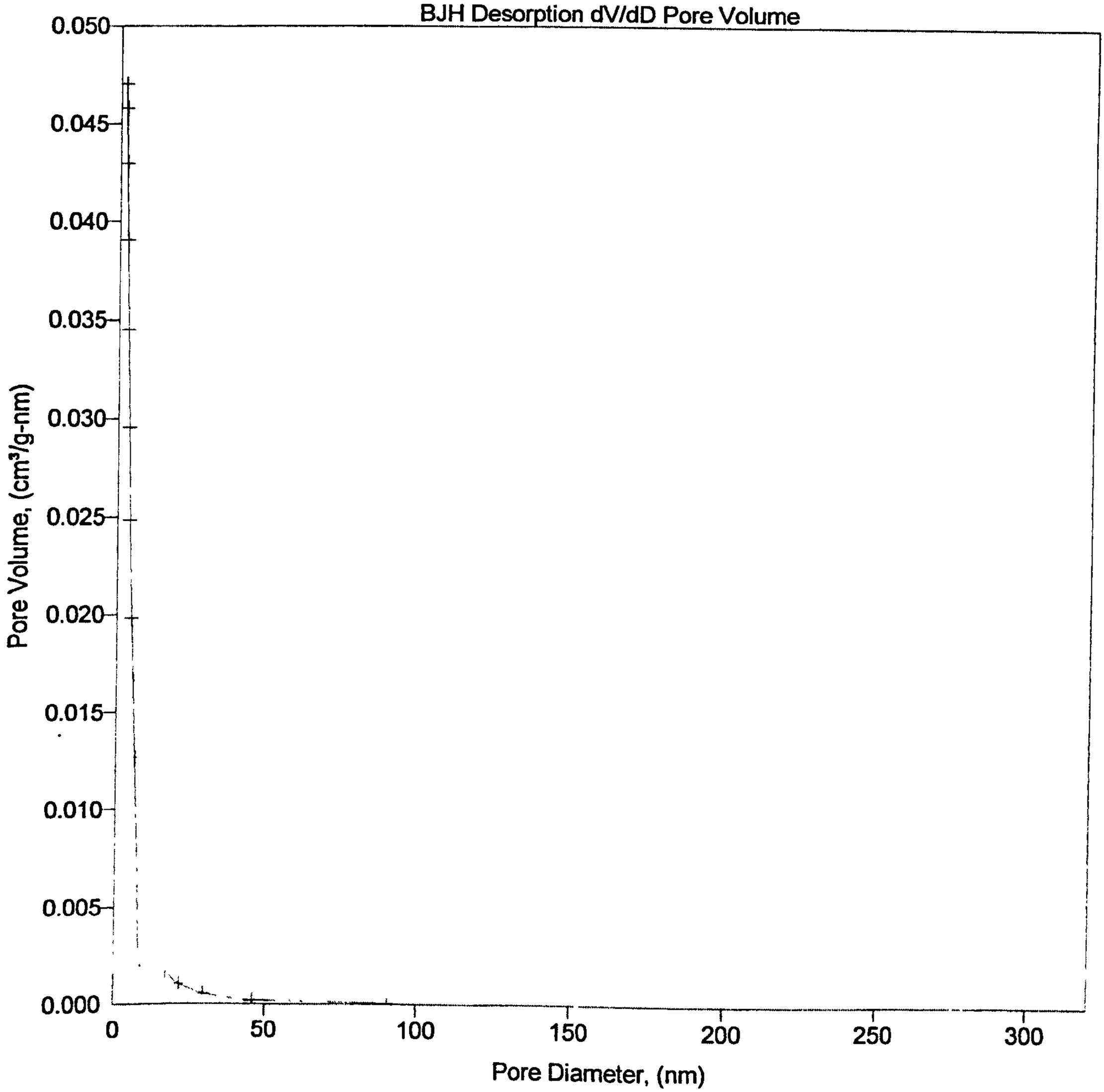

Sample: Second Rhodium coating
Operator: Susi Olsen
Submitter:
File Name: C:\ASAP2010\DATA\SY0505.SMP

Started: 29/05/03 09:30:16
Completed: 29/05/03 20:51:43
Report Time: 29/05/03 20:51:43
Sample Weight: 0.3000 g
Warm Freespace: 16.0000 cm³
Equil. Interval: 45 secs

Analysis Adsorptive: N2
Analysis Bath: 77.35 K
Thermal Correction: No
Smoothed Pressures: No
Cold Freespace: 45.0000 cm³
Low Pressure Dose: None

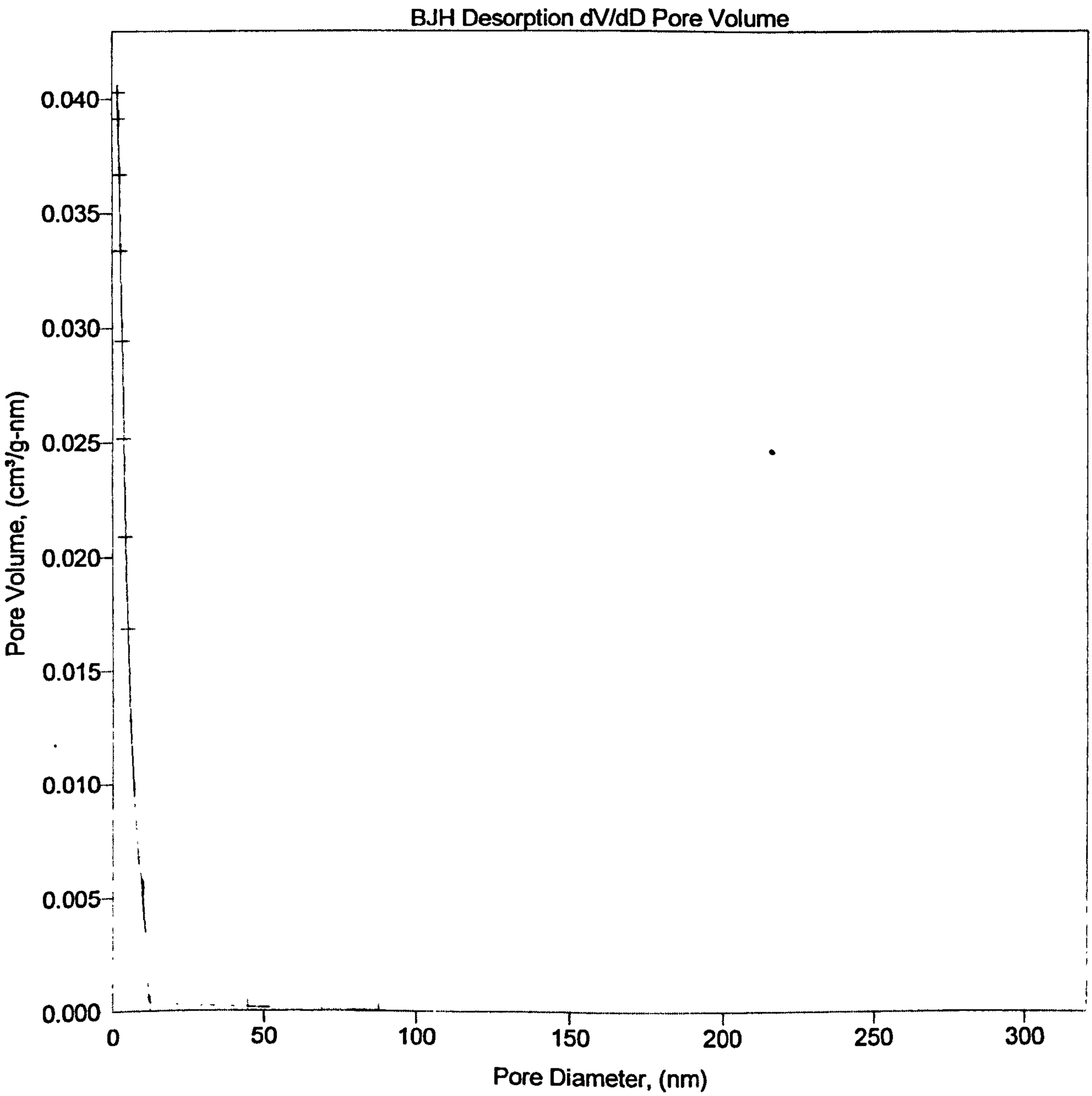

Sample: Third Rhodium coating
Operator: Susi Olsen
Submitter:
File Name: C:\ASAP2010\DATA\SY0506.SMP

Started: 30/05/03 09:06:26
Completed: 30/05/03 20:03:33
Report Time: 30/05/03 20:03:34
Sample Weight: 0.3000 g
Warm Freespace: 16.0000 cm³
Equil. Interval: 45 secs

Analysis Adsorptive: N2
Analysis Bath: 77.35 K
Thermal Correction: No
Smoothed Pressures: No
Cold Freespace: 45.0000 cm³
Low Pressure Dose: None

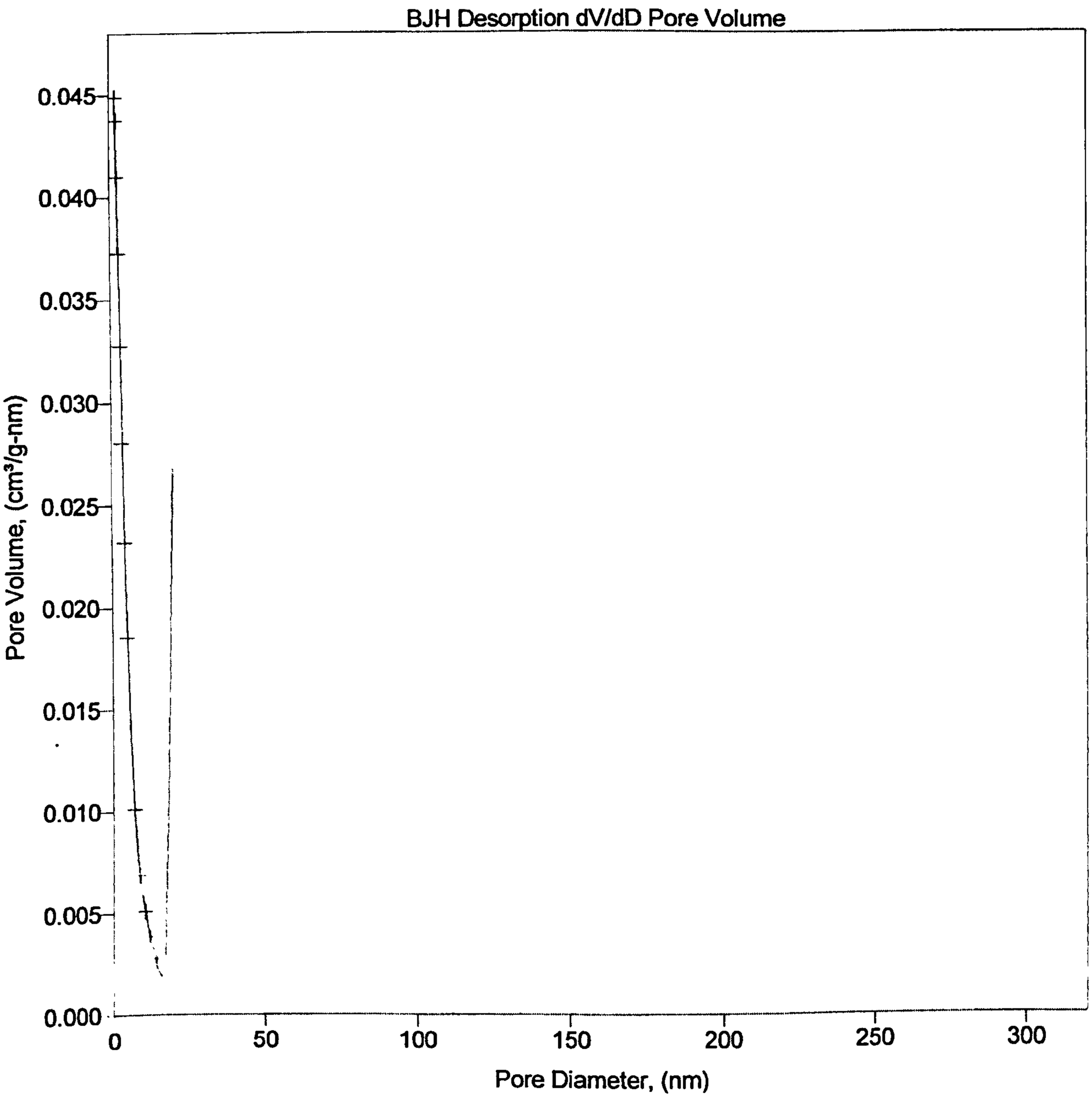

Sample: Forth Rhodium coating
Operator: Susi Olsen
Submitter:
File Name: C:\ASAP2010\DATA\SY0507.SMP

Started: 03/06/03 08:55:36
Completed: 03/06/03 20:23:40
Report Time: 03/06/03 20:23:40
Sample Weight: 0.3000 g
Warm Freespace: 16.0000 cm³
Equil. Interval: 45 secs

Analysis Adsorptive: N2
Analysis Bath: 77.35 K
Thermal Correction: No
Smoothed Pressures: No
Cold Freespace: 45.0000 cm³
Low Pressure Dose: None

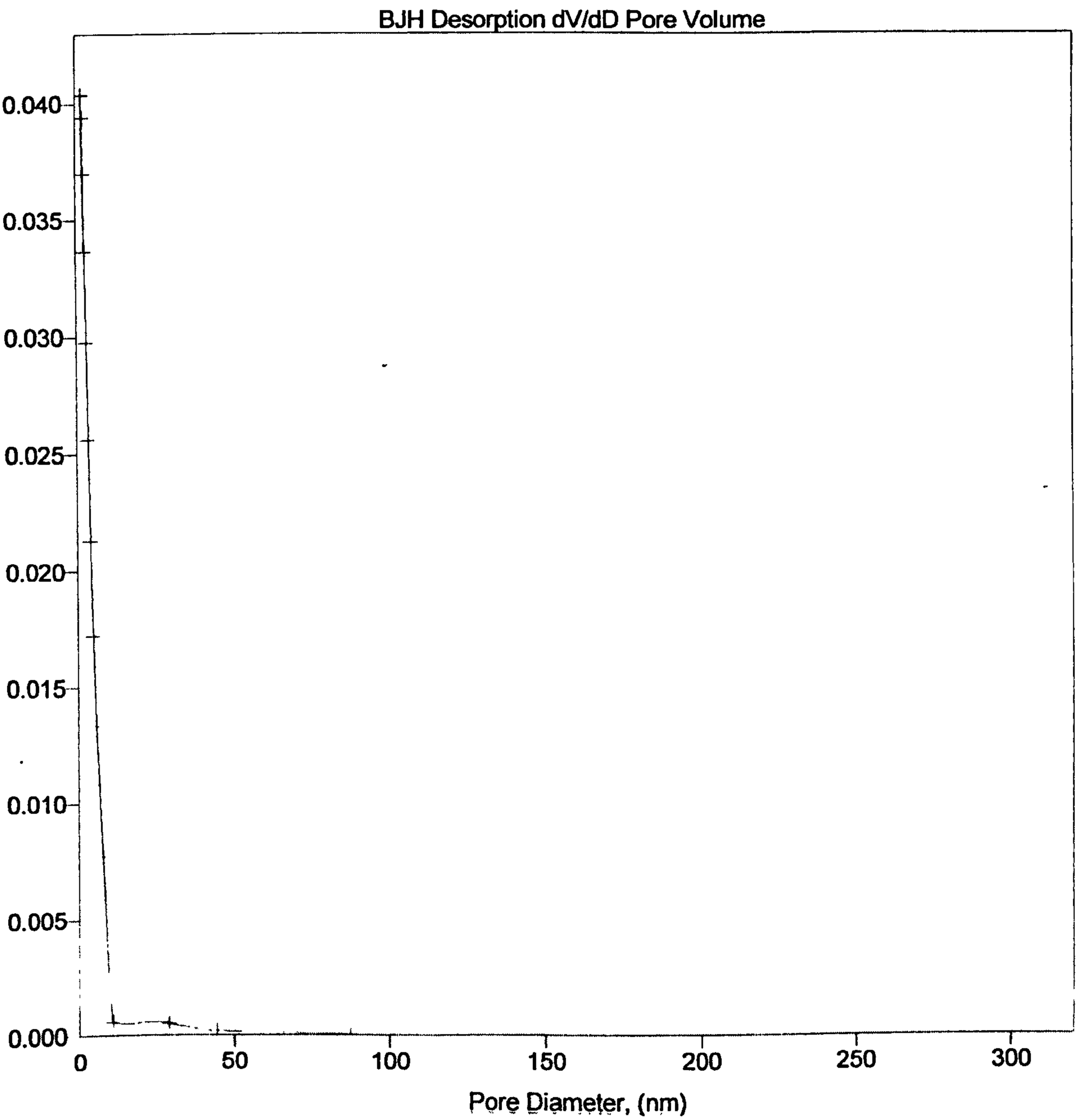

Sample: Forth Rhodium coating after H2 calcination
Operator: Susi Olsen
Submitter:
File Name: C:\ASAP2010\DATA\SY0508.SMP

Started: 04/06/03 10:23:00
Completed: 04/06/03 22:04:16
Report Time: 04/06/03 22:04:17
Sample Weight: 0.3000 g
Warm Freespace: 16.0000 cm³
Equil. Interval: 45 secs

Analysis Adsorptive: N2
Analysis Bath: 77.35 K
Thermal Correction: No
Smoothed Pressures: No
Cold Freespace: 45.0000 cm³
Low Pressure Dose: None

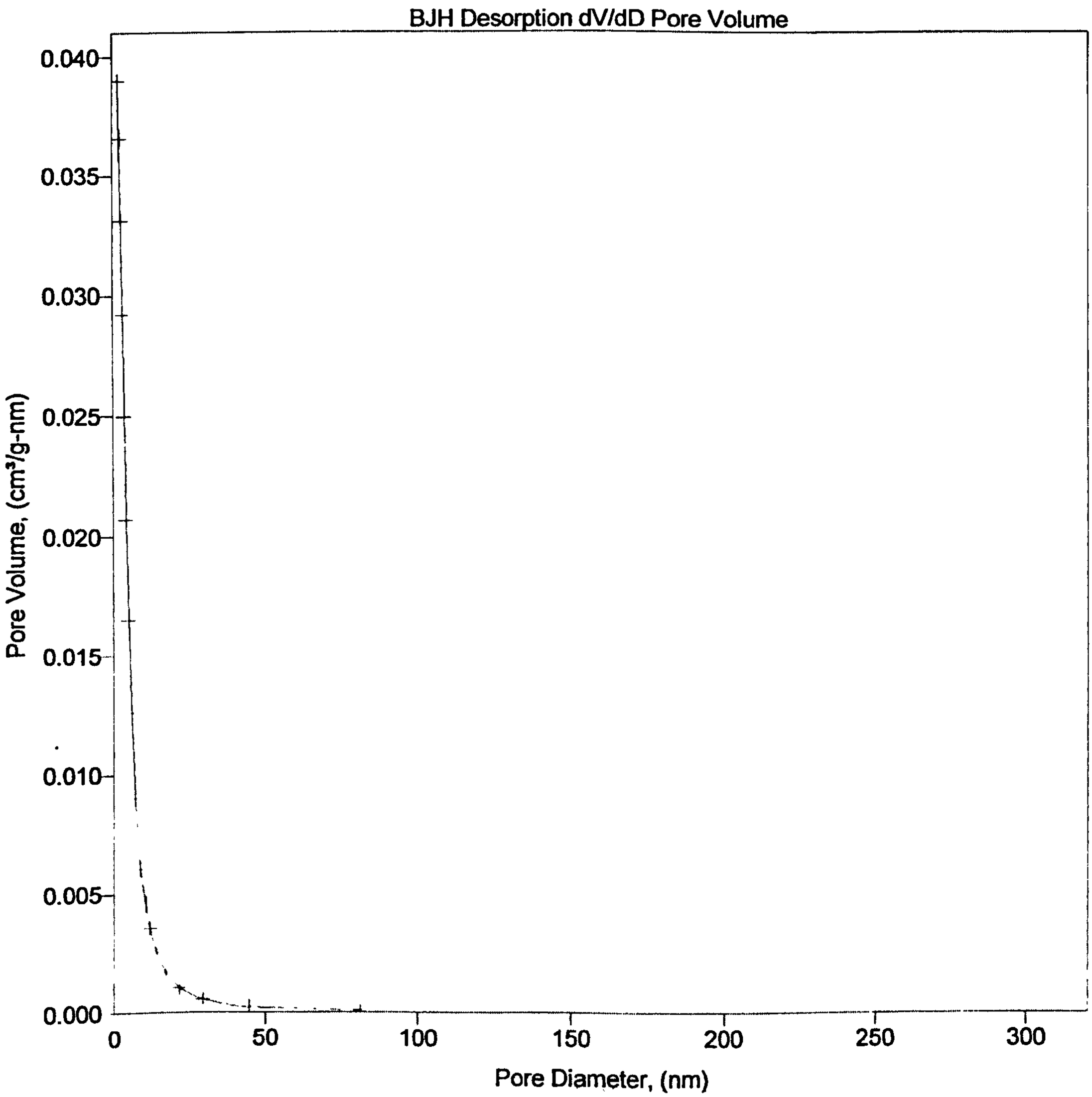

BJH DESORPTION dV / dlog (D) PORE VOLUME

Sample: Support
Operator: Susi Olsen
Submitter:
File Name: C:\ASAP2010\DATA\SY0501.SMP

Started: 22/05/03 09:26:19
Completed: 22/05/03 20:51:26
Report Time: 23/05/03 11:00:05
Sample Weight: 0.3000 g
Warm Freespace: 16.0000 cm³
Equil. Interval: 45 secs

Analysis Adsorptive: N2
Analysis Bath: 77.35 K
Thermal Correction: No
Smoothed Pressures: No
Cold Freespace: 45.0000 cm³
Low Pressure Dose: None

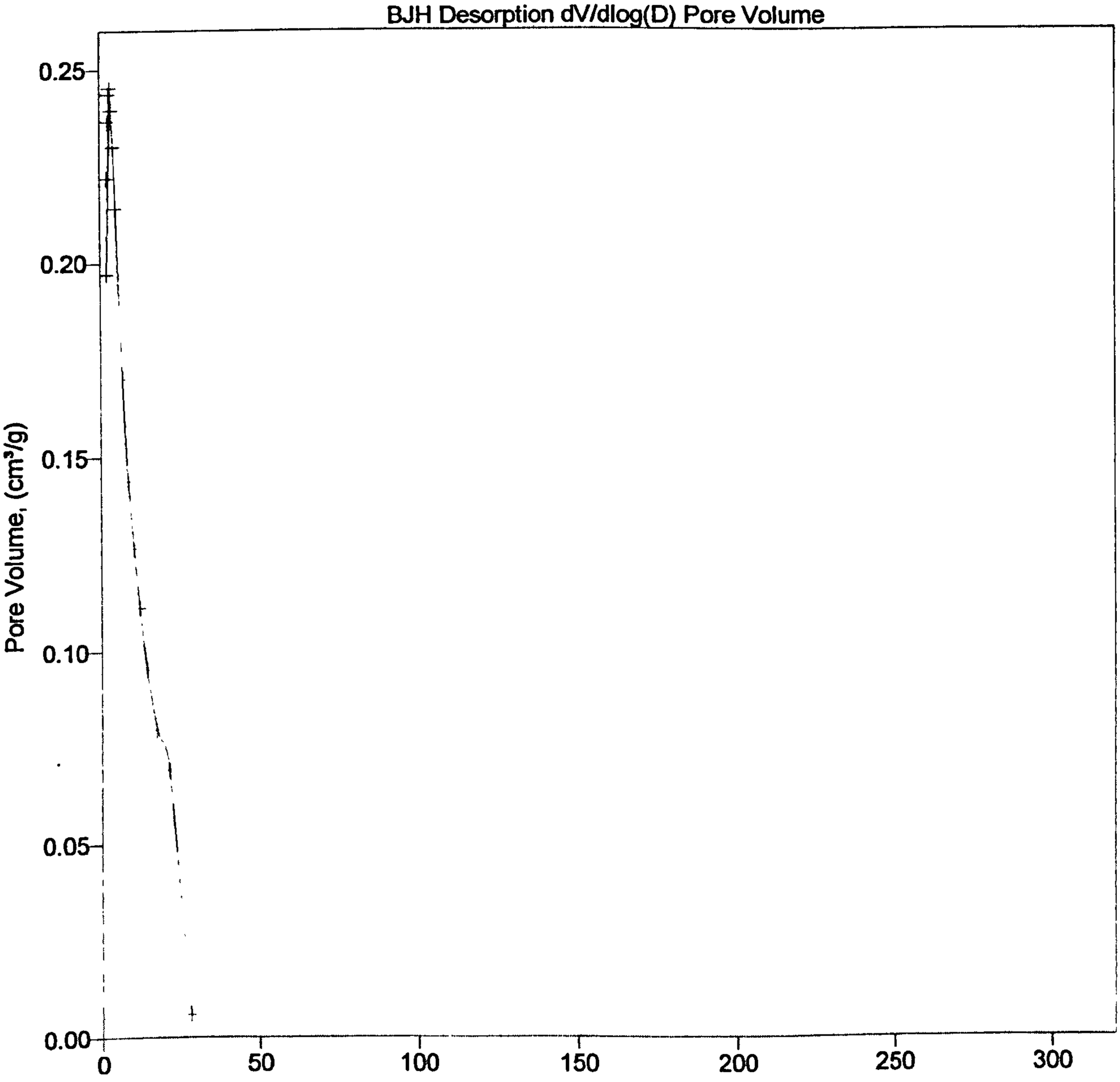

Sample:	First internal gamma alumina
Operator:	Susi Olsen
Submitter:	
File Name:	C:\ASAP2010\DATA\SY0502.SMP

Started:	21/05/03 10:15:22	Analysis Adsorptive:	N2
Completed:	21/05/03 21:25:24	Analysis Bath:	77.35 K
Report Time:	21/05/03 21:25:24	Thermal Correction:	No
Sample Weight:	0.3000 g	Smoothed Pressures:	No
Warm Freespace:	16.0000 cm³	Cold Freespace:	45.0000 cm³
Equil. Interval:	45 secs	Low Pressure Dose:	None

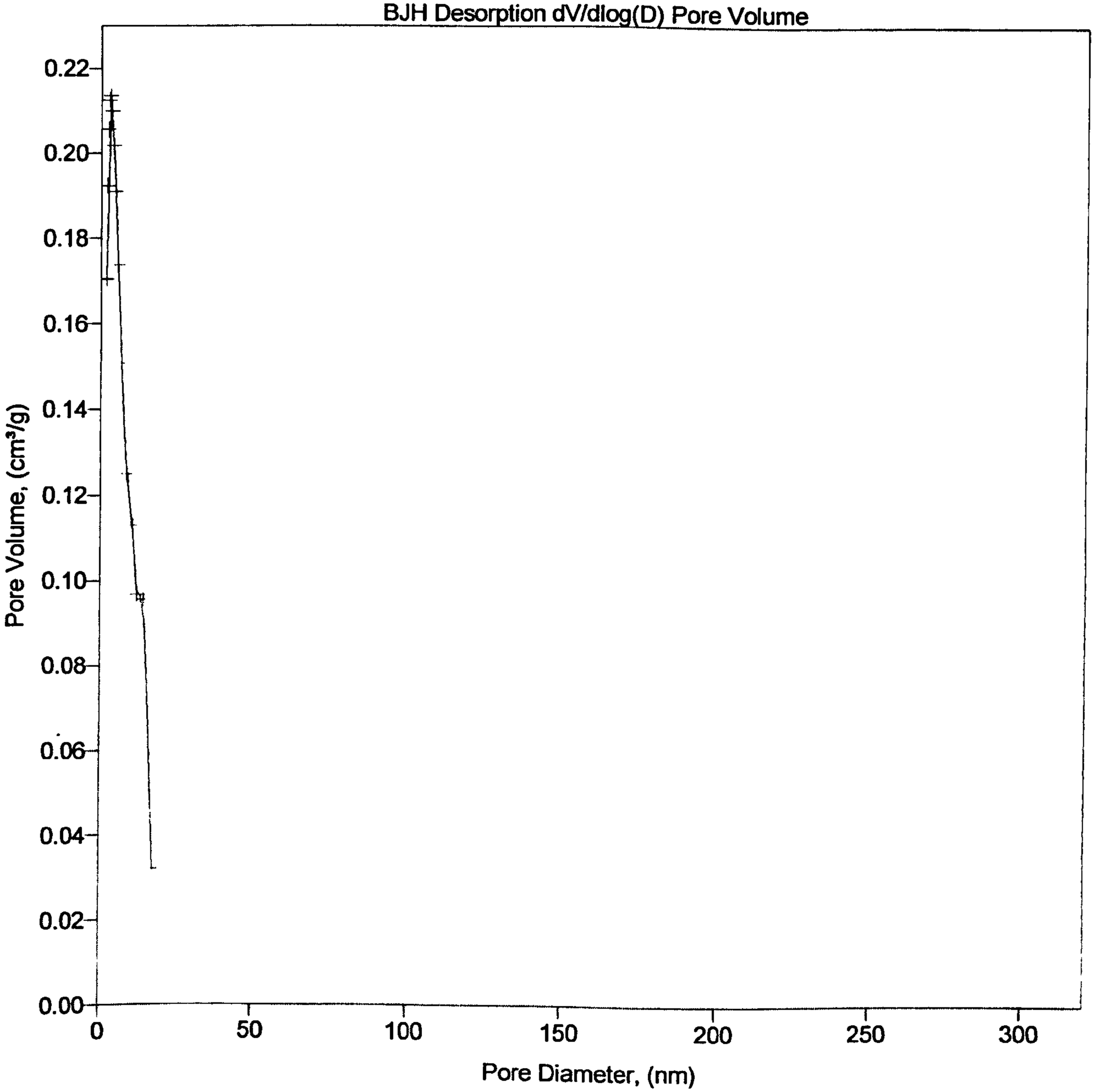

Sample: second internal gamma alumina coating
Operator: Susi Olsen
Submitter:
File Name: C:\ASAP2010\DATA\SY0503.SMP

Started: 27/05/03 09:24:51
Completed: 27/05/03 20:06:51
Report Time: 27/05/03 20:06:51
Sample Weight: 0.3000 g
Warm Freespace: 16.0000 cm³
Equil. Interval: 45 secs

Analysis Adsorptive: N2
Analysis Bath: 77.35 K
Thermal Correction: No
Smoothed Pressures: No
Cold Freespace: 45.0000 cm³
Low Pressure Dose: None

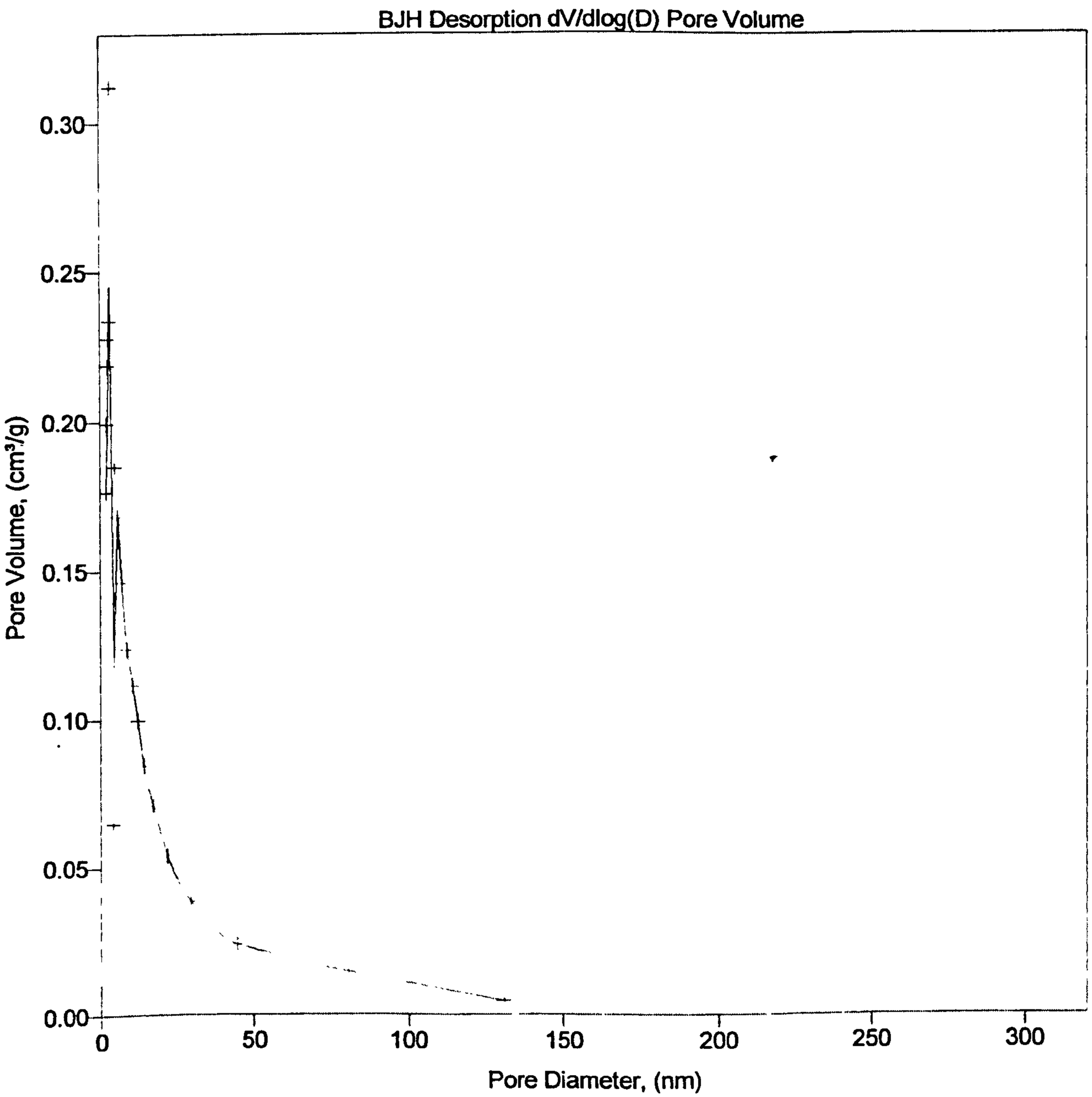

Sample: First Rhodium coating
Operator: Susi Olsen
Submitter:
File Name: C:\ASAP2010\DATA\SY0504.SMP

Started: 28/05/03 09:33:43
Completed: 28/05/03 20:47:16
Report Time: 28/05/03 20:47:16
Sample Weight: 0.3000 g
Warm Freespace: 16.0000 cm³
Equil. Interval: 45 secs

Analysis Adsorptive: N2
Analysis Bath: 77.35 K
Thermal Correction: No
Smoothed Pressures: No
Cold Freespace: 45.0000 cm³
Low Pressure Dose: None

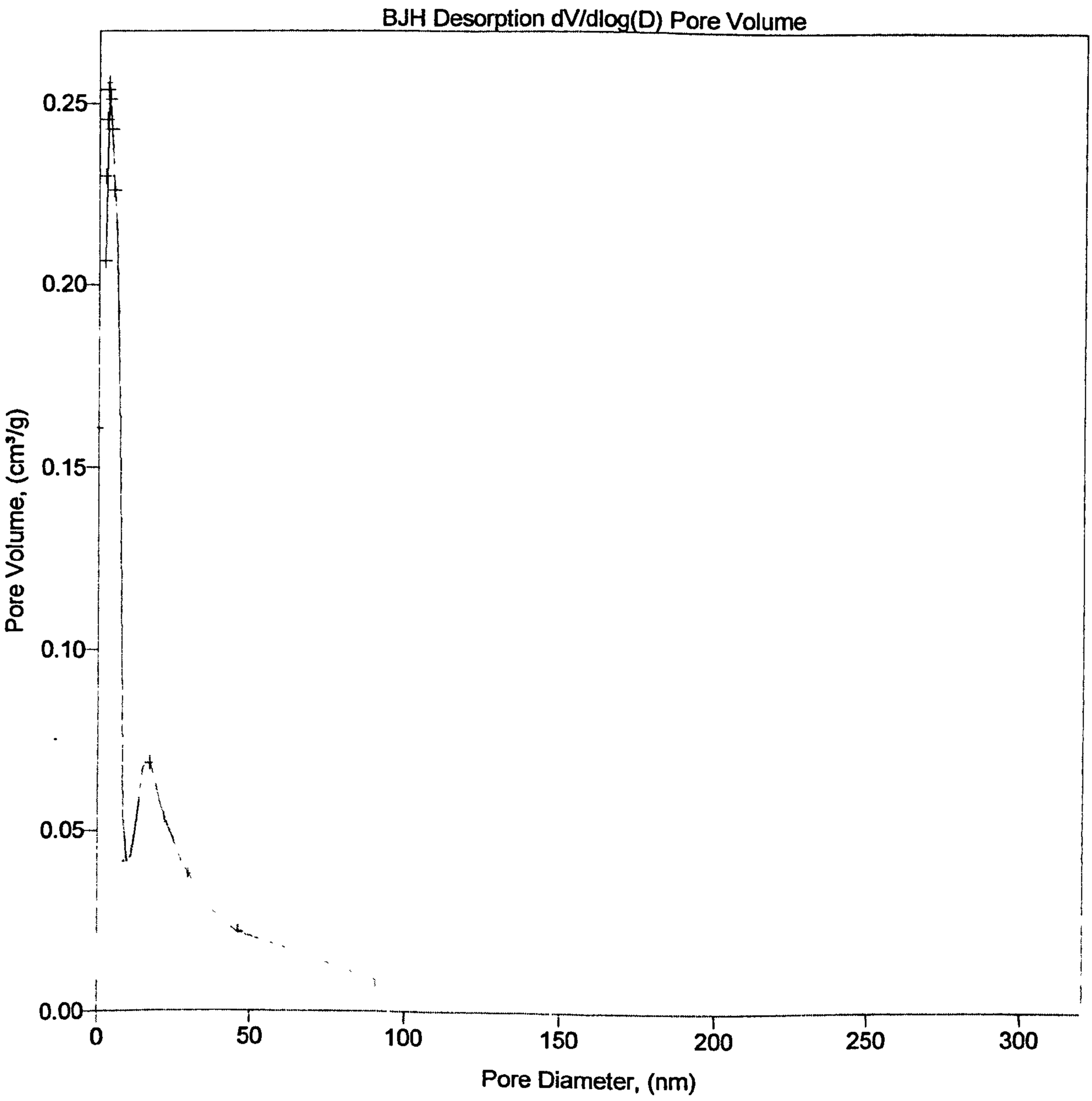

Sample: Second Rhodium coating
Operator: Susi Olsen
Submitter:
File Name: C:\ASAP2010\DATA\SY0505.SMP

Started: 29/05/03 09:30:16
Completed: 29/05/03 20:51:43
Report Time: 29/05/03 20:51:43
Sample Weight: 0.3000 g
Warm Freespace: 16.0000 cm³
Equil. Interval: 45 secs

Analysis Adsorptive: N2
Analysis Bath: 77.35 K
Thermal Correction: No
Smoothed Pressures: No
Cold Freespace: 45.0000 cm³
Low Pressure Dose: None

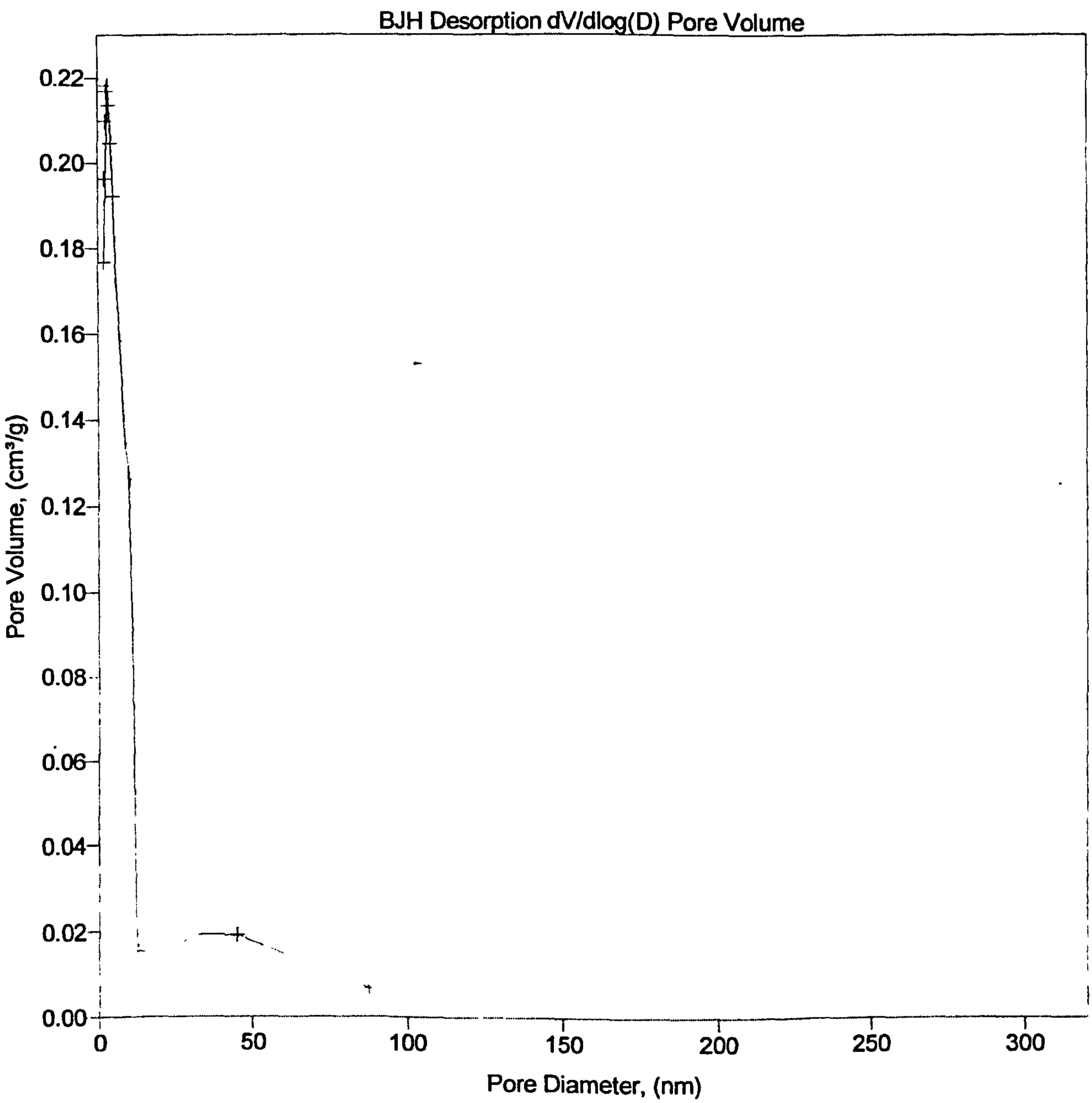

Sample: Third Rhodium coating
Operator: Susi Olsen
Submitter:
File Name: C:\ASAP2010\DATA\SY0506.SMP

Started:	30/05/03 09:06:26	Analysis Adsorptive:	N2
Completed:	30/05/03 20:03:33	Analysis Bath:	77.35 K
Report Time:	30/05/03 20:03:34	Thermal Correction:	No
Sample Weight:	0.3000 g	Smoothed Pressures:	No
Warm Freespace:	16.0000 cm³	Cold Freespace:	45.0000 cm³
Equil. Interval:	45 secs	Low Pressure Dose:	None

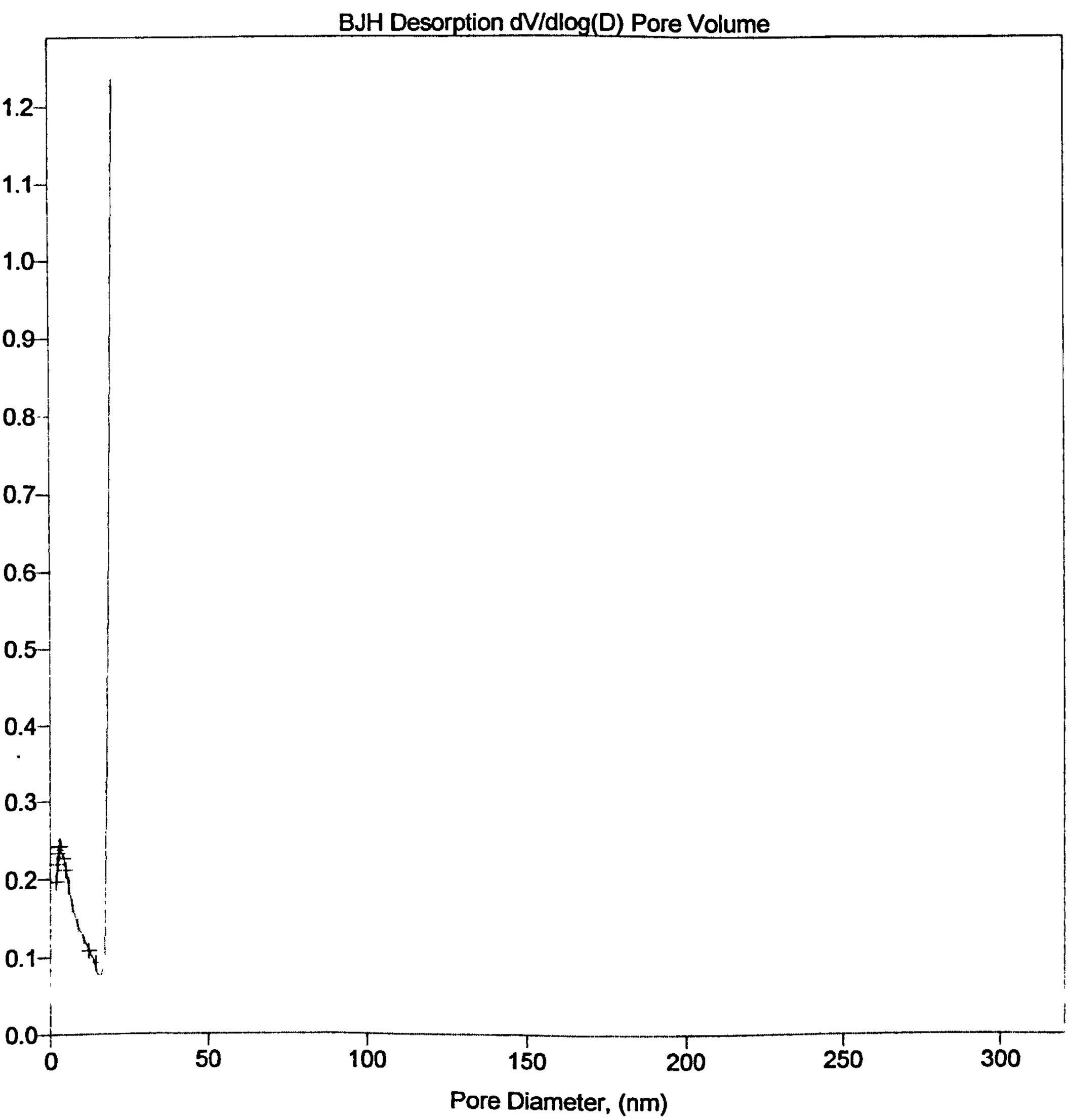

Sample: Forth Rhodium coating
Operator: Susi Olsen
Submitter:
File Name: C:\ASAP2010\DATA\SY0507.SMP

Started: 03/06/03 08:55:36
Completed: 03/06/03 20:23:40
Report Time: 03/06/03 20:23:40
Sample Weight: 0.3000 g
Warm Freespace: 16.0000 cm³
Equil. Interval: 45 secs

Analysis Adsorptive: N2
Analysis Bath: 77.35 K
Thermal Correction: No
Smoothed Pressures: No
Cold Freespace: 45.0000 cm³
Low Pressure Dose: None

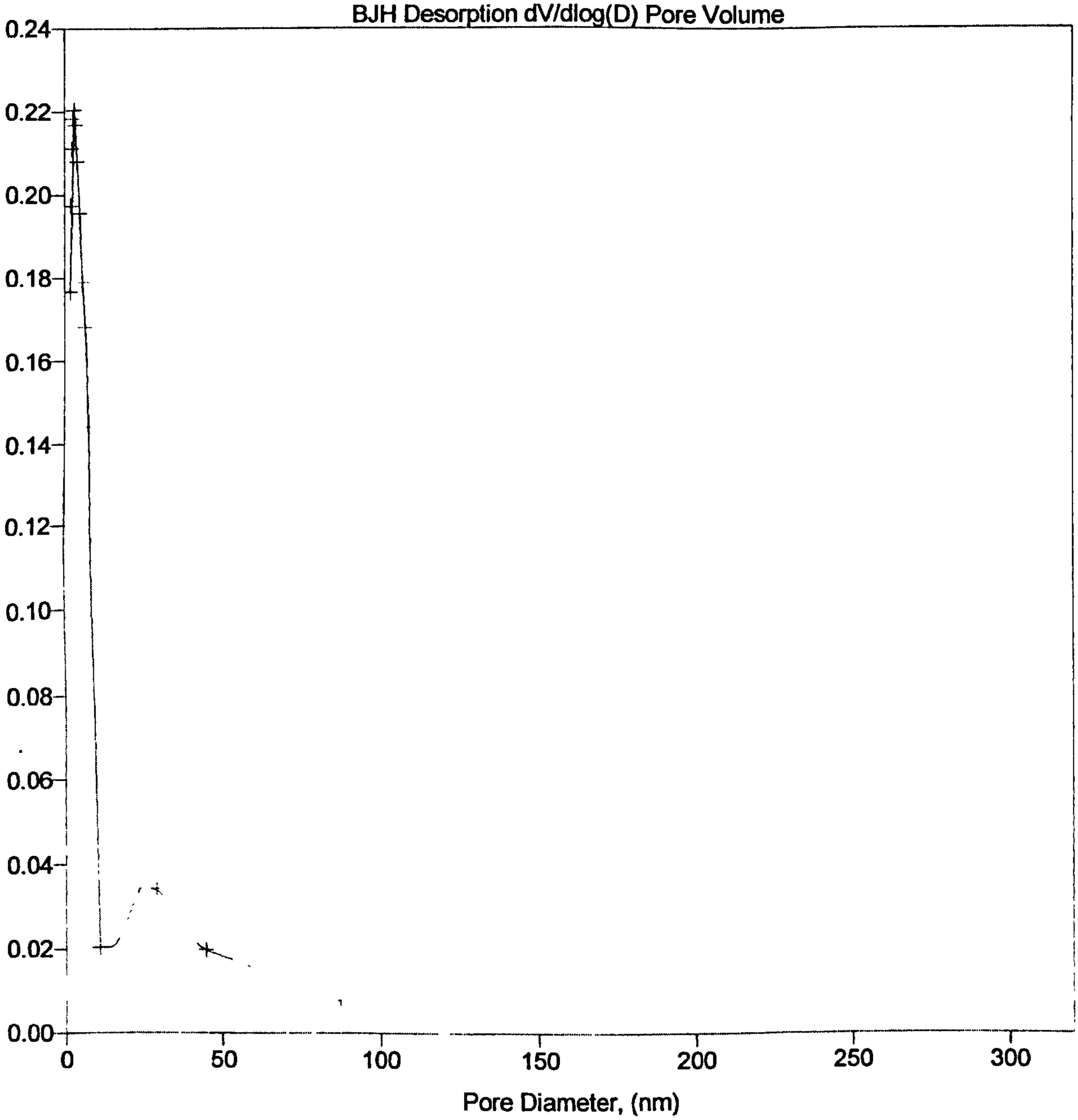

Sample: Forth Rhodium coating after H2 calcination
Operator: Susi Olsen
Submitter:
File Name: C:\ASAP2010\DATA\SY0508.SMP

Started: 04/06/03 10:23:00
Completed: 04/06/03 22:04:16
Report Time: 04/06/03 22:04:17
Sample Weight: 0.3000 g
Warm Freespace: 16.0000 cm³
Equil. Interval: 45 secs

Analysis Adsorptive: N2
Analysis Bath: 77.35 K
Thermal Correction: No
Smoothed Pressures: No
Cold Freespace: 45.0000 cm³
Low Pressure Dose: None